EFFECT OF SURFACE FINISH AND HARD COATINGS ON SCUFFING OF STEEL DISCS

by

Ajay Krishna Dhulipalla

Thesis submitted in candidature
for the degree of
Doctor of Philosophy at Cardiff University

Institute of Theoretical, Applied and Computational Mechanics
Cardiff School of Engineering
Cardiff University

March 2006

ProQuest LLC
789 East Eisenhower Parkway
P.O. Box 1346
Ann Arbor, MI 48106-1346

Summary

The principal purpose of the work described in this thesis was to develop an insight into the scuffing performance of steel discs used to simulate gear tooth contacts under severe conditions of load, sliding and high temperature. Different surface conditions of the discs such as ground, superfinished, ground/hard-coated, and superfinished/ hard-coated were investigated in various combinations and at sliding speeds of up to 16 m/s in order to obtain an understanding of the possible beneficial effect of improved surface finish and the application of hard coatings on scuffing performance under the severe conditions experienced in an aerospace transmission such as a helicopter main rotor gearbox. The lubricant used in all tests was an oil commonly used in aerospace transmissions. It was found that the diamond-like coating (DLC) investigated in this work had the effect of markedly improving the scuffing resistance of the hardened steel substrate. In tests using the ground/coated samples, for example, it was not found possible to produce scuffing within the load and temperature limits of the test rig used (2.0 GPa maximum Hertzian contact pressure or 300°C maximum disc bulk temperature) even at the high sliding speed of 16 m/s.

In addition to improving scuffing resistance it was found that the effect of the hard coating was to reduce friction and operating temperatures for a given load/speed combination. Superfinishing of the steel discs also led to a reduction in friction, but did not produce a significant improvement in scuffing resistance. It was found that the combination of ground/hard-coated discs running against ground/uncoated discs produced a remarkable behaviour of the discs' bulk temperatures, which suggests that the hard coating acts as a thermal barrier.

Micro-elastohydrodynamic lubrication (micro-EHL) analyses were conducted using surface profiles of discs used in the experimental work. These theoretical simulations demonstrated the very severe lubrication conditions which are present in the experiments. Pressure ripples far in excess of the calculated Hertzian pressure are predicted, and the films generated by hydrodynamic action are extremely thin. Under the most severe conditions transitory direct "dry" contact is predicted.

Acknowledgements

I was pleased to work under the supervision of Prof Ray Snidle, and indebted to him for making me believe I could achieve something, and extremely grateful to him for making it possible to secure funding from Cardiff School of Engineering. I would like to thank Dr Mark Alanou for making me acquainted with the experimental rig, other test equipment, and their various problems. A great deal of work from small things like thermocouple tools to major things like the finish-grinding of the test discs was done with the help of our experienced workshop staff and I thank Mr A Griffiths, head of the mechanical workshop, who was always cheerful and helpful. I would like to thank all my colleagues and friends in the Tribology and Contact Mechanics Group especially Dr C Davies (Chris as he was before) for his thoughts and supporting me through some messy times with the experimental rig. I am also grateful to Dr K J Sharif for his valuable suggestions and interesting talks, and Dr G Pugliese for his assistance with the EHL solver.

I am thankful to my family and parents who are very supportive and co-operative through all the phases of my life. They always respected my decisions and cared for me to the utmost. My brother is always a great pusher, always reminding me of my weaknesses, making me stay grounded all the time, and encouraging me to get more out of life, and I surely believe it to be a pleasure to be his brother.

I have been gifted since childhood with exceptionally good friends, who are very generous, understanding, and admirable. They always showed interest in the presentations I gave relating to Tribology after a good result or an interesting (as I think) fact I have discovered for my satisfaction. They have all been very helpful at all times and made me mesmerised regarding thoughts of home. I had a very interesting time both at Cardiff and in the University. I was always very well treated and always made to feel better. I enjoyed every moment of my stay in UK and Cardiff which gave me happy memories for life.

Contents

Notation

(Notation is given here for symbols that occur throughout the thesis. Other symbols are defined as they appear)

b	semi-dimension of Hertzian line contact
E'	effective modulus of elasticity
h	hydrodynamic film thickness
k	thermal conductivity
N	$=\pi q/\rho c u$
p	hydrodynamic pressure
q	heat flux density
Q	total heat flux or frictional power
R	radius of relative curvature
R_x, R_y	radii of relative curvature in axis directions
R_a	surface roughness parameter
t	time
u_s	sliding speed $=\lvert u_1 - u_2 \rvert$
u_1, u_2	surface speeds in x-direction relative to the contact
x, y	coordinates in the contact plane
α	proportion of total heat conducted into body 1
γ	coefficient in the density equation
Δt	time step
$\Delta x, \Delta y$	mesh spacing in coordinate directions
η	viscosity
η_0	viscosity at ambient pressure
κ	coefficient in the viscosity equation
λ	coefficient in the density equation
ρ	density
ρ_0	density at ambient pressure
Φ	surface roughness function
χ	coefficient in the viscosity equation
θ	temperature rise
μ	coefficient of friction
ρ	mass density of solid surface
σ	thermal resistivity ($=1/k$)

Chapter 1

Background, review of research and thesis aims

1.1. Introduction

The principal purpose of this work is to develop an insight into the scuffing performance of steel discs used to simulate gear tooth contacts under severe conditions of load, sliding and high temperature. Different surface conditions of the discs such as ground, superfinished, ground/hard coated, and superfinished/hard coated have been investigated in various combinations and at different sliding speeds in order to obtain an understanding of the possible benefits of improved surface finish and the application of hard coatings on the scuffing performance. This first chapter is intended as an introduction to the practical problem of scuffing and also provides a brief review of recent research in the subject. Finally the objectives of the current research project are described.

1.2. Scuffing – the background

There is little agreement in the literature on what scuffing is, what causes it, and how it can be predicted. This disagreement can be attributed, to some extent, to the different approaches taken to the problem such as those based mainly on hydrodynamic, temperature, material and chemical considerations. The definition of scuffing adopted by the Institution of Mechanical Engineers (1957) is: "gross damage characterised by the formation of local welds between the sliding surfaces". OECD (1969) adopts a similar definition: "localised surface damage caused by solid phase welding". In USA the term "scoring" is used for the same phenomenon, and in the field of rolling element bearings the term "smearing" is used to describe a type of failure which appears to be similar to that defined above.

An excellent review of scuffing which covered developments up to the mid 1970s was produced by Dyson (1975). Dyson explains that scuffing often appears in machinery which has been asked to carry heavier loads, transmit more power or operate at higher speed than before. Historically, at first the demand for increased duty led to forms of failure such as breakage of gear teeth because of the low strength materials in use at the time. This difficulty was overcome by using cast iron or steel in the place of wood. As loads and speeds were increased other limitations were encountered such as pitting of gear teeth. This form of failure was largely eliminated by through-hardening or case-hardening of the teeth and the use of cleaner steels with fewer inclusions. Finally scuffing became the failure mode, limiting the duty of gears and other mechanisms such as cams. The clear signs of scuffing failure are an increase in noise and vibration followed by a rapid increase in temperature of the surfaces involved. Smoke and sparks may be seen, in which case the surfaces usually become completely disrupted and unserviceable. The typical appearance of the surfaces of gear teeth which have been destroyed by scuffing is shown in Figure 1.1.

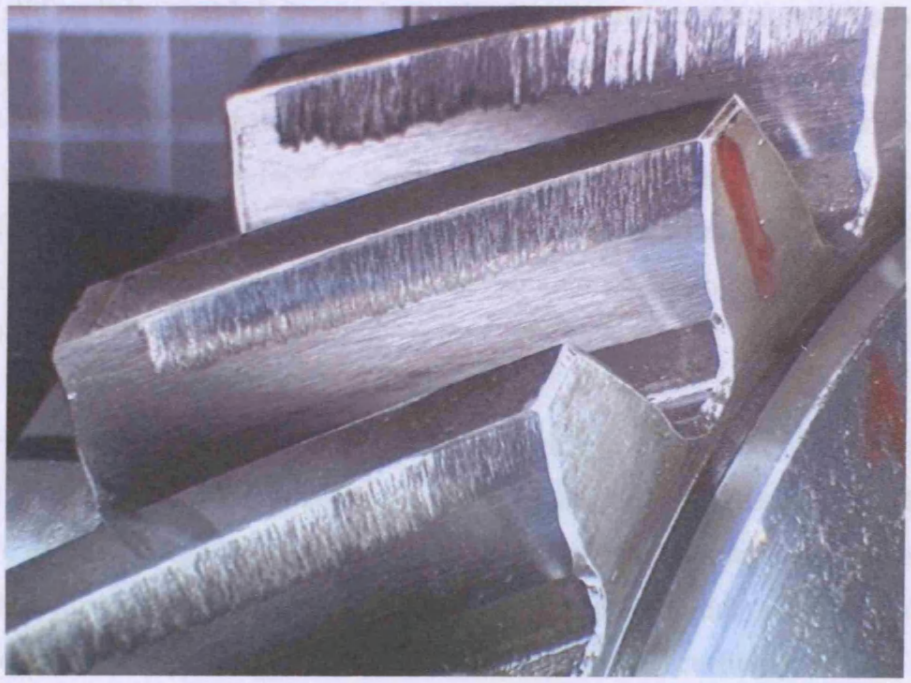

Figure 1.1. Gear teeth which have suffered severe scuffing failure.
(Design Unit, Newcastle University)

The abrupt rise in friction that accompanies scuffing was seen by Hirst (1974) as a cause of scuffing, but Dyson (1975) in his review called this a "chicken and egg" situation. In milder instances of scuffing "healing" may take place after scuffing has occurred at a light load, but this may then be followed by a more drastic scuffing failure at a subsequent higher load. When scuffing occurs in a disc test there is a very sharp increase in friction between the rolling/sliding surfaces, as will be seen in the results described in this thesis. The electrical contact resistance also falls during a scuffing episode (Leach and Kelley, 1965; Bell and Dyson, 1972). Metallurgical analysis of scuffed surfaces shows that the surface layer has undergone transformations associated with very high temperatures of the order of over 700°C (Padmore and Rushton, 1964). Practical measures to prevent scuffing have depended largely on materials and lubricant formulations in particular.

Scuffing can be postponed by the use of so-called "extreme pressure" (EP) additives in the lubricating oil. These chemically-active additives are not without unwanted side-effects, however, and whilst they may control scuffing they can also lower the resistance to pitting, for example. Scuffing is a serious problem in the design and operation of gears where a degree of sliding is inevitable between the teeth when contact occurs at positions other than at the pitch surface. Whereas strength considerations suggests the use of larger and fewer teeth on a gear, scuffing considerations favour smaller and therefore more teeth because of the lower sliding speed when teeth of smaller module are used. In high speed gearing, for example the reduction gearing in a gas-turbine driven naval vessel, the face width of the gears must be increased in order to transmit the required load using gears having relatively small teeth.

An important example of the way in which new design requirements can increase the likelihood of scuffing is the case of the hypoid rear axle gearing. This type of offset right-angle drive (Figure 1.2.) was introduced in the place of conventional bevel gears in order to lower the propeller shaft in passenger cars. The increased amount of sliding (compared to that in conventional bevel gears) present in hypoids led to scuffing problems, however, which were eventually cured by the introduction of special EP axle oils. A lower position of the propeller shaft can be achieved by using a worm drive, but in this case even the special EP oils cannot give protection when both gears are of steel, so one of the gears (the wheel) is made from a softer material (bronze) in order to avoid scuffing.

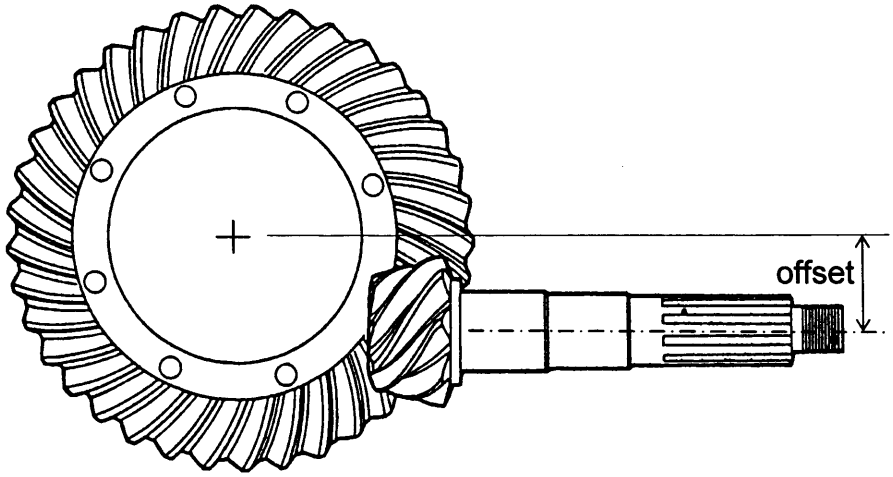

Figure 1.2. Hypoid gears
[British Gear Association]

When considering the factors which affect scuffing one of the main considerations is the sliding speed. In machinery in which there is no sliding scuffing is rare. Thus in rolling element bearings scuffing is not a serious problem, although it can arise in large high speed, lightly loaded bearings due to "ball skid" which is a situation that can occur in the main rotor bearings of a jet engine under certain conditions. The sliding speed, U_s, between two surfaces is defined as the difference between the two surface speeds U_1 and U_2, i.e. $U_s = U_1 - U_2$. The rolling, or entrainment speed, which is the mechanism by which oil is drawn into a gear tooth contact by viscous flow, is defined as $\overline{U} = (U_1 + U_2)/2$. The slide/roll ratio is defined as $U_s/\overline{U}$. This ratio expresses the relative effect of two velocities: rolling is beneficial (it generates an oil film which is capable of separating the surfaces) and sliding is the opposite because of its effect on friction and temperature. Thus in general it is better to avoid contacts in which the ratio is high, and this might be taken as a crude criterion in gear design, for example. In gears the ratio varies from zero at the pitch surface to a maximum (about 1.0, say) at the tooth tip contacts, but the ratio does not depend on the operating speed of the gears. A very severe case of sliding is when both surfaces have the same surface speed but in opposite directions. In this case the rolling speed is zero and hence the slide/roll ratio is infinite. This situation does not occur in gears but can happen in some types of cam/finger-follower valve operating mechanisms in IC engines.

The effect of chemistry is also very important. Tests with both discs and gears show that the complete exclusion of oxygen can lead to scuffing at very light loads (Bjerk, 1973). A review of the role of oxygen and oxides is given by Ludema (1984). As already noted the use of chemically active EP additives can also improve the resistance to scuffing, but high levels of chemical activity can cause corrosion problems as happened in naval reduction gearboxes when a new EP additive was found to give better scuffing resistance but unfortunately caused serious corrosion of the whitemetal bearings supporting the gears.

The choice of materials for lubricated contacts is of great importance. The pairing of two different materials is generally better than pairs of identical materials. This ideal is not easily realised in high duty gearing because of the need to use high strength, hardened steel for both parts in order to meet the basic tooth strength (bending and contact) requirements. Austenite is very inert chemically and a high content of this metallurgical phase in steel tends to cause scuffing. Alloy steels in which austenite can be controlled at a low level are preferable. Alloying elements which favour low austenite content are Cr, W, Mo, Va, and Si, and elements which tend to increase it (Ni, Mn, C, and N) are to be avoided (Niemann and Lechner, 1967).

Apart from the main factors of sliding, chemistry and materials, the geometry of contacting surfaces can have a major effect on the incidence of scuffing. The contacts between surfaces should, ideally, occur at a natural Hertzian conjunction in which there is a smooth distribution of pressure without any excessive points of high pressure caused by sharp discontinuities in the shape of the parts. The presence of sharp edges, such as those at the ends of gear teeth, should be avoided by suitable relief geometry as should heavy edge contacts cause by the omission of "tip relief" of the teeth. The effect of tooth profile modification on the scuffing resistance of case-hardened spur gears was studied by Yokoyama et al (1972) who found that a significant improvement in scuffing resistance could be achieved by better tooth geometry.

In spite of the usually sudden and experimentally reproducible nature of scuffing some authors (Tallian, 1972), for example have in the past believed that it is a cumulative or fatigue process. This view is discounted by present-day understanding which tends to see the importance of thermal effects and lubrication breakdown as the principal cause.

An extensive programme of experimental scuffing testing using discs was carried out by Bell and Dyson (1972) and by Bell, Dyson and Hadley (1974). The influence of various factors was investigated (rolling speed; sliding speed; surface finish; and oil additive). The sliding speed was found to be the most important factor influencing failure load. These authors also compared their experimental findings with theoretical predictions (see later).

Disc machines are widely used to simulate gear tooth action, but the question arises as to what extent disc machines can achieve this objective. Gear tooth action is kinematically more complex, giving conditions which pass from sliding, through pure rolling to sliding. However, it is very difficult to measure instantaneous values of friction in gear rigs, and the whole behaviour of gears is affected by the dynamics of tooth engagement and disengagement.

Surface finish of components, and the direction of finish, has been found to influence scuffing. Staph, Ku and Karper (1973) and Story, Archard and Baglin (1981) have suggested that an axial finish (i.e. finishing marks in a direction transverse to that of sliding) leads to a higher scuffing load on the basis that such a finish gives better EHL film formation. These earlier findings were supported by Paliwal (1987) who conducted scuffing tests on both circumferentially and axially ground discs and found that the scuffing load for axially-finished discs was typically twice that for circumferentially-finished surfaces.

Bishop (1981) investigated the effect of "running in" of steel discs. It was found that by pre-running in the discs at a high load using an EP additive it was then possible to achieve an increase in the base oil performance when the discs were run subsequently without the EP additive. This work drew attention to the important role of the running in process itself and its effect on scuffing performance. The conclusion of improved scuffing resistance with running in of the surfaces was also confirmed by Paliwal (1987).

Patching et al (1995) carried out scuffing tests on both axially finished (Ra = 0.4 μm) steel discs and the same discs which had been highly polished to a finish of Ra less than 0.1 μm. The "superfinished" discs were found to scuff at higher (typically twice) the loads at which

the ground surfaces failed and the friction and temperatures under conditions before scuffing were significantly lower.

Martin et al (2001) carried out scuffing tests on M50 bearing steel at very high sliding speeds of up to 30 m/s. This work was intended as a simulation of "ball skid" in high speed angular contact ball-bearings. In this industry a popular scuffing criterion is based on the "PV" value, i.e. the product of contact pressure and sliding speed. This was not found to be a reliable predictor of scuffing, however. A better indicator of failure was the calculated oil film thickness in relation to the surface roughness of the rollers. In general the performance of M50 material was found to be similar to superfinished, case-carburised steels when run with the same lubricant.

Alanou, et al (2004) followed up Patching's experiments on superfinished surfaces in their investigation of different combinations of surface hardening, finish and hard coatings. The results obtained confirmed the improvement in scuffing resistance as a result of superfinishing and also demonstrated the superior performance of nitrided surfaces as compared to case-carburised and hardened samples. These workers also carried out a short series of tests using hard-coated samples. The combination of a nitrided, superfinished, hard-coated sample produced a particularly scuff-resistant combination.

Kim (2001) presented an interesting paper relating the residual stresses on the lubricated sliding surfaces during break-in to the failure or scuffing resistance of the surfaces. The X-ray diffraction method was used to measure the residual stresses on a lubricated sliding surface and subsurface during break-in (running-in in our terminology). He concluded that the break-in procedure has a very important role in forming and increasing the distribution of the residual stresses at the surface and subsurface to overcome failures due to further sliding. Hershberger (2004) had done similar work with experiments on measuring dislocation densities by the X-ray diffraction method. Scuffing was predicted to occur when the rate of local thermal softening exceeded that of work hardening in the tribological contact.

Suh et al (2003) carried out controlled scuffing experiments to simulate failures in an air-conditioning compressor. The surfaces involved were measured at various stages of

running and the surface changes preparatory to scuffing. This work is interesting in that it emphasises the "fluid retention" role of surface roughness. It is suggested that the effects of progressive wear are translated into a decreased fluid retention capability and an increased bearing index, which both indicate that lubricant can no longer be retained sufficiently. The loss of lubricant retention capability means an increase of the real area of contact, leading to eventual direct metal-to-metal contact and scuffing.

Qu (2004) investigated different material characteristics using a scuffing detection method, which analyses the frictional changes on individual strokes, and thereby enables one to identify the starting locations and progressive spread of scuffing damage in heavy duty diesel fuel injectors. Rougher surfaces sustained thicker lubricant films with reduced asperity contact, preventing the scuffing longer, but the actual application of a good surface finish is needed to maintain high injection pressure. The ideas put forward in both these papers seem to suggest that perfectly smooth surfaces may not be ideal when trying to improve scuffing resistance.

Zhang (2004) worked on the scuffing behaviour at the contact between the end of the piston pin (often called the gudgeon pin in UK) and the cylinder bore. In this paper the effect of friction is examined in detail and scuffing is related to the shear strength of the surfaces involved. In spite of the considerable amount of experimental work on scuffing there has been little progress in understanding the detailed mechanism of this form of surface failure, and even less success with producing a viable criterion by which the possibility of scuffing may be predicted in advance.

Blok (1939) suggested that scuffing would occur if the total contact temperature exceeded a certain critical level, which in the extreme form of the hypothesis depends only on the lubricant and on the materials of the two surfaces. The total contact temperature is the sum of two components, first the bulk temperature of the parts, and second, the instantaneous increase of the temperature of the surfaces as they pass through the contact zone. The bulk temperature can be measured fairly easily (this is the temperature measured by the embedded thermocouples used in the present work). The second part, the so-called flash temperature, decays very rapidly once the surfaces leave the contact zone. The flash temperature cannot be measured in a simple way and it must be calculated based on an

assumed (or preferably measured) friction force. Blok gave a theory, in an earlier paper (Blok, 1937), for the calculation of the flash temperature based upon certain assumptions concerning the mode of heat conduction in the solid surfaces. Although Blok's approach has been widely used as a criterion of scuffing many investigators are highly sceptical about its ability to predict scuffing conditions. Bell, Dyson and Hadley (1974), for example, found that the Blok criterion failed to predict scuffing in their carefully controlled disc machine experiments in which the bulk temperature was measured and the flash temperature calculated from measured friction.

An alternative scuffing criterion, advanced by Matveevsky (1965), is based on the hypothesis of constancy of the frictional power intensity. The frictional power intensity is defined as the rate of production of energy by friction divided by the area of Hertzian contact. It is therefore the product of coefficient of friction, mean Hertzian contact pressure and sliding speed. Bell, Dyson and Hadley (1974) found, in their wide-ranging investigation of operating conditions, that this criterion was more reliable than the Blok total contact temperature, but still showed a wide variation over the range of conditions which they considered in their paper.

A new approach which attempted to model the physical conditions under which the EHL system would fail, and therefore cause scuffing, was put forward by Dyson (1976). In this theory the bulk temperature at which the EHL pressures just fail to be generated were calculated based upon the surface roughness of surfaces in the condition they reached just before scuffing. The calculated temperatures were found to be in reasonable agreement with the bulk temperatures which were measured just before scuffing in disc tests using circumferentially ground surfaces.

Snidle, Rossides and Dyson (1984) refined Dyson's method of calculation and ran a series of scuffing tests to compare theory with experiment that gave a closer agreement, but all the tests were done using one combination of steel and mineral oil. Dyson, Evans, Karami, Paliwal and Snidle (1990) ran further scuffing tests on steel discs with circumferential finish, with combinations of three types of steel and three different oils. There was reasonable agreement between theoretical predictions and experimental results, with experimental scuffing temperatures generally higher than the predicted values. It was

concluded that chemical factors, which were ignored in the theory, would be beneficial and probably explain the better than expected performance in the case of the additive oils. The results obtained in the latter paper are summarised in Figure 1.3.

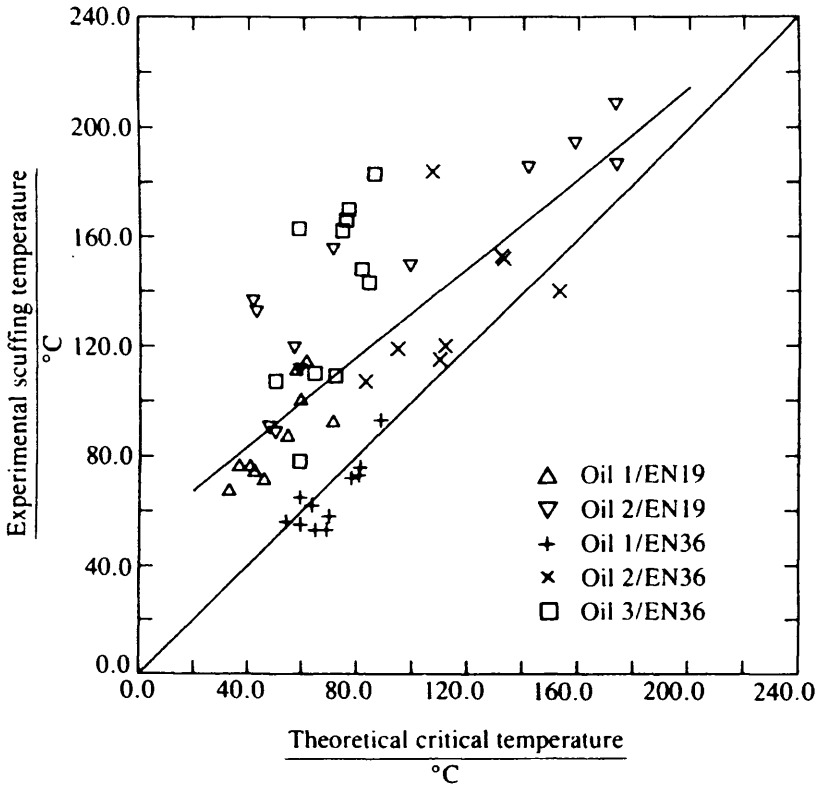

Figure 1.3. Experimental bulk temperature at scuffing versus calculated critical temperature. Lower line shows theory and upper line is least-squares mean line through experimental points.
[Dyson, Evans, Karami, Paliwal and Snidle (1990)]

The concept of "micro-elastohydrodynamic lubrication" (micro-EHL) in relation to both pitting and scuffing was explored by Cheng (1983). In this paper Cheng suggested that the origins of scuffing damage in EHL contacts occurred at individual asperity contacts where the failure mechanisms are influenced strongly by micro-EHL which is characterised by the local asperity oil film thickness, local pressure, shear stress and temperature.

Lee and Cheng (1991) carried out disc machine tests using circumferentially ground samples with the specific aim of verifying two existing scuffing theories based on breakdown of the EHL film (i.e. Dyson-type theories, and Cheng's micro-EHL approach as outlined in Cheng, 1983 – see above). Lee and Cheng developed an "average gap"

model of a rough EHL contact. The experimental results were categorised according to whether scuffing was "macroscopic" or "microscopic". It was found that the likelihood of micro-scuffing (i.e. scuffing at the asperity level) propagating to macro-scuffing (on the scale of the nominal Hertzian contact) was controlled by the effectiveness of the main EHL system.

Both the Dyson approach, which models the "main" EHL system under roughness conditions, and the Cheng approach (micro-EHL) are based on the analysis of circumferential roughness, i.e. roughness that is aligned in the direction of rolling/sliding. A possible criticism of this assumption about roughness geometry is that the analysis is only possible for circumferentially finished surfaces; real gears are effectively axially finished and a different approach to dealing with the failure of the hydrodynamic system is needed. A fundamental issue with axial finish is that the EHL problem is no longer "steady" because of the effect of "moving roughness" which makes the film thickness at any point in the conjunction a function of time as well as position. In recent years attention has been focussed on this problem and transverse-roughness, time dependent models for both line and point contact situations have emerged as a result of the development of micro-EHL theory at Cardiff University, as will be discussed in Chapter 5 of this thesis.

1.3. Hard Coatings

Two promising methods for improving both pitting and scuffing resistance of steel surfaces are superfinishing (polishing) and the use of super hard coatings. The need for longevity and quality in the field of contact mechanics was one of the reasons behind the evolution of hard coatings. Chemical vapour deposition (CVD) and physical vapour deposition (PVD) were very popular techniques in the initial development stages of hard coatings in the 1960s. PVD, which is a vacuum coating technique, has many variations and different techniques which are used for specific purposes. The current generation of hard coatings include "diamond like carbon" (DLC) coatings, a term which includes many sub groups depending on the type of material, method of deposition and the substrate used. The main aim of using hard coatings is to increase the life of the product, and most of the work done has been concerned with improving the fatigue performance of components. The progress made using these coatings in engineering contact situations in general, and as an anti-scuffing treatment in particular, is briefly reviewed as follows.

The effect of hard coatings on the fatigue life of rolling element bearings was studied by Polonsky et al (1997) who derived approximate analytical formulae to estimate the coating thickness required to protect the substrate effectively from the small-scale contact stress spikes produced by roughness, and thus prevent near-surface rolling contact fatigue. The analysis showed that to be truly effective the coating should be relatively thick, of the order 3 μm or greater.

Wong (1996) analysed the effect of hard and stiff overlay coatings on the strength of surfaces in repeated sliding and concluded that hard coatings can only be effective when they are thicker than a critical value, which depends on the elastic and plastic properties of the coating, substrate and their roughness. Kodali (1997) used pin on disc tests to find the fracture toughness and tribological properties of amorphous DLC coatings. It was found that the hardness and fracture toughness, both of which affect wear resistance, depend on the thickness of the coating. Hardness and thickness influenced the initiation of cracks, but residual stress in the coating influenced their propagation. The good wear resistance of the coatings was attributed to their low friction, high hardness and high fracture toughness.

Grill (1997) in a review paper on the tribology of diamond like carbon and related materials points out that the friction behaviour of diamond like carbon (DLC) depends strongly on the tribotesting environment and is controlled by tribochemical effects, which also depends on the deposition technique. Grill concludes that the observed low friction of DLC coatings is explained by the low shear strength of a transfer layer formed during sliding of the surfaces in contact. The importance of incorporating other elements, such as F, Si, N, metal, which can modify the physical properties of DLC layers while maintaining their tribological properties is also stressed.

Holmberg et al (1998) presented an excellent, wide-ranging review of coatings tribology and "surface design". It is the view of these authors that, from a tribological point of view, DLC coatings represent the most dramatic new coating concept introduced during the last few decades. An interesting aspect of this paper, in relation to the present study, is the section which deals with the effect of oil lubrication on the friction of hard coatings.

Donnet (1998) provided a review on the progress of the tribology of "doped" DLC coatings and carbon alloy coatings. The review shows how the incorporation of various "dopants" in the DLC structure has been used to achieve combinations of low friction and high wear resistance. This author also echoes the view that the tribological behaviour of hard coatings strongly depends on the testing conditions and the nature of film deposition.

Donnet and Grill (1997) also commented on the effect of the deposition process on the observed friction behaviour of DLC coatings used as dry lubricants. A wide range of friction coefficients from less than 0.01 to more than 0.5 were found. This variation was explained by tribochemical effects and the build up of an easy-shear transfer film in particular.

Hogmark et al (2000) reviewed the tribological response of coatings and their design. The author evaluated and explained the current trends in coating and types of coatings and the methods of deposition for attaining maximum scuff resistance. The authors emphasised the importance of developing versatile and reliable techniques for evaluation of coated components.

The effect of load on the abrasion of steel by metal-containing DLC was reported by Harris et al (1999) who ran tungsten-containing DLC-coated coupons against steel balls. The steel surfaces had a hardness of about 7GPa and the coating hardness, measured by nano-indentation, was about 10GPa. At low loads the initial abrasion rate was found to increase with load, but at higher loads the initial abrasion rate was almost independent of load. The authors conclude that the factors controlling the loss in abrasiveness of DLC coatings is not yet understood.

Abrasiveness was also the subject of a paper by Borodich et al (2003) in which the authors put forward two ball on disk wear models which are shown to agree with the experimentally observed power-law relationship between the abrasion rate of coatings and the number of wear cycles (n) which was of the following typical form (k = constant)

$$\text{average abrasion rate} = kn^{-0.8}$$

In an important paper Krantz et al (2004) reported the results of work in which spur gears both with and without a metal-containing DLC coating were run in surface fatigue tests. The surface fatigue lives of the gears were evaluated by accelerated tests. For the uncoated gears all of the 15 tests resulted in fatigue failure before completing 275 million revolutions. For coated gears 11 of the 14 tests were suspended with no surface fatigue (pitting) failure after 275 million revolutions. The improved durability as a result of coating gave an approximately sixfold increase in life and was a statistically significant result. The results of this series of tests are summarised in Figure 1.4 which shows the Weibull plot of the results for the coated and uncoated gears.

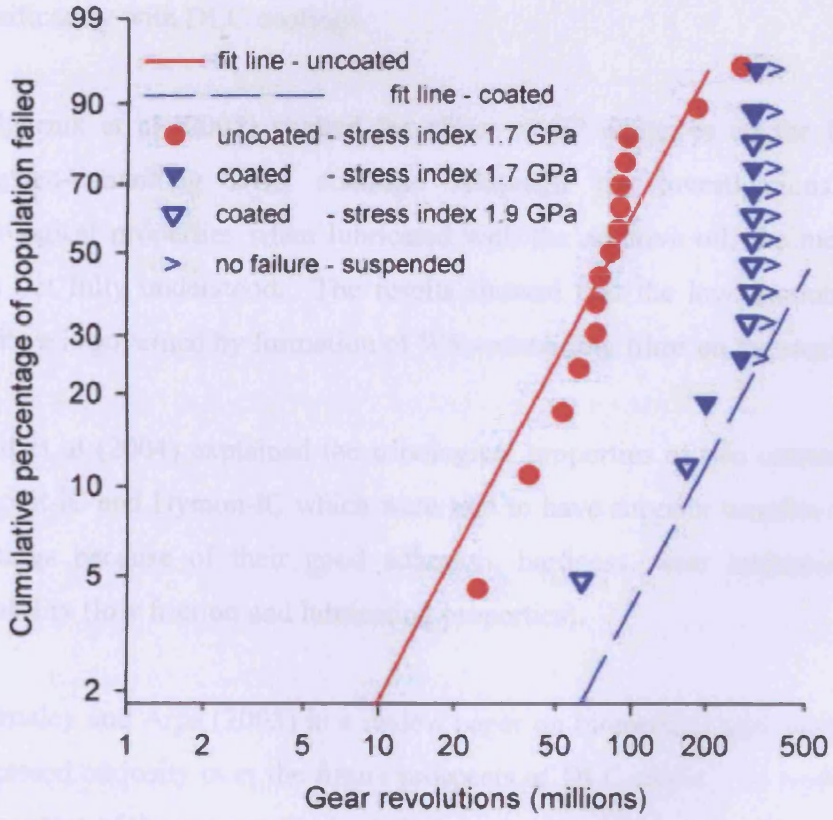

Figure 1.4. Weibull plot of the fatigue test results with best fit lines as was estimated using the maximum likelihood method [Krantz, 2004]

Various authors have experimented with different DLC formulations and methods of applying the coating. Chang et al (2004) tribologically tested Ti-containing films deposited by unbalanced magnetron sputtering with an intermediate layer of different kinds

of elements, showing low friction. Metal doped hydrogenated carbon films showed decreased residual stress and low dependence of the coefficient of friction on humidity.

Sheeja et al (2003) experimented on superfinished coated surfaces with single and multi layer coatings sliding one on another. A multi-layer DLC coated steel surface rubbing against a single-layer DLC coating was found to give superior performance at relatively low loads, but for high load situations, such as orthopaedic implants single layer coatings were found to be more reliable. Persson and Gahlin (2003) worked on the tribological performance of DLC coatings in combination with water based lubricants and showed that the performance of tribological systems with water based lubricants can be improved significantly with DLC coatings.

Podgornik et al (2005) studied the effect of EP additives on the friction behaviour of tungsten-containing DLC coatings. Although the investigations showed improved tribological properties when lubricated with the additive oil, the mechanism responsible was not fully understood. The results showed that the low friction behaviour with the additive is governed by formation of WS_2-containing films on the steel counterface.

Field et al (2004) explained the tribological properties of two commercial DLC coatings Graphit-iC and Dymon-iC which were said to have superior benefits over traditional DLC coatings because of their good adhesion, hardness, wear resistance and load bearing capability (low friction and lubricating properties).

Dearnaley and Arps (2005) in a review paper on biomedical applications of DLC coatings expressed curiosity over the future prospects of DLC coatings in medical applications. In the context of the present thesis study a point to note from the review is that DLC coatings when coated on highly polished surfaces (super finished surfaces) produce optimum results, depending on the type of deposition.

Alanou et al (2004) experimented on different surface finishes and coatings and the effect they have on the scuffing performance of hardened steel discs at high sliding speeds. This work showed that nitriding, superfinishing, and hard coating gave impressive scuffing resistance. The author expressed his view that superfinishing and coatings are the two

treatments which can enhance the scuffing performance of surfaces in practice. Using hard coatings on highly polished or superfinished surfaces gives a double benefit which is the present trend of countering scuffing more efficiently.

Kalin and Vizintin (2005a) performed various experiments with combinations of steel/steel, steel/DLC and DLC/DLC contacts with mineral/biodegradable oils using an *Optimol* reciprocating sliding wear apparatus to compare their tribological behaviour. Surprisingly, perhaps, the steel/steel combination gave the lowest wear rate with all three lubricants tested. The use of additives significantly reduced the wear in all types of contacts and the highest reduction was with DLC/DLC. This clearly indicated the beneficial boundary lubrication effects of additives on these "inert" DLC coatings. Kalin and Vizintin (2005b) also carried out tests on DLC coated gears in an FZG back-to-back rig lubricated with biodegradable oil with various material combinations.

The main conclusions from this important work are as follows.

- With DLC/DLC coated gears the oil temperature was lower and the gears showed good wear resistance up to contact pressures of 1.4GPa.
- Scuffing was prevented, which was attributed by the authors to the coating preventing adhesive wear.
- A "mixed" combination of steel/DLC is only suitable for low loads because of the extremely high wear of the steel (uncoated) gears at high loads.
- Contrary to these findings, perhaps, it was again found that the steel/steel combination gave the lowest wear.

To summarise these results it would seem from the work of Kalin and Vizintin that DLC coatings: reduce temperature (by lowering friction); they prevent scuffing; but under conditions less severe than scuffing they do not give better wear prevention than uncoated gears.

1.4. Thesis aims and layout

The main aim of the work described in this thesis was to obtain an understanding of the performance of hard-coated steel surfaces under realistically severe conditions that might be experienced in an aerospace transmission such as a helicopter rotor gearbox.

It was considered essential to use materials, lubricant, temperature and operating conditions of load and speed that could simulate gearing. The operating conditions used in much of the work covered in the preceding review, in which reciprocating wear rigs and 4-ball tests have been used, are mild compared to the real world of transmission gears.

Notable exceptions to this trend are the efforts of Alanou et al (2004) at Cardiff and the Slovenian team of Kalin and Vizintin.

A wide range of rolling/sliding conditions are to be covered, up to a maximum sliding speed of 16 m/s with contact pressures of up to 2.0GPa. The work undertaken is divided into the following chapters as follows.

The two disc machine used and other issues related to the rig are presented in *Chapter 2.* The chapter includes a description of the special grinding arrangement used to produce axial finish of the test discs.

The substantial series of tests carried out with various combinations of ground steel, superfinished steel, hard-coated steel using a steel substrate provided by UTRC of USA is described in *Chapter 3.* Full details of the test including friction and temperatures measured during the test are shown together with surface profiles of specimens before and after testing. Photographs and SEM images are shown as an aid to description of the effects of running and failure of the surfaces.

A shorter series of test using un-coated steel supplied by Rolls-Royce is described in *Chapter 4.*

Numerical simulations of three experimental tests using profiles acquired from the run surfaces are described in *Chapter 5.* The solver used in this work was provided by

Professor HP Evans and help in its use was provided by Mr Giovanni Pugliese, a visiting researcher in the School of Engineering.

Chapter 6 is a summary of the results obtained in this work and includes a discussion of the results, comparisons between the performance of different materials combinations and operating conditions. The conclusions to be drawn from the project are listed in a concise form. Finally the author makes his suggestions for a continuation of the work on scuffing and hard-coated surfaces in relation to improved durability of high duty gearing.

Chapter 2

Experimental Rig and Instrumentation

2.1 Introduction

In this chapter the special rig which has been used in all experiments is described together with the instrumentation used to acquire data such as load, speed, friction and temperatures. The basic rig was first devised by Patching *et al* (1994) and various enhancements have since been made. The rig was designed and built in the Cardiff School of Engineering for the study of scuffing in gears and uses two equal discs of 76.2 mm (3.00 inches) diameter.

Scuffing tests on actual gears are expensive, and if a fundamental understanding of scuffing is required then the geometry and kinematics of the gear meshing cycle tend to complicate the behaviour of the lubricated contact. For these reasons researchers have adopted disc (or roller) machines in which the basic non-conforming contact between gear teeth is simulated by that between two cylindrical rollers. The relative geometry at the tooth contact can be represented by appropriate choice of the size of the rollers; and a given combination of rolling and sliding at the contact is obtained by suitable gearing between them. The Hertzian contact pressure at the tooth contact is obtained in the corresponding disc rig by suitable choice of the load, given the relative geometry between the rollers.

A further advantage of the roller rig is that sliding friction at the contact can be measured relatively easily, a task which is difficult to perform in the case of gears. Disc rig simulations are open to criticism, of course, since they do not reproduce the time-varying rolling/sliding/geometry/loading that takes place at tooth contacts during the meshing of gear teeth, but from a scientific point of view it is recognised that the disc rig, which

avoids these complications, can provide better insight into the fundamentals of lubricated contacts under scuffing conditions. For these reasons disc rig testing is well established (see, for example, Bell and Dyson, 1972; Bell, Dyson and Hadley, 1975) as a technique for simulating the basic mechanism of gear tooth contacts.

2.2. Tooth contact Conditions in Gears

Conventional spur gears have teeth of involute profile and during the meshing cycle the relative geometry at the contact between a pair of teeth changes as does the relative velocity of sliding and the entrainment or "rolling" velocity. Figure 2.1 shows a pair of gears in contact at point *P*. The two base circles (of fixed diameter) define the involute profiles of the teeth on the two gears.

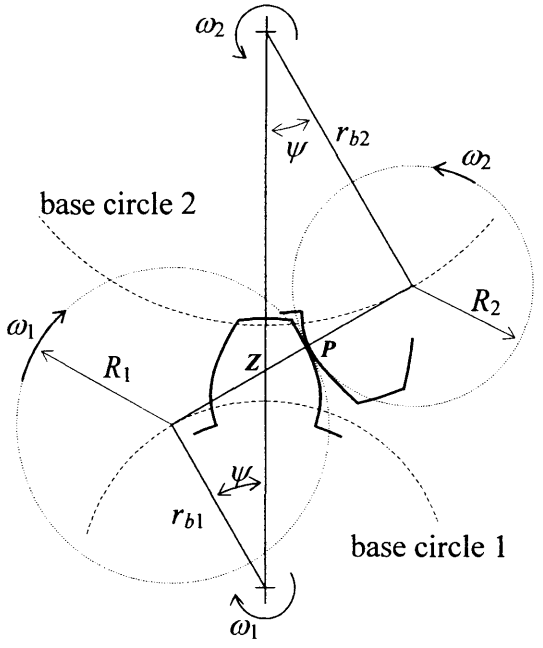

Figure 2.1. Illustration of gear teeth in contact showing equivalent rolling/sliding circles. Sliding is proportional to $s = ZP$, where Z is the pitch point and P is the instantaneous contact between the teeth.

The normal force on each tooth is F_n and the number of teeth in contact at any stage in the meshing cycle is n (for gears of standard design there are either one or two teeth in contact at any instant).

The total normal force acts on the gear in a direction which is tangential to both the base circles, hence, assuming equal sharing of the total load by n simultaneous contacts,

$$nF_n r_b = torque \qquad \text{hence} \qquad F_n = \frac{torque}{nr_b}$$

The elastic contact between involute gear teeth of spur form occurs along a line, which becomes a narrow band of contact under load. The geometrical conformity at this "line contact" is relatively low and it is therefore usual to assume that the contact stresses and deformation can be obtained from the Hertz equations. In order to apply Hertzian theory, which assumes that contact occurs between cylinders (or, more strictly, between parabolic surfaces), we require the radius of relative curvature of the two surfaces at their contact. As already noted this quantity varies during the meshing cycle.

When contact occurs at an arbitrary position defined by the distance s (= ZP) as shown in Figure 2.1 the involute profiles of the two teeth close to their contact may be represented by two circular arcs of radii R_1 and R_2 as shown, where

$$R_1 = r_{b1}\tan\psi + s \qquad \text{and} \qquad R_2 = r_{b2}\tan\psi - s$$

Note that s may take negative as well as positive values. The radius of relative curvature at the contact is defined as

$$\frac{1}{R} = \frac{1}{R_1} + \frac{1}{R_2}$$

which gives

$$R = \frac{(r_{b1}\tan\psi + s)(r_{b2}\tan\psi - s)}{(r_{b1} + r_{b2})\tan\psi}$$

The Hertz equations for the maximum elastic contact pressure (p_0) and semi-width of the band of contact (b) are

$$p_0 = \left[\frac{W'E'}{2\pi R}\right]^{1/2} \qquad \text{and} \qquad b = \left[\frac{8W'R}{\pi E'}\right]^{1/2}$$

where the load per unit width of tooth, W', and the quantity E' are obtained from

$$W' = \frac{F_n}{t} \qquad \text{and} \qquad \frac{2}{E'} = \frac{1-\nu_1^2}{E_1} + \frac{1-\nu_2^2}{E_2}$$

We may note that the radius of relative curvature depends on the base radii of the gears and not the "size" of the teeth.

Rolling at the contact between the gear teeth is the mechanism by which an elastohydrodynamic oil film is generated. The rolling or mean entraining velocity ($\bar{u}$) is defined as the mean of the two surface velocities relative to the instantaneous contact

$$\bar{u} = \frac{u_1 + u_2}{2}$$

The tooth surface velocities relative to the contact point P are u_1 and u_2 and these may be obtained from Figure 2.1 directly since the straight, fixed path of contact (i.e. the line which is tangent to both base circles) does not rotate. They are

$$u_1 = (r_{b1} \tan\psi + s)\omega_1 \qquad \text{and} \qquad u_2 = (r_{b2} \tan\psi - s)\omega_2$$

Since $r_{b1}\omega_1 = r_{b2}\omega_2$, the relative sliding velocity, $v_s = u_1 - u_2$, is then given by

$$v_s = (\omega_1 + \omega_2)s$$

The *slide/roll ratio* (*SRR*) is often quoted in the context of elastohydrodynamic lubrication (EHL) and is defined as

$$SRR = \frac{v_s}{\bar{u}} = \frac{2(u_1 - u_2)}{(u_1 + u_2)}$$

In order to give an indication of the size of gears that are effectively simulated using discs of a given diameter we may take the situation when contact occurs at the pitch point as our reference condition (i.e. when $s = 0$ in Figure 2.1). If we assume two equal gears with a

typical working pressure angle of 20° then from the above equation with $r_{b1} = r_{b2} = r_b$ and a value of R = 19 mm, (which is equivalent to the radius of relative curvature at the line contact between two rollers of 76 mm diameter as used in the Cardiff rig – see later), the equivalent pair of gears would have a base diameter r_b of about 200 mm. This approximate equivalence of gears and discs is illustrated schematically in Figure 2.2.

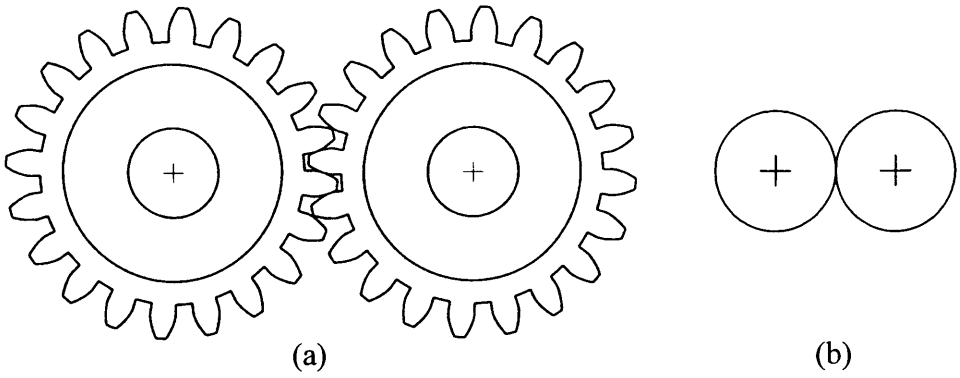

Figure 2.2. Illustration of a pair of equal gears (a) and corresponding pair of equal rollers (b) which give the same relative contact geometry between the gear teeth when contact occurs at the pitch point as shown.

2.3. Description of the Disc Machine

The test machine was originally designed with the aim of reproducing the rolling/sliding speeds and contact pressures found in typical gear meshes. The outline of the original specification is as follows:

Sliding speed up to 25 m/s (maximum of 16 m/s used in this work);
Maximum Hertzian contact pressure up to 1.7GPa (increased to 2GPa in this work);
Oil feed temperature up to 200 deg C (maximum of 100 deg C in this work);
Lubricant: synthetic (di-ester) meeting MIL-L-23699 C requirement (Mobiljet 2).

A general view of the machine is shown in Figure 2.3. The test discs of 76.2 mm diameter are fixed to shafts which are supported on rolling element bearings. At one end a double row spherical roller bearing provides axial and radial location and at the other end a cylindrical roller bearing is used which gives only radial support. The test shafts are manufactured from EN36 (AMS 9310) steel which is case-carburised and hardened to approximately 680 Vickers Hardness Number (30 kg). In order to ensure accurate running

of the shafts they were finish-ground on dead centres. Six sets of shafts were available. The test discs are pressed onto the shafts with interference fit (minimum of 0.015 mm, maximum 0.025 mm on diameter). The discs were further secured by a key and locknut. Each shaft has an axial hole which connects with a pair of radial holes for wiring of a thermocouple mounted in each test disc for the measurement of the metal temperatures of the discs.

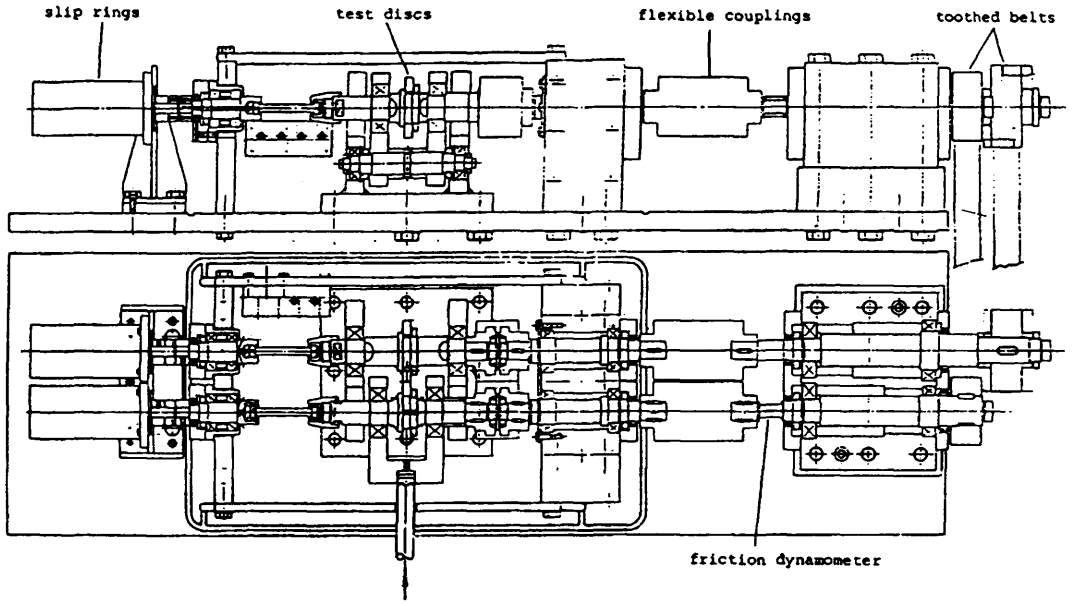

Figure 2.3. General arrangement of the main parts of the disc machine. Upper drawing shows side view and lower drawing is a plan view. Note slip rings for thermocouple connections on the left and toothed belt drive from splitter gearbox below (not shown) on right.

A photograph of the two shafts is shown in Figure 2.4. An overall photograph of the rig is shown in Figure 2.5 and a close up view of the test head with discs in position is shown in Figure 2.6. A more detailed isometric drawing of the test head is shown in Figure 2.7

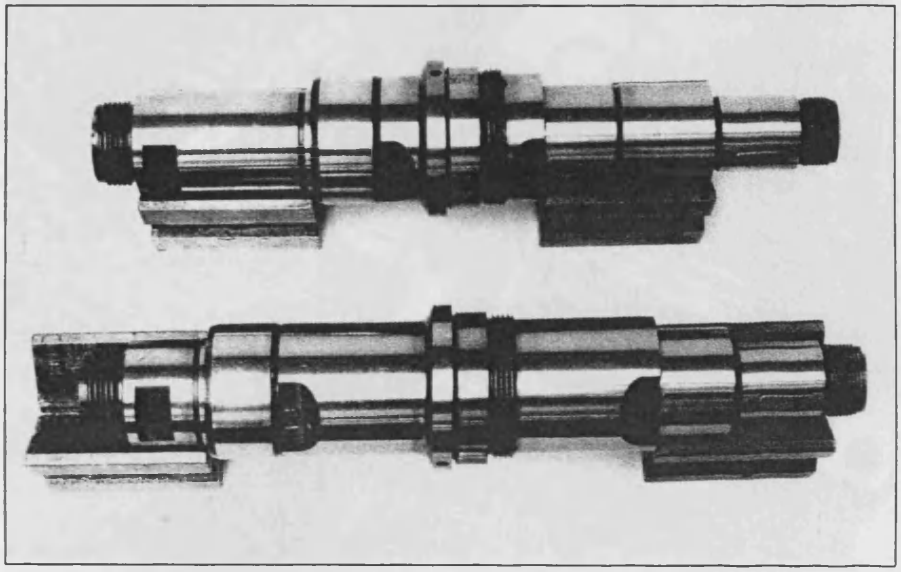

Figure 2.4. Photograph of the test shafts before fitting of the discs. Note that support bearing locations are spaced differently on the slow (upper) and fast (lower) shafts.

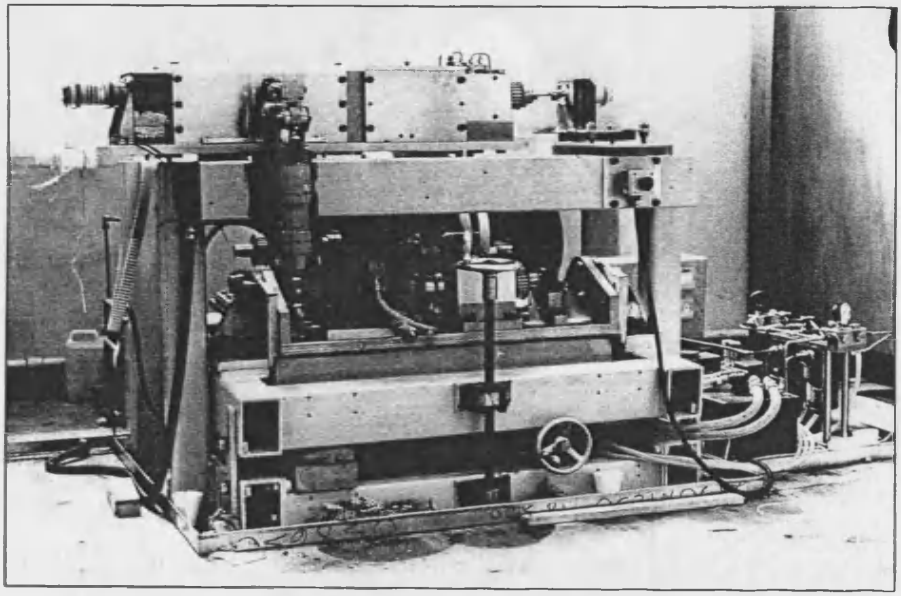

Figure 2.5. General view of the test rig with covers removed to expose splitter gearbox. Drive motor is hidden from view behind the rig.

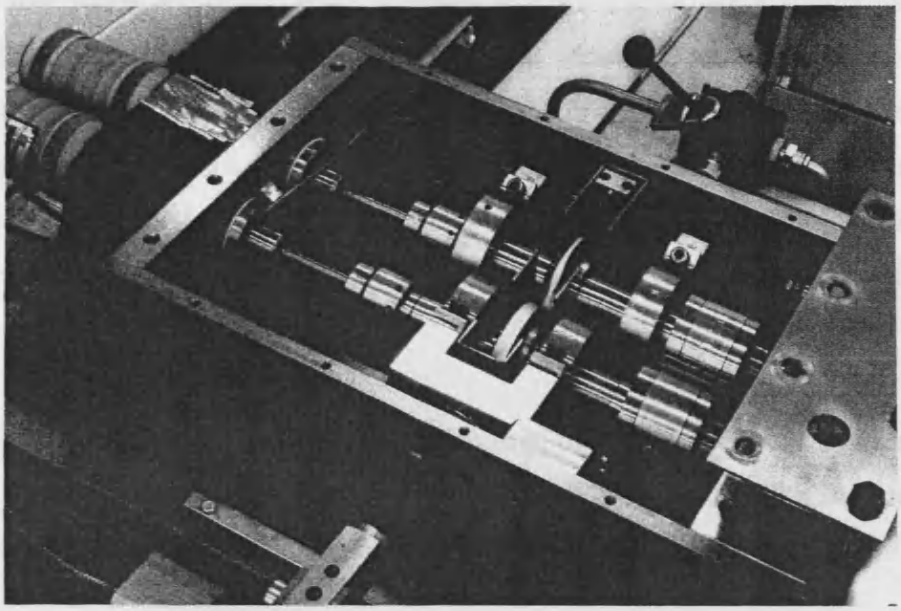

Figure 2.6. Photograph of test head of disc rig showing test discs in position. Slip rings for connection of disc thermocouples are just visible on the extreme left

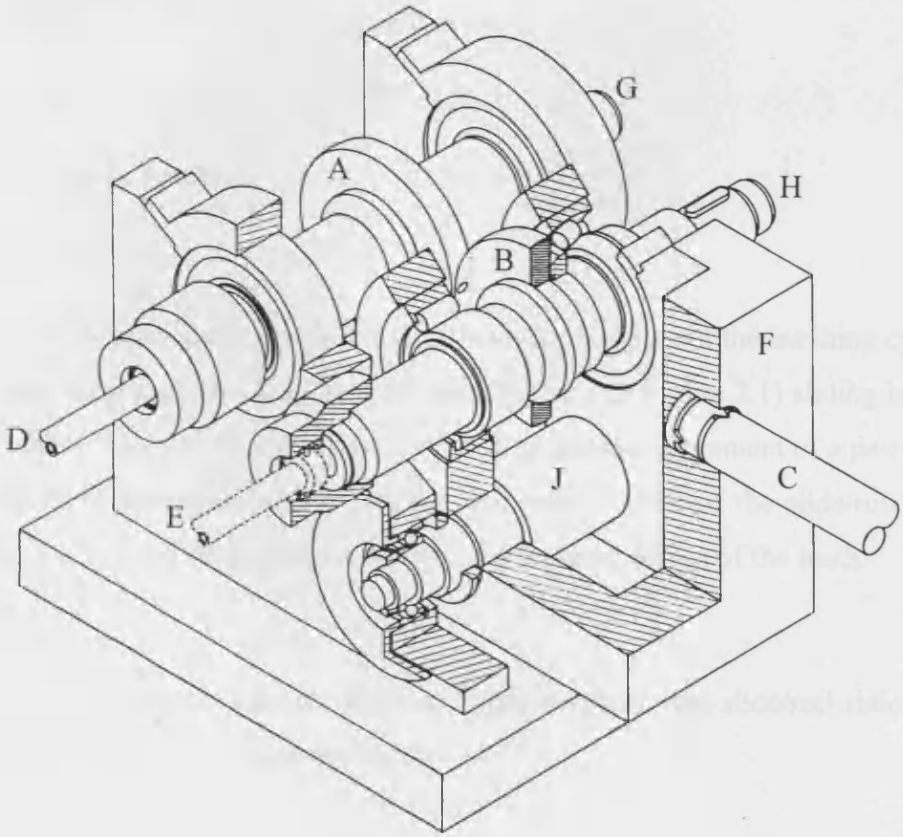

Figure 2.7. Details of the test head.
A fast disc; B slow disc; C loading pushrod; D & E slip-ring shafts; F yoke; G & H drive shafts; J yoke pivot shaft.

The two test shafts are driven from a single 18.5 kW motor via a splitter gearbox and toothed belts/pulleys. The drive motor is of the variable speed *TASC* type and has a maximum speed of 2800 rpm. Different combinations of pulleys can be used to achieve a wide range of speeds and ratios of speeds between the two shafts. In the work reported here the ratio of the shaft speeds was fixed at 4.24. The two discs rotate in opposite directions so that their surfaces both move in the same direction relative to their contact as is the case in conventional gears.

The ratio of the relative sliding speed to the rolling, or entrainment, speed is known as the slide/roll ratio. When two surfaces are rolling and sliding together with surface velocities relative to their conjunction of U_1 and U_2 then the sliding speed is defined as:

$$U_s = U_1 - U_2$$

and the entraining, or rolling velocity is defined as: $U_r = \frac{U_1 + U_2}{2}$

The slide/roll ratio is therefore: $$SRR = 2\frac{(U_1 - U_2)}{(U_1 + U_2)}$$

In conventional involute gears the slide/roll ratio varies throughout the meshing cycle. In the special case where contact is at the pitch point (point Z in Figure 2.1) sliding is absent, and when contact occurs at the tips of the teeth during initial engagement of a pair of teeth the sliding is at its maximum value. Typical maximum values of the slide/roll ratio in gears are about 0.4 to 0.8 depending on the size and detailed design of the teeth.

In the disc machine, which has two discs of equal diameter, the slide/roll ratio can be written in terms of the ratio of their speeds as

$$SRR = 2\frac{(G-1)}{(G+1)}$$

where G is the "gear ratio" between the two discs' shafts $= U_1/U_2 \geq 1$.

As mentioned above the gear ratio used in this work is 4.24, which therefore gives a slide/roll ratio of 1.24. This value of the *SRR* is rather higher than that experienced in typical gears. In previous work it was found that if a SRR more typical of gears was used then it was difficult or impossible to achieve scuffing conditions in the disc rig. This was found to be the case with discs having the standard uncoated, ground finish. In the present work, in which advanced anti-scuffing coatings were to be used, it was realised that scuffing would be even less easily obtained and hence the high SRR was retained. In the event, as will become clear, even this high value of relative sliding could not produce scuffing in some of the cases with coated surfaces.

A second modification which was introduced to help produce sufficiently severe conditions with the coated discs was the increase in the load capacity of the machine. The rig was originally designed to impose a maximum load of 4 KN at the contact which, for the geometry chosen (i.e. 76.2 mm diameter discs, each with 304.8 mm crown radius) gives a maximum Hertzian contact pressure of about 1.7GPa. In the present work coated discs were used which were found to have very high scuffing resistance, so the maximum load was increased to 6758 N to produce a maximum Hertzian contact pressure of 2.0GPa.

The discs are loaded together by means of a hydraulic ram which acts via a bell-crank and push rod mechanism as shown in Figure 2.8. The pressure applied to the ram was controlled via a variable voltage applied to an electro-hydraulic pressure relief valve. The slower speed disc is mounted in a swinging yoke as shown and the end of the push rod in contact with this yoke is made through a crossed knife edge so that the load is applied accurately in line with the discs both in the vertical and horizontal directions. This arrangement also limits any twisting of the yoke which would tend to misalign the discs. An electrical resistance load cell mounted in line with the push rod provides a direct measurement of the load. The load cell (seen in Figure 2.8) was calibrated using a special in-situ dead weight loading arrangement. When scuffing was detected during an experiment it was necessary to reduce the load as rapidly as possible so as to leave some of the "run-in" surface of the discs for profile measurements and to prevent a rapid increase in temperature to a dangerous level due to the high friction that occurs under scuffing conditions. This was achieved by providing a manually operated quick-release valve in the hydraulic supply to the ram.

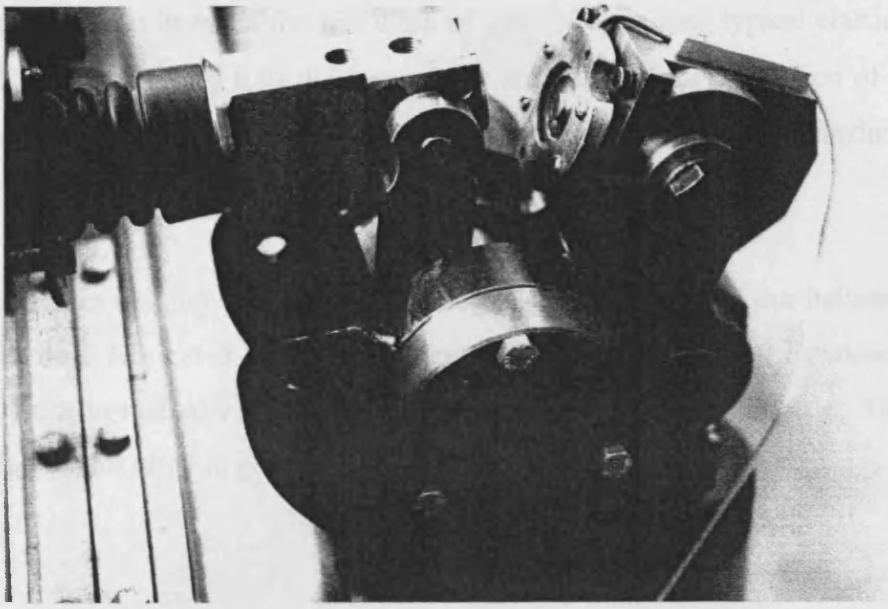

Figure 2.8. Photograph of the loading mechanism showing load pushrod and load cell. (The load cell is the disc-shaped unit which has a cable protruding from its top edge)

The test oil was heated in a special electrically-heated tank which is suitable for temperatures up to 300 deg C. In this work the temperature of the oil in the tank was fixed at 100 deg C. Built-in stirrers ensured that hot spots did not occur in the tank. The test oil passed through a 1μm pressure filter before delivery to the test head. The filter was of the steel mesh type. All oil pipes were of stainless steel so as to minimise contamination of the oil.

2.4. The Test Discs: Geometry and Materials

The test discs used in this work were of a standard geometrical design. The discs were 76.2 mm (3.00 inches) diameter with a crown radius of 304.8 mm (12.00 inches). The Hertzian dry contact area between the discs is therefore in the form of an ellipse. Contact dimensions and pressure for elliptical Hertzian contacts may be found using the simple iterative algorithm described by Dyson et al (1992). The radii of relative curvature at the contact are 19.05 mm in the circumferential direction and 152.4 mm in the axial direction giving a ratio of principal radii of 8.0.

The axis ratio of the Hertzian contact ellipse calculated using the above method is 3.91. For an assumed load between the test discs of 5000 N and using typical elastic properties of steel (E = 200GPa; ν = 0.3) the semi-major and semi-minor dimension of the contact ellipse are calculated to be 2.29 mm and 0.59 mm, respectively, and the maximum contact pressure at this load is predicted to be 1.77GPa.

The discs used in Chapter 3 (coated experiments) were supplied by our industrial partners UTRC and were fabricated from the Carpenter Technology Fe alloy *Pyrowear 53* in the vacuum-induction-melted/vacuum-arc-remelted (VIM-VAR) condition. The nominal composition of this alloy is given in Table 2.1.

Table 2.1.

Nominal composition of *Pyrowear 53* Fe alloy

Element	C	Si	Mn	Cu	V	Ni	Cr	Mo
% mass	0.1	1.0	0.35	2.0	0.1	2.0	1.0	3.3

W (tungsten) DLC coating is used for the discs used for the experiments with the coated discs. The deposition of the coating is done after the grinding using an unbalanced magnetron sputter deposition process. The roughness of ground discs after coating is about 0.30 to 0.36 μm, with respect to the nominal roughness values of ground discs of 0.36 to 0.40 μm. The roughness values of the super finished discs increase from around 0.04 μm to nominally 0.1 μm. So it can be noted that the roughness values of the ground surfaces decreases and roughness of the superfinished surfaces increases with coating.

The discs used in Chapter 4 (un-coated experiments) were of steel supplied by Rolls-Royce Ltd which is a material closely related to US specification AMS 6260 (AISI 9310).

A 2.2 mm diameter hole was provided 3 mm below the working surface of the discs for location of a thermocouple (J-type). This enabled measurement to be made of the bulk temperature of the disc. A drawing of the discs used is shown in Figure 2.9.

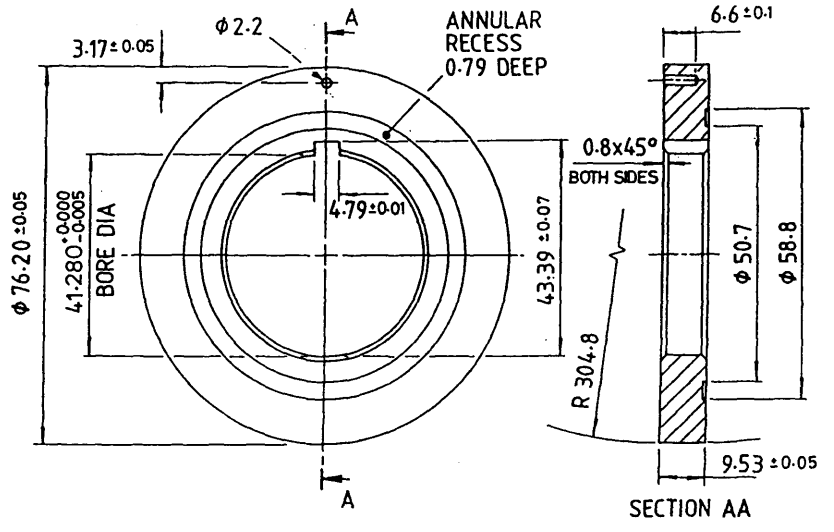

Figure 2.9. Drawing of test disc

A widely used steel for high quality gearing, such as that in aerospace transmissions, is a case-carburising Fe alloy that meets the US specification AMS 6260 (AISI 9310). In the early work performed by Patching (1994) a material supplied by Rolls-Royce was used described as RR6010 which is very similar to the foregoing specification. In this work a further bar of the same steel was kindly supplied by Rolls-Royce for the tests on uncoated discs described in Chapter 4. The composition of this steel was provided by Rolls-Royce and is given in Table 2.2.

Table 2.2.

Composition of RR6010 steel (% wt)

Element	C	Si	Mn	P	S	Ni	Cr	Mo
max	0.18	0.35	0.55	0.015	0.012	4.30	1.4	0.30
min	0.14	0.10	0.25	0.0	0.0	3.80	1.0	0.20

Heat treatment was performed using a typical aerospace specification, as outlined in Table 2.3. by Colledge & Morley Gears Ltd, an approved subcontractor of the UK aerospace industry. This particular company carried out manufacture and heat treatment of the "RR6010" discs, but not the final axial grinding which was performed in-house by the Cardiff School of Engineering Workshop.

Table 2.3.

Heat treatment specification for RR6010 discs.

Normalize @ 930°C ± 10°C	3 Hours ±15 minutes
Harden @ 850°c ±10°C	3 Hours ± 15 minutes
Temper @ 530°C ± 5°C	3 Hours ± 30 minutes
Carburize @ 927° ± 10°C to yield a carburized case depth (RC 50) of 0.036 to 0.042 inch, with a surface carbon (second 0.002" cut) of 0.65 to 0.95% Carbon.	
Cool to room temperature after carburizing and then	
Stress Relieve @ 566 to 621°C 4 hours ± 15 minutes air cool	
Copper plate all over, for protection during hardening.	
Harden @ 788 to 829 °C for 30 minutes at temperature	
Quench in oil 24 to 60°C	
Subzero treat, within 60 minutes of quenching, for 3 hours minimum @ –79°C or lower.	
Temper @ 160°C ± 5°C for 3 hours ± 15 minutes	
Final hardness values to be as follows:	
Carburized surface hardness HRC 60 to 63	
RC 60 depth to be 45% of 0.036" (0.016" of as-carburized case)	
Core hardness to be HRC 36 to 41	
As carburized case depth (HRC 50) 0.036 to 0.042"	

2.5. Axial Grinding of the Discs

After heat treatment all discs (both UTRC and Rolls-Royce) were finish ground. A very important feature of the discs is the direction of surface finish produced by the final grinding process. The work described in this thesis is designed to be relevant to gears so it was considered vital to reproduce the direction of finish as found on typical gear teeth as well as the roughness magnitude as measured by the Roughness Average parameter, Ra. Gear tooth flanks finished by the usual type of grinding have a finish direction perpendicular to the rolling/sliding direction on the teeth (i.e. in a direction to/from root from/to tip). In order to reproduce this effect in the disc machine the surfaces of the discs must be ground in the axial direction. A special method which involved a purpose-built

grinding arrangement was developed at Cardiff University to achieve axial finish on the discs as follows.

The rig is based on a combination of a surface grinder and a small cylindrical grinder. The principle of the process is illustrated in Figure 2.10(a). The working surface of the disc is produced by a generating line which is a circle on the conical surface of an internally conical abrasive wheel. This process gives a finish on the disc which is effectively in the axial direction and also produces a crown on the disc. The radius of the crown is determined by the combination of the cone angle of the abrasive wheel and the radius of generation of the wheel. If R is the required crown radius, r is the radius of the test disc and α is the angle of the cone as shown then the required distance d between the axis of the abrasive wheel and that of the test disc may be obtained from the geometry of Figure 2.9 and is given by

$$d = (R - r)\sin\alpha$$

Ideally, the generating radius should be large so that the finishing marks are close to axial in direction, but in practice the largest generating radius possible is limited by the size of abrasive wheel that can be used. In the rig provided a maximum abrasive wheel diameter of 180 mm was possible. This practical limitation led to the choice of a cone angle, α, of 15 degrees and a generating radius, d, of 69.1 mm. A scale drawing of the arrangement used is shown in Figure 2.10(b). The abrasive wheels were supplied in a pre-formed state as shown with a recess to allow for dressing of the wheel as wear occurred. Preparatory to axial grinding the discs were first cylindrically ground so that a minimum of material was removed by axial grinding. In this way the life of the conical surface of the abrasive wheel was preserved. The correct cone angle of the abrasive wheel was accurately set up and maintained by regularly dressing it with a diamond tool set in an angled slide. Care was taken to align the test disc relative to the abrasive wheel during grinding so that the crown was "centred" on the test disc. Figure 2.11 shows a disc being finish-ground in this way. Figure 2.12 shows the approximately axial grinding marks generated using this technique and also illustrates the equivalent Hertzian contact at the load which produced the clearly discernible running track on the disc.

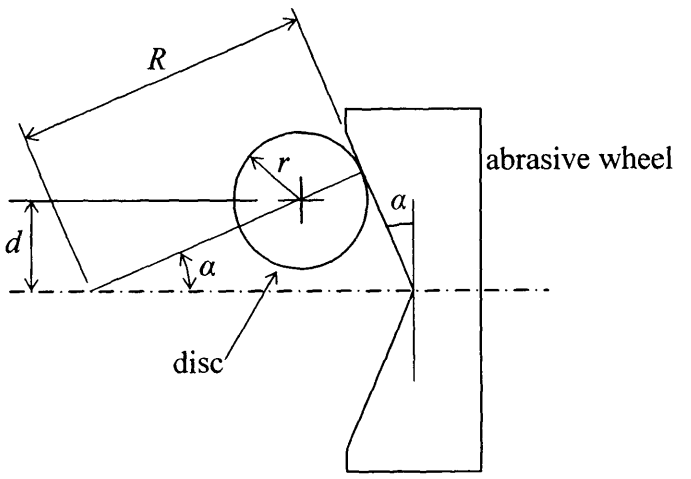

(a)

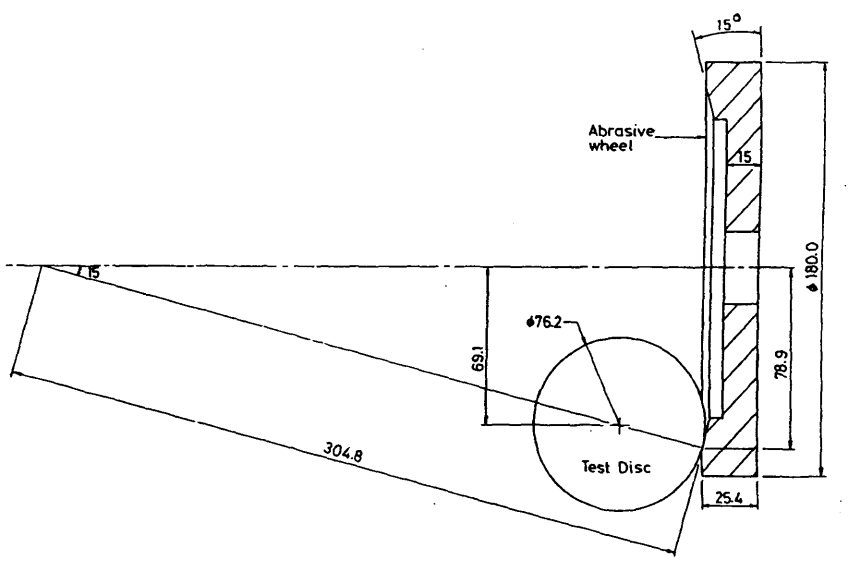

(b)

Figure 2.10. Axial grinding of discs: (a) Illustrating the principle of disc crowning using a conical abrasive wheel; (b) scale drawing of the grinding configuration with dimensions used.

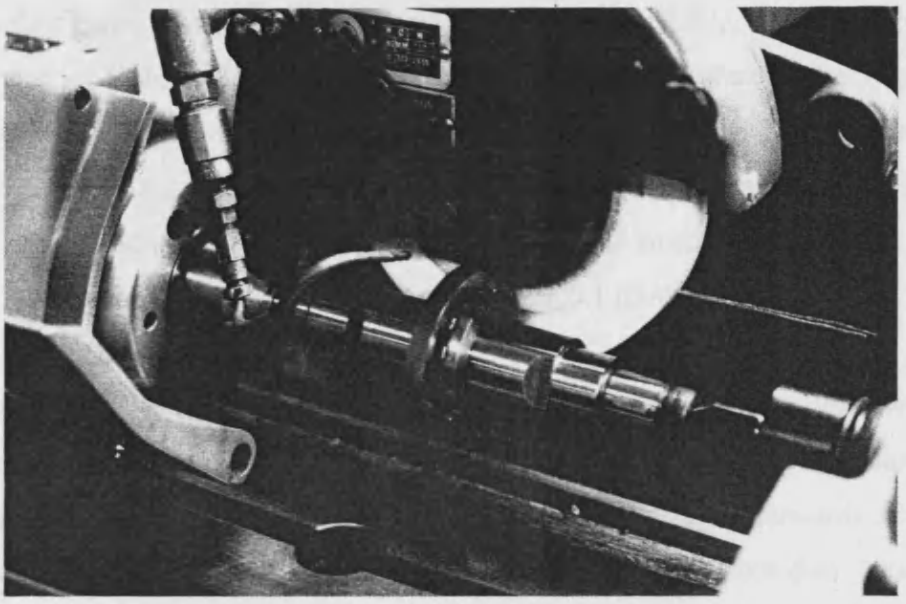

Figure 2.11. A disc being finish-ground on its test shaft in the special grinding rig

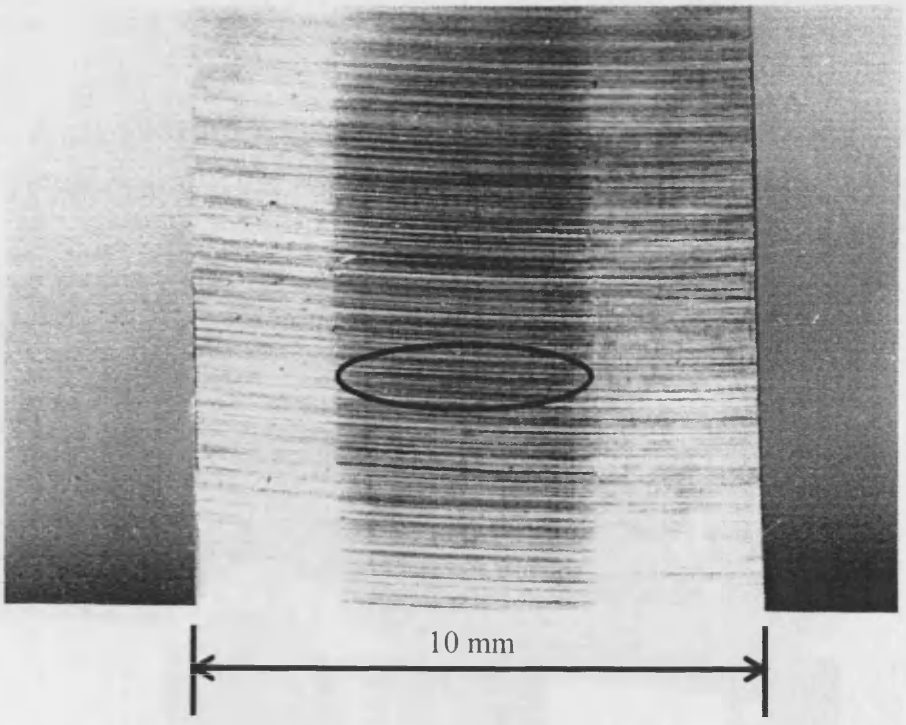

Figure 2.12. Photograph of an axially-ground disc showing finishing marks. The darkened central band corresponds to a running track. The superimposed ellipse shows the size and shape of the corresponding Hertzian contact at the load used.

The crowning radius of the discs was checked by taking a profile, in the axial direction, using the Taylor Hobson Form Talysurf 2. The form radius feature of the Talysurf was used to check the crown radius of the test samples as well as their surface finish (measured in the circumferential direction). A maximum deviation of ± 1mm from the specified crown radius of 304.8 mm was achieved. The maximum deviation from the specified outer diameter of the discs (76.2 mm) was ± 0.1 mm.

The appropriate direction in which to measure the roughness of the discs was in the circumferential direction (i.e. perpendicular to the lay of the roughness). Talysurf profiles were taken from all discs used in this study both before testing and afterwards. Figure 2.13 shows the configuration for taking a circumferential profile from a test disc. After the raw profiles were acquired they were filtered to remove the longer wavelength components of finish (waviness) using a digital filter (Gaussian type) with a cut-off wavelength of 0.25 mm. The roughness average (Ra) was then computed. In all tests performed with ground discs the roughness was controlled to give a Ra value of 0.4μm ± 0.05μm. A typical circumferential profile from a ground disc is shown on Figure 2.14.

Thanks are due to Mr Godfrey Jordan for his skill and dedication in carrying out the final grinding of all discs used in this work.

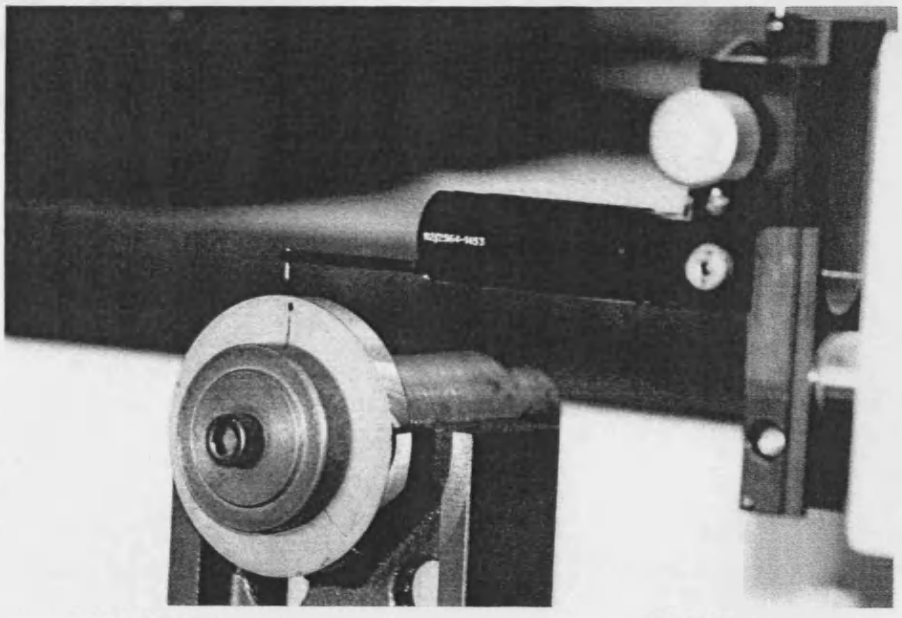

Figure 2.13. Photograph showing measurement of a surface profile in the circumferential direction using the Form Talysurf.

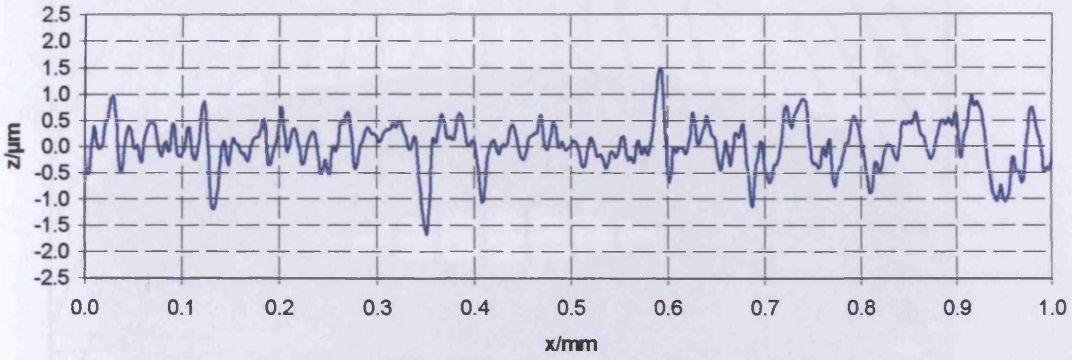

Figure 2.14. Typical circumferential profile taken from test discs. In this particular case, the type of surface finish corresponds to a ground disc, Unrun condition.

2.6. Superfinishing

In some of the experiments with both the UTRC steel (coated and uncoated) and the Rolls-Royce steel the discs were superfinished. Discs to be superfinished were first ground as described above to give the correct crowned geometry. A proprietary superfinishing method was available in-house at Cardiff and was used in the present work. In this method, known as the Abral process, the discs are immersed in a vibrating bath containing water, abrasive powder (Al_2O_3) and small zinc pellets. After several hours of treatment the discs take on an almost mirror finish as may be seen from the photograph of one such disc shown in Figure 2.15. In terms of roughness average (Ra), the level of roughness after superfinishing is better than 0.1 µm and typically 0.05 µm starting from a ground state. Typical circumferential profiles from both a ground and a superfinished disc are compared (at the same scale) in Figure 2.16.

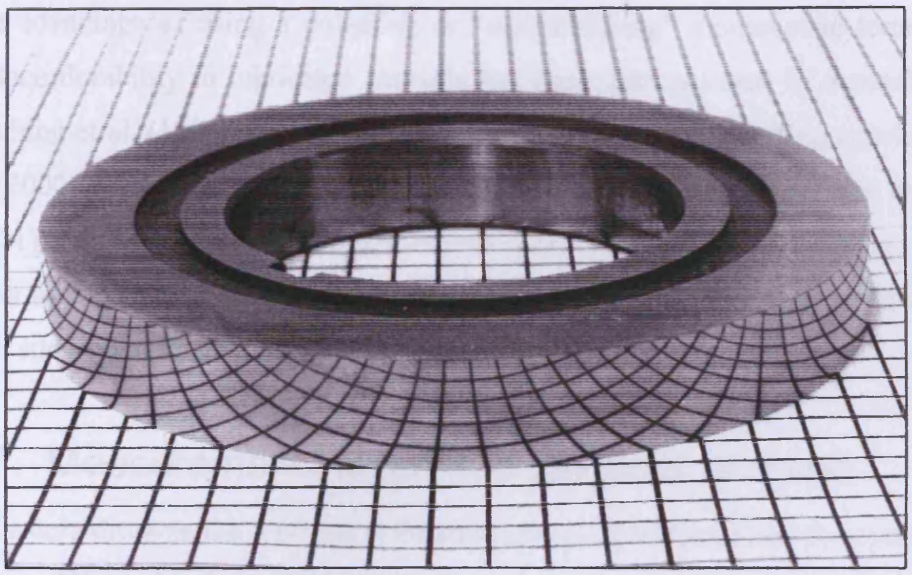

Figure 2.15. Superfinished disc showing highly-reflective surface

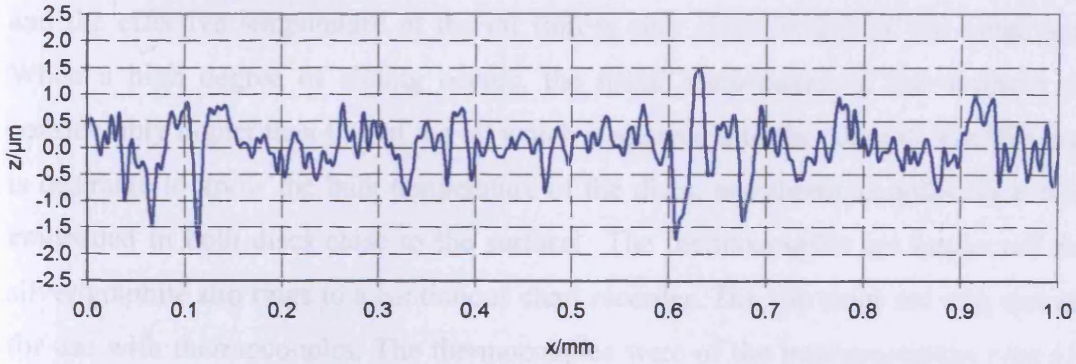

Figure 2.16.(a) Typical circumferential profile taken from test discs. In this particular case, the type of surface finish corresponds to a ground disc, Unrun condition.

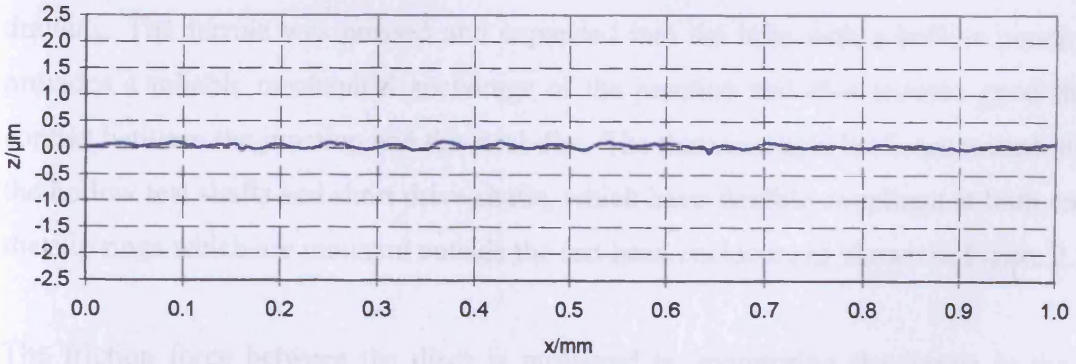

Figure 2.16.(b) Typical circumferential profile taken from test discs. In this particular case, the type of surface finish corresponds to a superfinished disc, Unrun condition.

The advantage of using a polishing or "superfinishing" treatment in terms of improved surface durability in lubricated contacts has been demonstrated by a number of authors. Patching et al. (1995) showed how superfinishing improved scuffing resistance. Britton et al. (2000) demonstrated its effect in reducing the friction of gear contacts, and Krantz et al. (2001) have reported a significant improvement of surface (micropitting) fatigue life of gears as a result of superfinishing. In this work superfinishing was used in combination with super-hard coatings.

2.7. Measurements taken and progress of a test

In elastohydrodynamic lubrication the entrainment of lubricant into the contact is governed by conditions in the inlet region. The important quantities in this respect are the entrainment velocity, as defined above, and the viscosity of the lubricant. Under thin film conditions in the inlet to the EHL contact heat transfer is dominated by conduction effects and the effective temperature of the oil film is very close to that of the metal surfaces. When a high degree of sliding occurs, the metal temperature of the surfaces can be considerably higher than that of the oil which is sprayed into the contact. For this reason it is desirable to know the bulk temperature of the discs, and thermocouples were therefore embedded in both discs close to the surface. The thermocouples are connected through silver/graphite slip rings to a continuous chart recorder. The slip rings are of a special type for use with thermocouples. The thermocouples were of the iron/constantan type (J type) insulated with PTFE. The thermocouple junction is made in a small copper ferrule of 2.0 mm diameter which is a close fit in a hole provided in the test discs as shown in the above drawing. The ferrule was pressed and expanded into the hole with a hollow punch. This provides a reliable mechanical anchorage of the junction and also ensures good thermal contact between the junction and the steel disc. The thermocouple leads are routed through the hollow test shafts and short drive shafts, which have flexible couplings at both ends, to the slip rings which are mounted outside the test head enclosure as shown in Figure 2.3.

The friction force between the discs is measured by monitoring the torque in the shaft driving (or, strictly, braking) the slower speed test shaft. A reduced section of the shaft was fitted with electrical resistance strain gauges, which are connected to a suitable electronic unit through a third silver/graphite slip ring unit. The strain gauge units were bonded to the dynamometer shaft and temperature sensitive compensating elements were incorporated to

eliminate thermal drift of the unit. At the start of the present project the strain gauges were renewed by a specialist supplier and the electronic unit which powered the resistance bridge was also replaced. The output from the torque unit was recorded on the chart recorder and connected to the computer data acquisition system.

The load steps are applied to the contact in a standard sequence. The load was increased at intervals of 3 minutes until either scuffing failure was detected or the load limit of the machine was reached before a scuff occurred. The step by which the load was raised at each stage was chosen to give a constant increase of 0.1GPa in the Hertzian pressure. The loading sequence is shown in Table 2.4.

Table 2.4.

Standard loading sequence

Load Stage	Time/min	Load/N	Max Hertz Pressure/GPa
1	0	180	0.6
2	3	290	0.7
3	6	430	0.8
4	9	620	0.9
5	12	850	1.0
6	15	1120	1.1
7	18	1460	1.2
8	21	1850	1.3
9	24	2320	1.4
10	27	2850	1.5
11	30	3450	1.6
12	33	4150	1.7
13	36	4927	1.8
14	39	5794	1.9
15	42	6758	2.0

The progress of a typical test is as follows. Following assembly of the discs on their shafts they were placed in position and couplings and slip rings connected. The test oil was heated and circulated until it reached a tank temperature of 100°C and the temperature of the discs reached a steady level and the splitter gearbox oil (which has a separate supply) reached 45°C. A light load of about 100N was then applied to the discs so as to keep them in contact. Both the chart recorder and the computer data acquisition system were started at this stage and the zero position of the friction readings checked. The drive motor was then started and the speed of the rig gradually increased to the steady value selected for the particular run being undertaken. After checking the speed on the digital readouts the machine was run for about three minutes before the loading sequence was begun. The first load (180 N) was then applied by setting a potentiometer that controlled the electro-hydraulic pressure relief valve controlling the hydraulic loading ram pressure.

The experiment was recorded using the analogue chart recorder which recorded the friction and the bulk temperatures of the two discs. The computer data acquisition system stored the same quantities plus load and speed. A typical chart from an experiment with ground/uncoated discs at a sliding speed of 12 m/s is shown in Figure 2.17. The corresponding printout of the computer-acquired data is shown in figure 2.18. It should be noted that the output from the chart recorder shows the uncorrected friction force which is lower than the corrected value. The zero level on the chart recorder is set at the line marked "10" which is 1 inch from the left side of the chart paper. This allows for negative values of friction that occur at light loads due to the effect of friction in the slow shaft bearings. It will be noted that the drive to the slow shaft is in fact a "braking" torque which explains this behaviour. Correction for bearing friction has been applied to the computer-acquired result. Details of the friction calibration procedure including the correction for bearing friction are included in Appendix E. Note that the friction trace is calibrated to give a tangential friction force of 40 N per major division (1 inch) on the chart recorder. The temperature traces are set to correspond to 0°C at the left edge of the chart and the full-scale deflection corresponds to a temperature of 400°C. The chart was set to run at 10 mm/minute. It is important to realise when examining the chart output that the three traces (two temperatures plus friction) are, apparently, offset in time. This is a necessary feature of multi-channel pen chart recorders which allows the pens to cross over during operation. This apparent lag is, of course, not seen in the computer-acquired output.

The periodic increase of load in the loading sequence was timed according to when the friction trace on the recorder passed every third major division (each major division is spaced at 10 mm) to give the required 3 minute period between load increments.

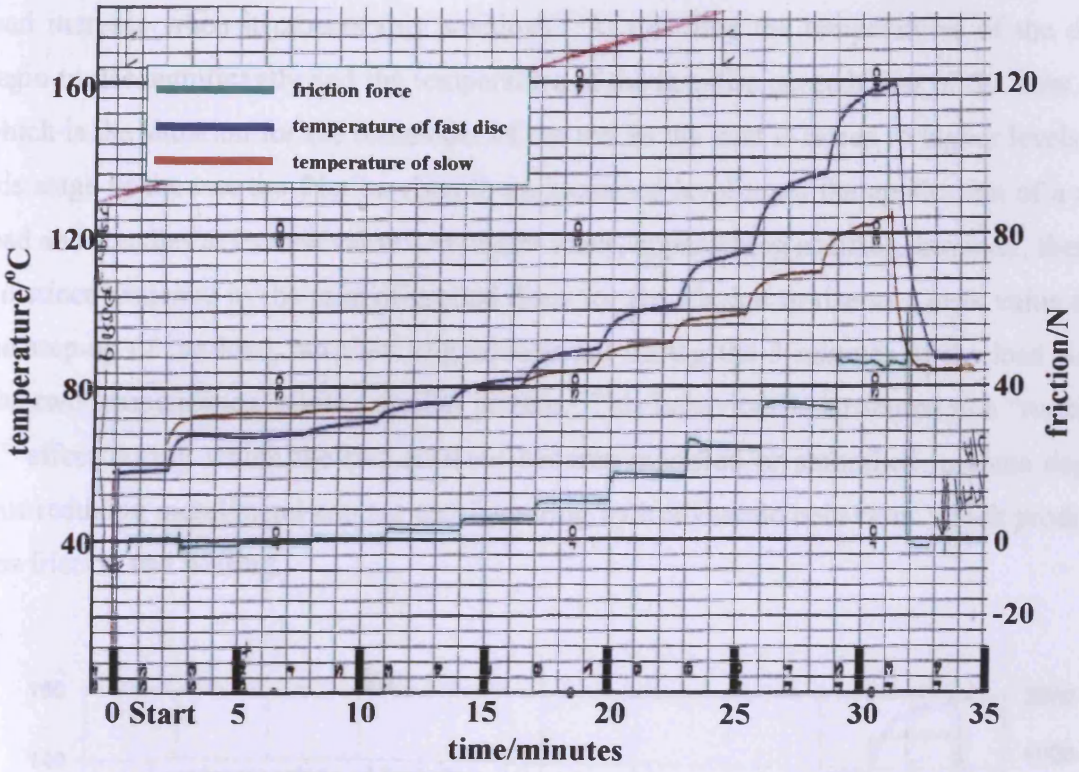

Fig 2.17. A typical test trace from the chart recorder record of scuffing test AD02, sliding speed of 12m/s slow disc: ground; fast disc: super finished

Figure 2.17 shows the progress of a typical scuffing test. With the test oil at a tank temperature of 100°C and the machine stationary the temperatures of the two discs are seen to be about 52°C (fast disc) and 58°C (slow disc). The small difference in temperature is due to the different stationary positions of the thermocouples in relation to the oil jets. Before the drive motor is started the friction trace can be seen to have been set at its zero position on the chart as indicated above. After starting the drive motor and bringing the machine up to the desired speed the friction reading becomes slightly negative indicating that the shaft support bearing friction is greater than the friction between the discs at the light, initial load of about 100 N. After running for a period of 4 minutes at the initial light load the first load in the standard sequence (180 N) is applied at the time when the friction trace crosses chart position 1.5.

The temperature of both discs rises in response as does the friction. At the lighter loads it is noticeable that the temperature of the slow disc is higher than that of the fast disc, whereas at higher loads the reverse is true. The second step in the load sequence (290 N) was applied at chart position 3.0 (again note that the friction trace is used as the signal for a load increase when it crosses this position). At this load the temperatures of the discs begin to rise significantly and the temperature of the fast disc exceeds that of the slow disc which is the situation for the remainder of the test as the load is raised to higher levels. At this stage in the test the friction rises to an increased level upon the application of a new load and steadies at its new value. At higher loads, approaching scuffing, however, there is a distinct tendency in the case of ground discs for the friction to rise to a peak value after the step-up of the load, but then to gradually fall during the 3 minutes of the load stage. The two temperatures follow a similar pattern. This behaviour is attributed to a "running-in" effect during which the two surfaces become modified or smoothed to some degree thus reducing metal/metal contact and favouring hydrodynamic behaviour which produces less friction and heating.

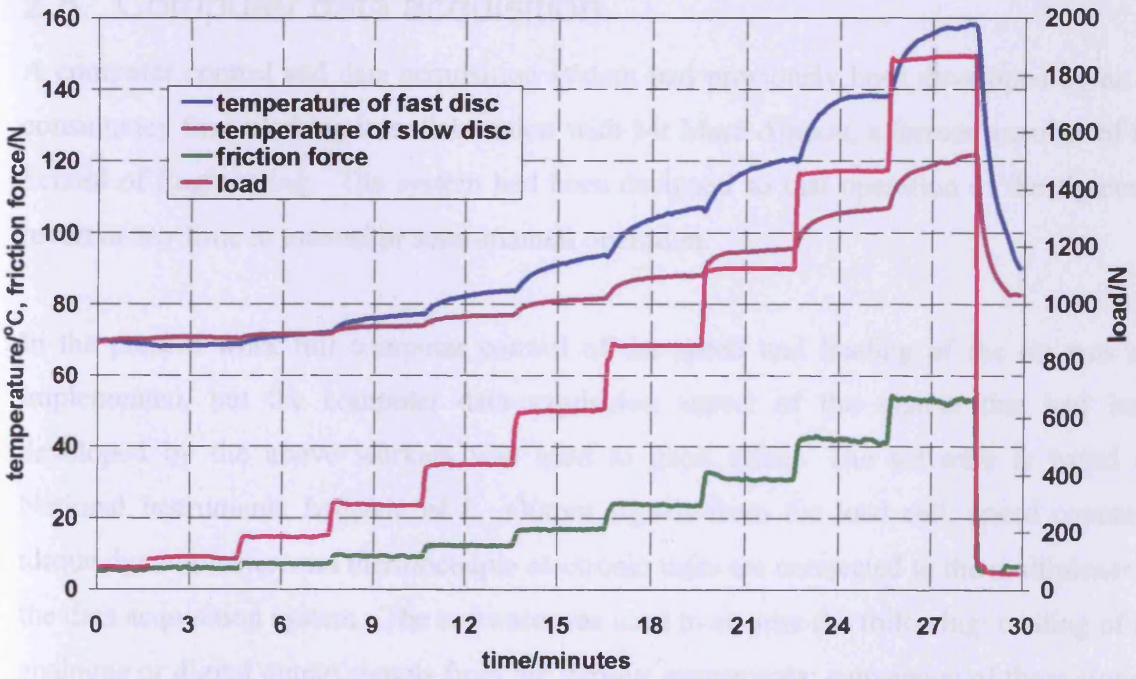

Figure 2.18. Typical test trace from the data acquisition software of scuffing test AD02, sliding speed of 12m/s slow disc: ground: fast disc: super finished

Based upon experience of using the rig a stage is reached at which scuffing failure is anticipated. This is finally indicated by a very sudden and unmistakable rise in the friction reading in the case of uncoated discs (the behaviour with coated discs is less clear-cut in some cases as will be seen in the following chapter). At this point the load is rapidly removed by opening a quick-release valve in the pressure line to the loading ram. This action is necessary if some of the run, but un-scuffed, part of the discs is to be retained for subsequent examination. It is also clear that the rapid rise in the temperature of the discs under high sliding at heavy loads with the severe friction of scuffed surfaces would quickly lead to dangerously high temperatures in the test head if unchecked. This situation is clear at chart position 13. Once the load is removed the friction falls back and the temperatures of both discs subside under the cooling effect of the oil jet which is at a much lower temperature. The rig is left to cool for an hour or so before the test shafts are removed and the discs are then available for inspection. In every case scuffing, as indicated by the friction behaviour during the test, was confirmed by subsequent visual inspection of the surfaces which had severely disrupted and torn bands of damage.

2.8. Computer data acquisition

A computer control and data acquisition system had previously been developed by an IT consultancy firm working in collaboration with Mr Marc Alanou, a former member of the School of Engineering. The system had been designed so that operation of the rig could revert at any time to manual or semi-manual operation.

In the present work full computer control of the speed and loading of the rig was not implemented, but the computer data-acquisition aspect of the system that had been developed by the above workers was used to good effect. The software is based on National Instruments *Labview v4.1.* Output signals from the load cell, speed counters, torque dynamometer, and thermocouple electronic units are connected to the multiplexer in the data acquisition system. The software was used to acquire the following: reading of all analogue or digital output signals from the various instruments; conversion of these signals into relevant physical quantities; generation of files for storing these quantities (the rate used was 1 datum/sec).

At the end of the test the data acquired by the system during the test were available in a Windows file which was then copied and backed up for further processing. One aspect of the data that required processing was the friction history which was corrected to allow for the effect of load on bearing friction as described in Appendix D.

Chapter 3

The effect of a hard coating on scuffing performance

3.1. Introduction

This chapter reports on the series of experiments designed to investigate the effects of a particular hard coating on the scuffing performance of steel discs. Both the steel from which the discs were manufactured and the coating were supplied by United Technologies Research Center (UTRC). The coating is a proprietary treatment developed by UTRC, and as such its composition and method of application are not known in detail. However it can be stated that the coating is of the thin film diamond-like carbon (DLC) type.

Thin hard coatings have been used by industry for engineering applications for over 20 years, and their advantages in terms of wear resistance, chemical inertness and low values of the friction coefficient have been demonstrated in a number of applications. The coatings are usually applied using some variation on the physical vapour deposition (PVD) process. The DLC types have been extensively exploited in applications such as tooling and various machine parts to reduce wear. Within the general family of DLC coatings are the so-called metal doped type (Me-DLC) which appear to offer improved adherence and higher toughness values than the straight DLC types. The base structure of DLC coatings is amorphous and contains a mixture of sp3 and sp2 carbon. The sp3 atomic structure corresponds to a "diamond-like" form, whereas the sp2 form is a "graphite-like" structure. The ratio of sp3 to sp2 (diamond/graphite) is critical to the performance of the coating as is clear from the work of Zaidi, *et al* (2000).

The metal-doped coatings include metals in the form of small nano-crystallites of pure metal or metal carbides which are dispersed in the carbon network (Donnet, 1998). As an aid to promoting good adhesion between the coating and the substrate a metal layer (typically chromium) is first laid down on the surface. This interlayer is controlled to be very thin. It is emphasised by Wanstrand, et al (1999), for example, that the thinner the interlayer the better the tribological properties of low wear and friction.

Wanstrand et al (1999) observed that the type of structure seen in these coatings is usually columnar. The temperature at which deposition takes place is usually in the range 200°C to 250°C, and the thickness of the coating is typically 1-3 μm. The most significant mechanical property of the coatings is its hardness, which is typically above 10GPa, see for example, Harris, et al (1997).

3.2. Tests on un-coated discs

In order to establish a reference level of performance against which the improvement, if any, due to the application of the hard coating could be measured, scuffing tests were first carried out on the un-coated UTRC steel discs. The discs were finish-ground using the technique described in the previous chapter (section 2.5). The roughness was controlled so that the ground discs had a Ra roughness value (measured in the circumferential direction) of 0.4 μm ± 0.05 μm. Following axial grinding (which was necessary to produce the desired crowned geometry) some of the discs were superfinished to a Ra value < 0.1 μm so that tests could be carried out with un-coated discs in both the ground and superfinished state. It was of interest to know if superfinishing could provide an improvement in scuffing performance that could compare with that anticipated as a result of hard-coating.

The operating conditions for the scuffing tests were as already outlined in Chapter 2. All tests were run with a test oil tank temperature of 100°C and the standard loading sequence was followed as given in Table 2.4. The gear ratio between the discs was fixed at 4.24 which gave a slide/roll ratio of 1.24. Tests were carried out at a series of different sliding speeds (i.e. the difference in surface speeds of the two discs). Tests were carried out at three different sliding speeds of 7 m/s; 12 m/s and 16 m/s. These conditions corresponded to the fast shaft running at 2293 rpm; 3938 rpm; and 5251 rpm, respectively. The slow

shaft ran at correspondingly lower speeds of 539 rpm; 929 rpm; and 1238 rpm, respectively.

3.2.1. Ground discs running against ground discs

Eight tests were carried out with ground (un-coated) discs on both shafts. Four tests were undertaken at a sliding speed of 16 m/s (tests UTRC 1,2, 23,,25); two tests at 12 m/s (tests UTRC 7, 28); and two tests at 7 m/s (tests UTRC 5, 27). As already noted the computer data acquisition system was not operative for the first half of the testing programme so computer-acquired output was only available for tests UTRC13 to UTRC28. Figure 3.1 shows the chart record of test UTRC01 at the sliding speed of 16 m/s. Note that in this and subsequent chart recorder records the copy of the chart has been mirrored so that time progresses from left to right. Also it should be noted that there is an offset in time between the three quantities recorded as is usual in a pen chart recorder. At the light, starting load and the first load in the standard sequence the friction trace is seen to give a negative reading indicating that the friction generated at the discs is insufficient to overcome the bearing friction. At the 290 N stage there is a positive friction output however. It is also at this load that the temperature of the fast discs overtakes that of the slow disc. At loads up to and including the 430 N stage the friction reading stays at a steady level after application of a new load, but following the application of the 620 N load there is a discernible falling off of the friction during the three-minute duration of this stage. This tendency becomes even more pronounced at the next and succeeding stages. As already commented upon this is thought to be due to a running in effect during which the surfaces of the discs become partially smoothed, thus promoting less metal/metal contact and hence lower friction. The temperatures of the two discs diverge considerably at the higher load stages and by the 2320 N stage there is a temperature difference of over 80°C between them. Upon application of the 2850 N load (stage 10) the temperatures and friction at first behave as they had done during previous load increases at the higher loads, but within one minute of the increase in load there is a very sudden rise in the friction force with a corresponding sharp increase in the temperature of both discs. At this point the load was rapidly removed as described above. The friction force dropped instantaneously and the temperatures of both discs fell with a sharp gradient as they were cooled by the test oil. Clearly, had the load not been removed at this point the temperatures of the two discs would have risen in an unchecked fashion to over 400°C within a few seconds.

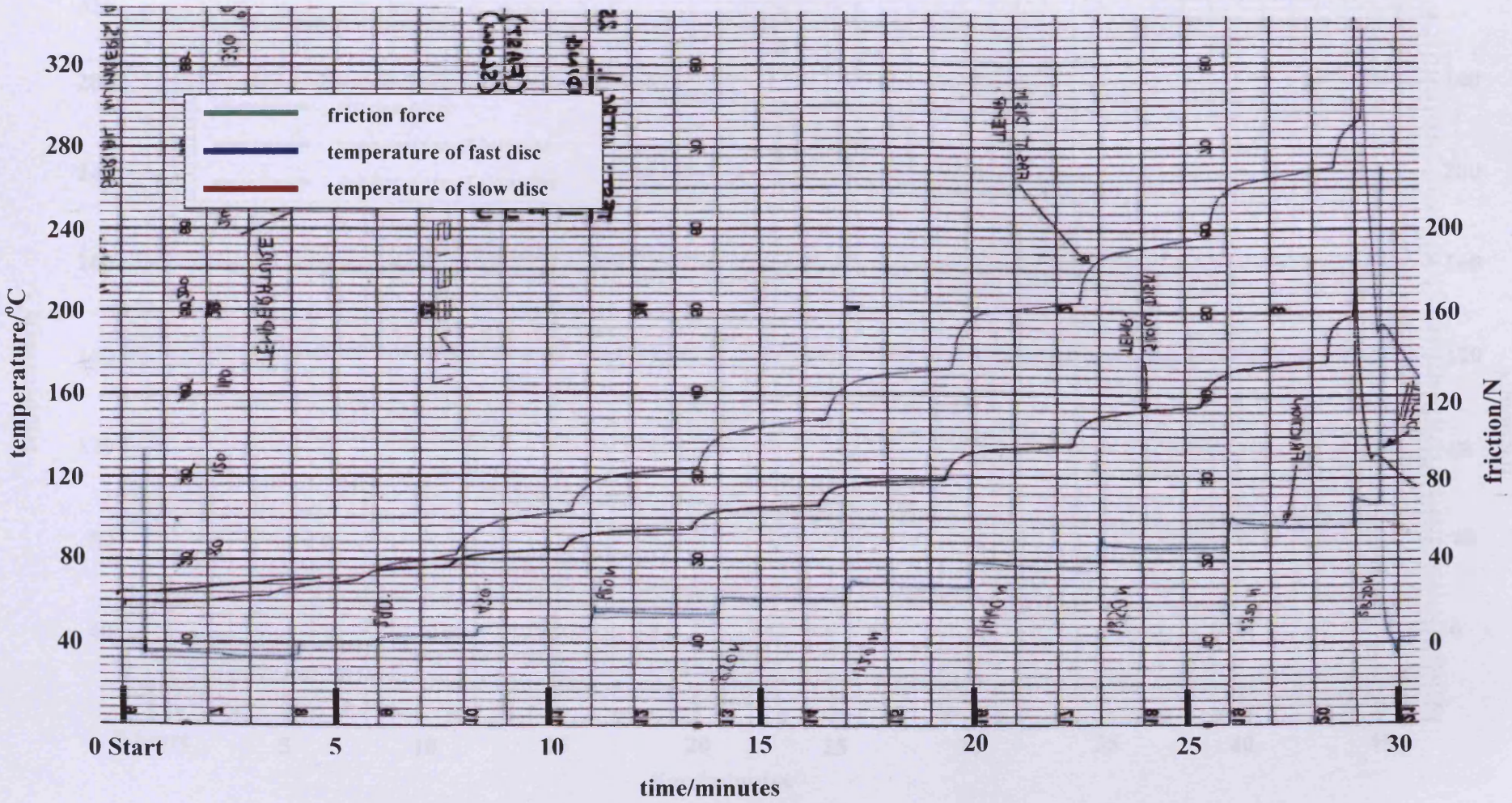

Figure 3.1. Chart recorder record of scuffing test UTRC01, , graph shows applied load and bulk temperatures of two discs

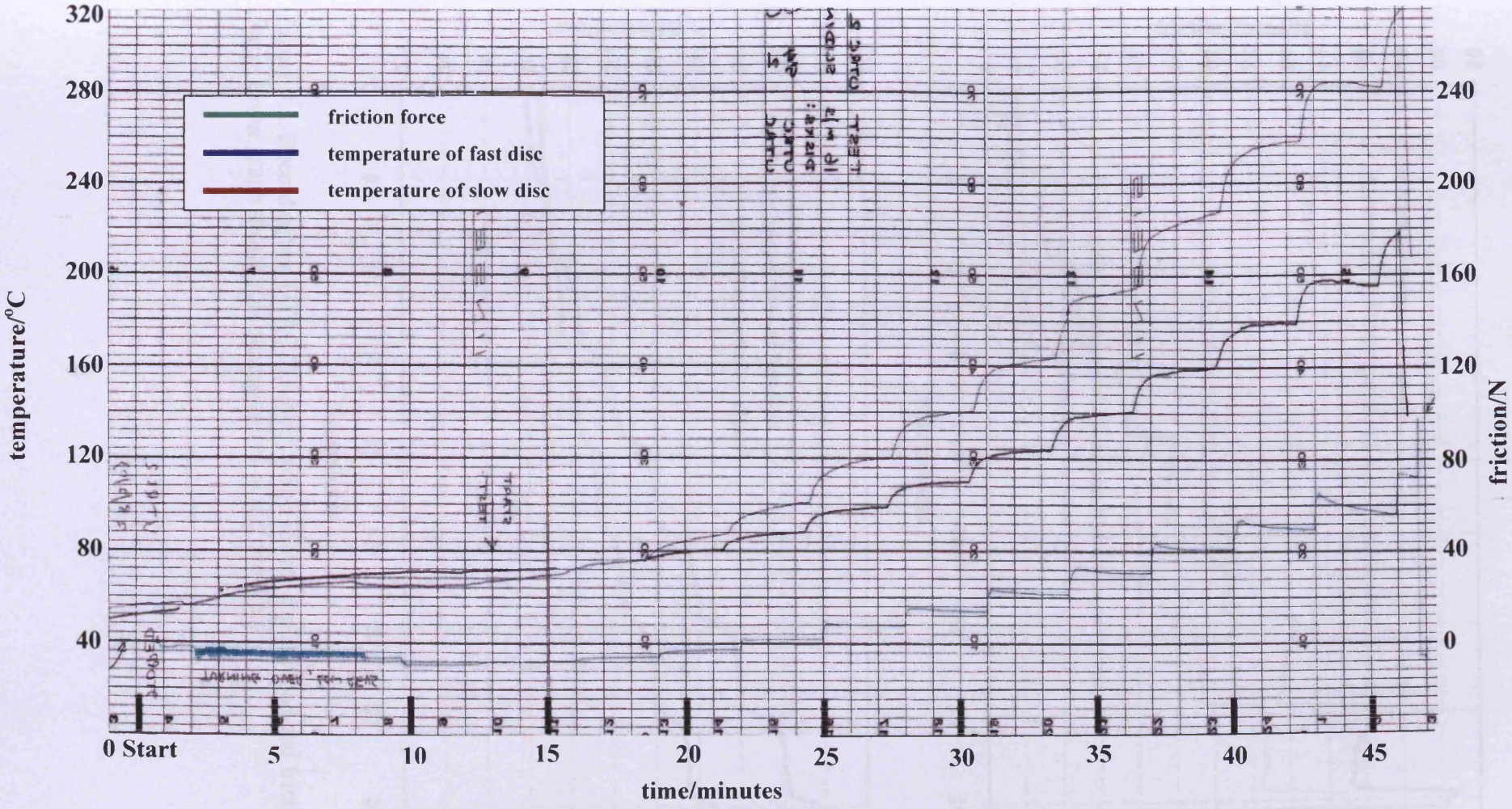

Figure 3.2. Chart recorder record of test UTRC02, graph shows friction force and bulk temperatures of two discs

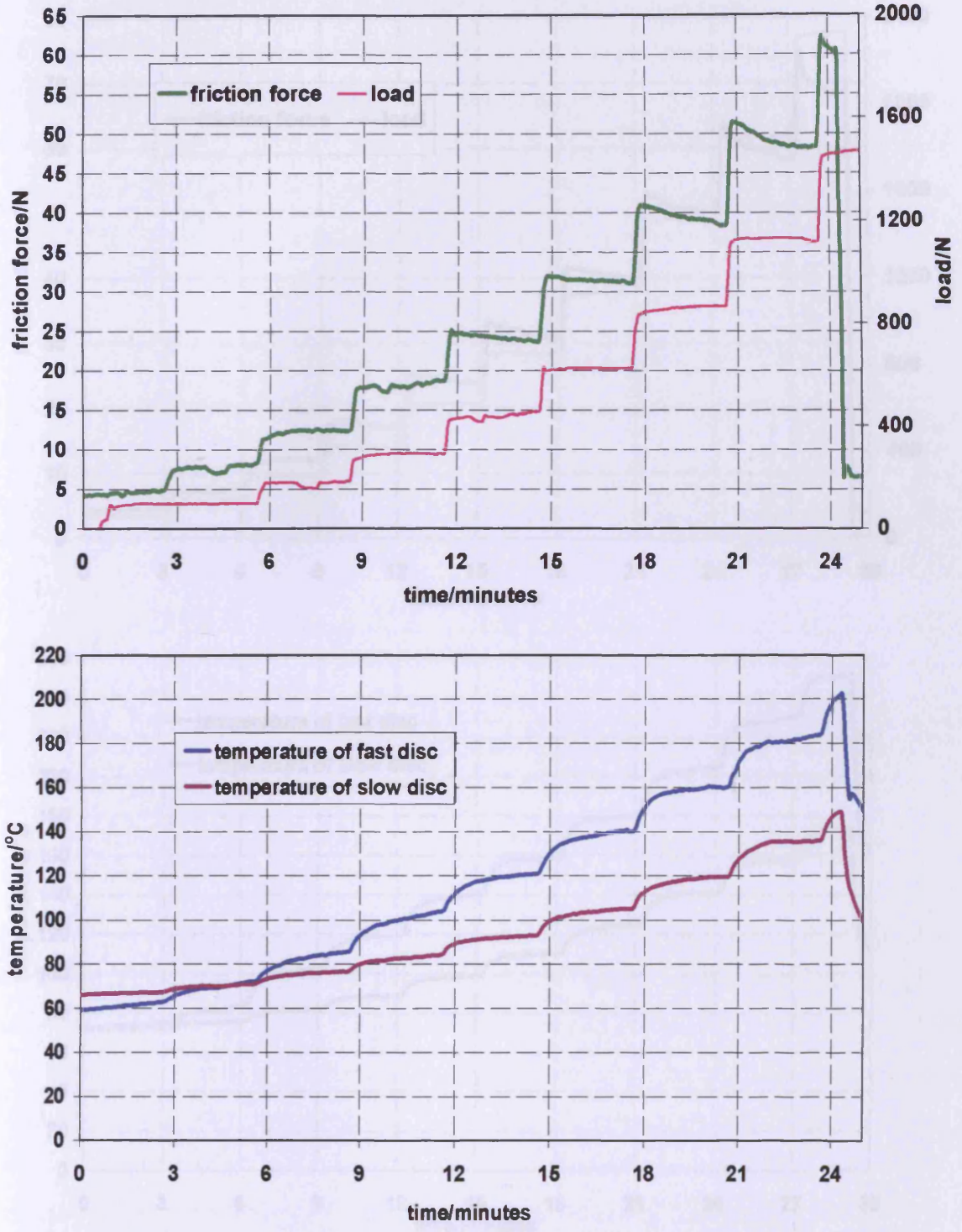

Figure 3.3. Record of test UTRC23; upper graph shows applied load and friction force; lower graph shows bulk temperatures of the two discs

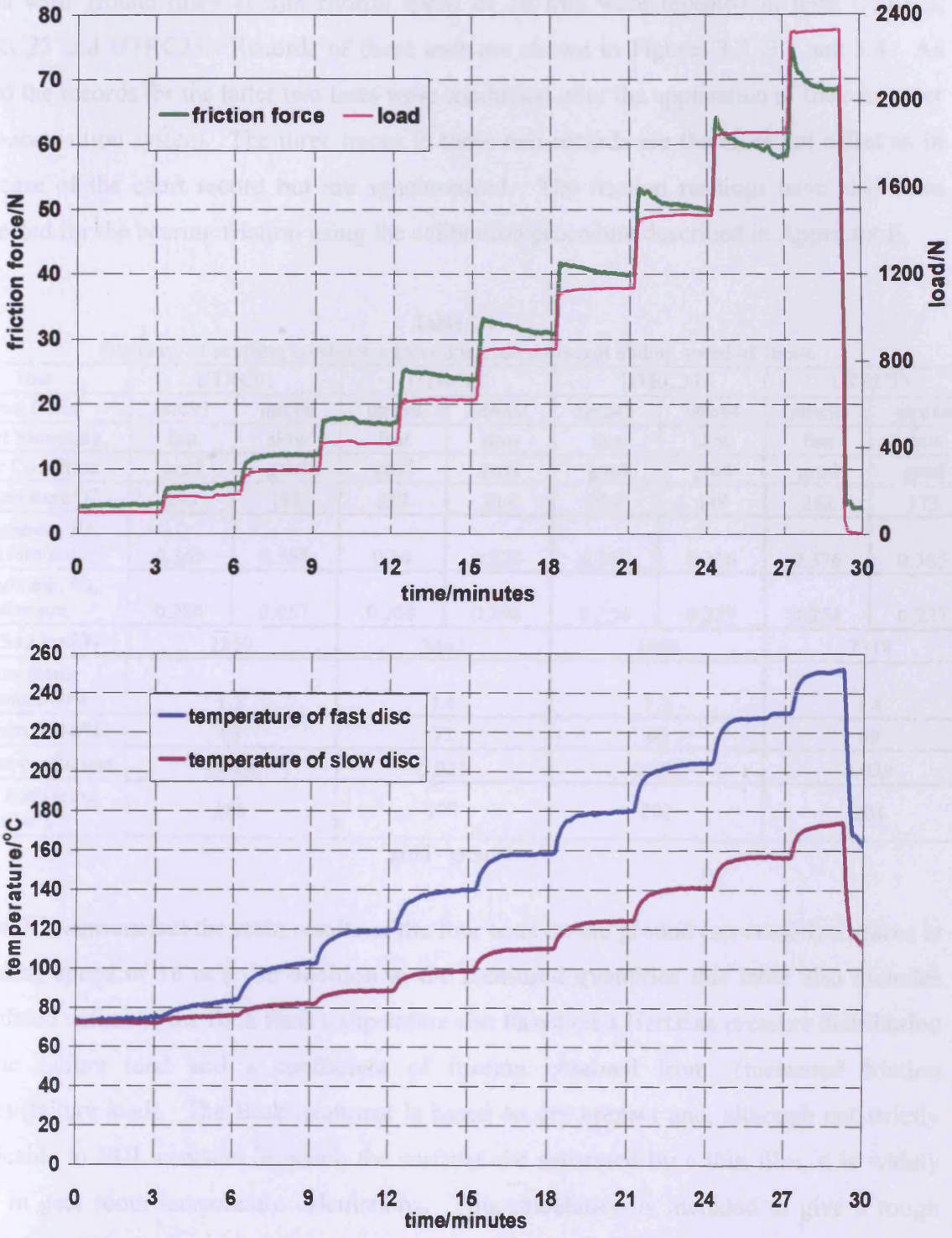

Figure 3.4. Record of scuffing test UTRC25, upper graph shows applied load and friction force; lower graph shows bulk temperatures of the two discs

Tests with ground discs at this sliding speed of 16 m/s were repeated in tests UTRC2, UTRC23 and UTRC25. Records of these tests are shown in Figures 3.2, 3.3 and 3.4. As noted the records for the latter two tests were conducted after the application of the computer data-acquisition system. The three traces in these two records are therefore not offset as in the case of the chart record but are synchronised. The friction readings have also been corrected for the bearing friction using the calibration procedure described in Appendix E.

Table 3.1.
Summary of scuffing conditions-ground/uncoated discs at sliding speed of 16m/s

Test	UTRC01		UTRC02		UTRC23		UTRC25	
Test Discs	utrc93	utrc66	utrc94	utrc02	utrc45	utrc44	utrc58	utrc18
Shaft Mounting	fast	slow	fast	slow	fast	slow	fast	slow
Disc Condition	grnd	grnd	grnd	grnd	grnd	grnd	grnd	grnd
temperature/°C	292	198	317	218	202	149	252	173
Roughness, Ra, before/μm	0.362	0.388	0.34	0.328	0.352	0.356	0.376	0.385
Roughness, Ra, after/μm	0.280	0.057	0.208	0.206	0.254	0.227	0.254	0.227
Scuffing load/N	2850		3462		1860		2318	
Max Hertz pressure/GPa	1.5		1.6		1.3		1.4	
Friction force/N	68		72		60		69	
Friction coefficient	0.024		0.021		0.032		0.029	
Blok flash temp. rise/°C	184		177		201		204	

grnd - ground

Table 3.1. summarises the main results of the four tests on the ground (un-coated) surfaces at a sliding speed of 16 m/s. In addition to the measured quantities this table also includes calculated values of the Blok flash temperature rise based on a Hertzian pressure distribution at the failure load and a coefficient of friction obtained from: (measured friction force)/(failure load). The Blok treatment is based on dry contact and, although not strictly applicable to EHL contacts in which the surfaces are separated by a thin film, it is widely used in gear tooth temperature calculations. This calculation is included to give a rough indication of the magnitude of the additional transient temperature rise that will occur whilst the surfaces are in contact. The complete derivation of the Blok flash temperature is given in Appendix A

The Blok formula for the temperature rise in a concentrated contact between two surfaces of the same material may be stated as follows:

$$\Delta\theta_{max} = \frac{1.658\mu\bar{p}|u_1 - u_2|b^{\frac{1}{2}}}{(k\rho c)^{\frac{1}{2}}\left(u_1^{1/2} + u_2^{1/2}\right)}$$

Where μ is the coefficient of friction; $\bar{p}$ is the mean contact pressure; u_1 and u_2 are the surface velocities; k, ρ, c are the thermal conductivity, mass density and specific heat of the surface, respectively. The Blok formula applies to a "line" contact and in this case the formula has been applied on the elliptical contact centre line. The contact semi-dimension in the formula (b) is therefore the semi-dimension of the minor axis of the contact (in the rolling direction).

The appearances of the surfaces of both discs used in each test after failure are shown in Figure 3.5. In the case of test UTRC01 (Figure 3.1) the whole running track has been scuffed whereas in the other three cases scuffing has occurred only along the edge of the track. This difference is due to the fact that in test UTRC01 there was a longer delay in (manually) unloading the discs after scuffing had been detected. This is indicated by the friction force reaching a relatively high value at the end of the test. In most other cases the load was removed more rapidly by the operator so as to preserve as much of the run, but unscuffed, surface as possible. In the case of ground surfaces scuffing invariably begins at the edge of the running track. The scuffed surfaces have the typical heavily torn areas where they have welded together and torn apart.

Typical circumferential profiles from the discs used in these four tests are shown in Figure 3.6. The profiles are from the discs used in test UTRC23 before running and from run but un-scuffed parts of the discs after scuffing failure. In this figure the Ra values correspond to the individual profiles shown. The low value of roughness of the fast disc used in test UTRC01 reflects the fact that in this case the whole track was scuffed and the disc effectively had its roughness re-orientated from axial to circumferential. The averages of four Ra values taken from each disc are also given in Table 3.1.

In each case it can be seen both qualitatively (from the profiles), and numerically (from the Ra values), that there is evidence of running in of the surfaces prior to scuffing failure in all cases where it was possible to measure the run in but unscuffed parts of the discs.

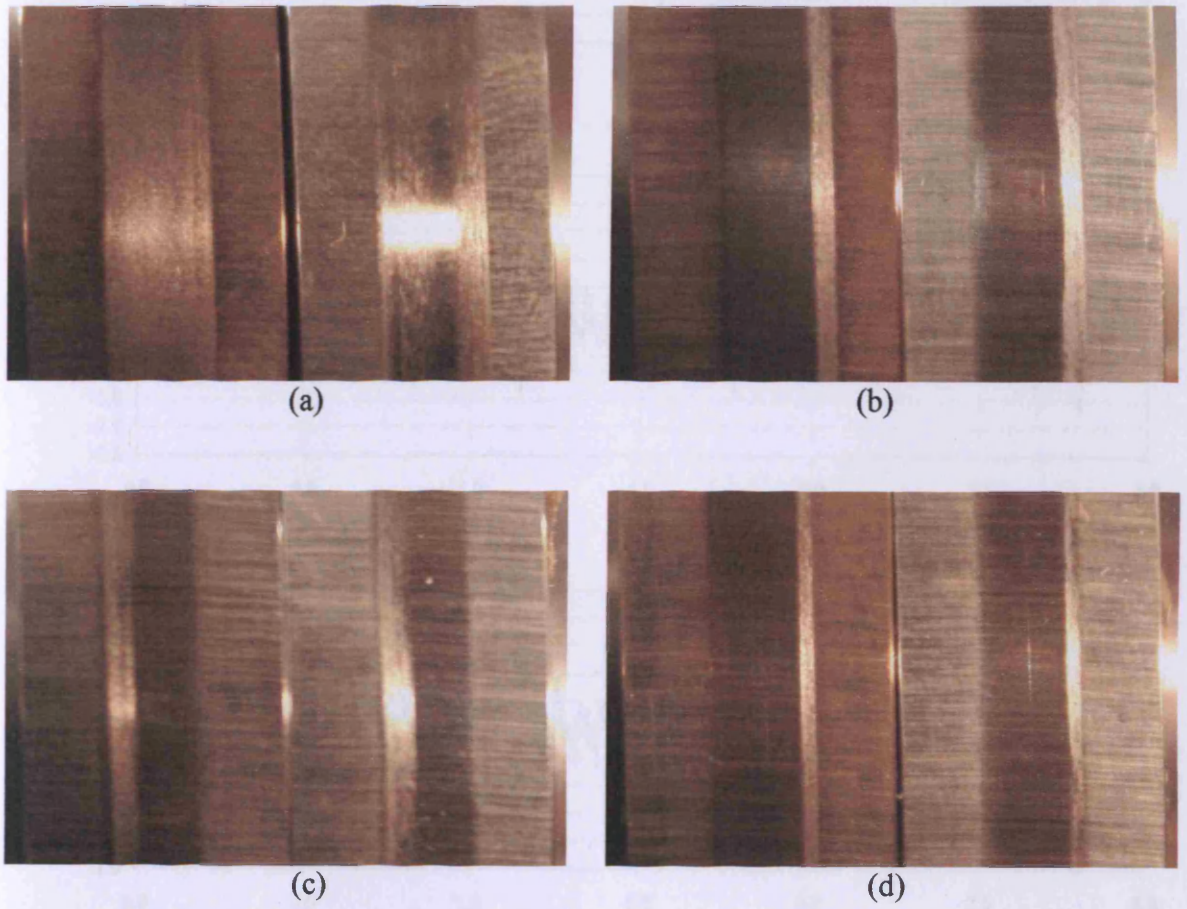

Figure 3.5. Photographs of discs following testing at 16m/s
(a) UTRC01; left: ground disc on fast shaft; right: ground disc on slow shaft
(b) UTRC02; left: ground disc on fast shaft; right: ground disc on slow shaft
(c) UTRC23; left: ground disc on fast shaft; right: ground disc on slow shaft
(d) UTRC25; left: ground disc on fast shaft; right: ground disc on slow shaft

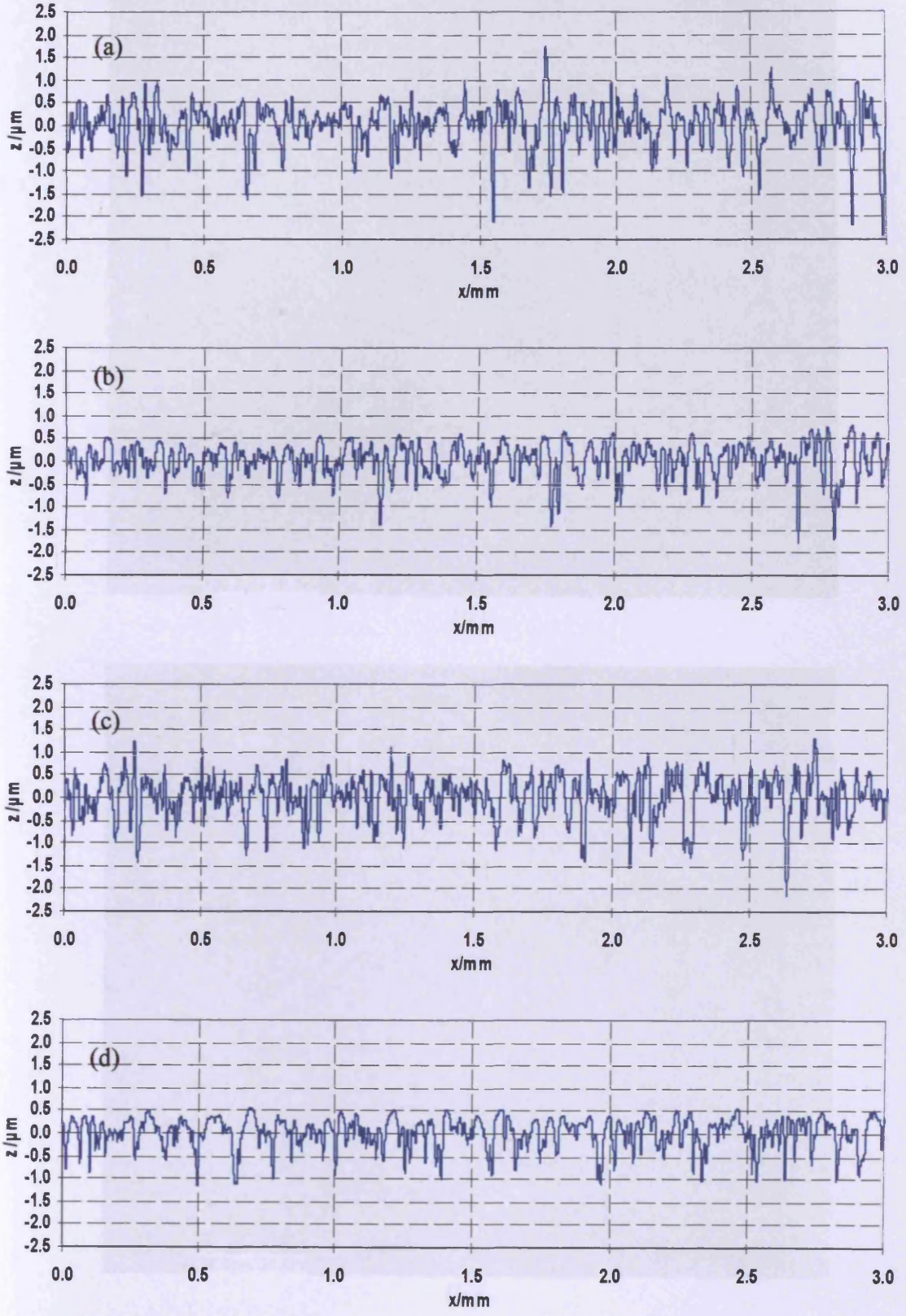

Figure 3.6. Surface profiles taken in the circumferential direction from discs used in test UTRC23, Profiles from fast disc (a) before test; Ra = 0.379 µm (b) after test; Ra = 0.259 µm
Profiles from slow disc (c) before test; Ra = 0.366 µm (d) after test; Ra = 0.226 µm

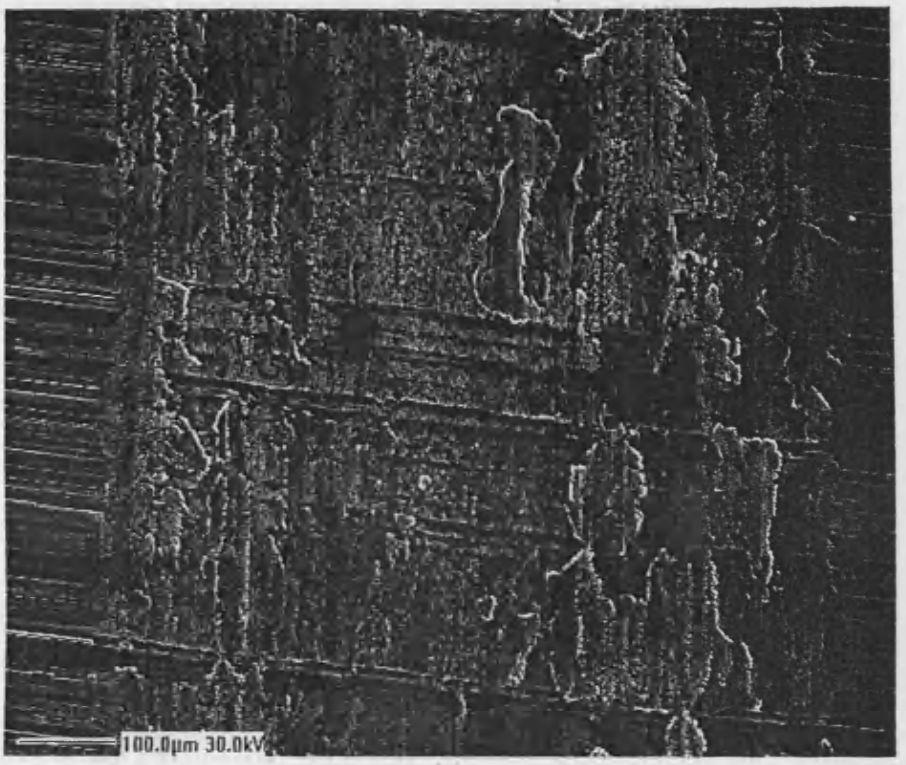

(a)

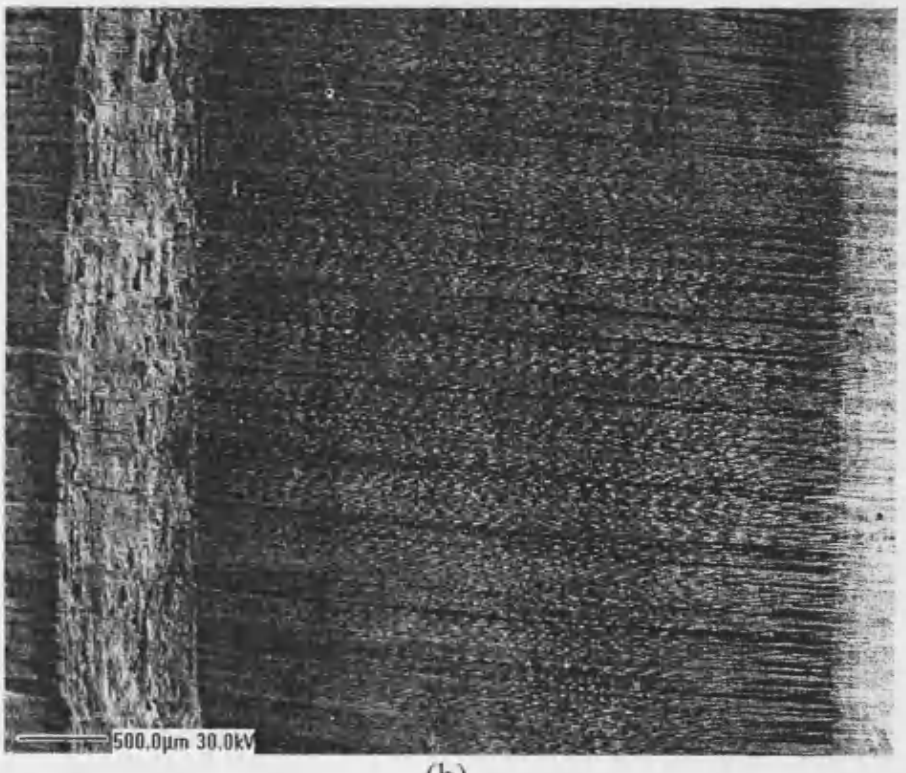

(b)

Figure 3.7. SEM images of surface of the fast disc used in test UTRC02.
(a) scuffing scar with unrun surface on the left and run in surface on right
(b) running track with scuffing scar on the edge

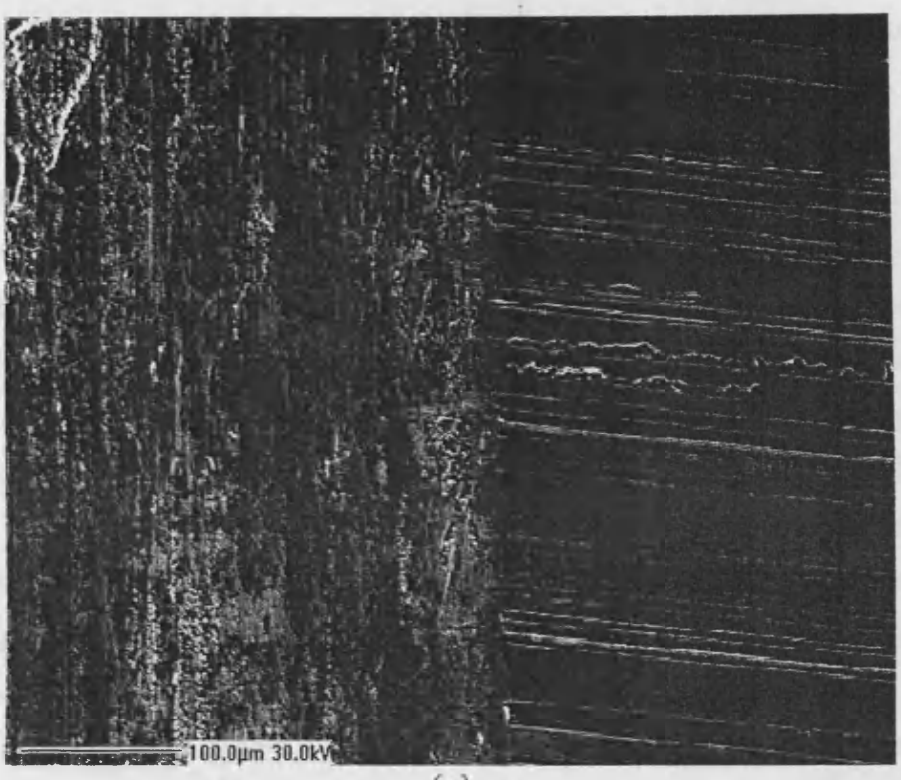

(a)

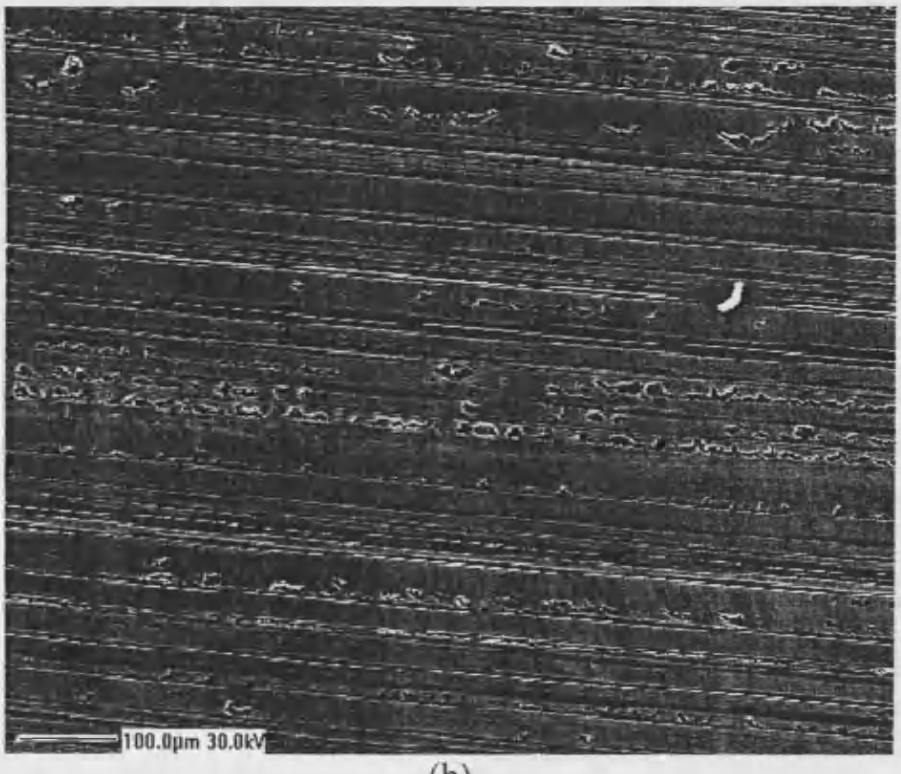

(b)

Figure 3.8. SEM images of surface of the slow disc used in test UTRC02.
(a) scuffing part with run in surface on the right (lands clearly visible)
(b) middle of the running track with clear indication of material removal

A more detailed picture of the changes that occur to the surfaces as a result of both running in and scuffing failure are shown in the following SEM images in Figures 3.7 and 3.8. Figure 3.7 shows SEM images from the fast disc used in experiment UTRC02. The upper image shows the characteristic scuffing scar at the edge of the running track. To the left of the scar is the un-run surface which is outside the contact, and to the right of the scar is the surface of the running track, but which has not become scuffed. In this case the load was released fairly quickly so that although the axial grinding marks (which appear as horizontal lines on the image) have become disrupted the deeper grinding scratches are still visible beneath the scuffing scar. The lower image in Figure 3.7 is at a lower magnification and shows the whole width of the running track with the scuffing scar on the left of the track. The run but unscuffed part of the track appears slightly darker than the un-run area on the extreme right. The total width of the track is about 4 mm as expected at the load reached (3462 N) during this test. Again, the underlying grinding marks (horizontal) are faintly visible within the scuffed region. In this case relative sliding is in the vertical upwards direction and the smearing of the surface can be seen to "overhang" into the valley features of the original surface.

Figure 3.8 shows similar SEM images from the slow disc used in the same test, UTRC02. In this case both images are at the higher magnification. The upper image of Figure 3.8 shows the scuffing scar on the left with run in but unscuffed track of the disc to the right. The creation of flat-looking "lands" can be seen in this image. These show that significant smoothing of the surfaces occurs in the heavily loaded stages prior to scuffing. The lower image shows the run in region near the middle of the track. The flattened lands are particularly clear in this view. In this case sliding is in the downwards direction and the smearing of the surface into the valley regions of the original roughness is again clearly seen.

Experiments UTRC07 and UTRC28 were carried out with uncoated ground discs at the intermediate sliding speed of 12 m/s. Records of these tests are shown in Figures 3.9 and 3.10. Again it is noted that the earlier tests in this series were carried out before the introduction of the computer data-acquisition system.

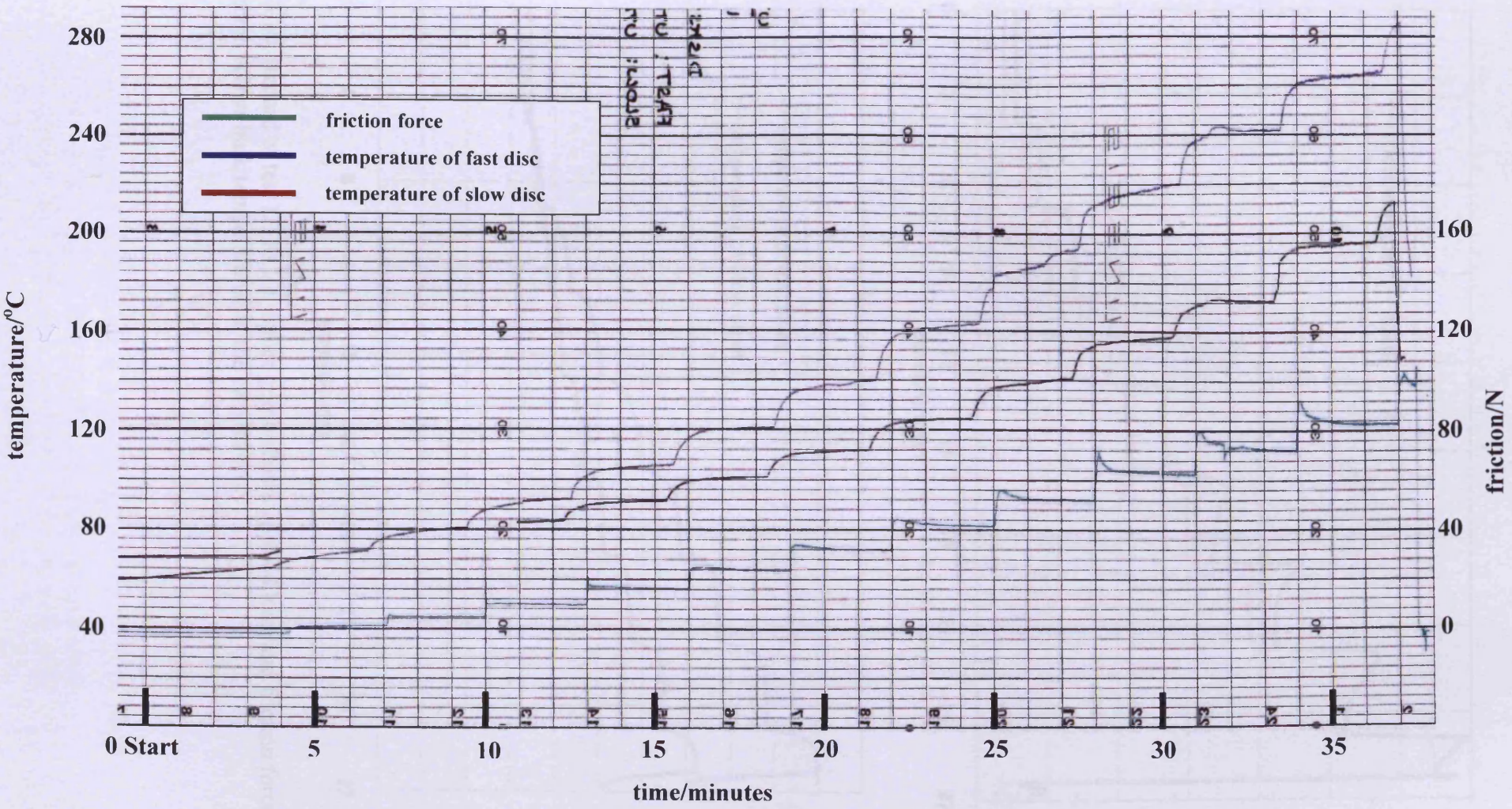

Figure 3.9. Record of scuffing test UTRC07, graph shows friction force and bulk temperatures of the two discs

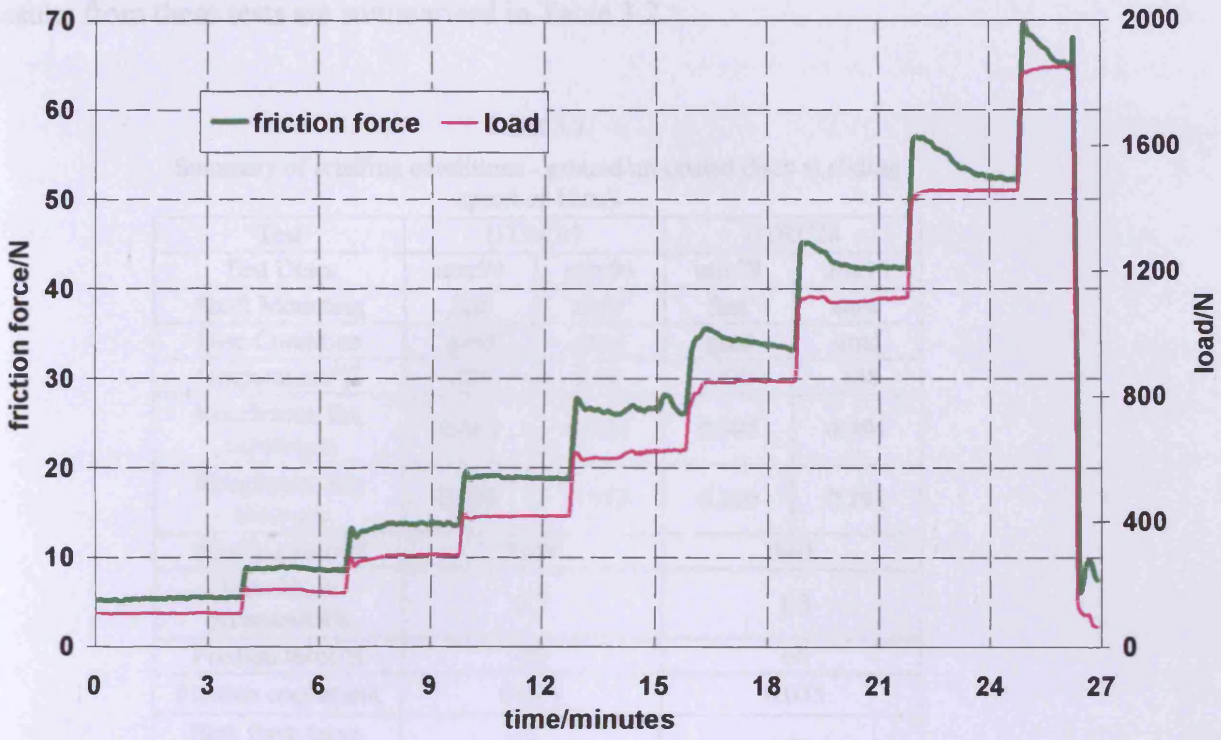

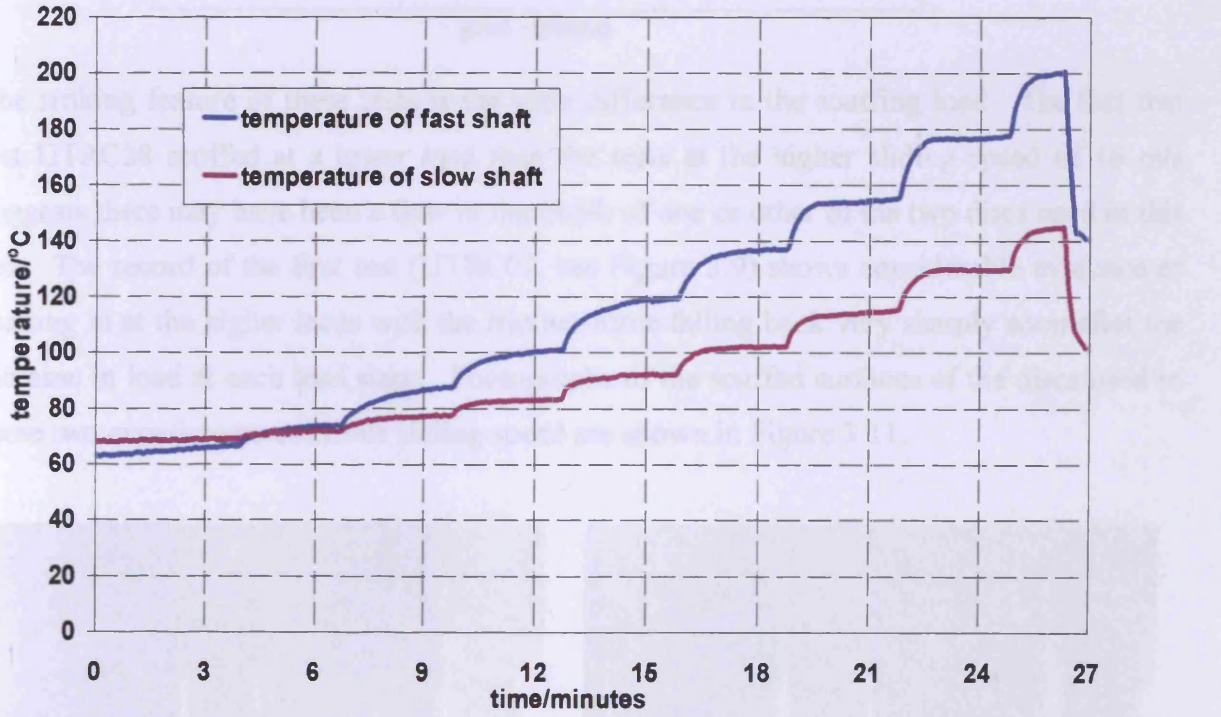

Figure 3.10. Record of test UTRC28, upper graph shows applied load and friction force; lower graph shows bulk temperatures of the two discs

Results from these tests are summarised in Table 3.2.

Table 3.2.

Summary of scuffing conditions - ground/un-coated discs at sliding speed of 12m/s

Test	UTRC07		UTRC28	
Test Discs	utrc90	utrc06	utrc78	utrc19
Shaft Mounting	fast	slow	fast	slow
Disc Condition	grnd	grnd	grnd	grnd
temperature/°C	286	212	200	148
Roughness, Ra, before/μm	0.363	0.356	0.385	0.394
Roughness, Ra, after/μm	0.225	0.212	0.210	0.191
Scuffing load/N	4149		1861	
Max Hertz pressure/GPa	1.7		1.3	
Friction force/N	98		66	
Friction coefficient	0.024		0.035	
Blok flash temp. rise/°C	190		191	

grnd - ground

The striking feature of these tests is the wide difference in the scuffing load. The fact that test UTRC28 scuffed at a lower load than the tests at the higher sliding speed of 16 m/s suggests there may have been a flaw in the finish of one or other of the two discs used in this test. The record of the first test (UTRC07, see Figure 3.9) shows considerable evidence of running in at the higher loads with the friction force falling back very sharply soon after the increase in load at each load stage. Photographs of the scuffed surfaces of the discs used in these two experiments at 12 m/s sliding speed are shown in Figure 3.11.

(a) (b)

Figure 3.11. Photographs of discs following testing at 12m/s
(a) UTRC07; left: ground disc on fast shaft; right: ground disc on slow shaft
(b) UTRC28; left: ground disc on fast shaft; right: ground disc on slow shaft

It may be noted that the fast disc from test UTRC07 (Figure 3.11a, left), which failed at the relatively high load of 4149N, and reached a bulk temperature of 286°C, has a rather dark-looking appearance compared to the other discs shown in this figure. This effect will be seen in other discs that reached high temperatures are probably due to oxidation of the oil on the surfaces under high temperature conditions. The darkening is more pronounced in the running track area where the discs are subjected to the additional transient "flash" temperature effect. Typical circumferential profiles from the discs before and after running are shown in Figure 3.12. As before the profiles taken from the discs after running are taken from the run in but unscuffed parts of the discs. Again, there is evidence of significant running in of the surfaces.

The high degree of surface modification taking place prior to scuffing is clearly evident in the SEM images shown in Figures 3.13 and 3.14. Figure 3.13(a) shows a high magnification of the surface of the fast disc at the boundary between the scuffing scar and the run, but unscuffed, part of the running track. In this case the scuffing is severe and the original grinding marks are completely removed due to heavy welding and smearing of the surface. The run but unscuffed region to the right of the scar shows the typical flattening behaviour and there is evidence of plastic displacement of the ridges with smearing of metal in the upwards direction. The lower image, at a lower magnification, shows the total width of the scuffing scar. Figure 3.14 shows images from the slow disc used in test UTRC07. The upper image, at a high magnification, shows the scuffing scar to the right and run in surface to the left. The lower image is taken from near the middle of the running track and shows what may be described as incipient scuffing, The smearing of the surface, in the downwards direction, is more pronounced than that seen in the usual run in region. It has disrupted the land features with pronounced transverse grooves. Again, it is clear that considerable plastic deformation occurs prior to gross welding and tearing.

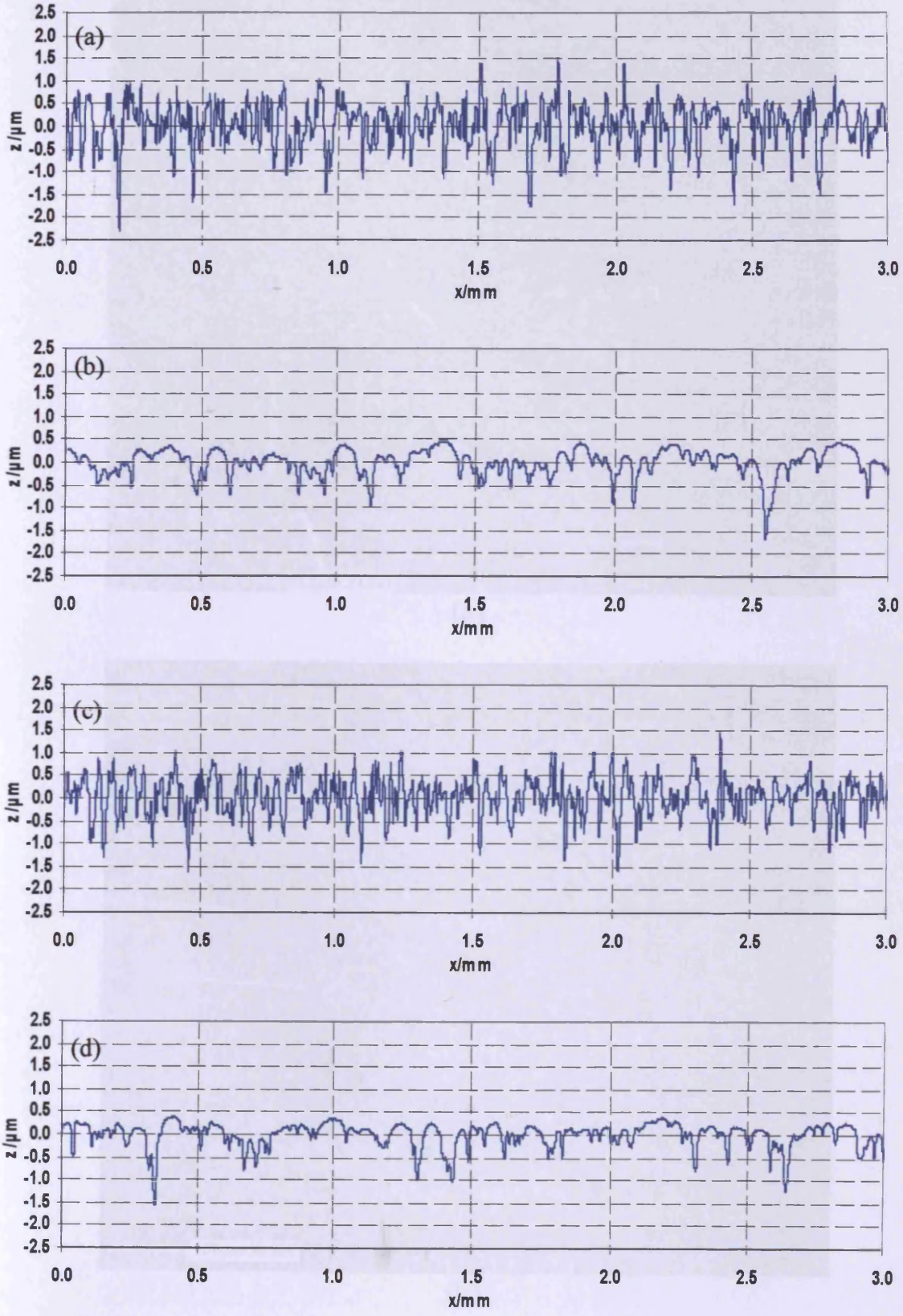

Figure 3.12. Surface profiles taken in the circumferential direction from discs used in test UTRC07
Profiles from fast disc (a) before test; Ra = 0.373 µm (b) after test; Ra = 0.214 µm
Profiles from slow disc (c) before test; Ra = 0.358 µm (d) after test; Ra = 0.206 µm

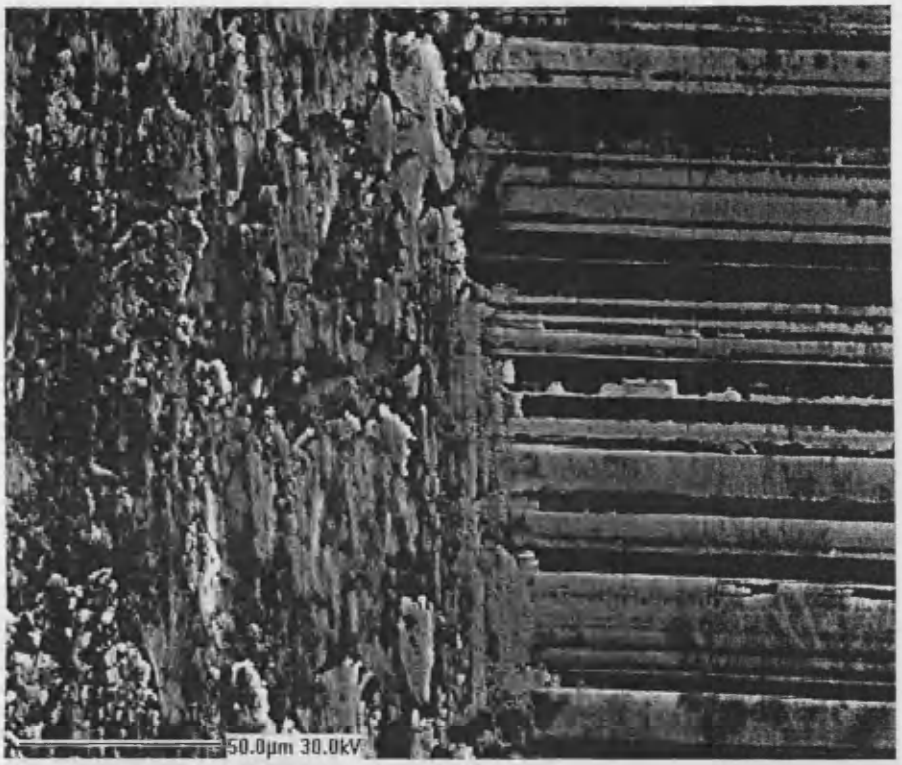

(a)

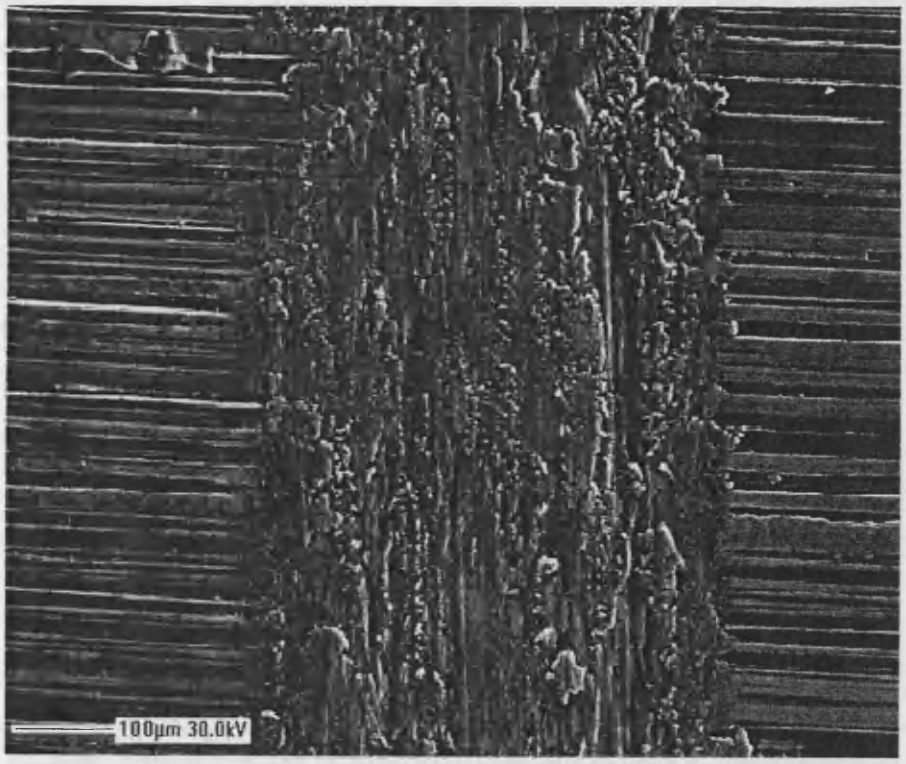

(b)

Figure 3.13. SEM images of surface of the slow disc used in test UTRC07.
(a) scuffed part with run in surface on the right
(b) scuffed part with run in surface on both sides

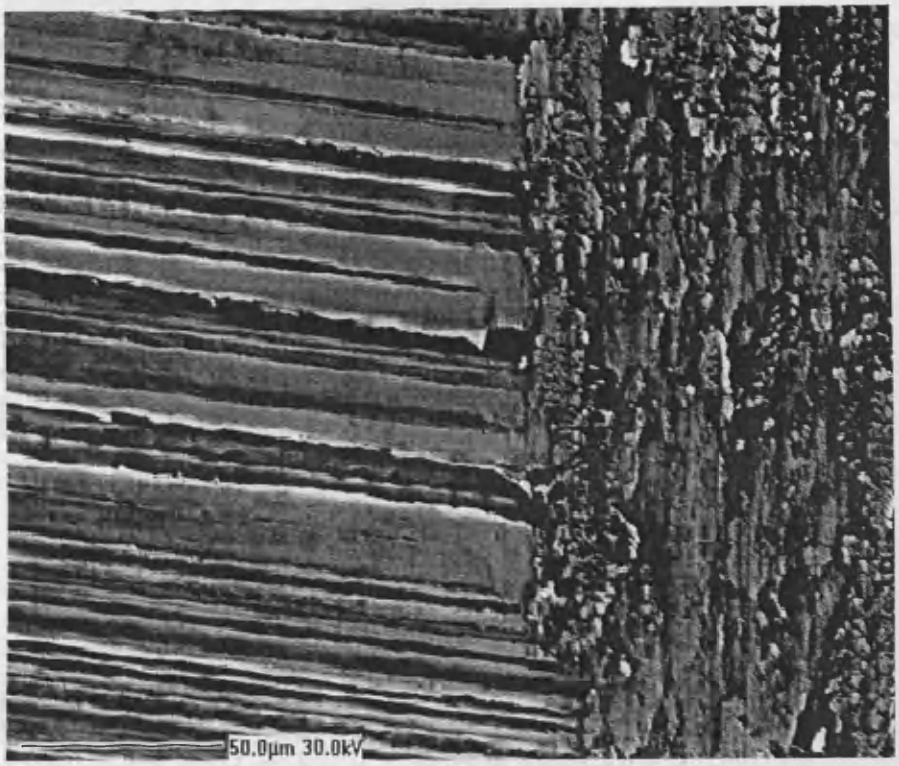

(a)

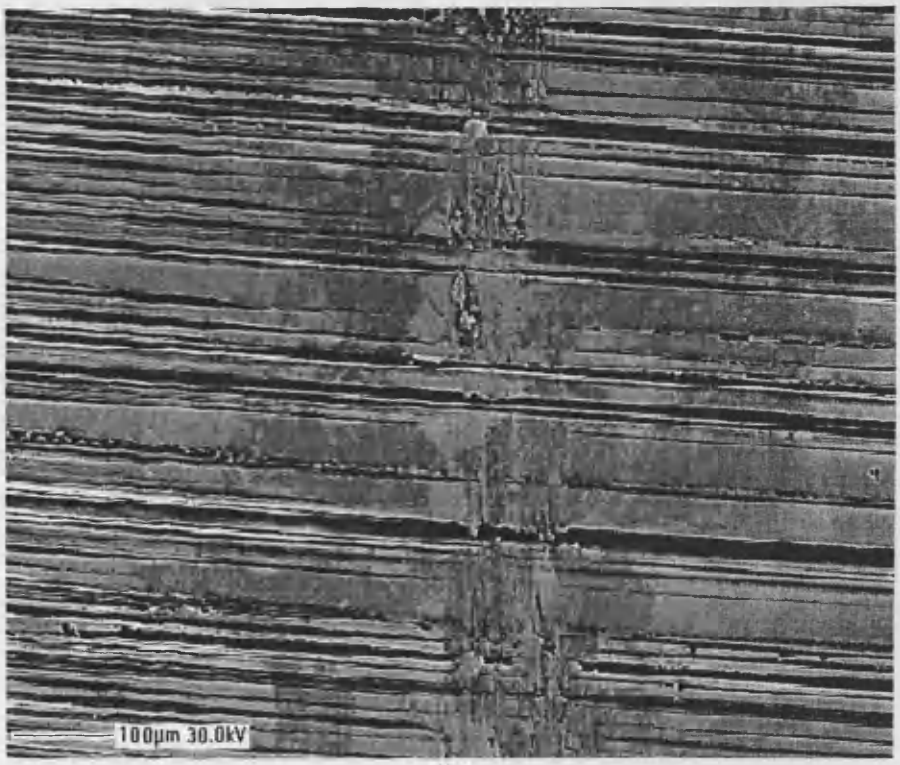

(b)

Figure 3.14. SEM images of surface of the slow disc used in test UTRC07.
(a) run in surface on the left and scuffed part on the right
(b) transition of scoring to scuffing with run in surface in the background

Experiments UTRC05 and UTRC27 were carried out with uncoated ground discs at the lowest sliding speed of 7 m/s. Records of these tests are shown in Figures 3.15 and 3.16. Again it is noted that the earlier tests in this series were carried out before the introduction of the computer data-acquisition system. Both tests resulted in scuffing at a relatively high load as might be expected at this lowest of the sliding speeds considered. In both Figures 3.15 and 3.16 we see considerable falling off of the friction force following application of an increase in load during the later stages of the test. This behaviour is particularly evident in the final stages preceding scuffing in test UTRC27. Photographs of the discs used in these two tests at 7 m/s are shown in Figure 3.17. It may be noted that scuffing occurs near the edge of the running track.

Results from these tests are summarised in Table 3.3.

Table 3.3.
Summary of scuffing conditions - ground/un-coated discs at sliding speed of 7m/s

Test	UTRC05		UTRC27	
Test Discs	utrc90	utrc06	utrc78	utrc19
Shaft Mounting	fast	slow	fast	slow
Disc Condition	grnd	grnd	grnd	grnd
temperature/°C	218	165	246	182
Roughness, Ra, before/μm	0.311	0.345	0.362	0.388
Roughness, Ra, after/μm	0.236	0.236	0.256	0.257
Scuffing load/N	4146		5790	
Max Hertz pressure/GPa	1.7		1.9	
Friction force/N	120		180	
Friction coefficient	0.029		0.031	
Blok flash temp. rise/°C	178		226	

grnd - ground

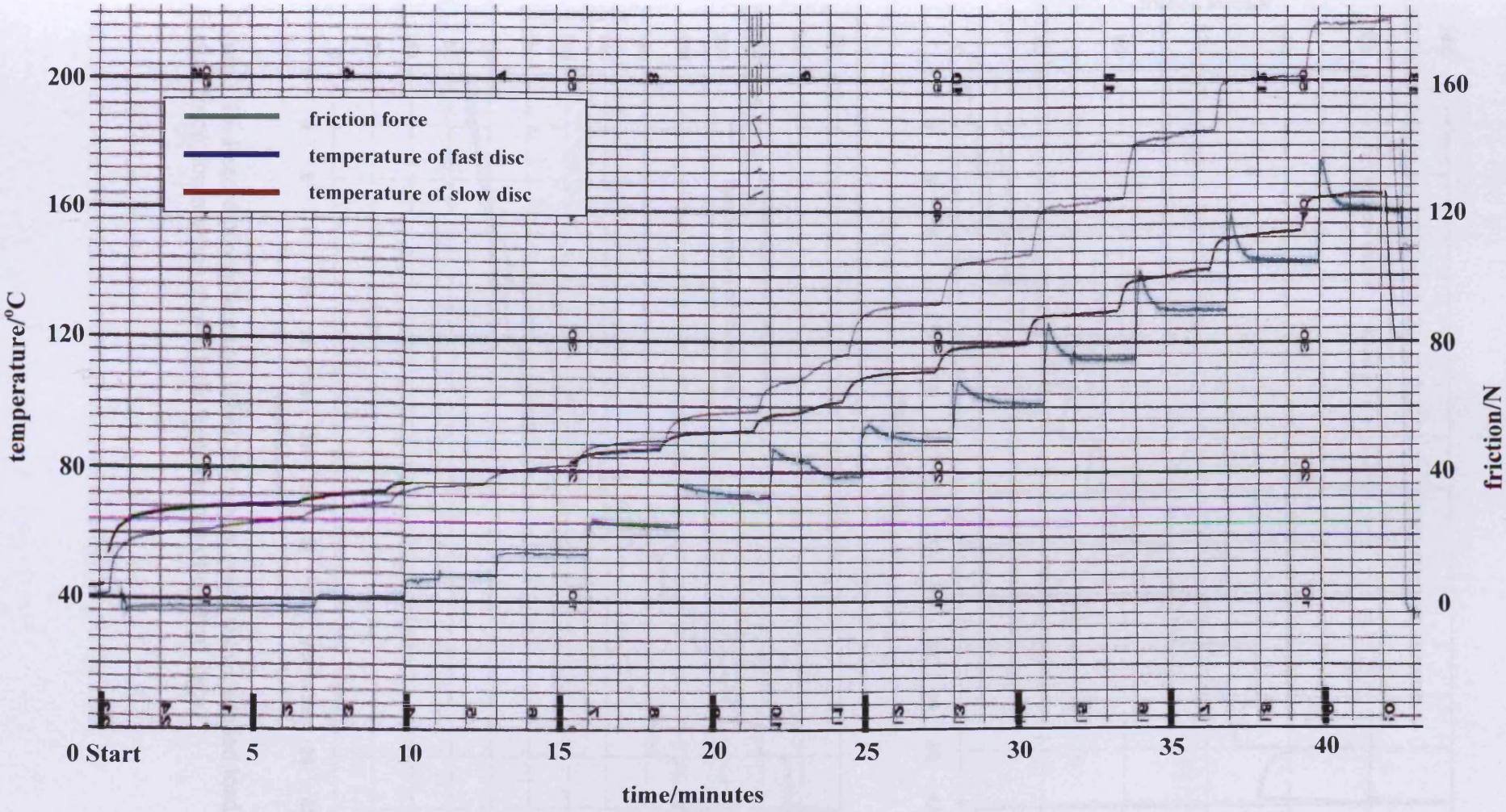

Figure 3.15. Chart recorder record of test UTRC05, graph shows friction force and bulk temperatures of two discs.

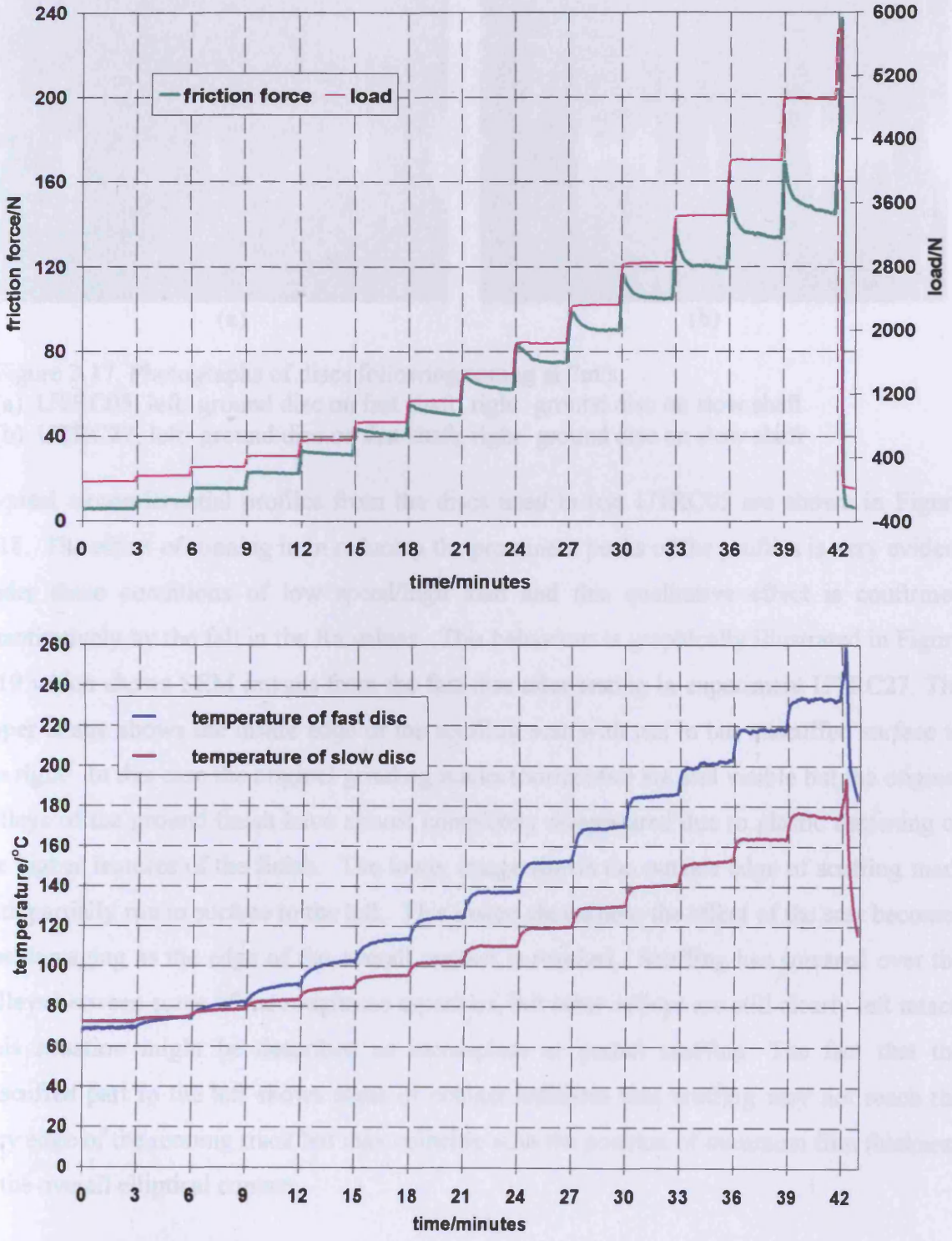

Figure 3.16. Record of scuffing test UTRC27, upper graph shows applied load and friction force; lower graph shows bulk temperatures of the two discs

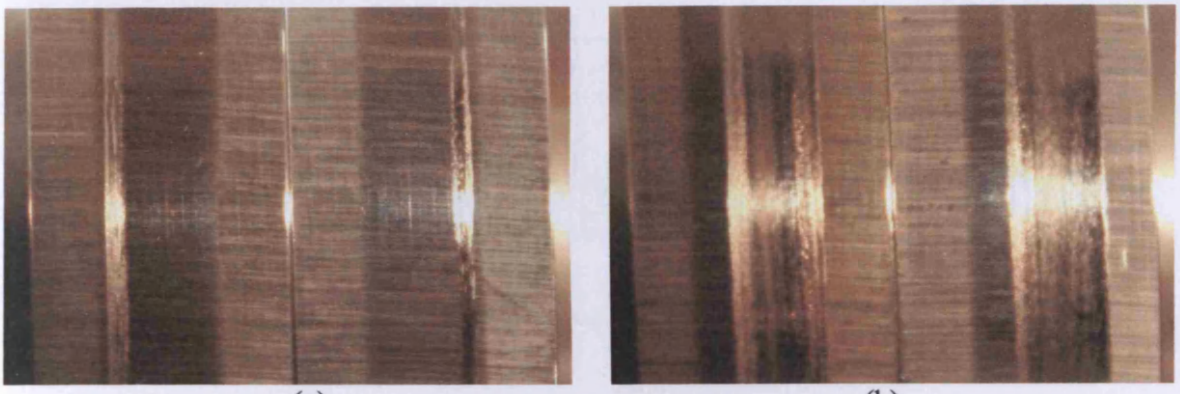

(a) (b)

Figure 3.17. Photographs of discs following testing at 7m/s
(a) UTRC05; left: ground disc on fast shaft; right: ground disc on slow shaft
(b) UTRC27; left: ground disc on fast shaft; right: ground disc on slow shaft

Typical circumferential profiles from the discs used in test UTRC05 are shown in Figure 3.18. The effect of running in in reducing the prominent peaks of the profiles is very evident under these conditions of low speed/high load and this qualitative effect is confirmed quantitatively by the fall in the Ra values. This behaviour is graphically illustrated in Figure 3.19 which shows SEM images from the fast disc after testing in experiment UTRC27. The upper image shows the inside edge of the scuffing scar with run in but unscuffed surface to the right. In this case the original grinding marks (horizontal) are still visible but the original valleys of the ground finish have almost completely disappeared due to plastic flattening of the higher features of the finish. The lower image shows the outside edge of scuffing mark with partially run in surface to the left. This image shows how the effect of the scar becomes less damaging as the edge of the overall contact is reached. Scuffing has smeared over the valleys between some of the roughness asperities, but other valleys are still clearly left intact. This situation might be described as incomplete or partial scuffing. The fact that the unscuffed part to the left shows signs of contact indicates that scuffing may not reach the very edge of the running track but may coincide with the position of minimum film thickness in the overall elliptical contact.

Figure 3.20 shows SEM images of the slow disc used in test UTRC27. The upper image shows the perfect unrun condition of the disc. The roughness features on the ground discs are clearly seen in the image which shows high peaks and deep valleys. In contrast the lower image shows the run in surface on the left and the scuffing scar in the right.

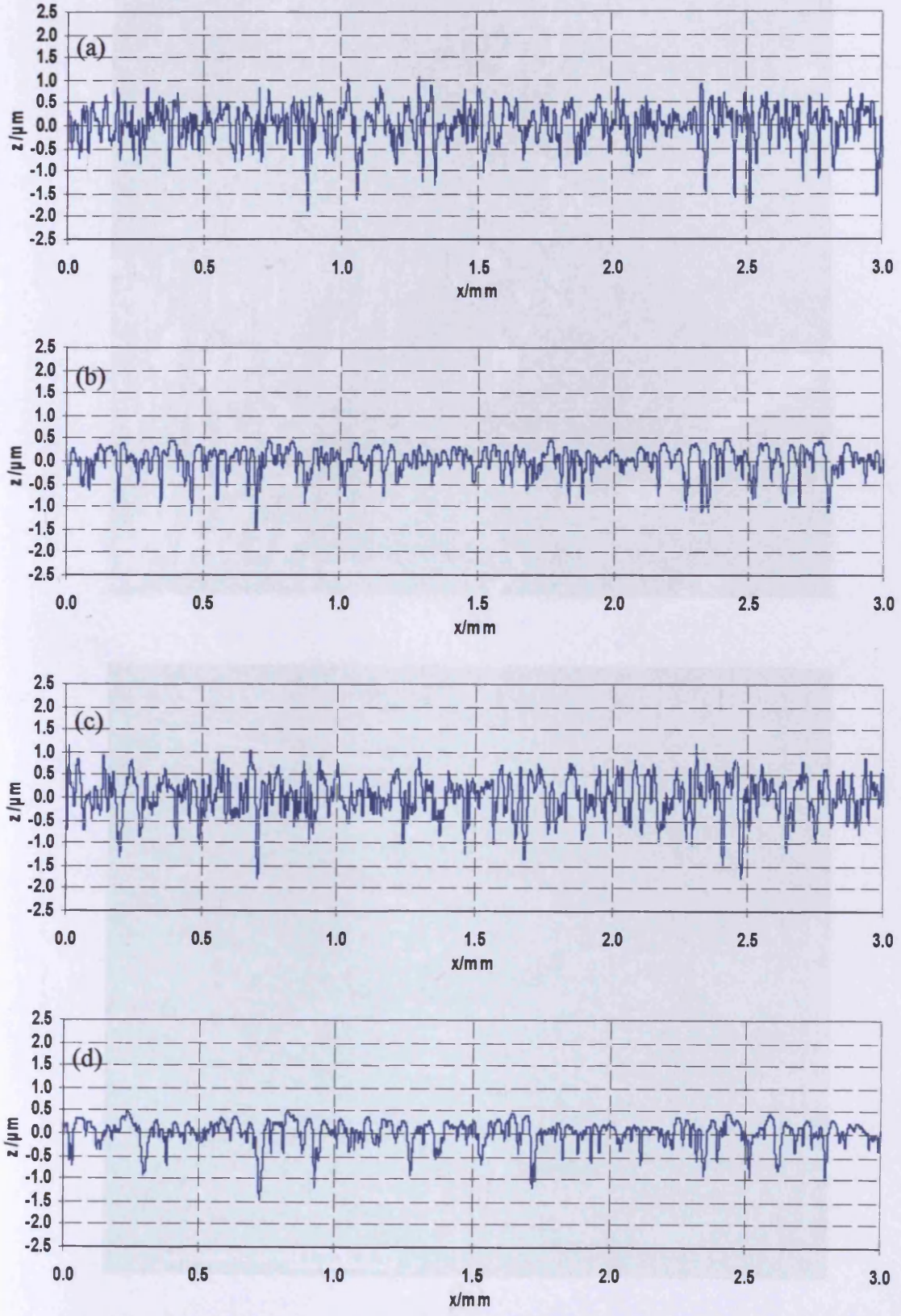

Figure 3.18. Surface profiles taken in the circumferential direction from discs used in test UTRC05
Profiles from fast disc (a) before test; Ra = 0.323 µm (b) after test; Ra = 0.221 µm
Profiles from slow disc (c) before test; Ra = 0.354 µm (d) after test; Ra = 0.214 µm

(a)

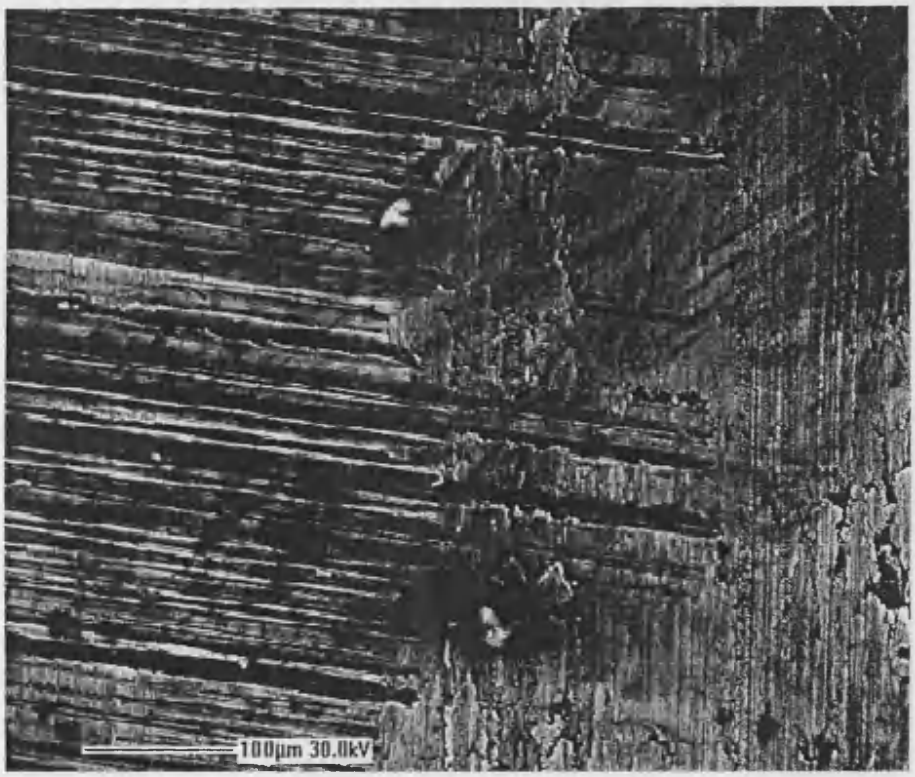

(b)

Figure 3.19. SEM images of surface of the slow disc used in test UTRC27.
(a) scuffing area on the left with run in surface to the right
(b) edge of the scuff with unrun part to the left

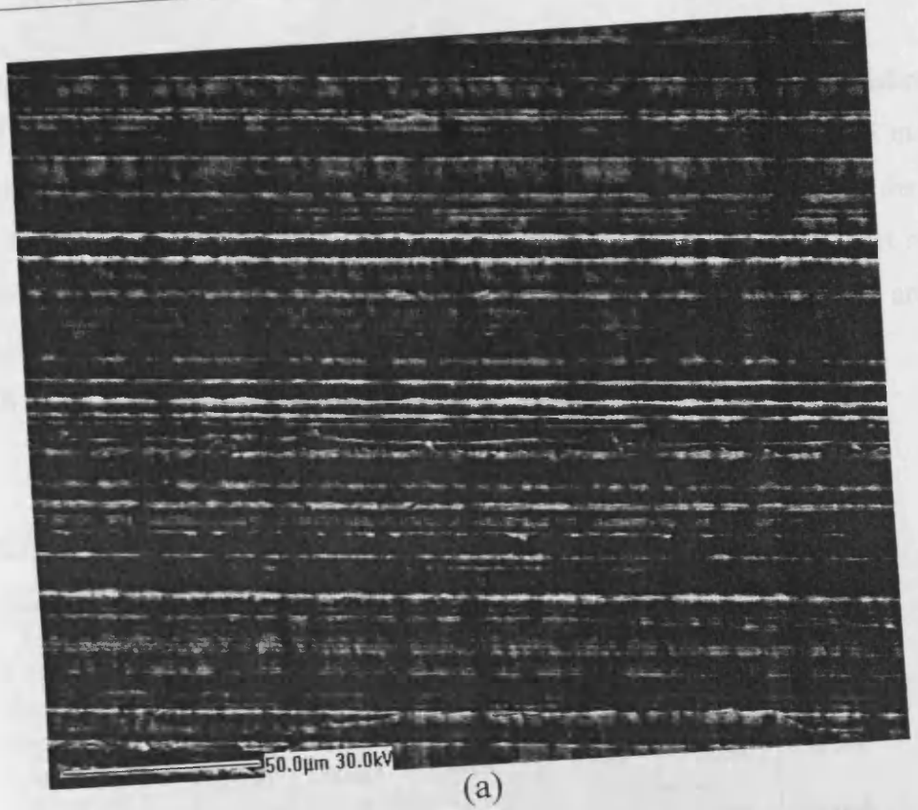

(a)

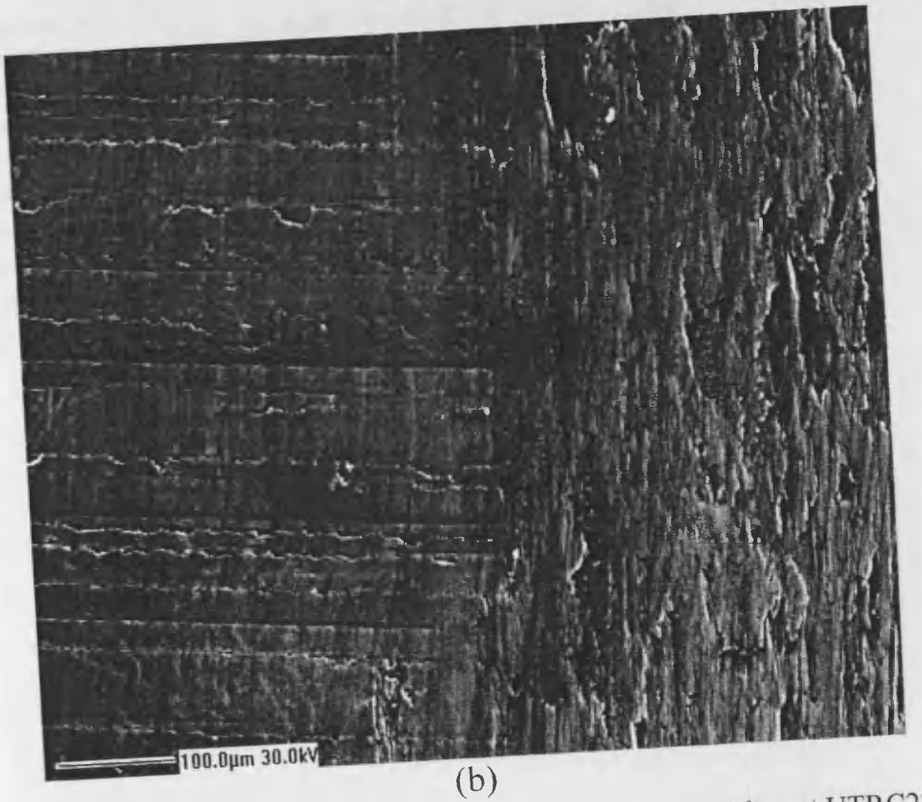

(b)

Figure 3.20. SEM images of surface of the slow disc used in test UTRC27.
(a) unrun section of the disc
(b) run in surface on the left with the scuffed part to the right

3.2.2. Superfinished discs running against superfinished discs

Three tests (UTRC03, UTRC04 and UTRC06) were carried out with superfinished discs running against superfinished discs as follows: two tests at the sliding speed of 16 m/s and a single test at 7 m/s. As all three tests were carried out during the early stages of the project the progress of the tests is recorded in the form of the paper charts from the chart recorder. These are shown in Figures 3.21, 3.22 and 3.23 and the main features of the tests are shown in table 3.4.

Table 3.4.
Summary of scuffing conditions-superfinished discs running against superfinished discs

Test	UTRC03		UTRC04		UTRC06	
Sliding Speed	16m/s				7m/s	
Test Discs	utrc86	utrc01	utrc79	utrc03	utrc75	utrc09
Shaft Mounting	fast	slow	fast	slow	fast	slow
Disc Condition	s.f	s.f.	s.f.	s.f.	s.f.	s.f.
temperature/°C	212	137	165	122	167	130
Roughness, Ra, before/μm	0.086	0.032	0.053	0.112	0.054	0.048
Roughness, Ra, after/μm	0.052	0.051	0.047	0.053	0.053	0.048
Scuffing load/N	4158		3456		5778	
Max Hertz pressure/GPa	1.7		1.6		1.9	
Friction force/N	44		24		78	
Friction coefficient	0.010		0.007		0.013	
Blok flash temp. rise/°C	99		59		98	

s.f. - super finished

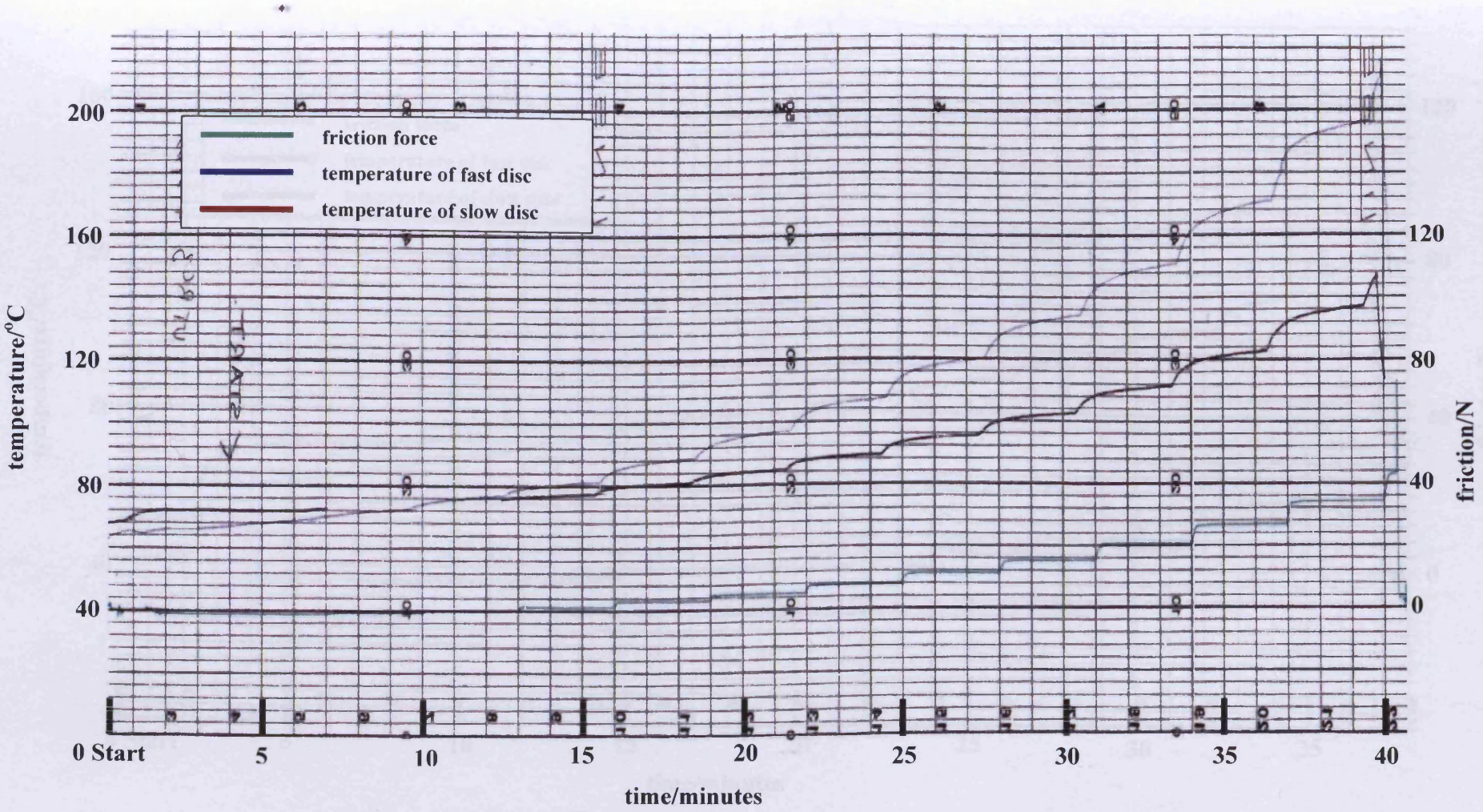

Figure 3.21. Chart recorder record of test UTRC03, graph shows friction force and bulk temperatures of two discs

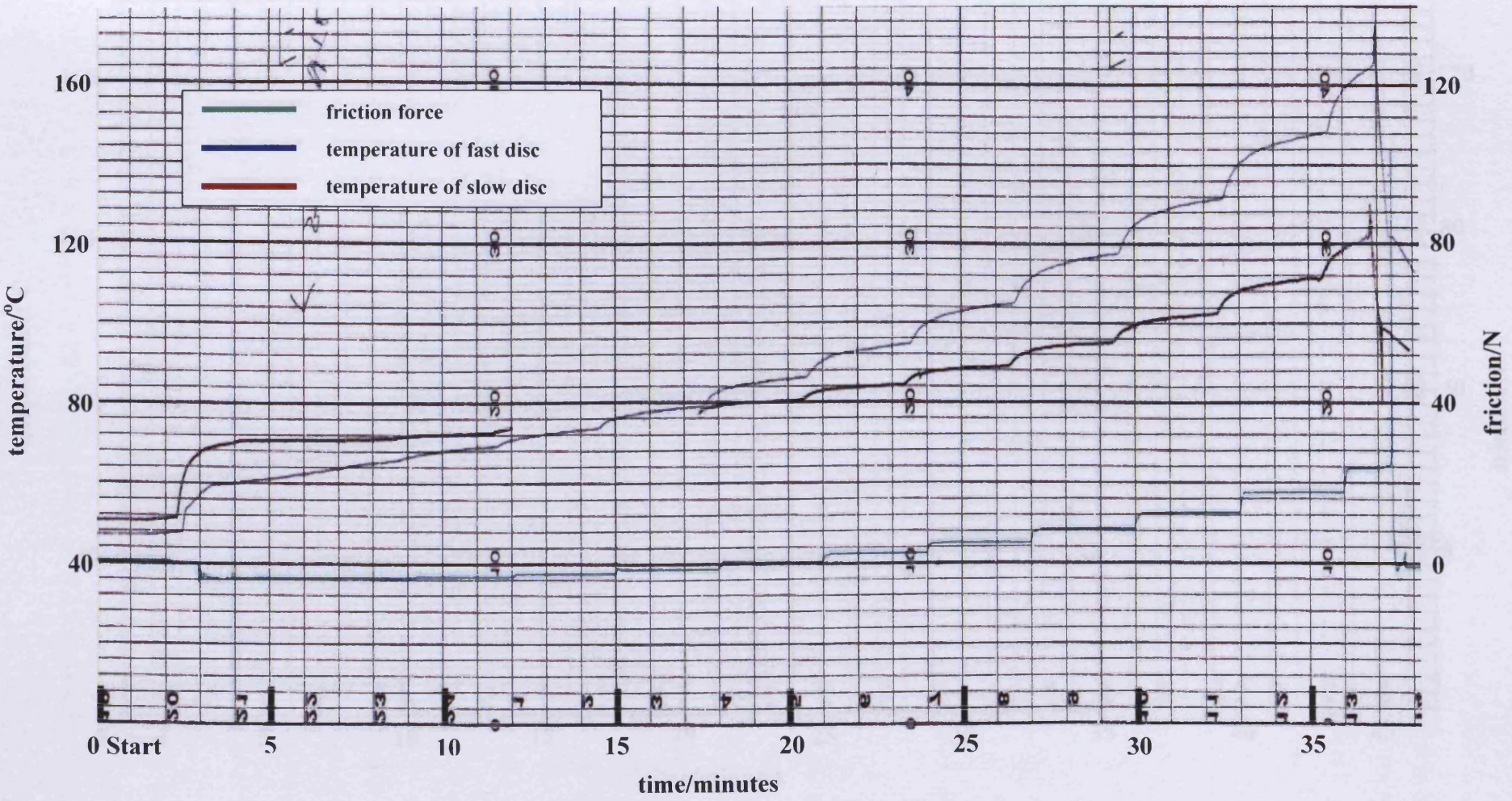

Figure 3.22. Chart recorder record of test UTRC04, graph shows friction force and bulk temperatures of two discs

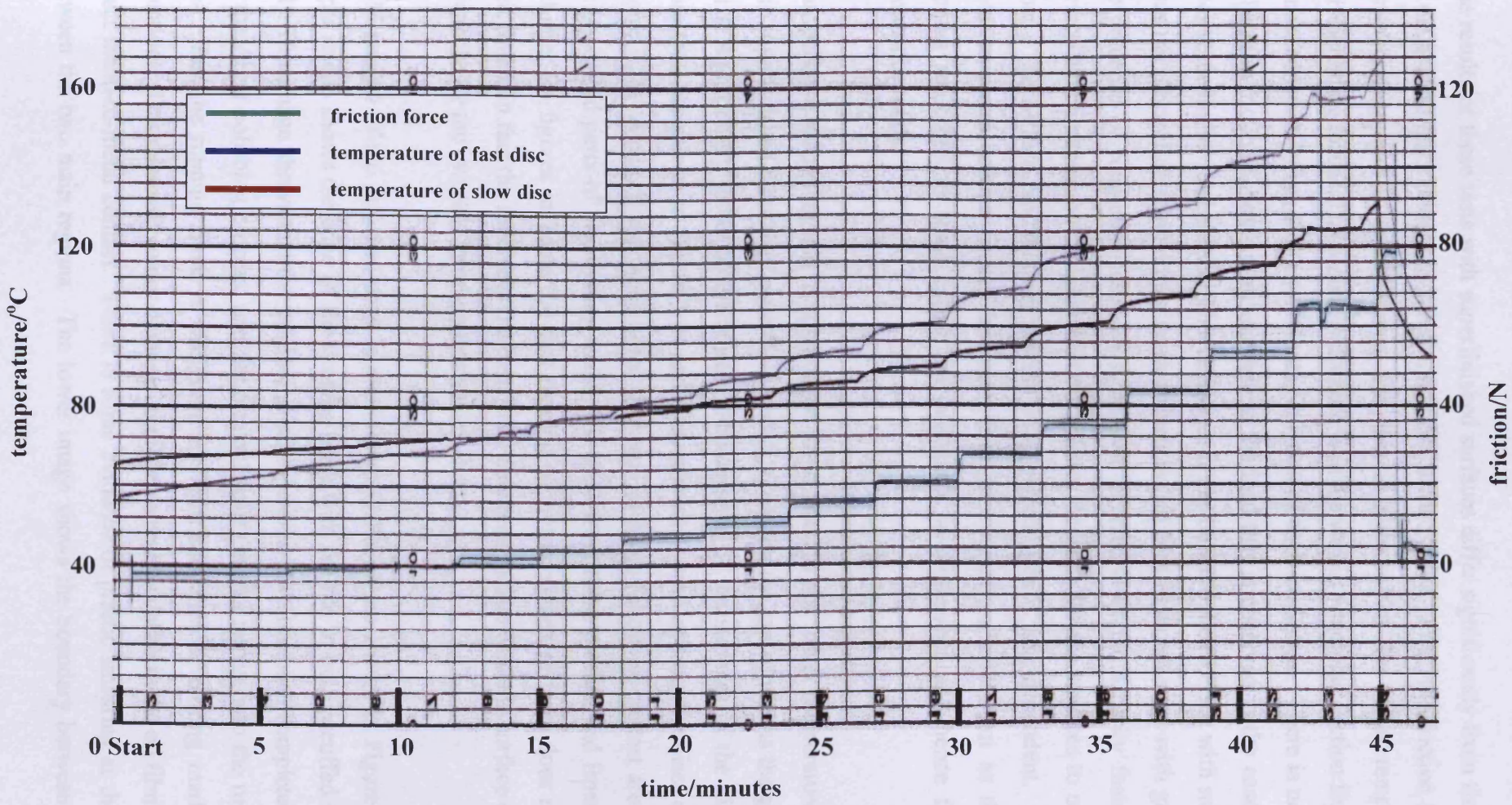

Figure 3.23. Chart recorder record of test UTRC06, graph shows friction force and bulk temperatures of two discs

The results of these tests with superfinished surfaces differ significantly from the behaviour of the ground discs under the same conditions in two ways. First, the friction force at the corresponding load is much lower, and this is reflected in the lower temperatures at corresponding loads. The second difference is in the way in which the friction force remains almost constant during the three minutes duration of each load stage. There is not the sharp fall in the friction following an increase in the load that is observed in the case of ground discs at the higher load stages. This behaviour is attributed to the fact that with superfinished discs the lubrication regime may be described as full film EHL, whereas with ground discs the presence of roughness leads to significant interaction of the asperity features of the surface which causes both higher friction and the tendency for the surfaces to modify each other. The surface modification process with ground discs is time-dependent. At first the metal to metal contact (mixed boundary/EHL lubrication) is severe but as the surfaces become smoothed to some extent the interaction is diminished and hence friction and temperatures fall.

It is, perhaps, surprising that in spite of the lower friction and lower temperatures observed with superfinished discs they nevertheless scuff at around the same loads as the ground discs but at significantly lower temperatures. Photographs of the surfaces of the discs used in these tests are shown in Figure 3.24 and circumferential profiles from the discs are given in Figure 3.25. Again, it should be noted that profiles taken following the test are taken from the unscuffed parts of the running track. It is clear from these profiles and from the before and after Ra figures in Table 3.4 that running of these polished surfaces does not improve their finish; in fact the reverse is the case since they tend to deteriorate in surface quality as is evidenced by the increase in roughness values.

SEM images of the fast disc used in experiment UTRC03 are shown in Figure 3.26. The upper image shows the edge of the running track with the run in but unscuffed track to the left. This image shows that the original grinding marks have not been completely removed by the Abral polishing process, and the original valley marks persist into the running track area. But the running track is disfigured by light scratches or scoring marks (vertical direction). This relatively minor damage might be caused by debris in the oil film rather than direct metal-to-metal contact. There is some evidence of plastic smearing at the boundary between the two main regions. The lower image shows the boundary between the run in

track (right) and the severe scuffing scar (left). Again, the original grinding marks (horizontal) have persisted in the running track region, but are now obliterated by the main scuffing damage. The slight damage to the polished surface in the running track area supports the earlier suggestion that the superfinished surfaces tend to become rougher rather than smoother during running prior to actual scuffing failure.

SEM images of the slow disc used in test UTRC03 are given in Figure 3.27. The upper image shows the edge of the contact depicting the run in surface having vertical scoring marks on the surface to the left of the image. The right part shows the scuffing area.

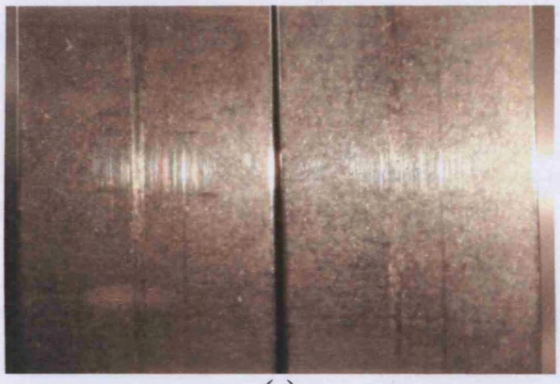

(a)

(b)

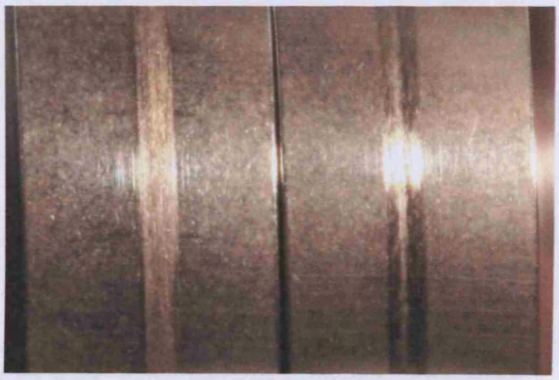

(c)

Figure 3.24. Photographs of discs following testing at 7m/s and 16m/s
(a) UTRC06; left: super finished disc on fast shaft; right: super finished disc on slow shaft
(b) UTRC03; left: super finished disc on fast shaft; right: super finished disc on slow shaft
(c) UTRC04; left: super finished disc on fast shaft; right: super finished disc on slow shaft

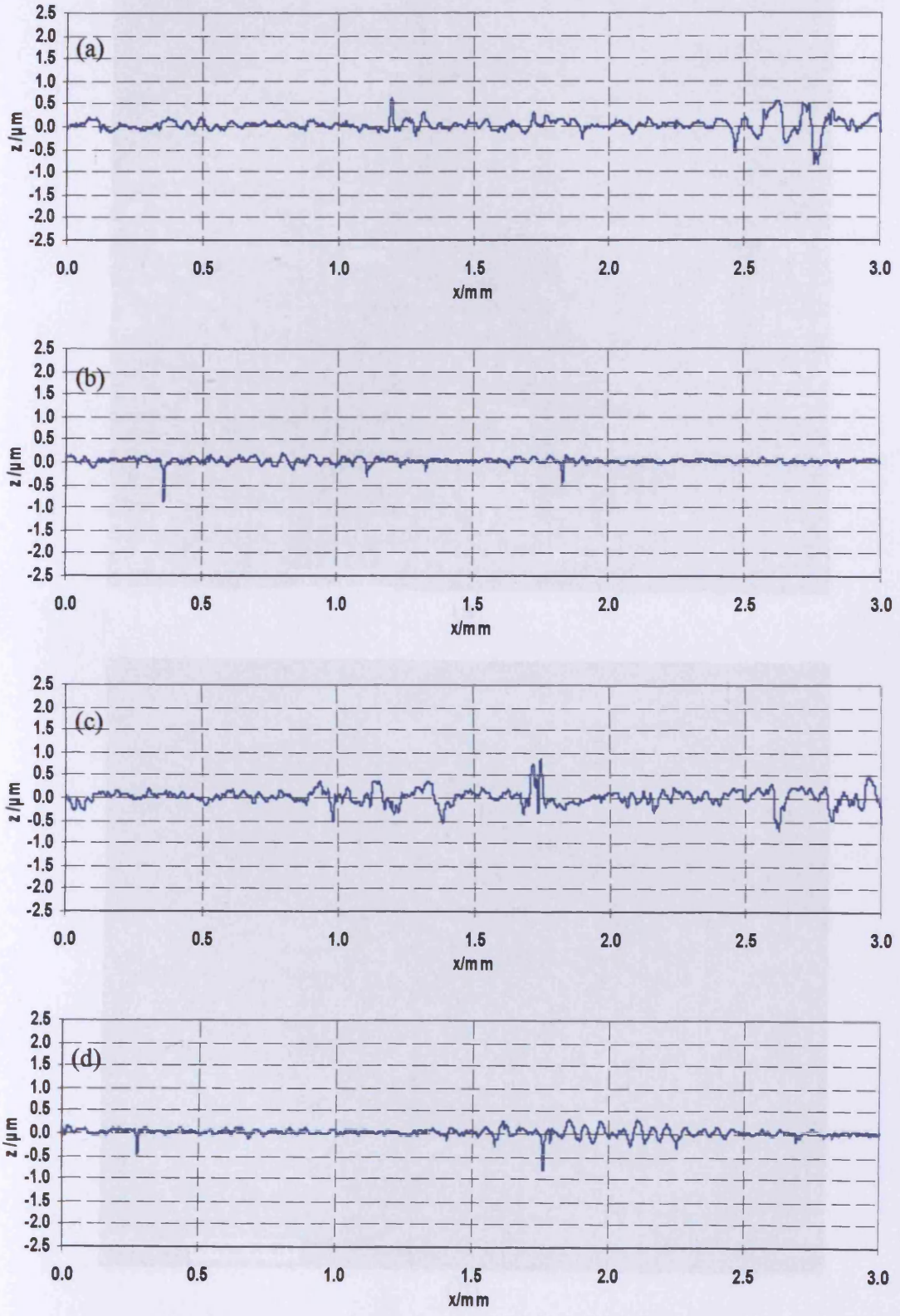

Figure 3.25. Surface profiles taken in the circumferential direction from discs used in test UTRC03
Profiles from fast disc (a) before test; Ra = 0.044 µm (b) after test; Ra = 0.051 µm
Profiles from slow disc (c) before test; Ra = 0.040 µm (d) after test; Ra = 0.062 µm

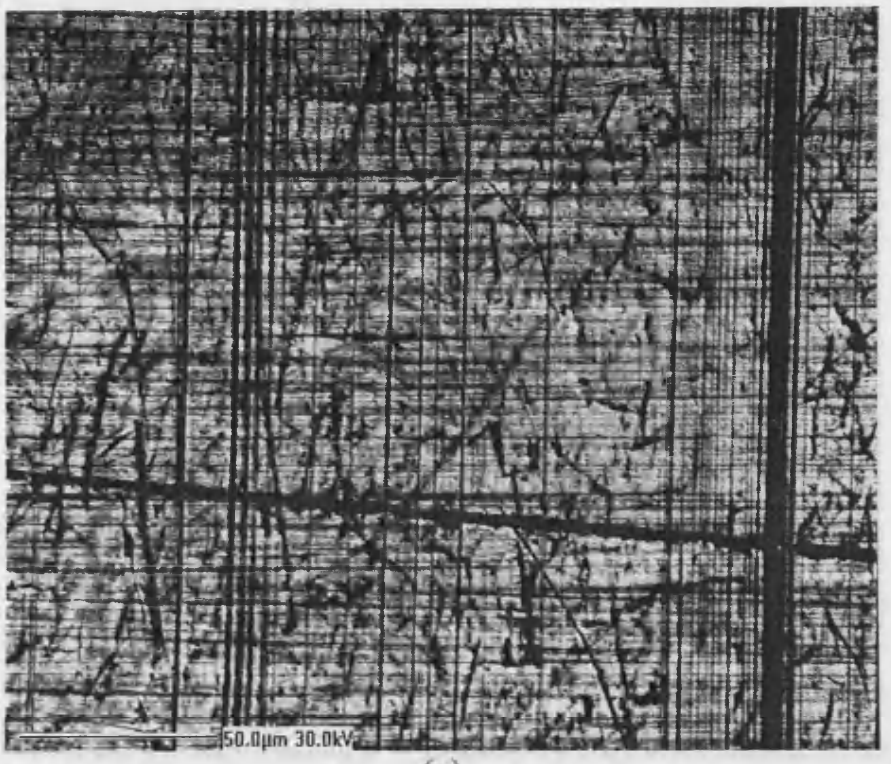

(a)

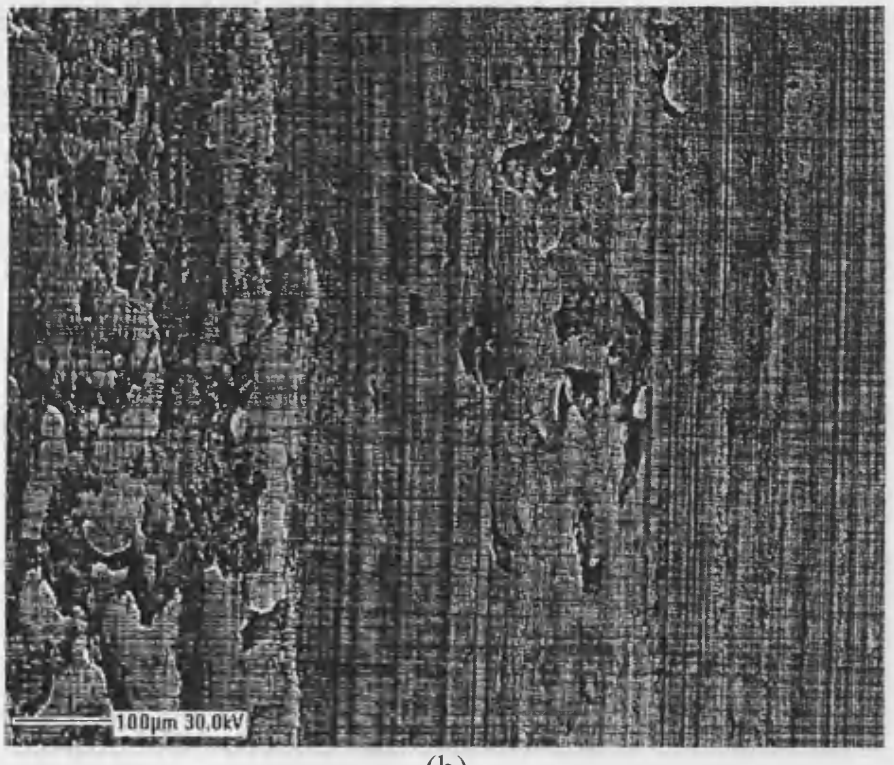

(b)

Figure 3.26. SEM images of surface of the fast disc used in test UTRC03.
(a) edge of the running track with slight scoring marks
(b) scuffing, severe on the left and more lightly on the right side

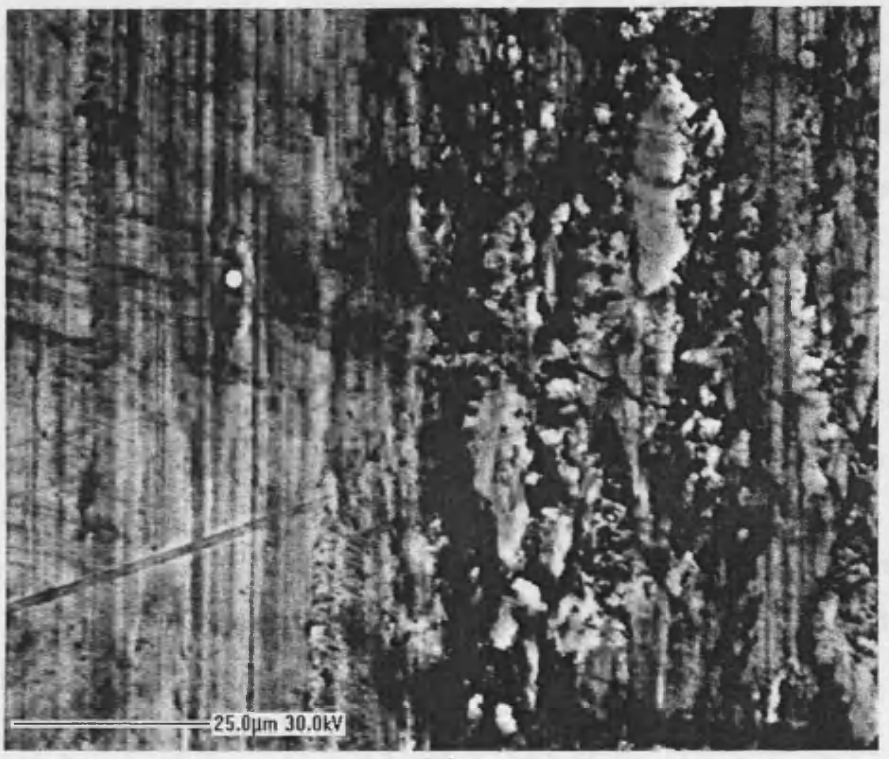

(a)

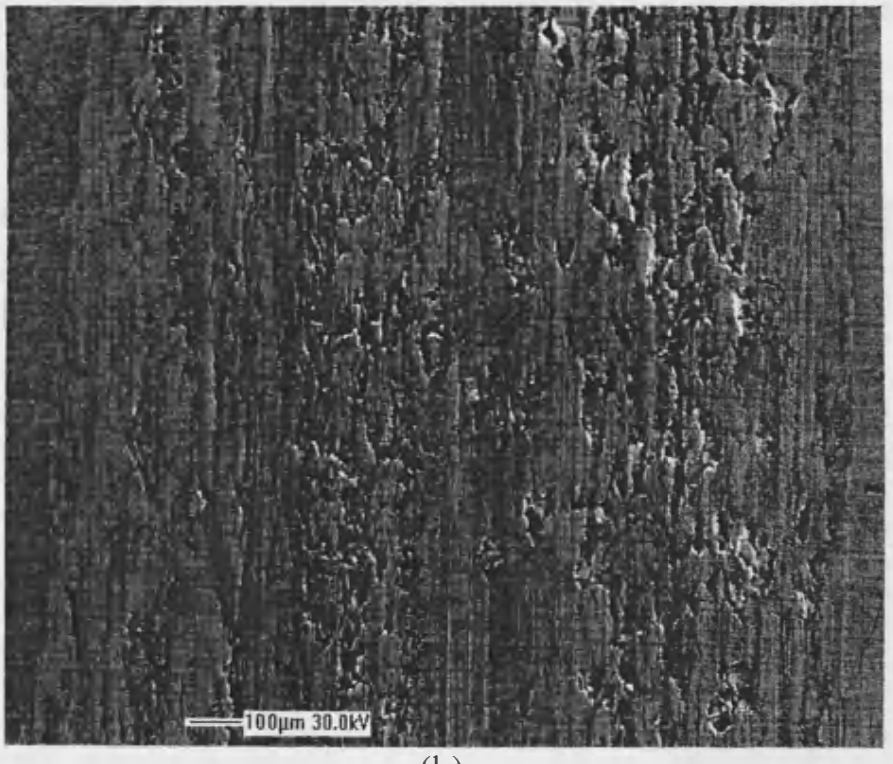

(b)

Figure 3.27. SEM images of surface of the slow disc used in test UTRC03.
(a) scuff taken at a very high magnification on the right with the run in surface
(b) scuffing track in the centre with run on surface on both the sides

3.2.3. Superfinished discs running against ground discs

It was considered to be of interest to investigate the scuffing behaviour of conventional axially finished ground discs running against superfinished discs. This combination of surfaces could occur, for example, in gearing in cases where it was economical to superfinish the smaller of two meshing gears (pinion) but not, perhaps, the larger one (wheel), with the aim of improving the surface durability of both. This arrangement might be particularly worth considering, for example, where the pinion was of a harder material than the wheel, which is often the case in practice. In the rig used in the present work there is a considerable difference in the surface speeds of the contacting discs and it is already clear from the preceding results that the temperatures of the two discs differ considerably, with the temperature of the faster disc achieving a significantly higher temperature than that of the slower disc. It was therefore decided to carry out experiments firstly with the polished disc mounted on the fast shaft and secondly with the ground disc in the fast position. Four tests were carried out at the high sliding speed of 16 m/s. Two tests (UTRC18 and UTRC20) were performed with the polished disc running faster, and two tests (UTRC17 and UTRC19) were undertaken with the ground disc running faster. The records of these four tests are shown in Figures 3.28 to 3.31 and a summary of the results is given in Table 3.5.

Table 3.5.
Summary of scuffing conditions-ground/uncoated discs with superfinished discs at sliding speed of 16m/s

Test	UTRC17		UTRC19		UTRC18		UTRC20	
Configuration	grnd disc on fast shaft				s.f. disc on fast shaft			
Test Discs	utrc84	utrc14	utrc81	utrc17	utrc71	utrc10	utrc73	utrc07
Shaft Mounting	fast	slow	fast	slow	fast	slow	fast	slow
Disc Condition	grnd	s.f.	grnd	s.f.	s.f.	grnd	s.f.	grnd
temperature/°C	297*	228	298*	237	238	151	265	162
Roughness, Ra, before/μm	0.380	0.062	0.394	0.057	0.056	0.371	0.052	0.395
Roughness, Ra, after/μm	0.201	0.152	0.242	0.156	0.179	0.167	0.157	0.202
Scuffing load/N	4922		4934		1850		2325	
Max Hertz pressure/GPa	1.8		1.8		1.3		1.4	
Friction force/N	87		89		68		74	
Friction coefficient	0.017		0.018		0.036		0.039	
Blok flash temp. rise/°C	179		183		228		248	

grnd - ground; s.f.-super finished
* maximum temperature - did not scuff

Figures 3.28 and 3.29 show the records of scuffing tests UTRC17 and UTRC19 respectively. There is evidence of significant running in with the ground disc on the fast shaft. The test was stopped due to high temperatures. Test UTRC 19 was allowed to run on for about six minutes after load stage 12 when the temperature approached 300°C. During this extended period both temperature and friction began to fall. Records of scuffing tests UTRC18 and UTRC20 with the superfinished surfaces on the fast shaft are given in Figures 3.30 and 3.31. This pair of tests show good repeatability and both the tests scuffed at load stage 8 (1850 N).

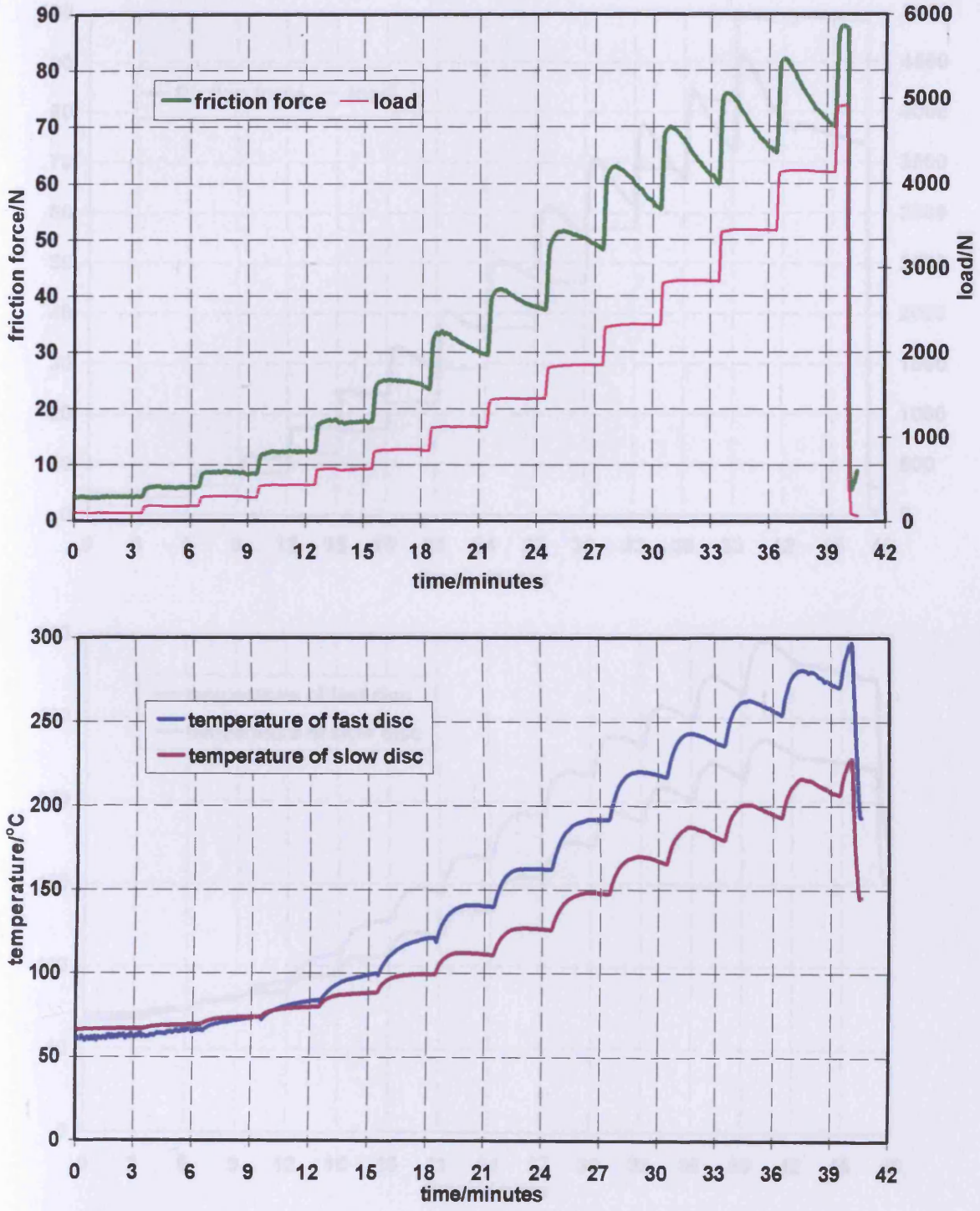

Figure 3.28. Record of scuffing test UTRC17, upper graph shows applied load and friction force; lower graph shows bulk temperatures of the two discs

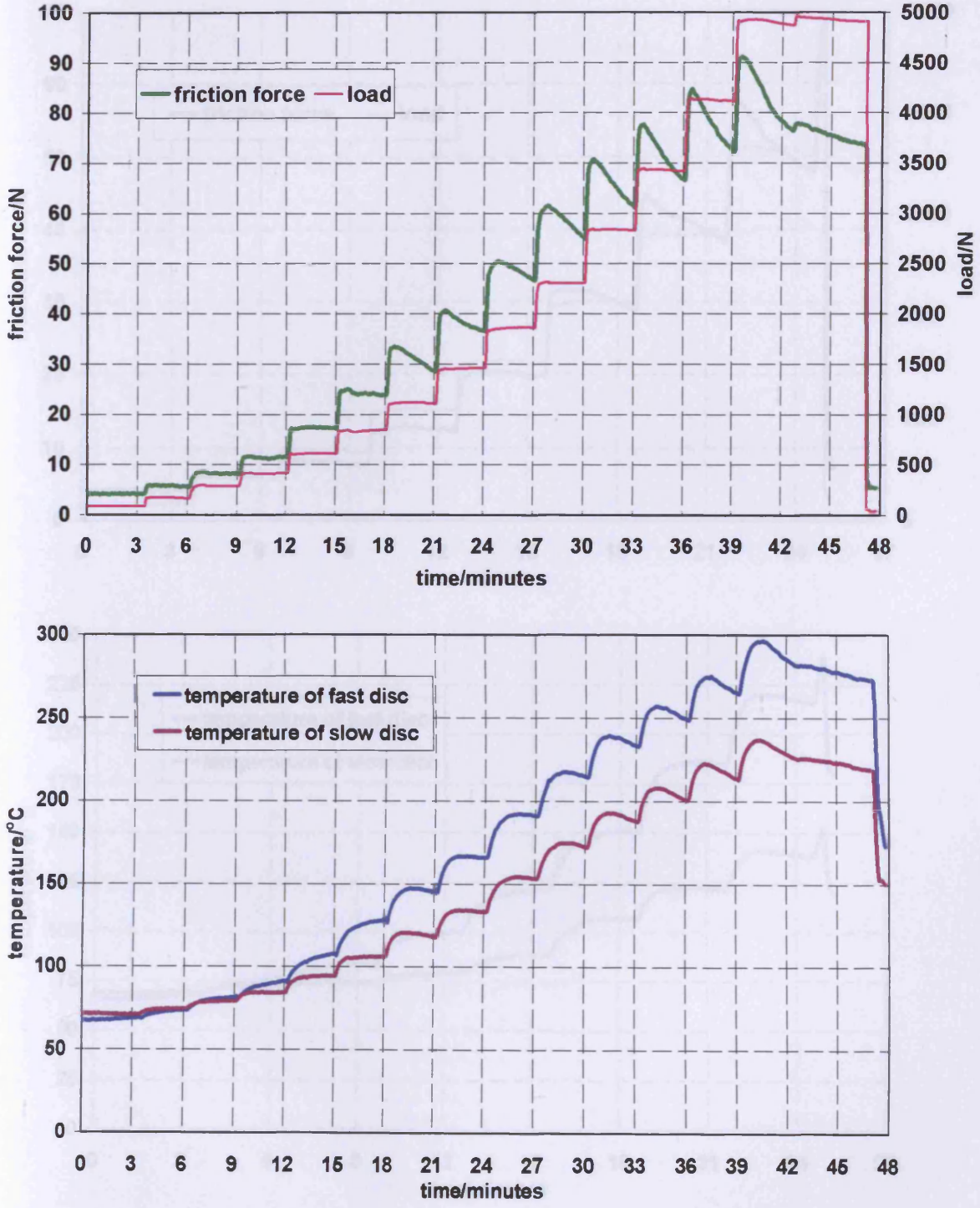

Figure 3.29. Record of scuffing test UTRC19, upper graph shows applied load and friction force; lower graph shows bulk temperatures of the two discs

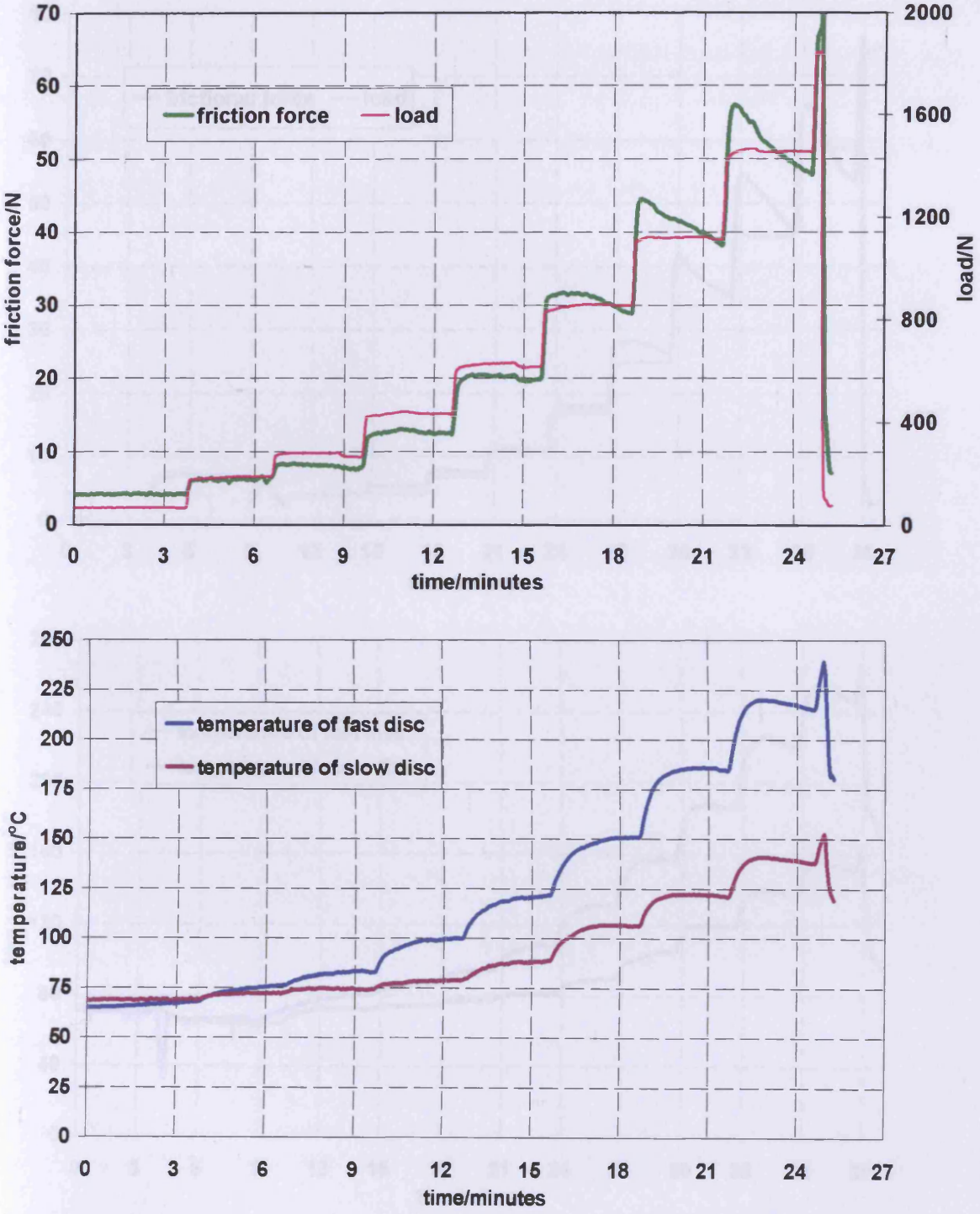

Figure 3.30. Record of scuffing test UTRC18, upper graph shows applied load and friction force; lower graph shows bulk temperatures of the two discs

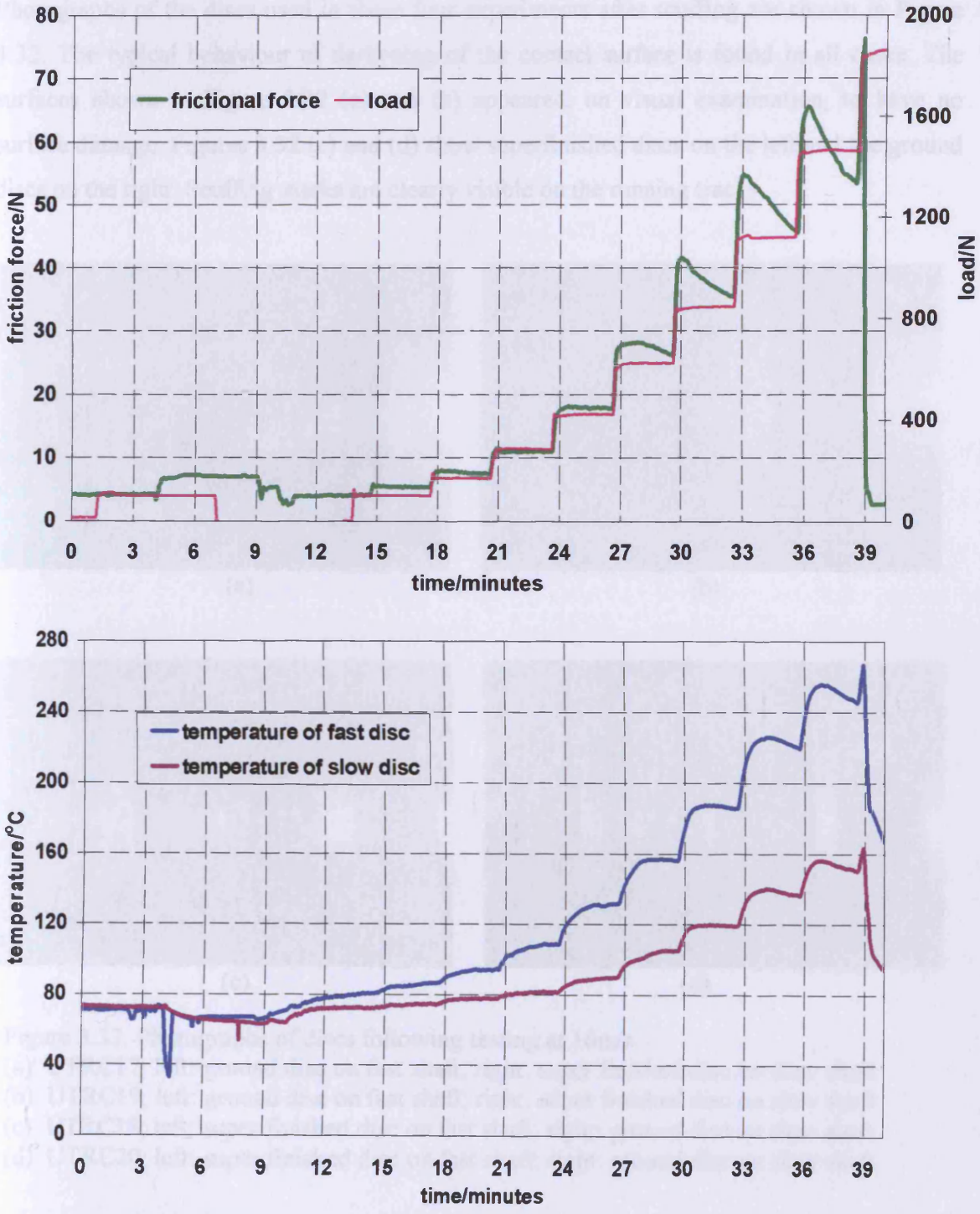

Figure 3.31. Record of scuffing test UTRC20, upper graph shows applied load and friction force; lower graph shows bulk temperatures of the two discs

Photographs of the discs used in these four experiments after scuffing are shown in Figure 3.32. The typical behaviour of darkening of the contact surface is found in all cases. The surfaces shown in Figure 3.32 (a) and (b) appeared, on visual examination, to have no surface damage. Figures 3.32 (c) and (d) show superfinished discs on the left and the ground discs on the right. Scuffing marks are clearly visible on the running tracks.

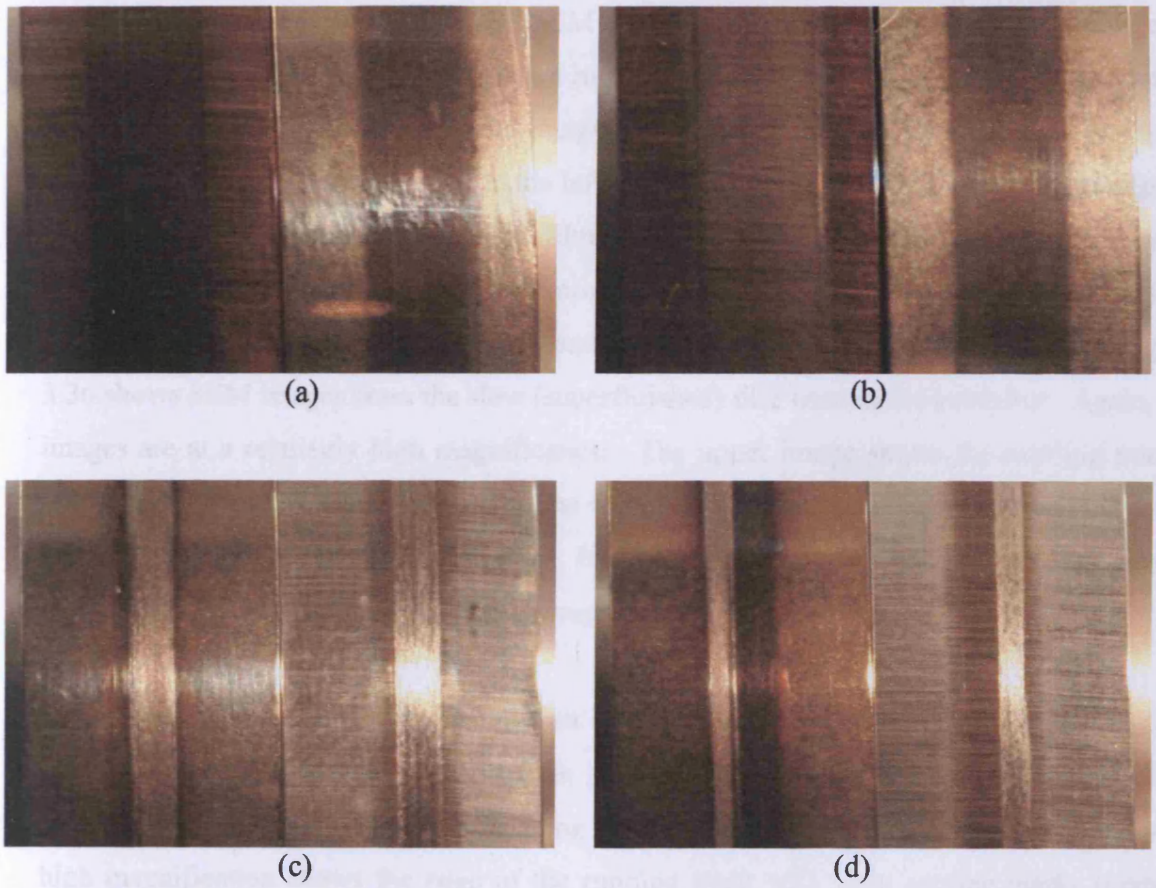

Figure 3.32. Photographs of discs following testing at 16m/s
(a) UTRC17; left: ground disc on fast shaft; right: super finished disc on slow shaft
(b) UTRC19; left: ground disc on fast shaft; right: super finished disc on slow shaft
(c) UTRC18; left: super finished disc on fast shaft; right: ground disc on slow shaft
(d) UTRC20; left: super finished disc on fast shaft; right: ground disc on slow shaft

Circumferential profiles from the discs used in test UTRC17 before and after scuffing are shown in Figure 3.33 for the case where the ground discs ran faster, and Figure 3.34 shows corresponding profiles from test UTRC18 in which the superfinished disc was on the fast shaft. Again, it should be noted that the profiles taken after scuffing are from the run but unscuffed parts of the discs. There is the now expected reduction in the roughness of the

ground surfaces as a result of running, particularly in the case of discs that failed at the higher loads.

The most interesting aspect of these experiments in which polished discs were run against rough ones is the significantly higher scuffing load experienced when the polished surface is the more slowly moving of the pair. This aspect will be examined further in the series of experiments reported in Chapter 4. SEM images from these experiments are shown in Figures 3.35 to 3.38. Figure 3.35 shows high magnification SEM images from the ground disc used in test UTRC17. The upper image shows the edge of the running track. The track is to the right and un-run surface is to the left. A slight scoring is present close to the edge of the track which suggests that the EHL film was thinner at this point. The lower image is taken from near the middle of the running track and shows evidence of severe plastic deformation in the form of smearing caused by sliding in the downwards direction. Figure 3.36 shows SEM images from the slow (superfinished) disc used in the same test. Again, the images are at a relatively high magnification. The upper image shows the scuffing scar to the left and un-run, polished, surface to the right. The lower image shows the run in part of the running track of the polished surface, but there is evidence of the ground disc, against which it ran, producing an imprinting of roughness.

Figure 3.37 shows SEM images of the fast disc (superfinished) used in test UTRC18. The upper image is a typical unrun part of the superfinished disc. This shows remaining deep grinding marks following the superfinishing treatment. The lower image taken at a relatively high magnification shows the edge of the running track with light scoring marks (vertical lines) and one of the deep grinding marks which is about 5 μm wide in this case. Figure 3.38 shows SEM images of the ground disc used on the slow shaft in the same test. The upper image shows the unrun ground surface with peaks and valleys. There is no evidence of running as would be expected since the image is from outside the running track. The lower image shows the edge of the contact with ground but run in surface to the left of the image and scuffing damage to the right. The run in area has the characteristic lands caused by flattening of the high points of the profile.

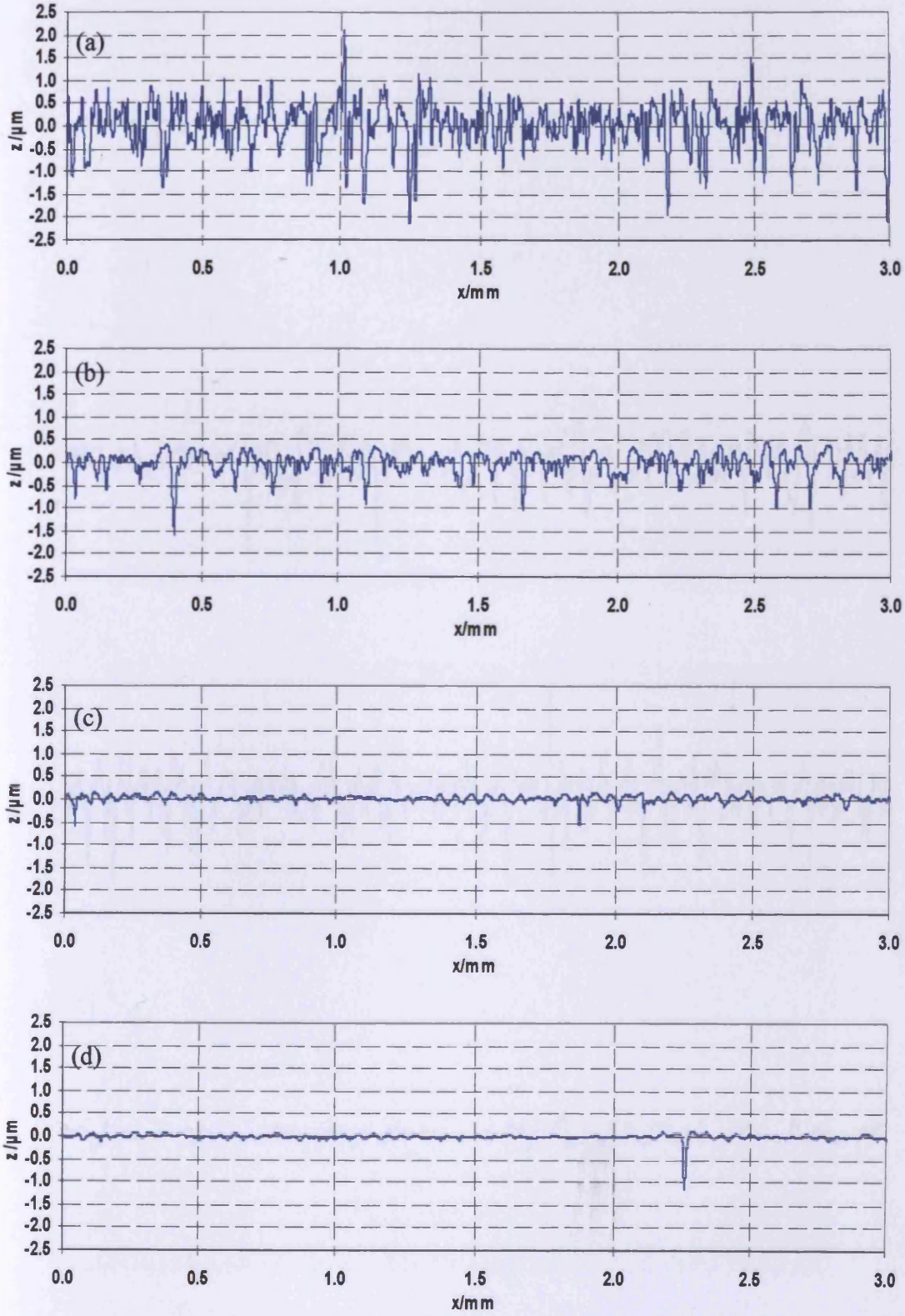

Figure 3.33. Surface profiles taken in the circumferential direction from discs used in test UTRC17
Profiles from fast disc (a) before test; Ra = 0.371 µm (b) after test; Ra = 0.216 µm
Profiles from slow disc (c) before test; Ra = 0.055 µm (d) after test; Ra = 0.148 µm

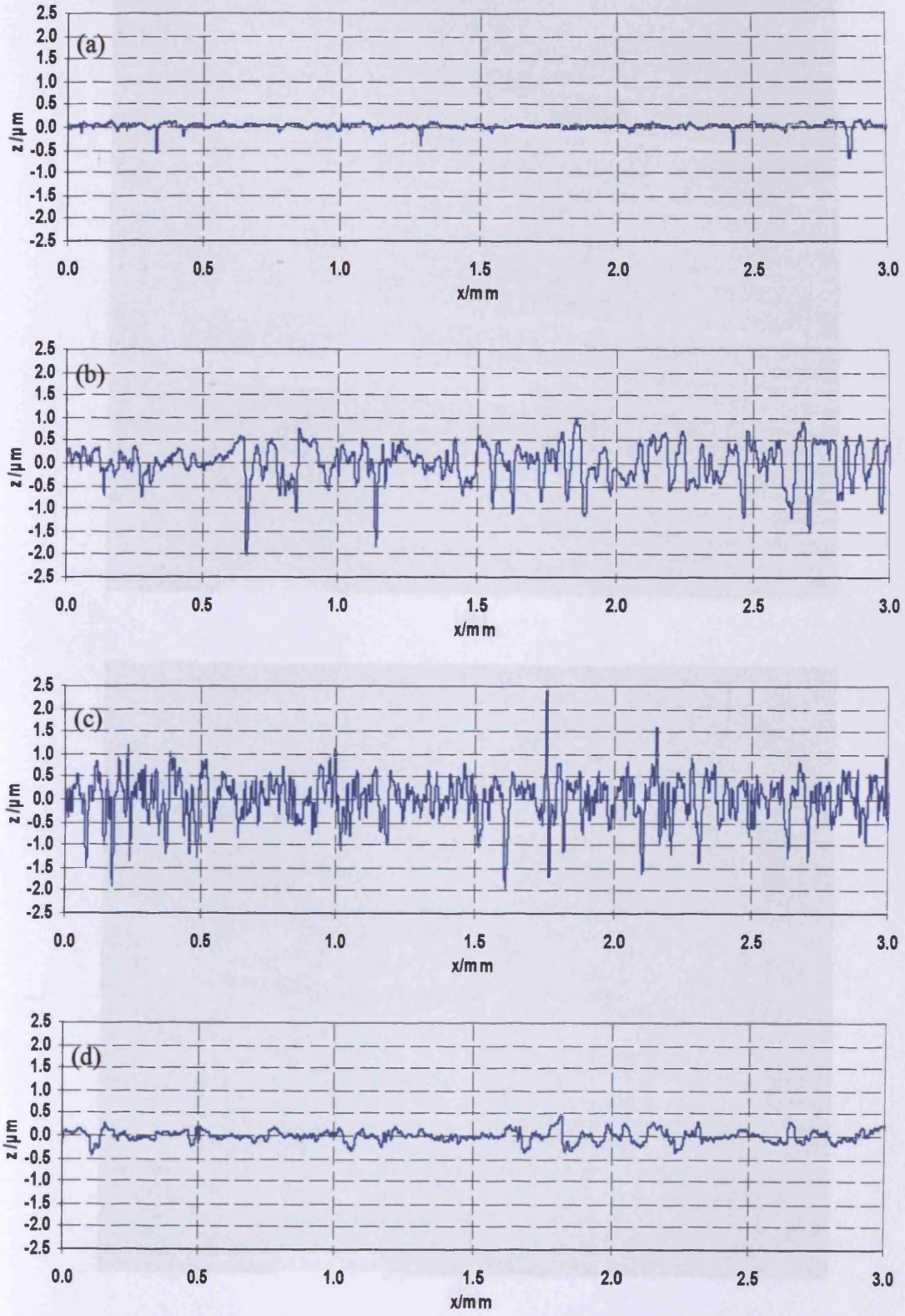

Figure 3.34. Surface profiles taken in the circumferential direction from discs used in test UTRC18
Profiles from fast disc (a) before test; Ra = 0.053 µm (b) after test; Ra = 0.251 µm
Profiles from slow disc (c) before test; Ra = 0.354 µm (d) after test; Ra = 0.199 µm

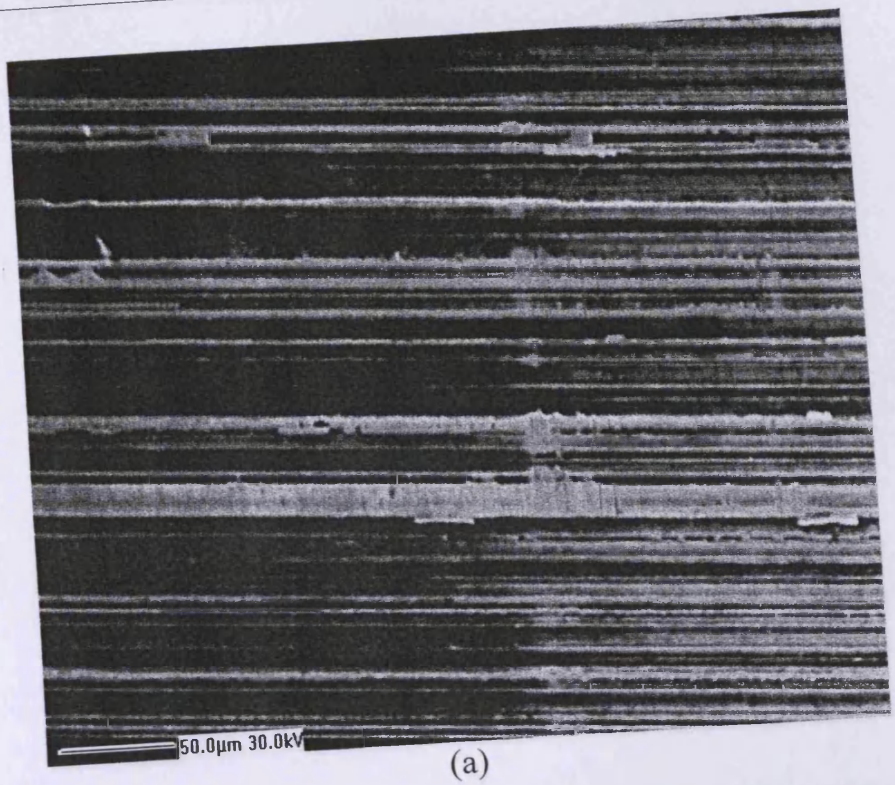

(a)

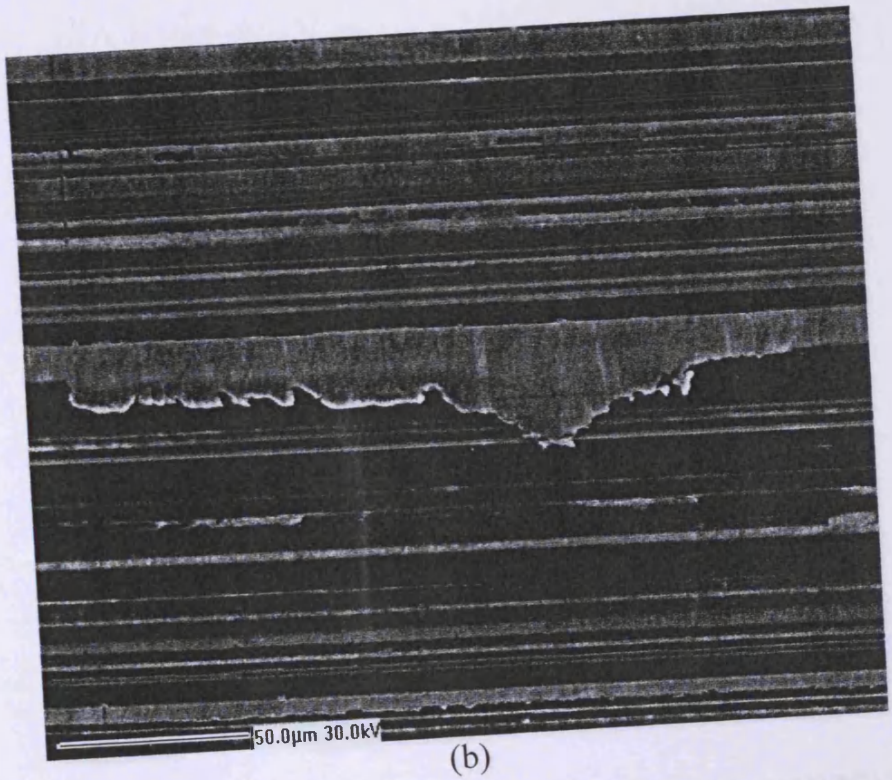

(b)

Figure 3.35. SEM images of surface of the fast disc used in test UTRC17.
(a) the edge of unrun surface with the run part of the disc to the right
(b) evidence of material movement or removal in the run part

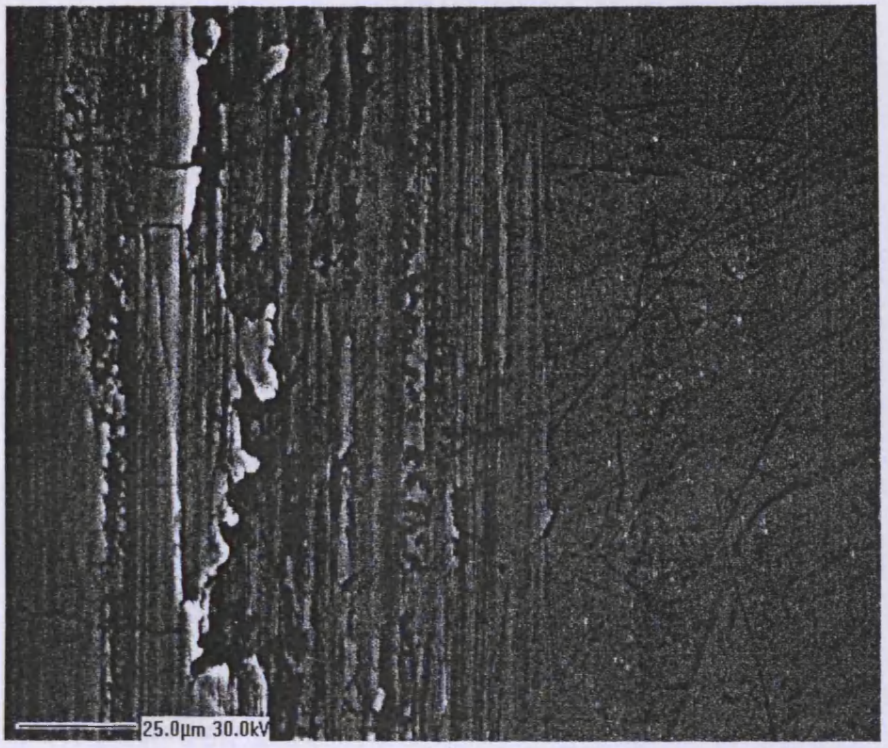

(a)

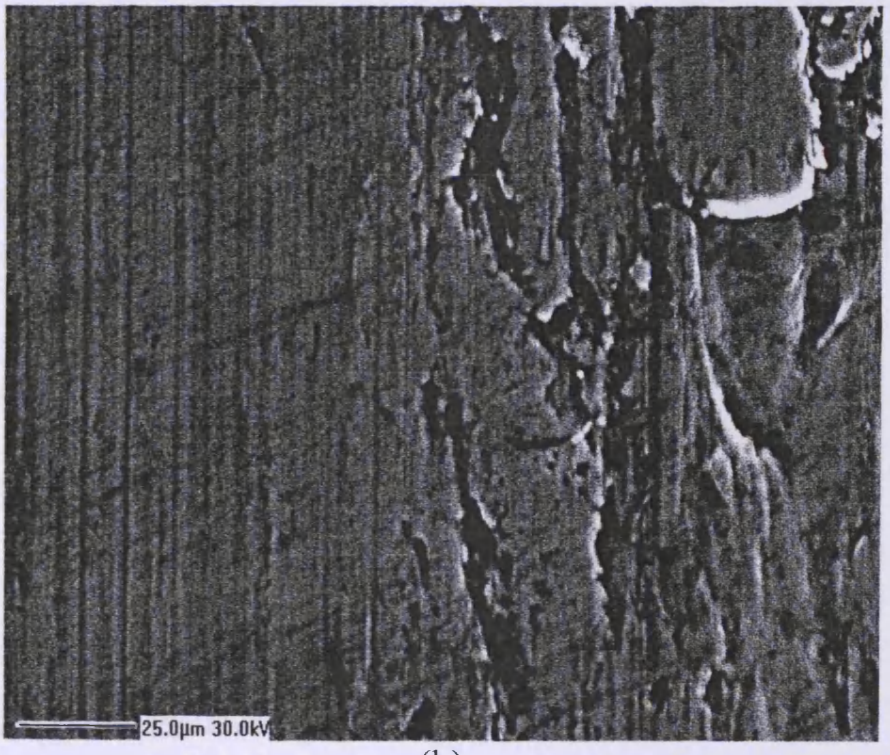

(b)

Figure 3.36. SEM images of surface of the slow disc used in test UTRC17.
(a) scuffed part on the edge of the contact on the left with unrun part to the right
(b) run in part on the left with the scuffed region on the right

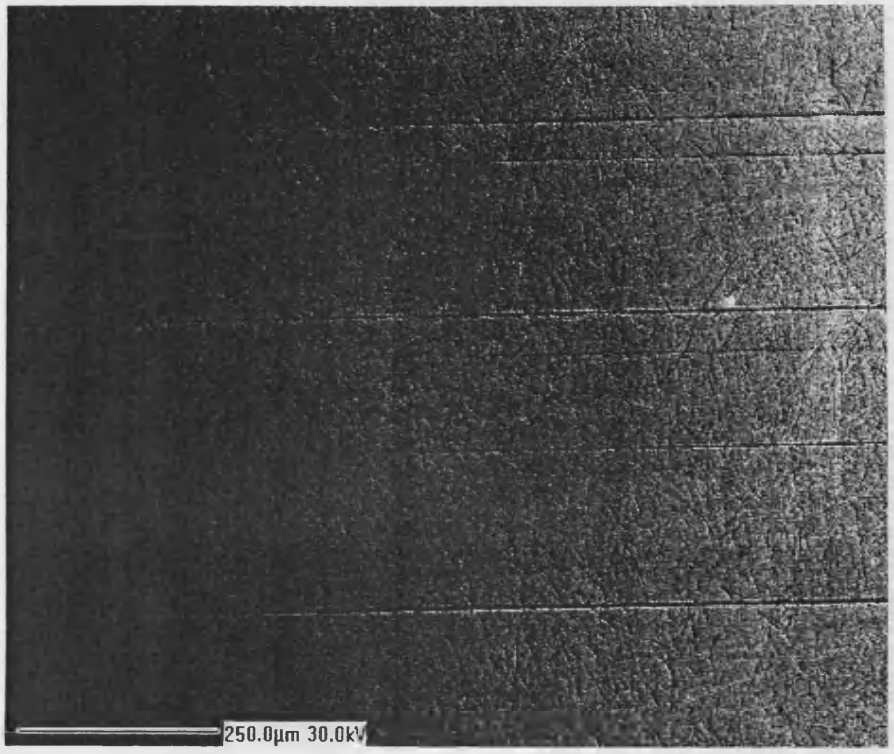

(a)

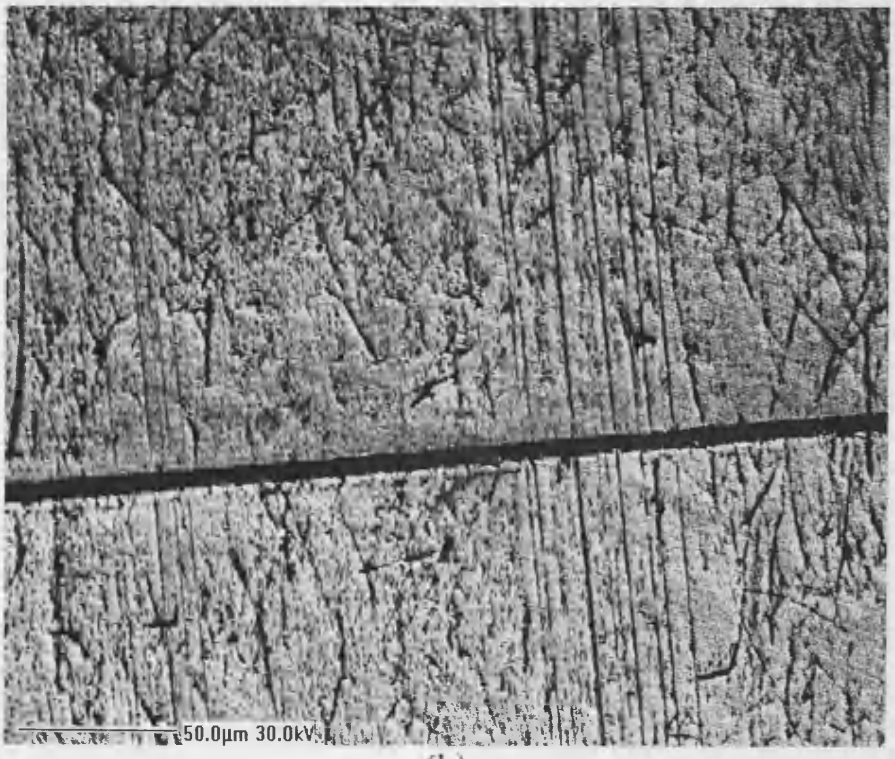

(b)

Figure 3.37. SEM images of surface of the fast disc used in test UTRC18.
(a) unrun condition of the superfinished disc
(b) edge of the running track with light scoring and a deep grinding mark

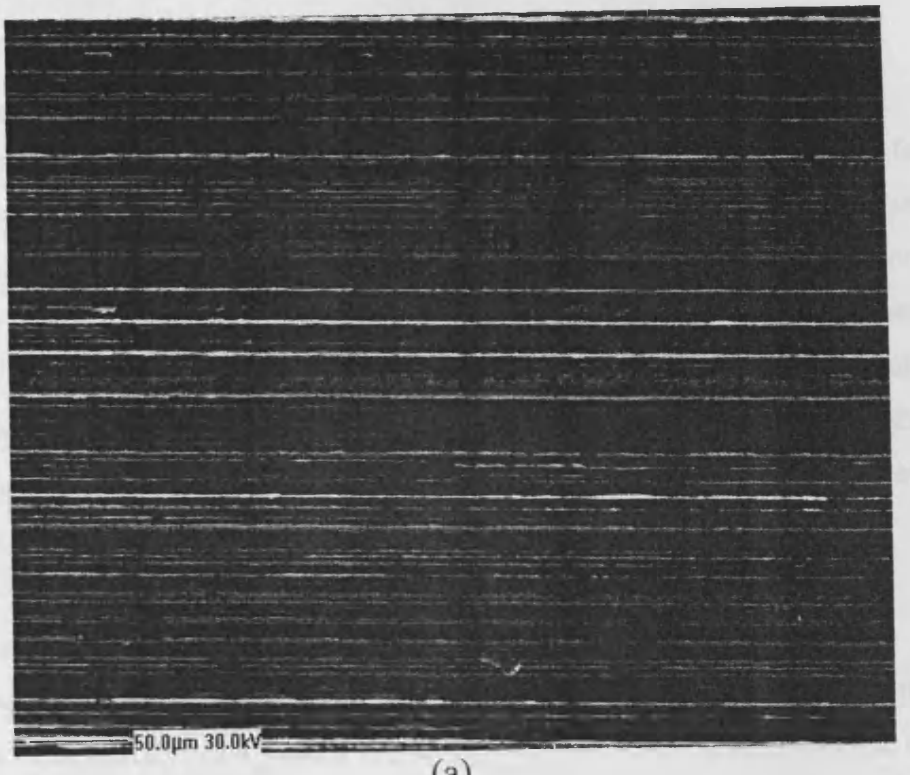

(a)

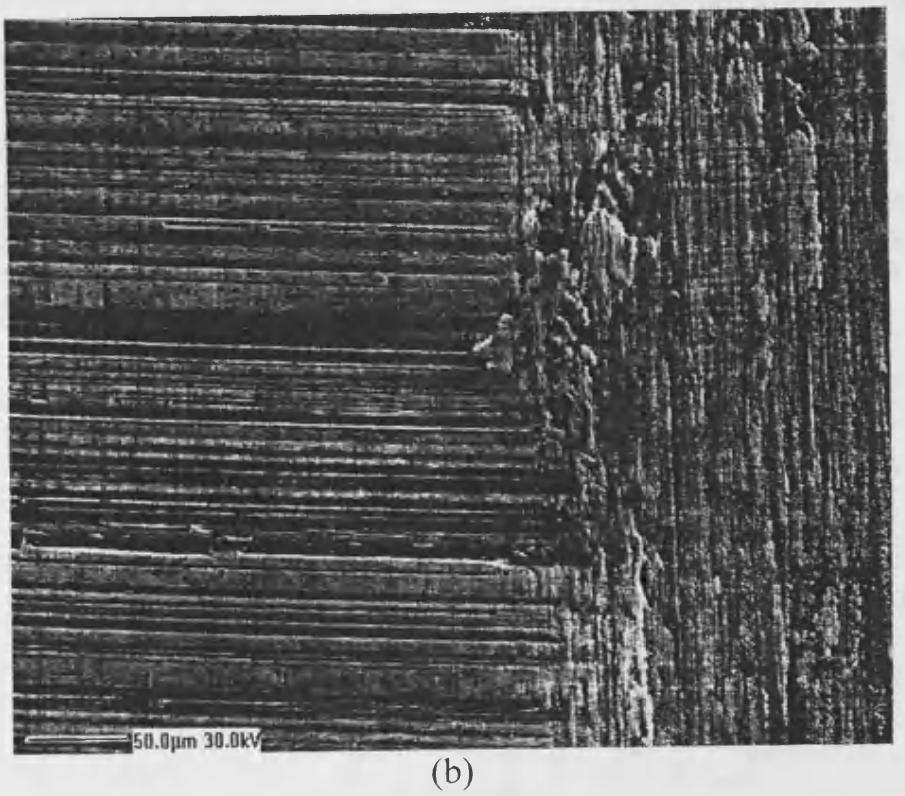

(b)

Figure 3.38. SEM images of surface of the slow disc used in test UTRC18.
(a) unrun condition of the disc
(b) edge of scuff with the run in surface to the left

3.3. Tests on coated discs

3.3.1. Introduction

Three kinds of test were performed involving coated discs as follows. In the first series axially ground and coated discs were used on both shafts of the rig. The second series used superfinished and coated discs, and in the third series ground/coated discs were run against ground but uncoated specimens. A point of general interest in these tests with ground/coated samples is that after coating the roughness of the discs decreased slightly, typically falling from about 0.4 μm Ra to about 0.35 μm Ra. The reverse effect occurred in the case of superfinished discs, i.e. the roughness of superfinished discs after coating was slightly higher than the un-coated sample.

3.3.2. Ground/coated discs running against ground/coated discs

Six experiments were conducted with this combination of surfaces with two tests being carried out at each of the three sliding speeds of 16.0, 12.0 and 7.0 m/s. Records of the two tests at 16 m/s (tests UTRC09 and UTRC12) are shown in Figures 3.39 and 3.40, and a summary of the conditions at the heaviest load attained are shown in Table 3.6.

Table 3.6.
Summary of scuffing conditions - ground/hard coated discs at sliding speed of 16m/s

Test	UTRC09		UTRC12	
Test Discs	utrc83	utrc12	utrc70	utrc21
Shaft Mounting	fast	slow	fast	slow
Disc Condition	grnd/h.c.	grnd/h.c.	grnd/h.c.	grnd/h.c.
temperature/°C	272*	186	284*	160
Roughness, Ra, before/μm	0.369	0.343	0.340	0.318
Roughness, Ra, after/μm	0.193	0.169	0.159	0.192
Scuffing load/N	3466		3454	
Max Hertz pressure/GPa	1.6		1.6	
Friction force/N	63		42	
Friction coefficient	0.018		0.012	
Blok flash temp. rise/°C	155		103	

grnd/h.c. - hard coated
* maximum temperature – did not scuff

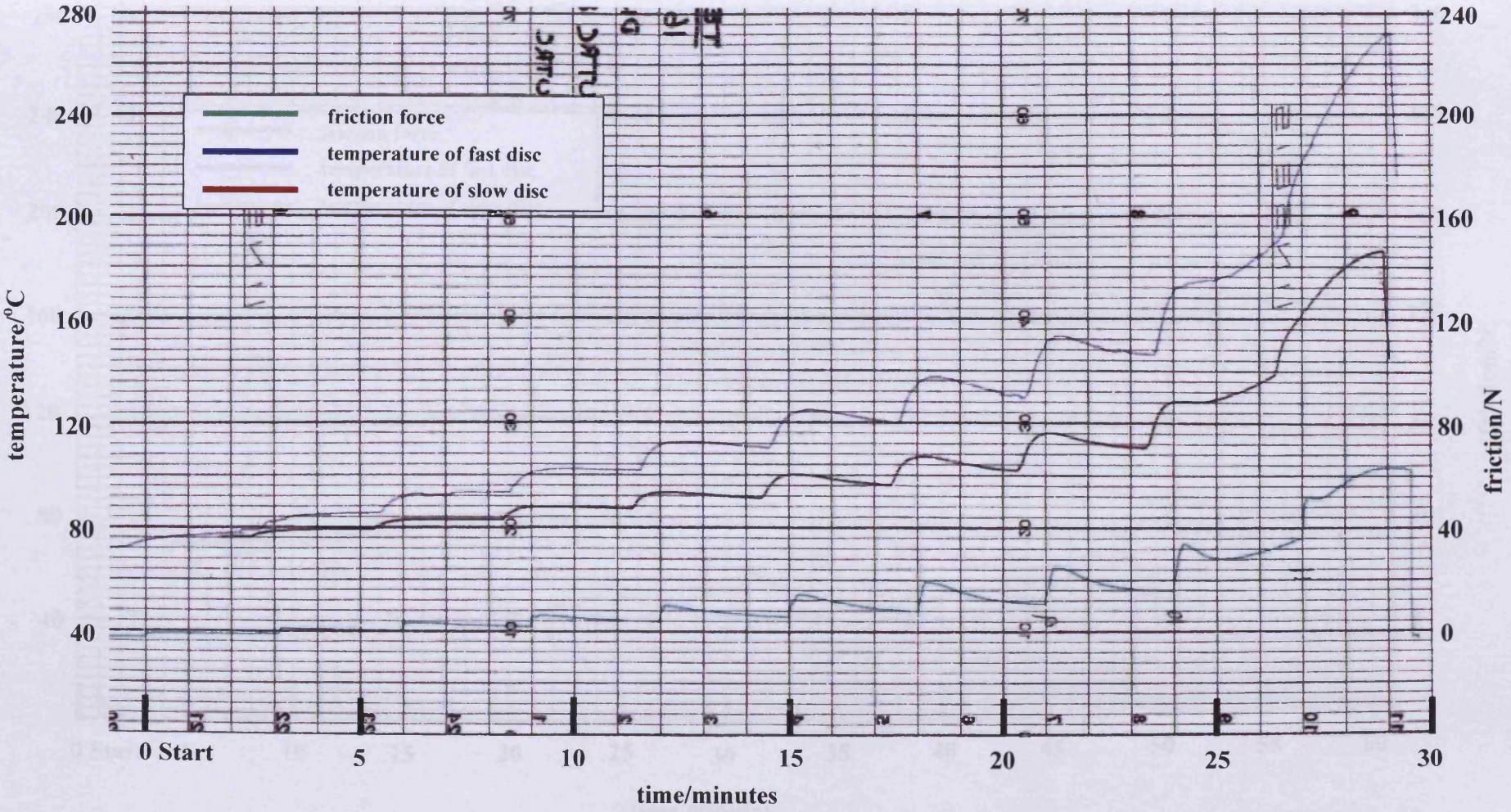

Figure 3.39. Chart recorder record of test UTRC09, graph shows friction force and bulk temperatures of two discs

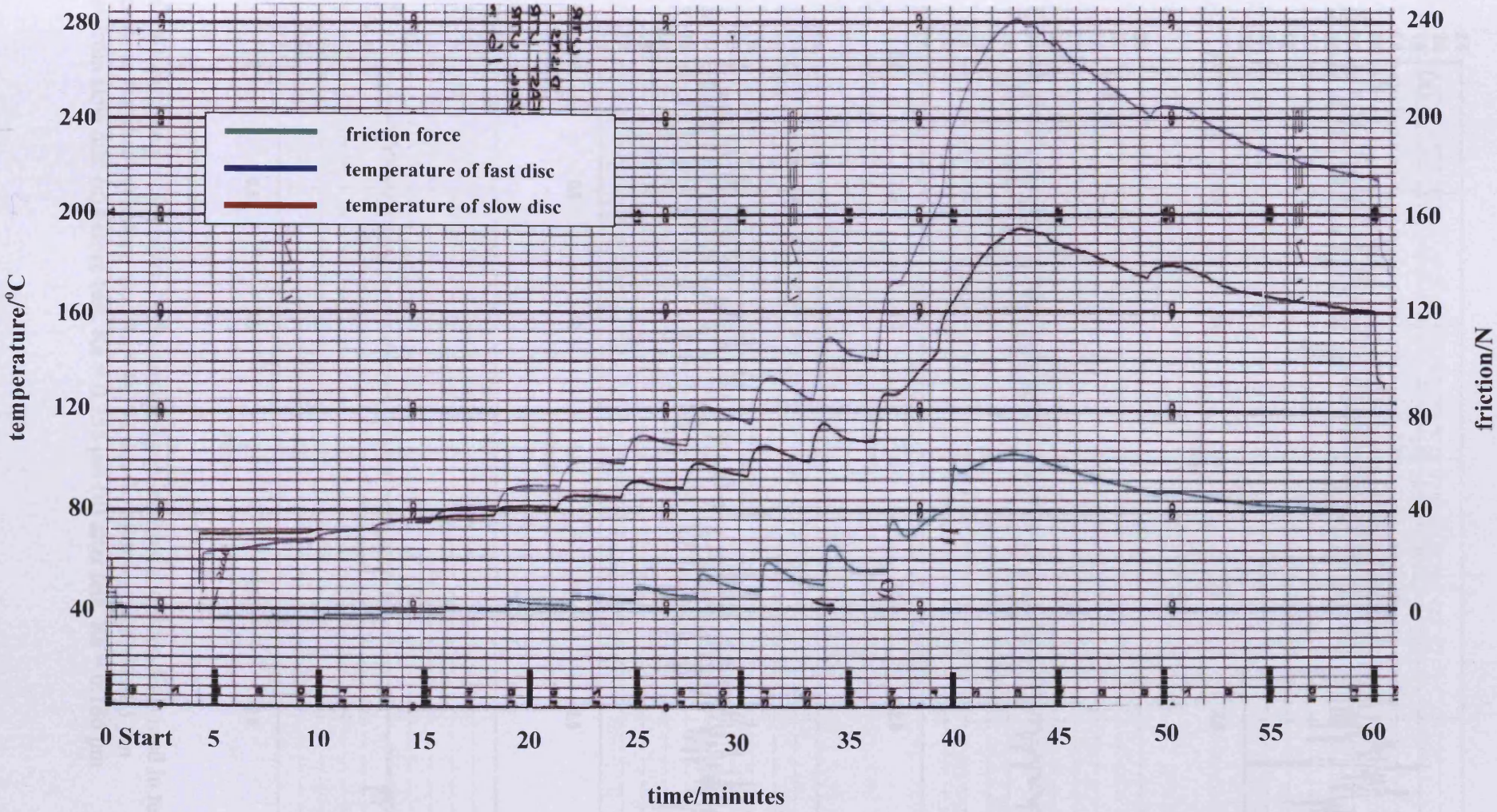

Figure 3.40. Chart recorder record of test UTRC12, graph shows friction force and bulk temperatures of two discs

In neither of these tests at the severe sliding speed of 16 m/s was scuffing achieved. In test UTRC09 the test progressed in the expected way until load stage 11 at which point the friction and temperatures began to rise in what appeared to be a situation leading to scuffing. The test was discontinued towards the end of this stage because the temperature of the fast disc had reached over 270°C. This behaviour suggested a deterioration of the coating, but upon visual examination the surface did not appear to have scuffed in the accustomed fashion. The relatively undamaged appearance of the surfaces is illustrated in the photograph of the discs used in this test shown in figure 3.41(a). The operating conditions of this test were repeated in test UTRC12. The record of this test is shown in Figure 3.40. The same behaviour seen in the previous test recurred. During the same load stage (stage 11) the friction and temperatures began to rise as in the previous test. In this case the test was not stopped immediately but was allowed to run on for approximately 25 minutes. During this extended period the temperature of the fast disc reached a maximum level of approximately 280°C, after which the friction and temperatures fell back. After a further period of running the test was eventually stopped at which stage the temperature of the fast disc had fallen to about 220°C. Again, upon visual inspection there was no indication of a conventional scuffing failure. The surfaces are shown in the photograph given in Figure 3.41(b). It is again very noticeable that the faster of the two discs in both these tests became very discoloured with a dark appearance. There is also a very striking "edge effect" present on the discs corresponding to a dark circumferential band; this is particularly evident in Figure 3.41 (a), left and (b), right. This local effect is probably associated with thinning of the EHL film at the edge of the running track.

(a) (b)

Figure 3.41. Photographs of discs following testing at 16m/s
(a) UTRC09; left: ground coated disc on fast shaft; right: ground coated disc on slow shaft
(b) UTRC12; left: ground coated disc on fast shaft; right: ground coated disc on slow shaft

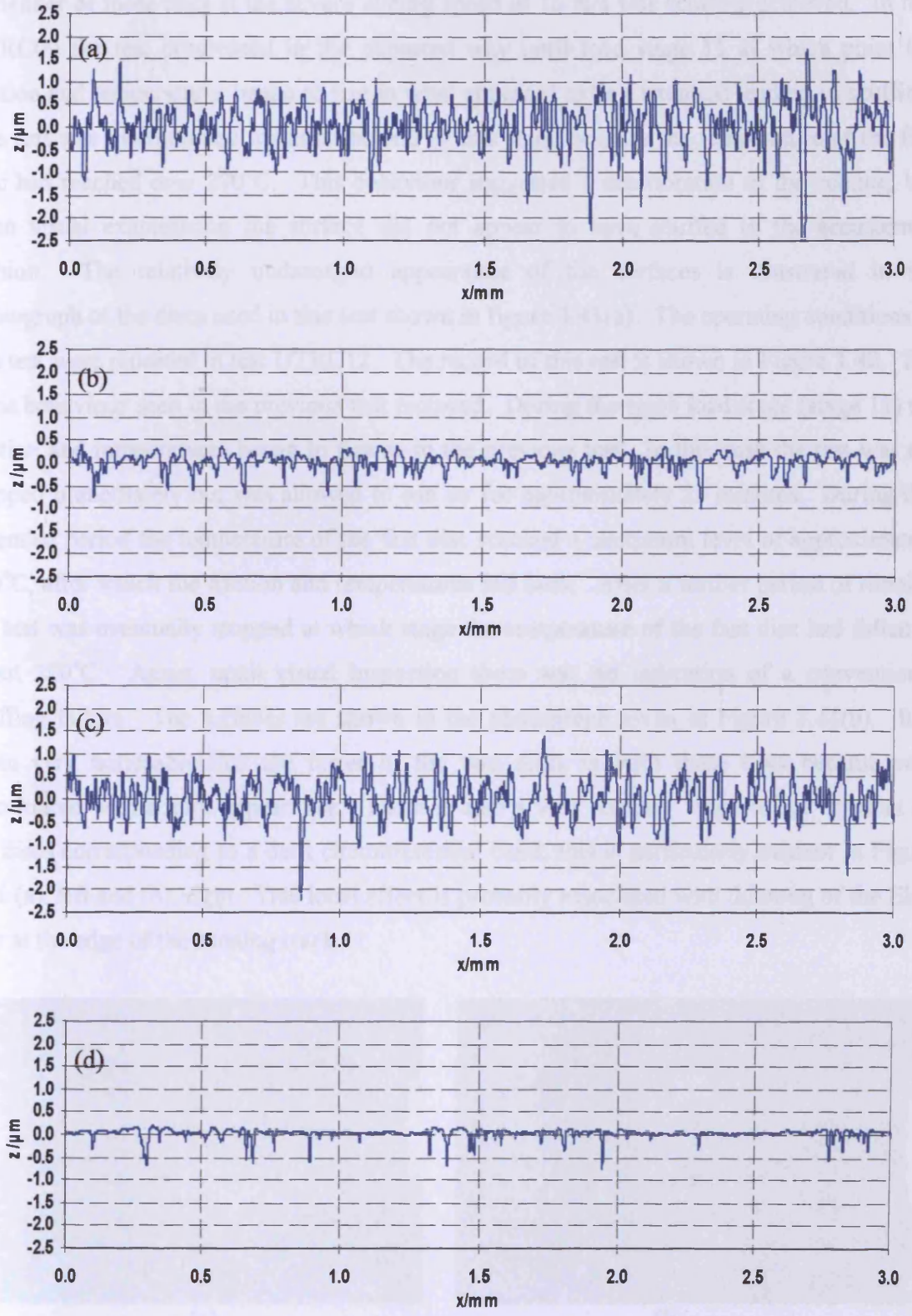

Figure 3.42. Surface profiles taken in the circumferential direction from discs used in test UTRC09
Profiles from fast disc (a) before test; Ra = 0.392 µm (b) after test; Ra = 0.203 µm
Profiles from slow disc (c) before test; Ra = 0.355 µm (d) after test; Ra = 0.186 µm

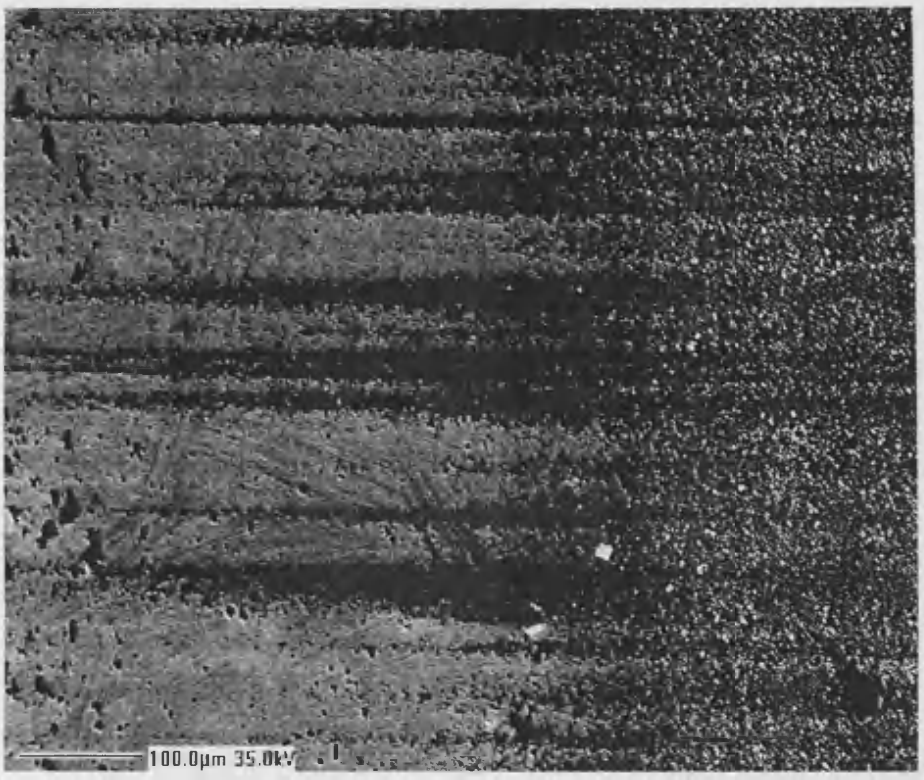

(a)

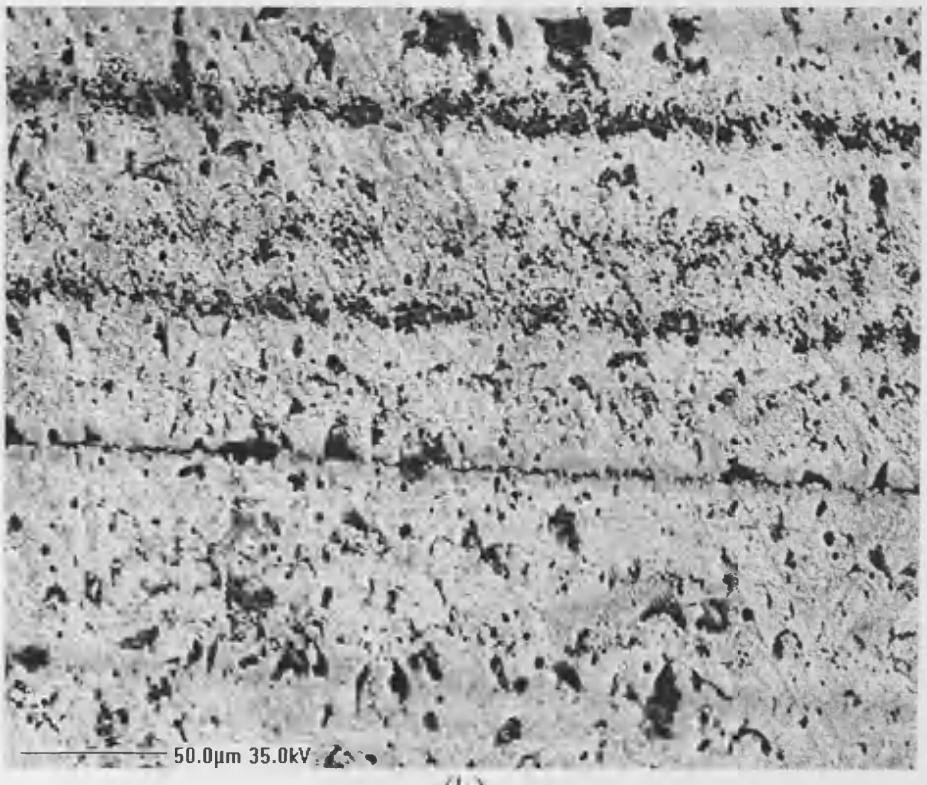

(b)

Figure 3.43. SEM images of surface of the fast disc used in test UTRC12.
(a) unrun condition of the disc on the right with the run in surface to left
(b) middle of the running track showing polished appearance

(a)

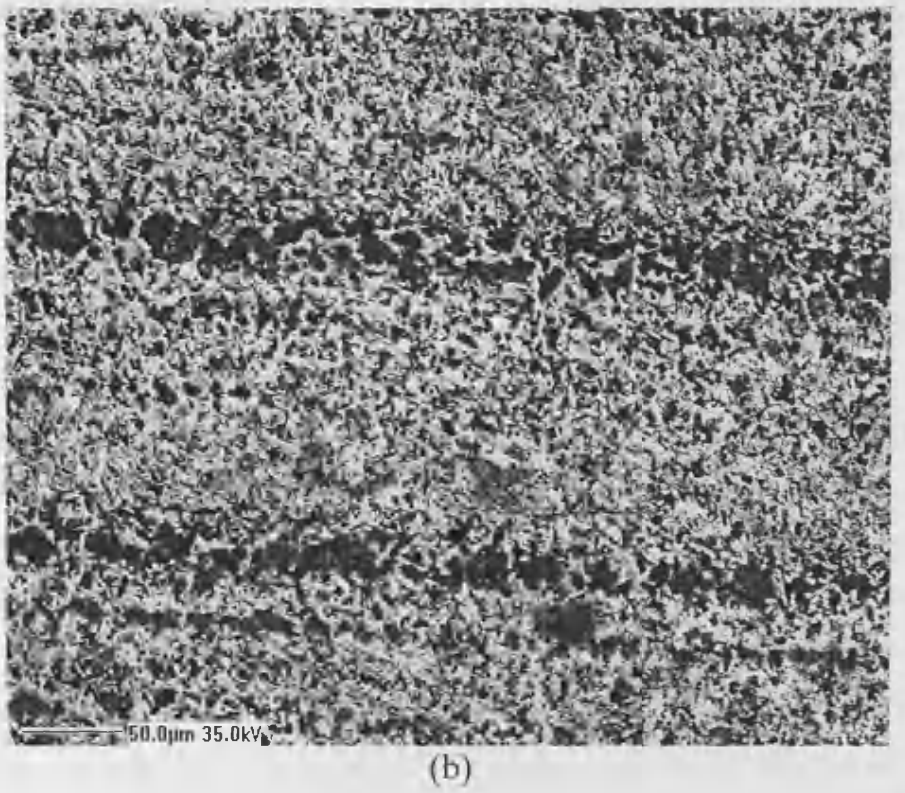

(b)

Figure 3.44. SEM images of surface of the slow disc used in test UTRC12.
(a) evidence of coating removal from the running track
(b) middle of the running track with removal of coating

Circumferential profiles from the two discs used in test UTRC09 are shown in Figure 3.42. Figure 3.42 (a) and (b) show profiles from the fast disc before and after test, respectively, and Figure 3.42 (c) and (d) are profiles from the slow disc before and after test, respectively. There is strong evidence of running in in both cases. The slower disc is particularly affected and becomes significantly smoother as a result of running under these severe conditions.

SEM images from the discs used in test UTRC12 are shown in Figures 3.43 and 3.44. Figure 3.43 shows images from the fast disc. The upper image shows the edge of the running track with unrun surface to the right and run surface to the left. Running produces a brightening or polished appearance of the coating, leaving the deepest valleys untouched and darker in appearance. The lower image is from near the middle of the running track and again shows the polished high points of the surface and the remaining, untouched valley features. A similar behaviour is seen in the case of the slow disc as shown in Figure 3.44. The upper image is again from the edge of the running track and the lower image, at a higher magnification is from the middle of the running track. The run surface has a characteristic grainy or mottled appearance.

Records of the tests run at the intermediate sliding speed of 12 m/s are shown in Figures 3.45 and 3.46. The same behaviour as seen in the test at the high sliding speed of 16 m/s is repeated in both cases. The running in tendency is less pronounced which indicates less interaction of the surfaces. Test UTRC10 was run to load stage 14. Up to the end of load stage 10 the test progressed in a familiar pattern, with friction at first rising and then falling slightly. After the application of load stage 11, however, the friction continued to rise during the load stage. It was decided to progress with further load stages in spite of this behaviour. During load stage 12 the situation appeared to stabilise and friction steadied as did the temperatures towards the end of this interval. The test was continued with application of load stages 13 and 14. But shortly after the start of stage 14 the test was aborted because of a very high temperature reading on the fast disc of about 280°C. The conditions of this test were repeated in test UTRC 11 with much the same results as shown in the record of Figure 3.46. In this case load stage 12 was the highest load achieved and the test was run on at this load for about 20 minutes, during which period the friction and temperatures fell back and appeared to stabilise with a maximum fast disc temperature of about 200°C.

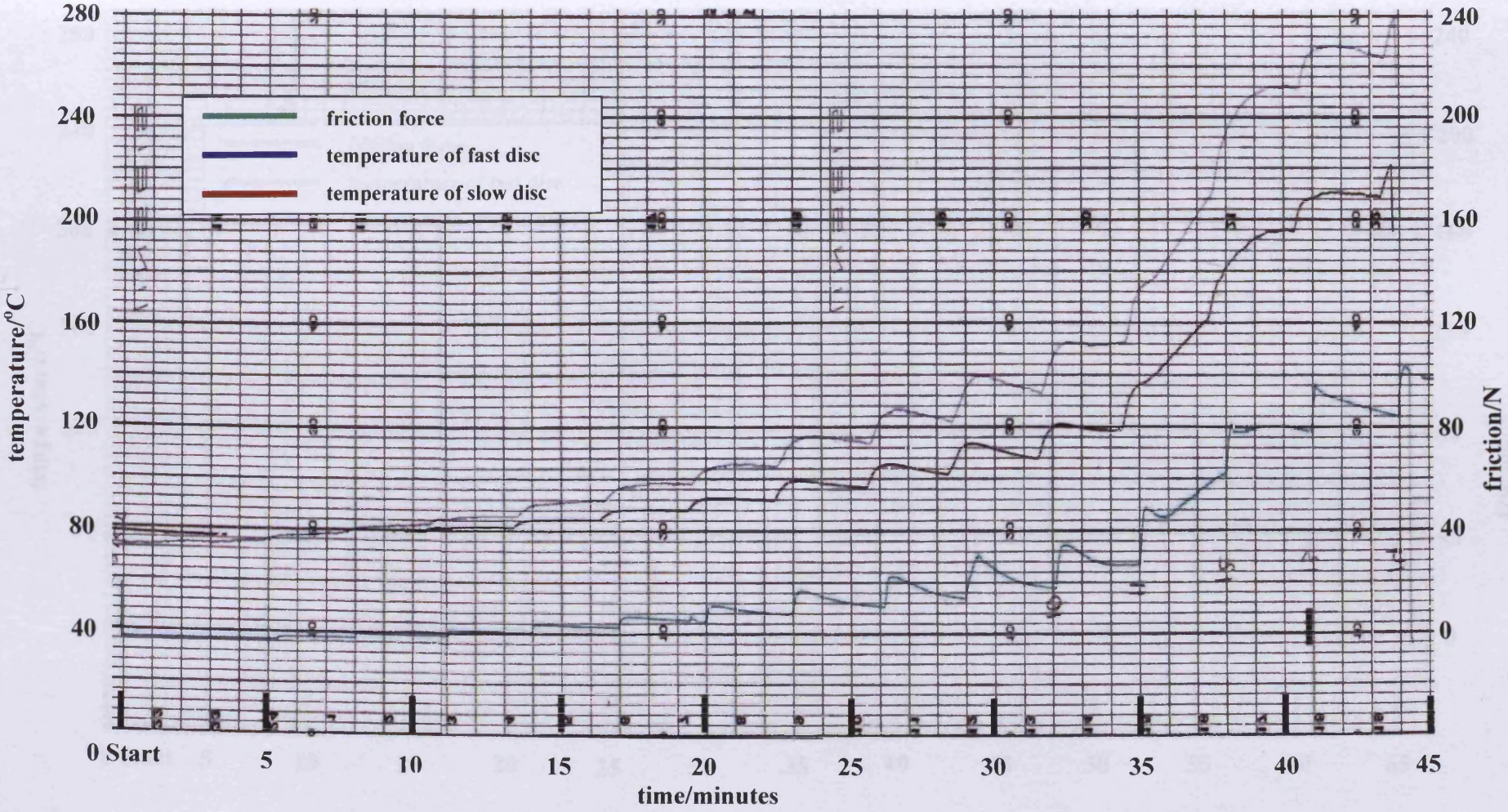

Figure 3.45. Chart recorder record of test UTRC10, graph shows friction force and bulk temperatures of two discs

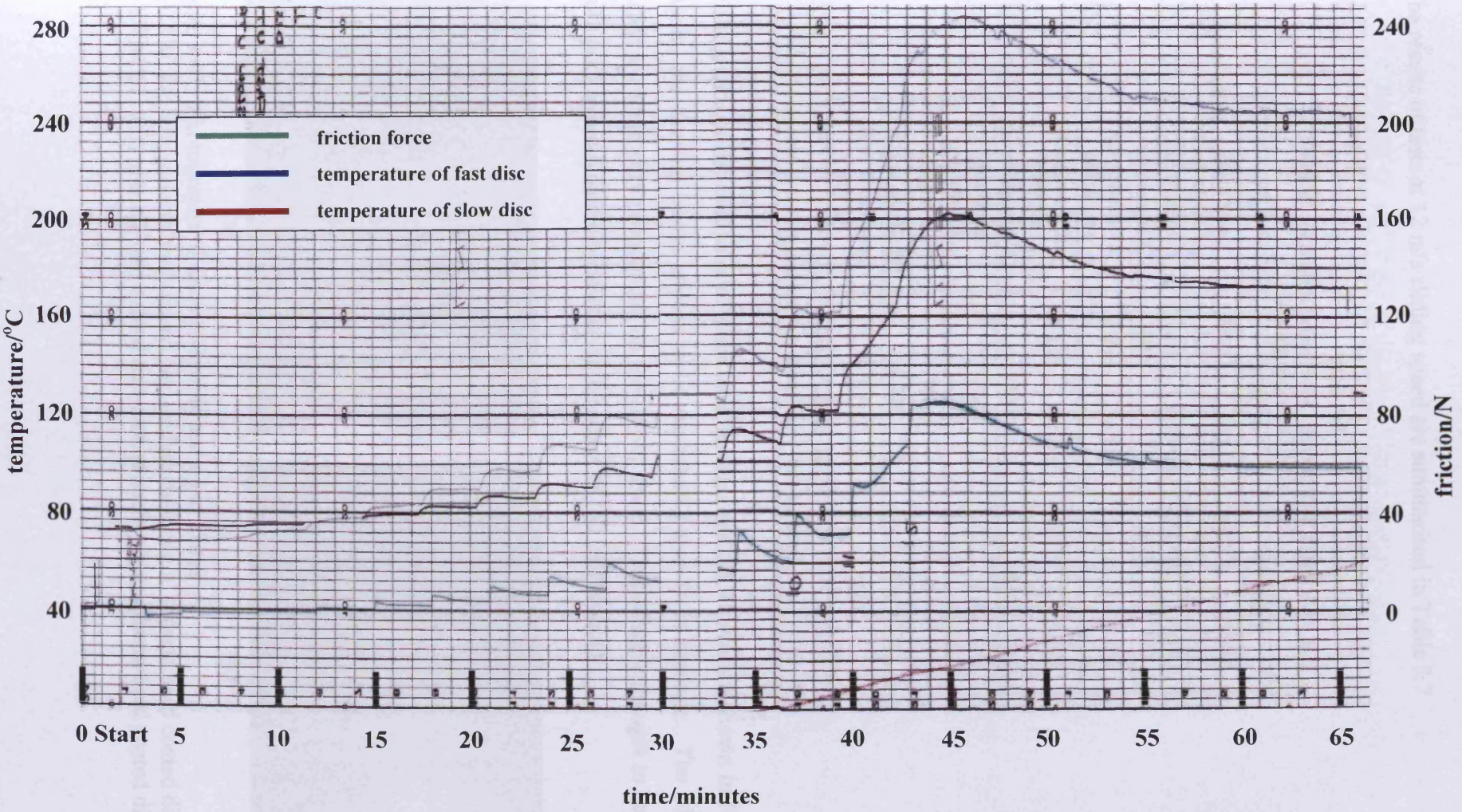

Figure 3.46. Chart recorder record of test UTRC11, graph shows friction force and bulk temperatures of two discs

The results of tests at 12 m/s sliding speed are summarised in Table 3.7.

Table 3.7.
Summary of scuffing conditions - ground/hard coated discs at sliding speed of 12m/s

Test	UTRC10		UTRC11	
Test Discs	utrc95	utrc11	utrc74	utrc13
Shaft Mounting	fast	slow	fast	slow
Disc Condition	grnd/h.c.	grnd/h.c.	grnd/h.c.	grnd/h.c.
temperature/°C	280*	221	282*	172
Roughness, Ra, before/μm	0.370	0.347	0.326	0.369
Roughness, Ra, after/μm	0.160	0.189	0.172	0.195
Scuffing load/N	5786		4157	
Max Hertz pressure/GPa	1.9		1.7	
Friction force/N	104		58	
Friction coefficient	0.018		0.014	
Blok flash temp. rise/°C	171		113	

grnd/h.c. - hard coated
* maximum temperature – did not scuff

Photographs of the two pairs of discs used in these tests at 12 m/s are shown in Figure 3.47. Again, the running tracks appear to be remarkably free from damage. The edge contact bands are again very pronounced on the slower discs. This effect is thought to be associated with poor hydrodynamic behaviour at the edges of the EHL contact.

(a) (b)

Figure 3.47. Photographs of discs following testing at 12m/s
(a) UTRC14; left: ground/hard coated disc on fast shaft; right: ground/hard coated disc on slow shaft
(b) UTRC11; left: ground/hard coated disc on fast shaft; right: ground/hard coated disc on slow shaft

Circumferential profiles from the pair of discs used in test UTRC10 are shown in Figure 3.48. The effect of running at the high load and temperatures experienced in this test is to produce a very striking smoothing of the surfaces of both discs. The surface of the fast disc, in particular, becomes almost polished in appearance.

SEM images from the two discs used in this test are shown in Figures 3.49 and 3.50. Figure 3.49 shows the fast disc from test UTRC10. The upper image shows the edge of the contact track and illustrates the brightened appearance of the coating where contact has occurred. Again, the valley features of the ground surface remain intact. The lower image shows the middle part of the running track which has become highly polished as a result of running. The original ground finish of the disc is faintly visible. This striking improvement in surface finish is further confirmed by the profile of this disc shown in Figure 3.48(b). SEM images of the slow disc are shown in Figure 3.50. The upper image shows the edge of the running track with un-run surface to the left and the running track to the right. In this case there appears to be more deterioration of the coating in the running area. The lower image shows the opposite side of the running track and again we observe the same appearance. The slower disc does not become as polished as the faster one, and this is confirmed by the profile shown in Figure 3.48(d).

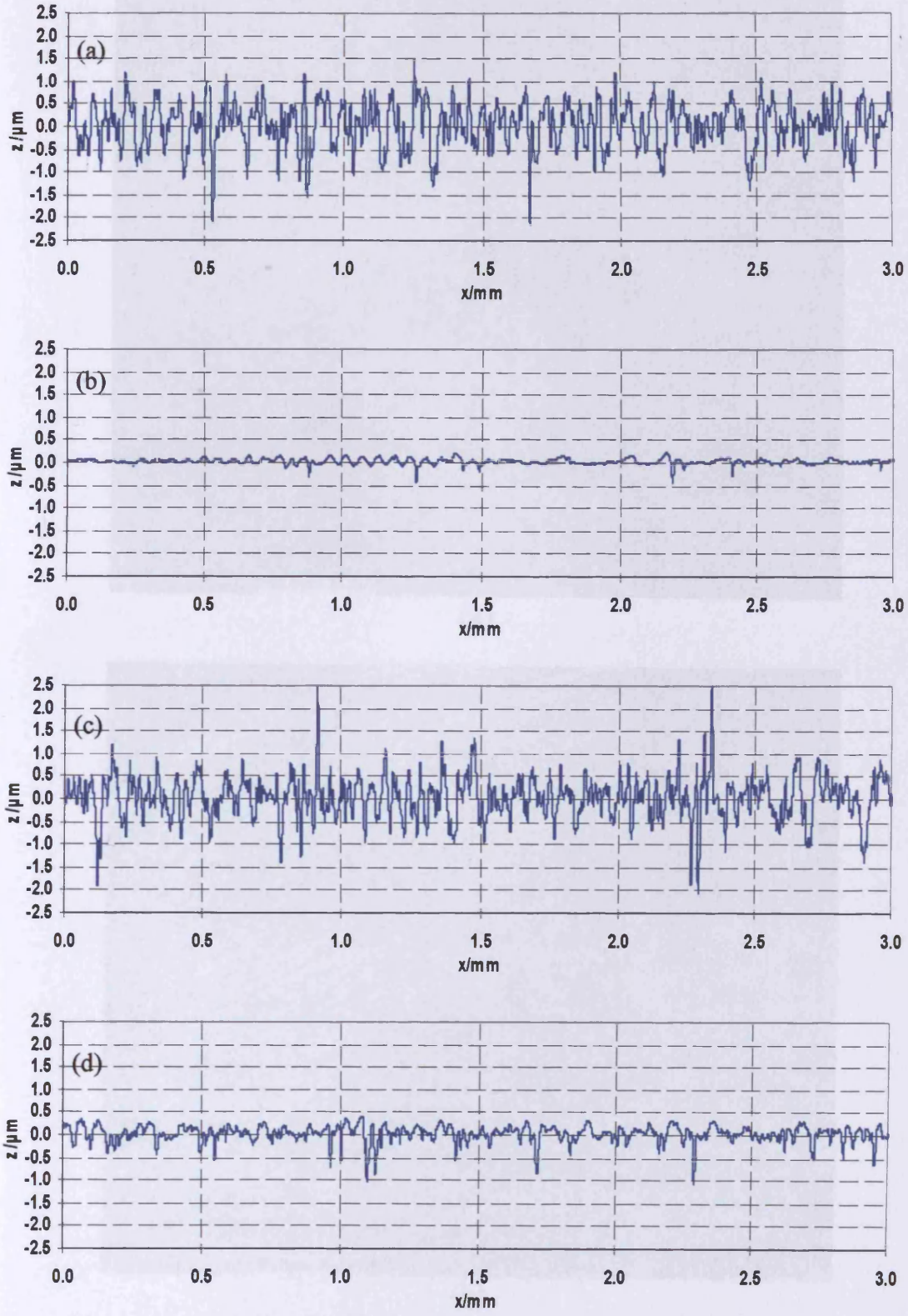

Figure 3.48. Surface profiles taken in the circumferential direction from discs used in test UTRC10
Profiles from fast disc (a) before test; Ra = 0.395 µm (b) after test; Ra = 0.159 µm
Profiles from slow disc (c) before test; Ra = 0.353 µm (d) after test; Ra = 0.20 µm

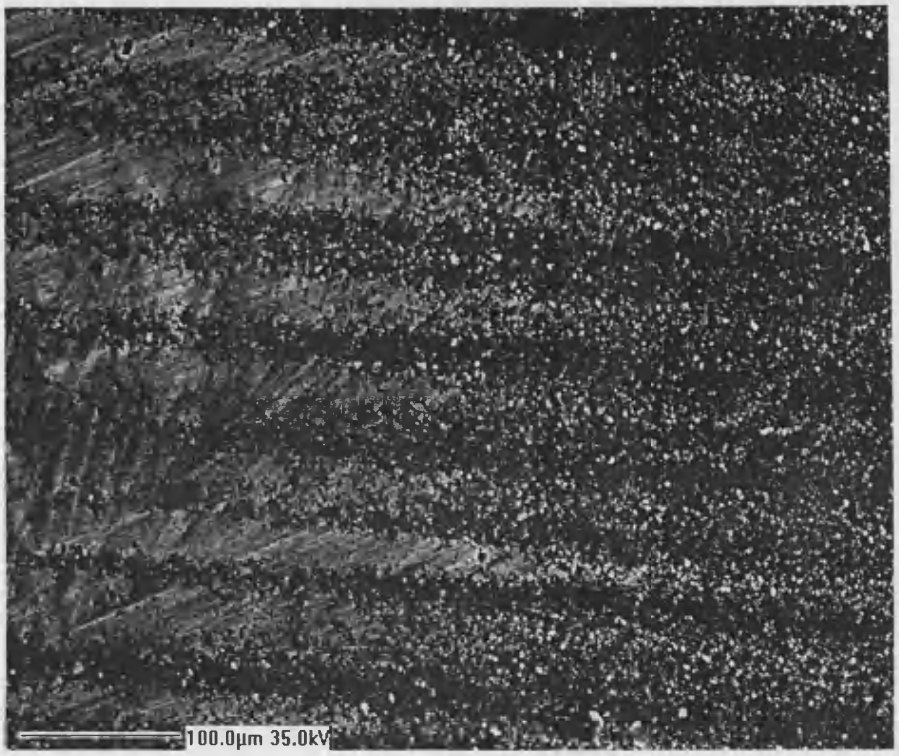

(a)

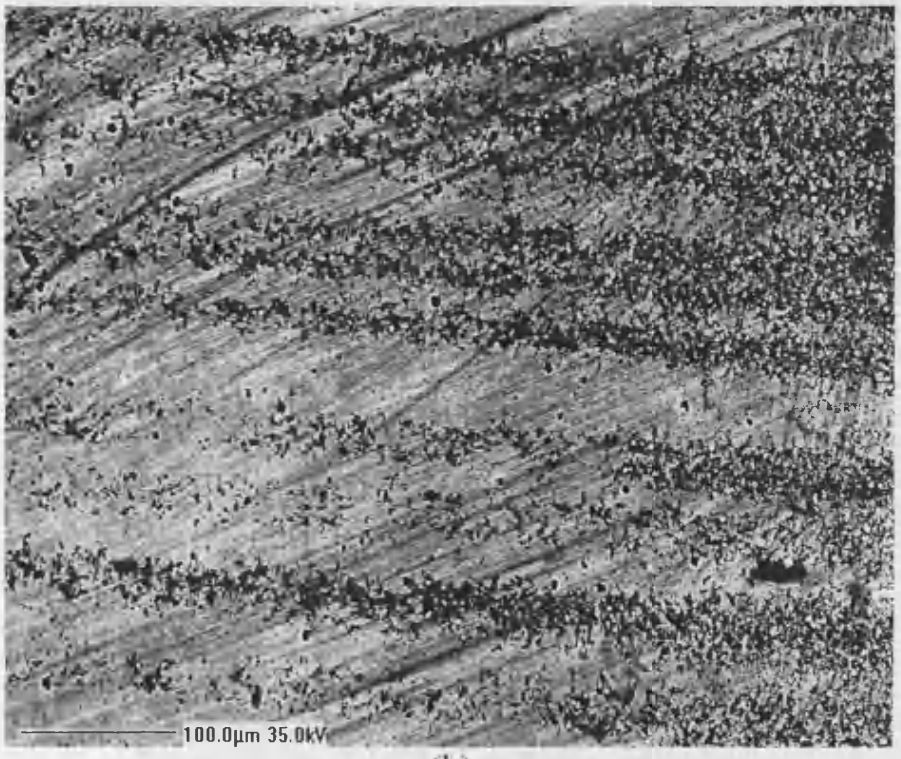

(b)

Figure 3.49. SEM images of surface of the fast disc used in test UTRC10.
(a) unrun surface to the right with the edge of running track on the left
(b) middle of the running track with coating still remaining

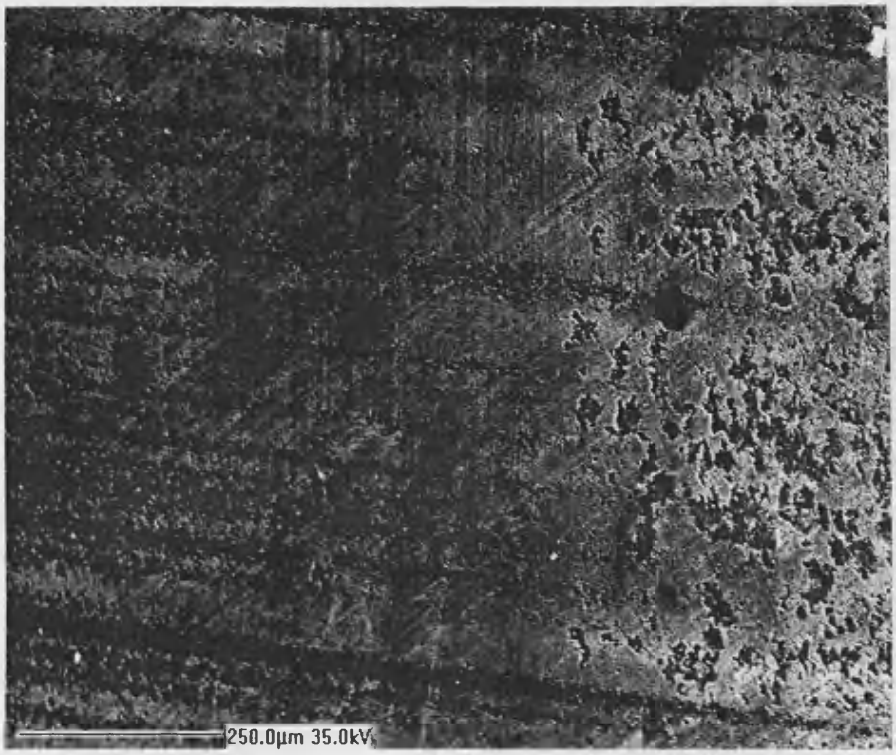

(a)

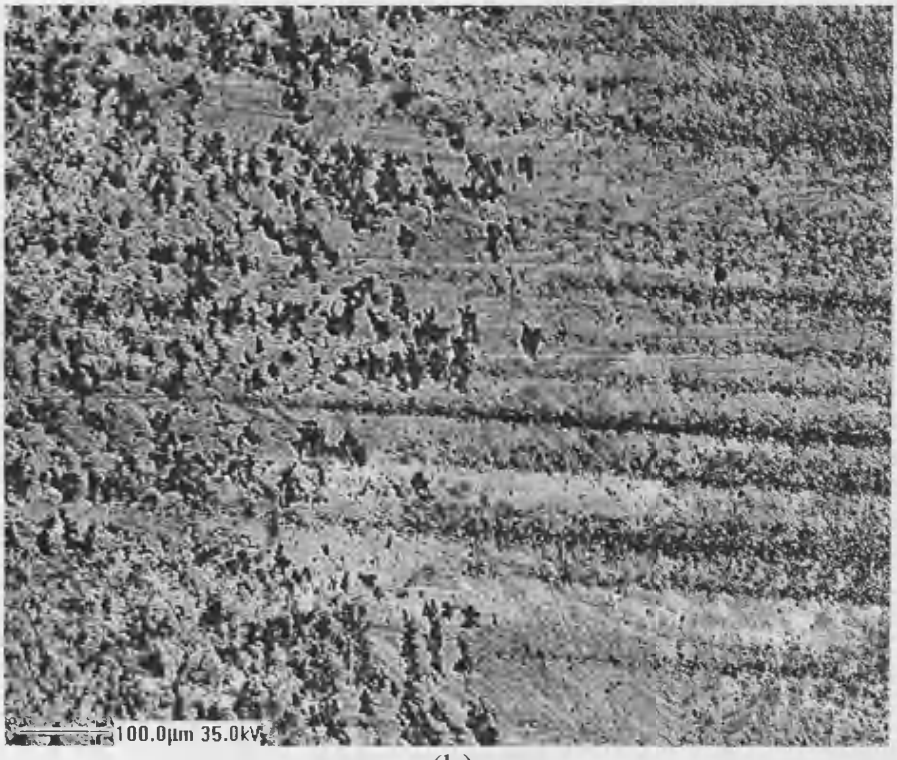

(b)

Figure 3.50. SEM images of surface of the slow disc used in test UTRC10.
(a) edge of the running track with little coating still remaining
(b) middle of the running track

The records of tests carried out with ground/coated discs at a sliding speed of 7 m/s are shown in Figures 3.51 and 3.52. In neither of these tests at the lowest sliding speed was it possible to achieve scuffing even at the increased maximum load (6758 N) used in this project. In both tests there was considerable evidence of running in as indicated by the way in which the friction force declined after each load increment was applied. In both tests at load stage 14 the friction force quickly steadied and remained at a constant level for the last two minutes of the stage. The application of load stage 15 proved to be problematic in that the magnitude of the load was rather difficult to control due to the response of the hydraulic valve at the high pressure used. However, the behaviour seen in the previous stages was at first repeated, but after about one minute at this load stage the friction began to climb as in the test at the higher speeds (12m/s and 16m/s). The test was allowed to run on at this maximum load for about 10 minutes during which the friction and temperatures appeared to stabilise, although this was confused to some extent by the variation of load as mentioned earlier. The summary of results for tests at 7m/s is given in Table 3.8.

Table 3.8.
Summary of scuffing conditions - ground/hard coated discs at sliding speed of 7m/s

Test	UTRC8		UTRC13	
Test Discs	utrc87	utrc08	utrc64	utrc15
Shaft Mounting	fast	slow	fast	slow
Disc Condition	grnd/h.c.	grnd/h.c.	grnd/h.c.	grnd/h.c.
temperature/°C	190	148	268	148
Roughness, Ra, before/μm	0.331	0.358	0.367	0.357
Roughness, Ra, after/μm	0.171	0.181	0.211	0.200
Scuffing load/N	6655#		6612 #	
Max Hertz pressure/GPa	2.0		2.0	
Friction force/N	92		90	
Friction coefficient	0.014		0.013	
Blok flash temp. rise/°C	108		106	

grnd/h.c. - hard coated
maximum load – did not scuff

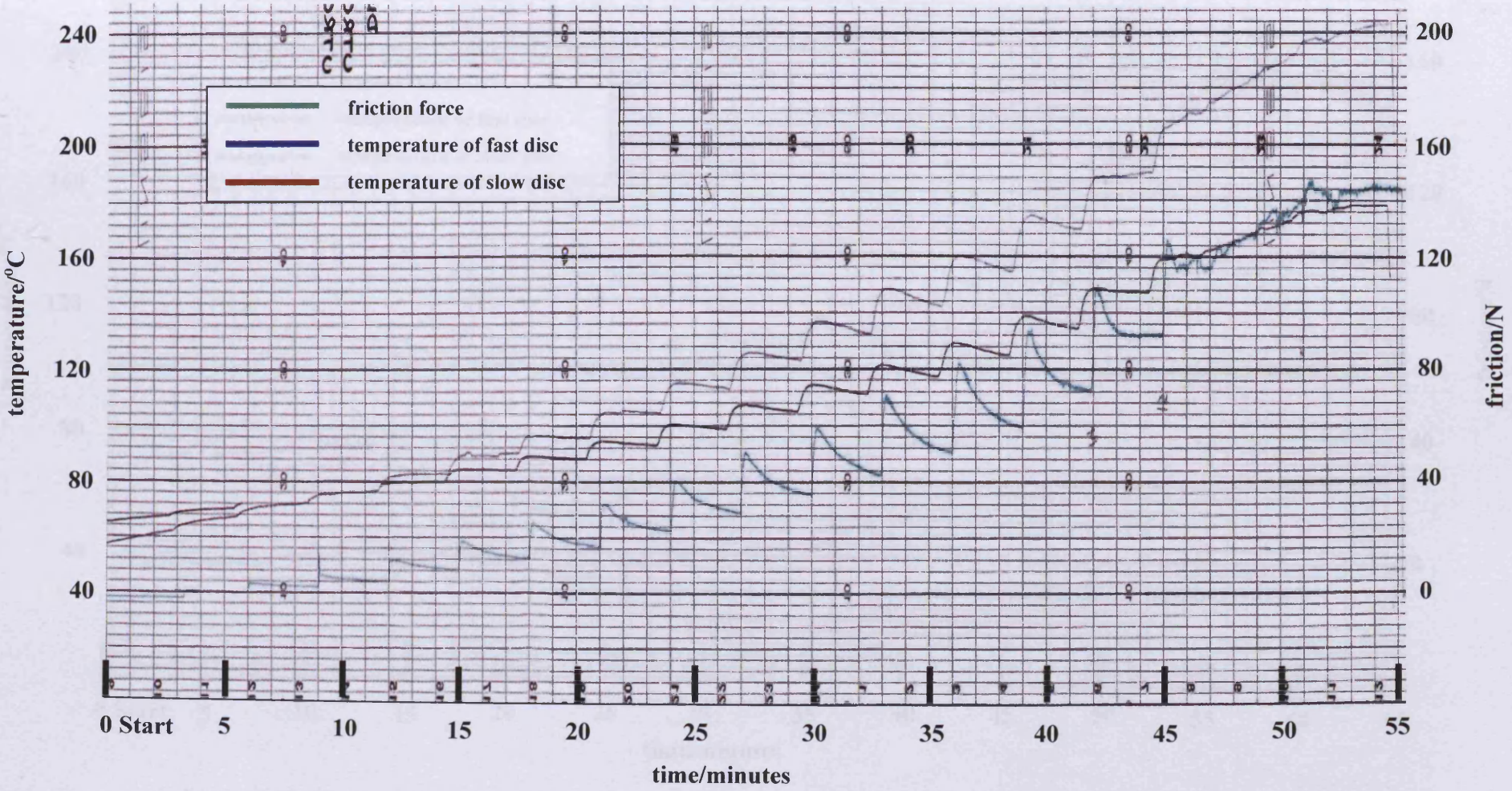

Figure 3.51. Chart recorder record of test UTRC08, graph shows friction force and bulk temperatures of two discs

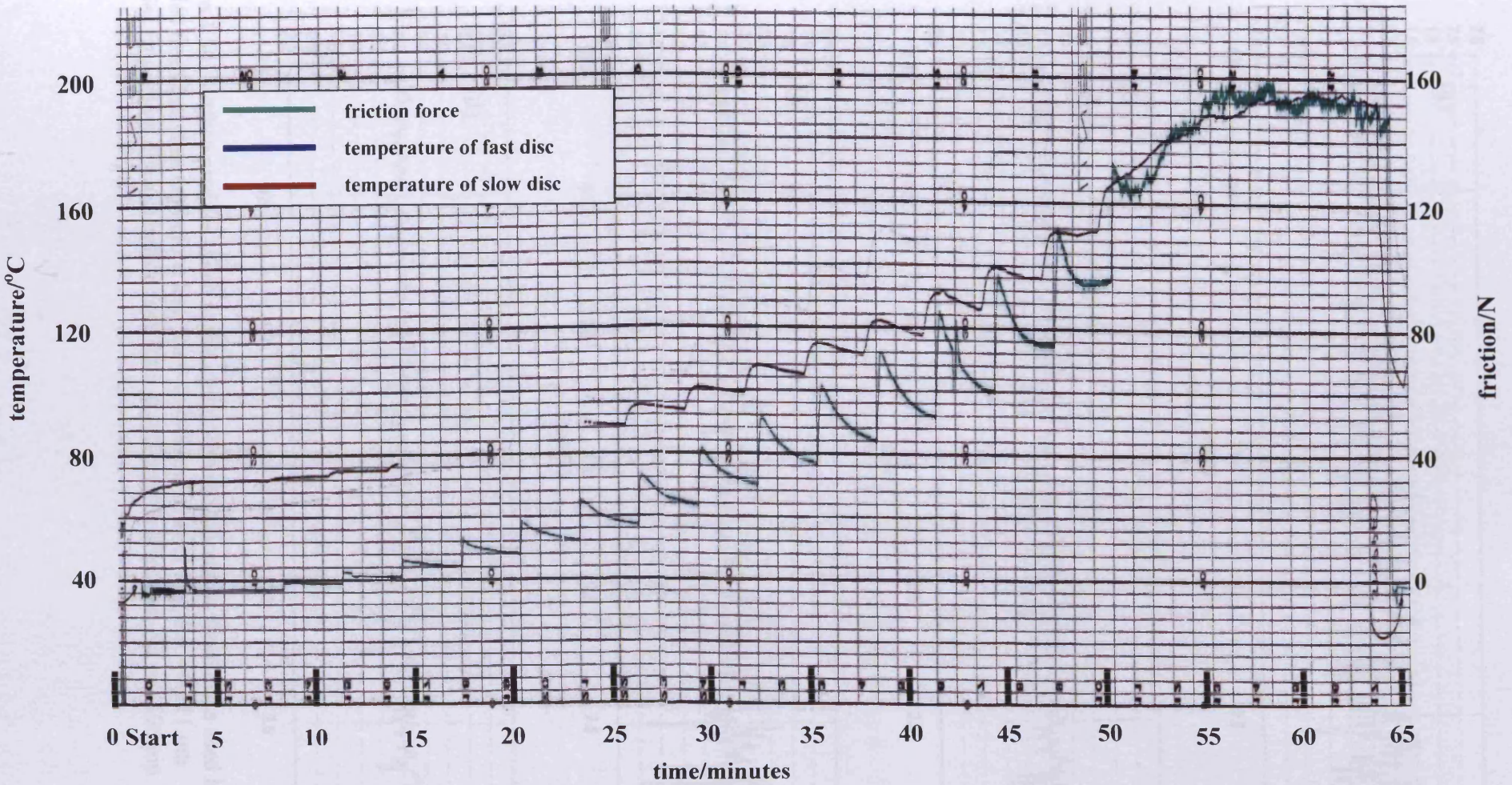

Figure 3.52. Chart recorder record of test UTRC13, graph shows friction force and bulk temperatures of two discs

Photographs of the discs used in these tests are shown in Figure 3.53. None of the discs show any indication of scuffing as defined conventionally. The original axial grinding marks persist and are not interrupted by circumferential scratching or scoring. Again there is very clear evidence of more severe contact at the edges of the running track, which we believe is due to the thinning of the EHL film in this region.

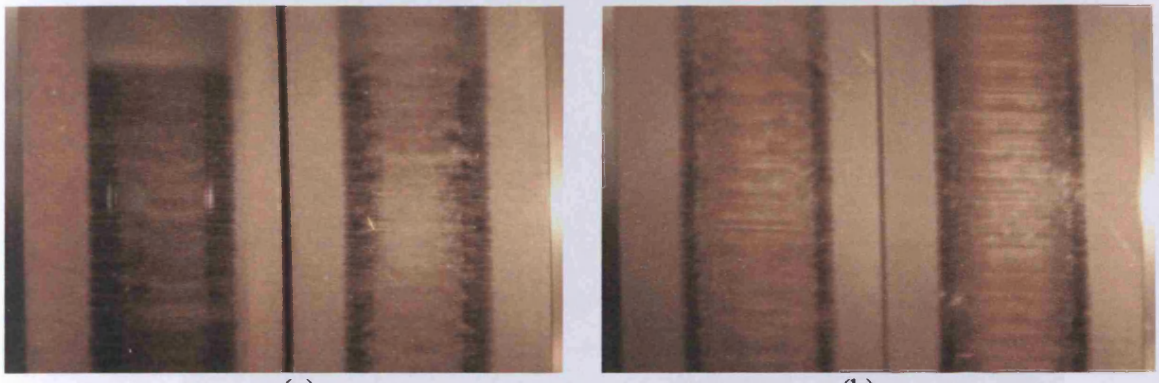

(a) (b)

Figure 3.53. Photographs of discs following testing at 7m/s
(a) UTRC08; left: ground/hard coated disc on fast shaft; right: ground/hard coated disc on slow shaft
(b) UTRC13; left: ground/hard coated disc on fast shaft; right: ground/hard coated disc on slow shaft

The circumferential profiles given in Figure 3.54 show that running leads to smoothing of both fast and slow discs, but not to the extent observed in the test at the higher sliding speeds with ground/coated discs.

SEM images from test UTRC13 are given in Figures 3.55 and 3.56. As in the previous tests in this section the images show the edge and middle parts of the running track and the same brightening effect is observed. It may be noted that these four images are at a relatively high magnification.

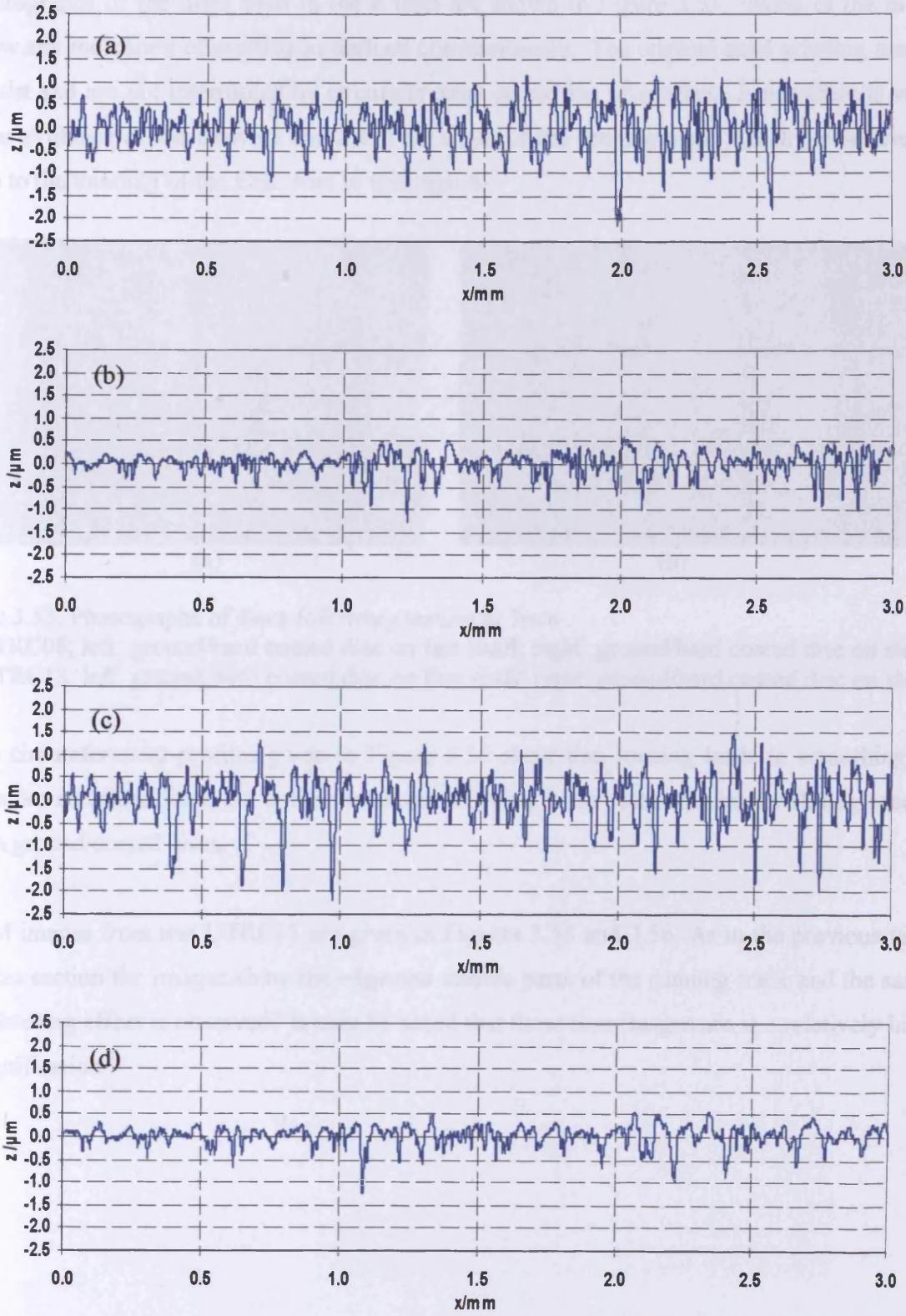

Figure 3.54. Surface profiles taken in the circumferential direction from discs used in test UTRC13
Profiles from fast disc (a) before test; Ra = 0.380 µm (b) after test; Ra = 0.211 µm
Profiles from slow disc (c) before test; Ra = 0.403 µm (d) after test; Ra = 0.196 µm

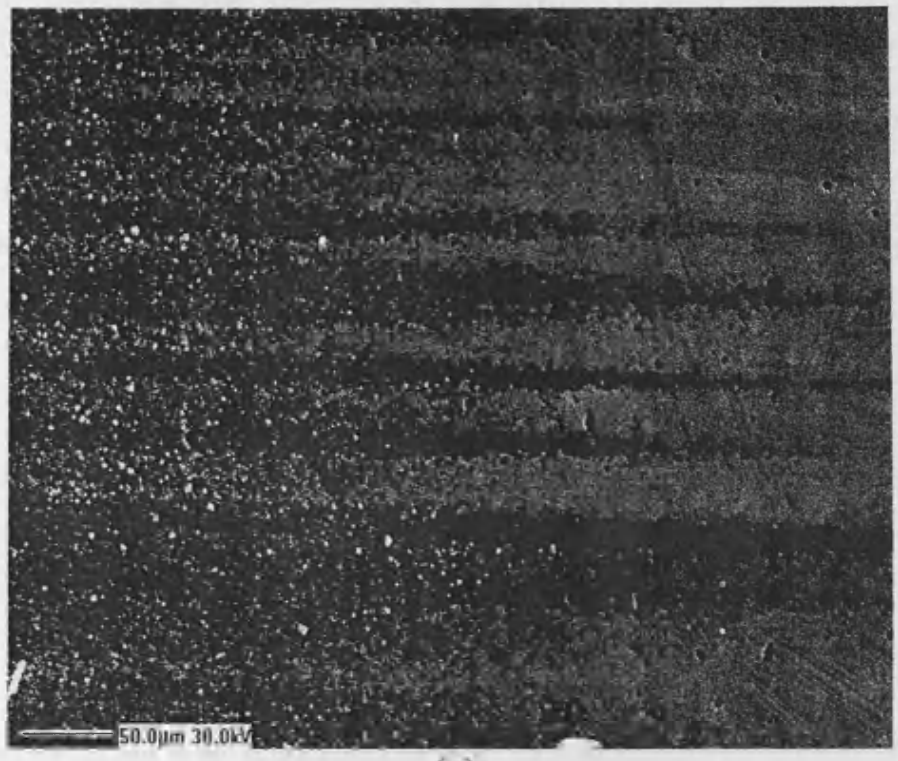

(a)

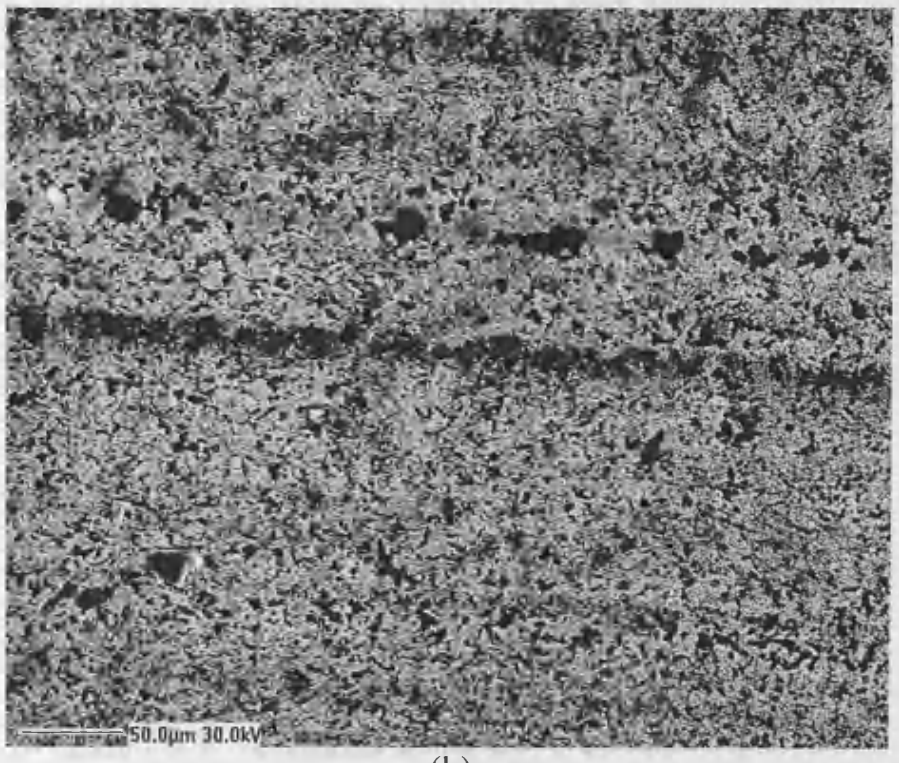

(b)

Figure 3.55. SEM images of surface of the fast disc used in test UTRC13.
(a) unrun surface with a polished running track to the right of the image
(b) middle of the running track with evidence of coating still remaining

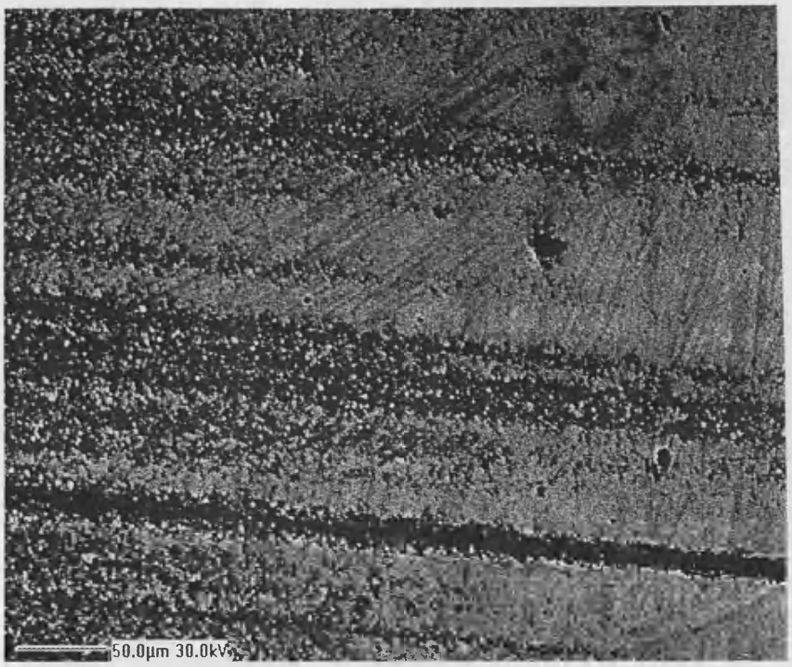

(a)

(b)

Figure 3.56. SEM images of surface of the slow disc used in test UTRC13.
(a) edge of the running track showing polishing effect
(b) middle of the running track with coating still remaining

3.3.3. Superfinished/coated discs running against superfinished/coated discs

Three tests were carried out with superfinished/coated discs on both shafts, one test being at a sliding speed of 7 m/s (test UTRC15) and two tests at 16 m/s (tests UTRC14 and UTRC16). Records of these tests are shown in Figures 3.57, 3.58 and 3.59 and a summary of the conditions at scuffing failure are given in Table 3.9.

Table 3.9.
Summary of scufing conditions-superfinished coated discs

Test	UTRC15		UTRC14		UTRC16	
Sliding Speed	7m/s		16m/s			
Test Discs	utrc55	utrc38	utrc51	utrc40	utrc54	utrc43
Shaft Mounting	fast	slow	fast	slow	fast	slow
Disc Condition	s.f./h.c.	s.f./h.c.	s.f./h.c.	s.f./h.c.	s.f./h.c.	s.f./h.c.
temperature/°C	271	184	293	214	221	169
Roughness, Ra, before/μm	0.106	0.120	0.083	0.107	0.176	0.064
Roughness, Ra, after/μm	0.226	0.231	0.159	0.188	0.160	0.168
Scuffing load/N	6403 #		5781		4923	
Max Hertz pressure/GPa	2.0		1.9		1.8	
Friction force/N	162		79		62	
Friction coefficient	0.025		0.014		0.013	
Blok flash temp. rise/°C	193		150		128	

s.f./h.c. - super finished hard coated
maximum load

In view of the durability of the ground surfaces when coated as reported in the preceding section it is, perhaps, surprising that these tests with superfinished surfaces led to clear scuffing failures in all three cases. In these tests there was no evidence of running in at the lower load stages (as indicated by the friction force remaining at a constant level during the three minute period of a load stage) but at high load stages, for example at stage 11 in test UTRC15 (7 m/s), the friction force continued to rise after application of this load. In this test, scuffing occurred towards the end of load stage 15. The same behaviour was repeated in the following load stage. This behaviour occurred at the higher load stages in the case of the two tests at the higher sliding speed (test UTRC14 and UTRC16 at 16 m/s).

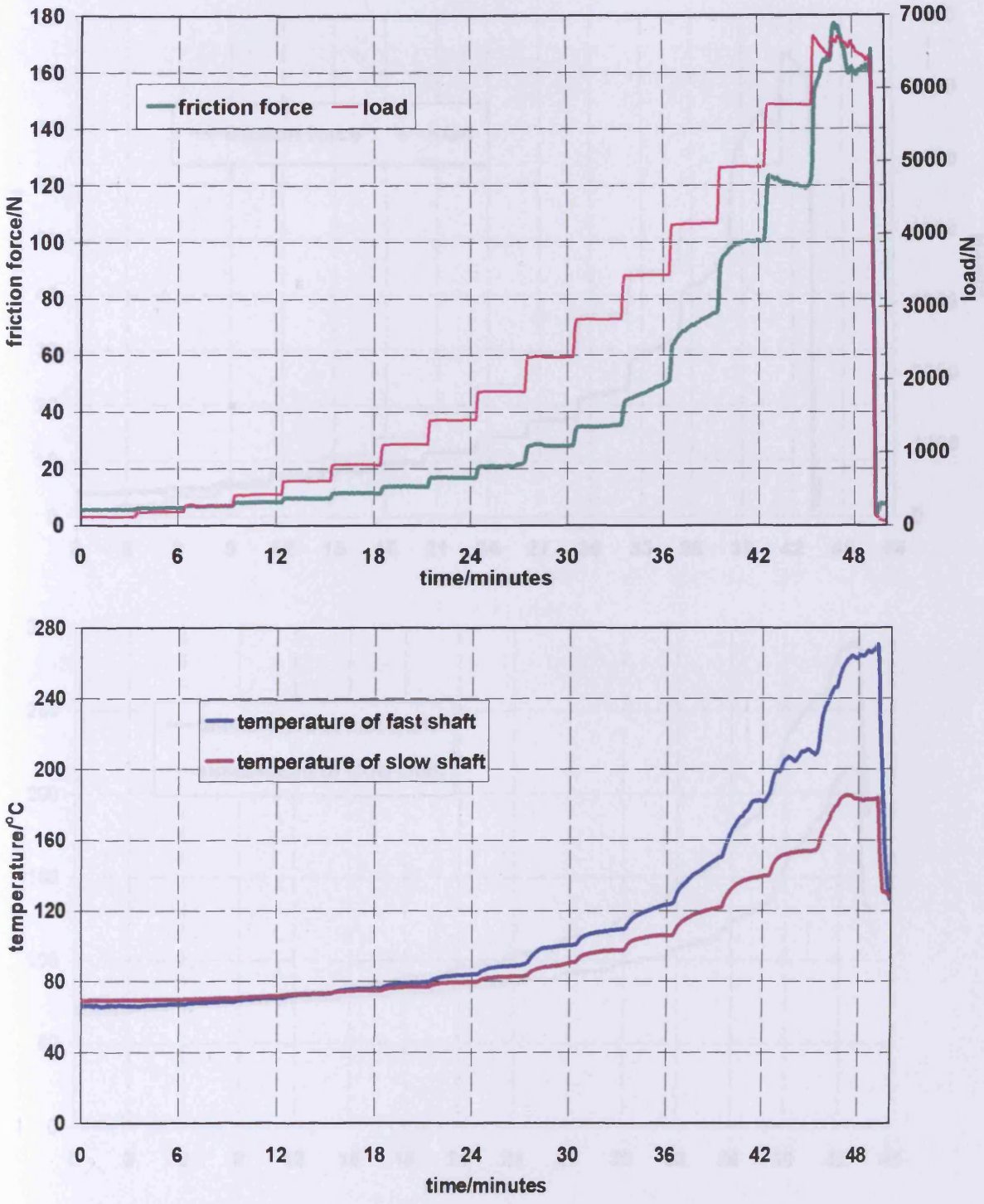

Figure 3.57. Record of scuffing test UTRC15, upper graph shows applied load and friction force; lower graph shows bulk temperatures of the two discs

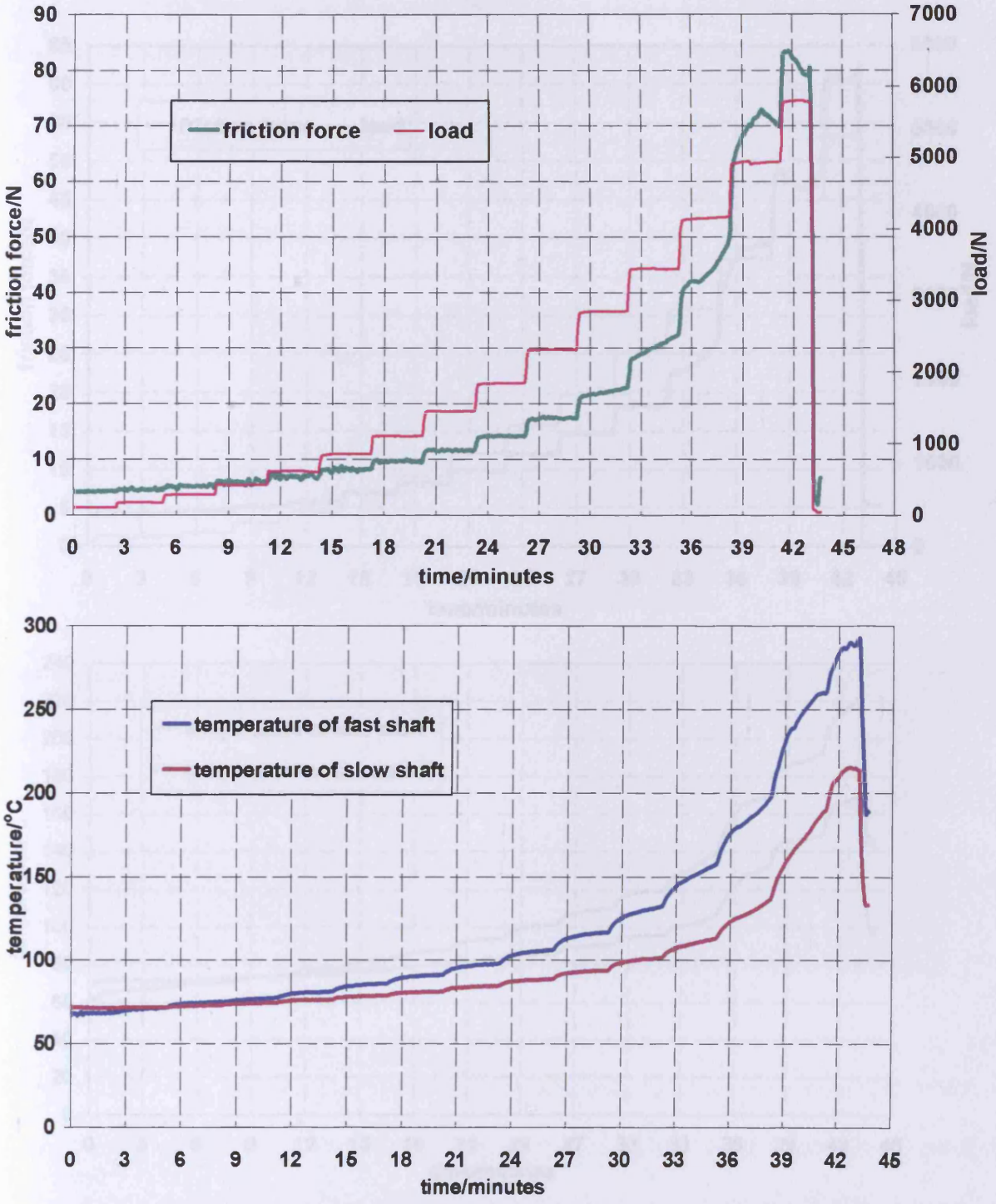

Figure 3.58. Record of scuffing test UTRC14, upper graph shows applied load and friction force; lower graph shows bulk temperatures of the two discs

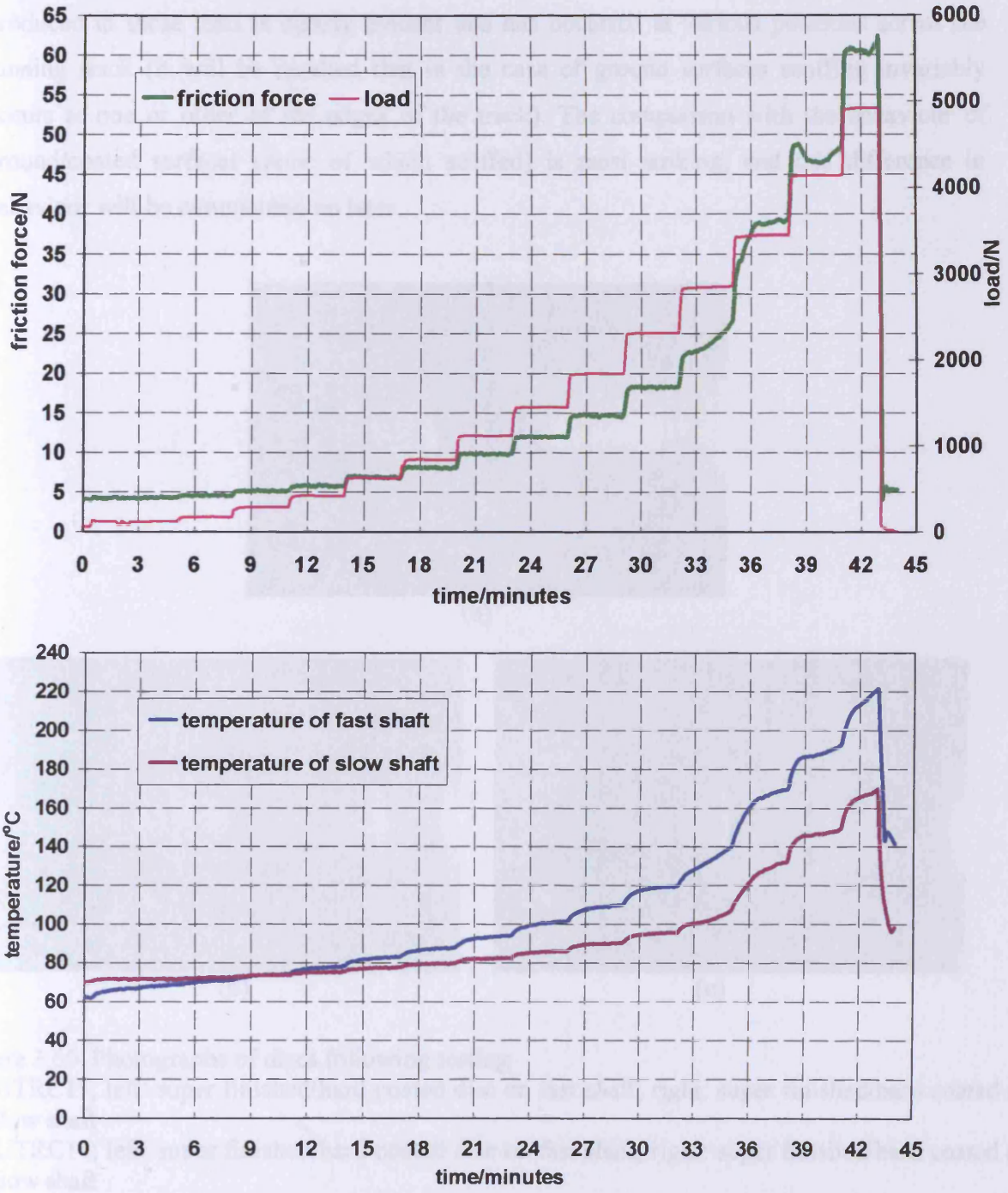

Figure 3.59. Record of scuffing test UTRC16, upper graph shows applied load and friction force; lower graph shows bulk temperatures of the two discs

Photographs of the discs used in these tests are shown in Figure 3.60. The scuffing damage produced in these tests is clearly evident and has occurred at various positions across the running track (it will be recalled that in the case of ground surfaces scuffing invariably occurs at one or other of the edges of the track). The comparison with the behaviour of ground/coated surfaces (none of which scuffed) is most striking, and this difference in behaviour will be commented on later.

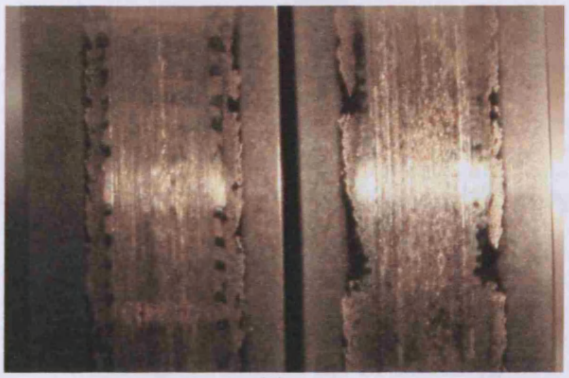

(a)

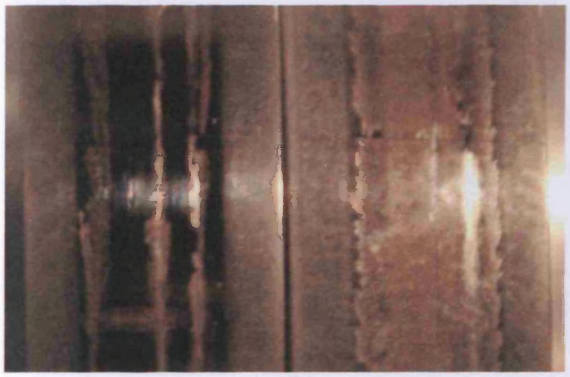

(b)

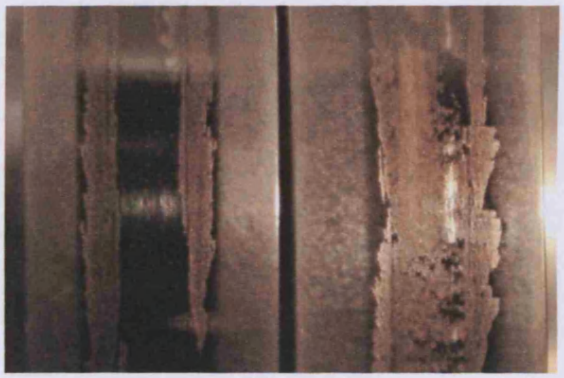

(c)

Figure 3.60. Photographs of discs following testing
(a) UTRC15; left: super finished/hard coated disc on fast shaft; right: super finished/hard coated disc on slow shaft
(b) UTRC14; left: super finished/hard coated disc on fast shaft; right: super finished/hard coated disc on slow shaft
(c) UTRC16; left: super finished/hard coated disc on fast shaft; right: super finished/hard coated disc on slow shaft

Circumferential profiles from the discs used in test UTRC15 at a sliding speed of 7 m/s are shown in Figure 3.61.

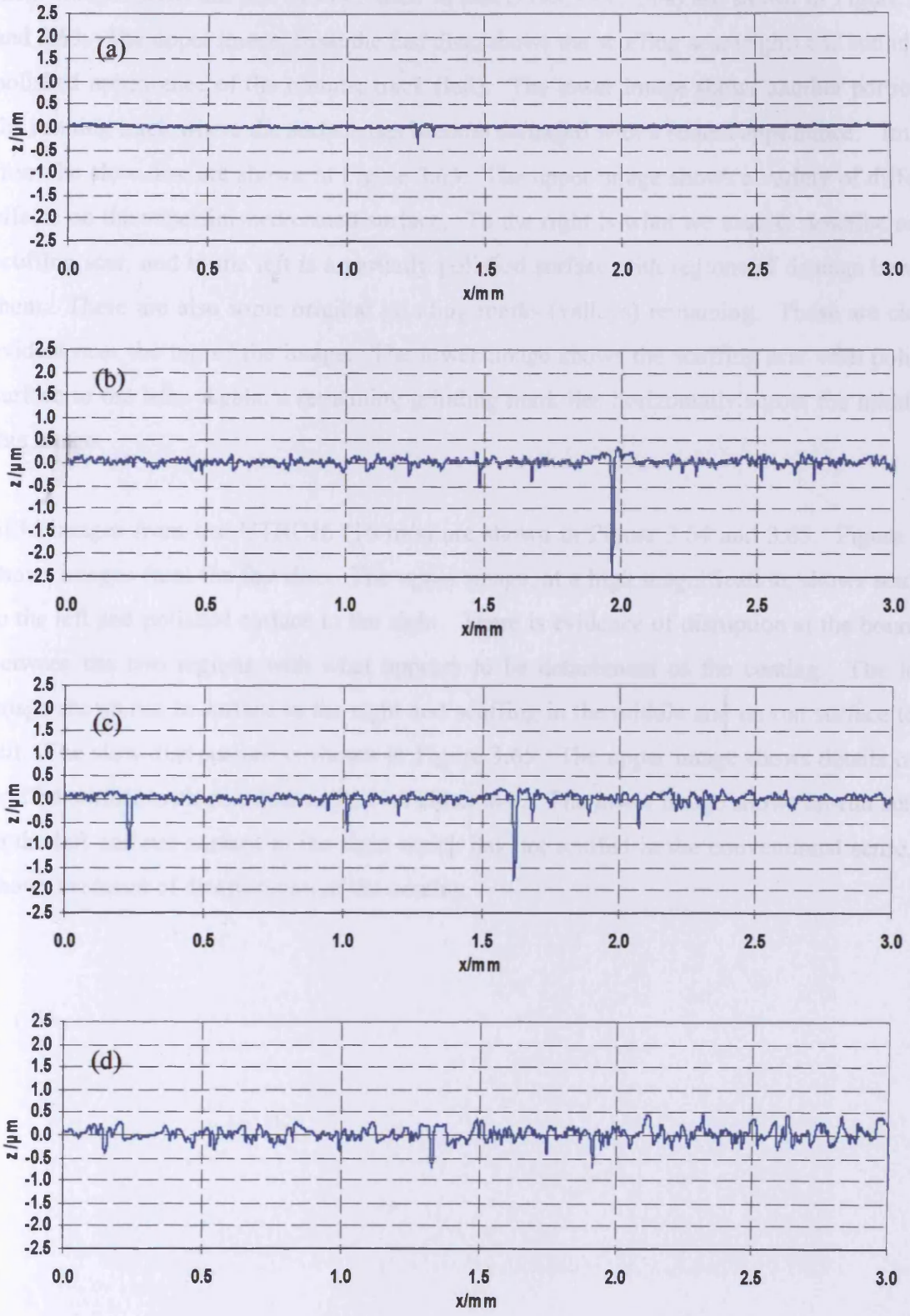

Figure 3.61. Surface profiles taken in the circumferential direction from discs used in test UTRC15
Profiles from fast disc (a) before test; Ra = 0.084 µm (b) after test; Ra = 0.153 µm
Profiles from slow disc (c) before test; Ra = 0.091 µm (d) after test; Ra = 0.182 µm

SEM images from the pair of discs used in test UTRC15 (7 m/s) are shown in Figure 3.62 and 3.63. The upper image, from the fast disc, shows the scuffing scar (right) and run in and polished appearance of the running track (left). The lower image shows another portion of the running track where the surface has become damaged with a scored appearance. Images from the slow disc are shown in Figure 3.63. The upper image shows a variety of different effects on the superfinished/coated surface. To the right is what we usually describe as the scuffing scar, and to the left is a partially polished surface with regions of damage between them. There are also some original grinding marks (valleys) remaining. These are clearly evident near the top of the image. The lower image shows the scuffing scar with polished surface to the left. Again, a remaining grinding mark lies horizontally across the middle of this image.

SEM images from test UTRC16 (16 m/s) are shown in Figure 3.64 and 3.65. Figure 3.64 shows images from the fast disc. The upper image, at a high magnification, shows scuffing to the left and polished surface to the right. There is evidence of disruption at the boundary between the two regions with what appears to be detachment of the coating. The lower image shows run in surface to the right and scuffing in the middle and un run surface to the left. The slow disc surface is shown in Figure 3.65. The upper image shows details of the scuffed surface with polished surface on either side. The lower image shows un-run surface to the left and run surface to the right which has not scuffed in the conventional sense, but shows evidence of deterioration of the coating.

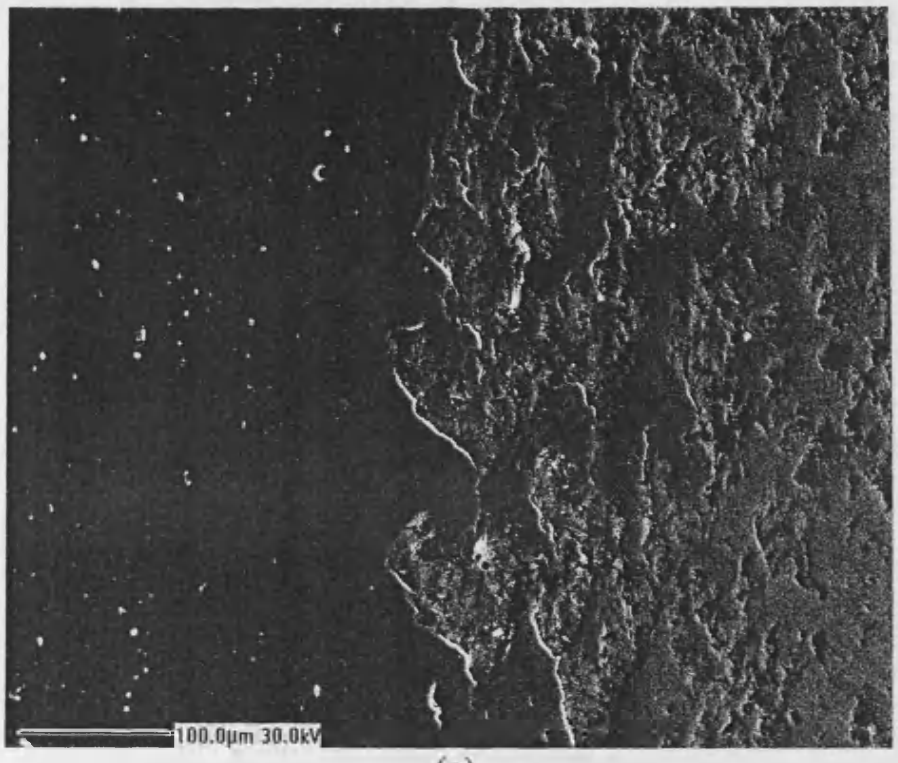

(a)

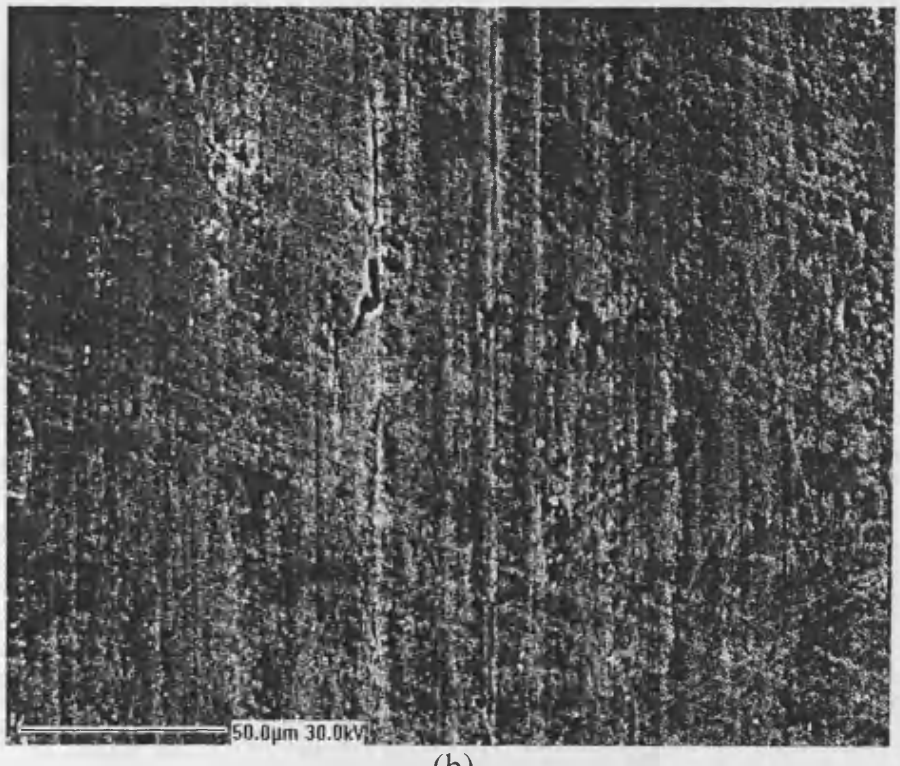

(b)

Figure 3.62. SEM images of surface of the fast disc used in test UTRC15.
(a) scuff track with run, undamaged surface on the left
(b) scoring marks in the middle of the running track

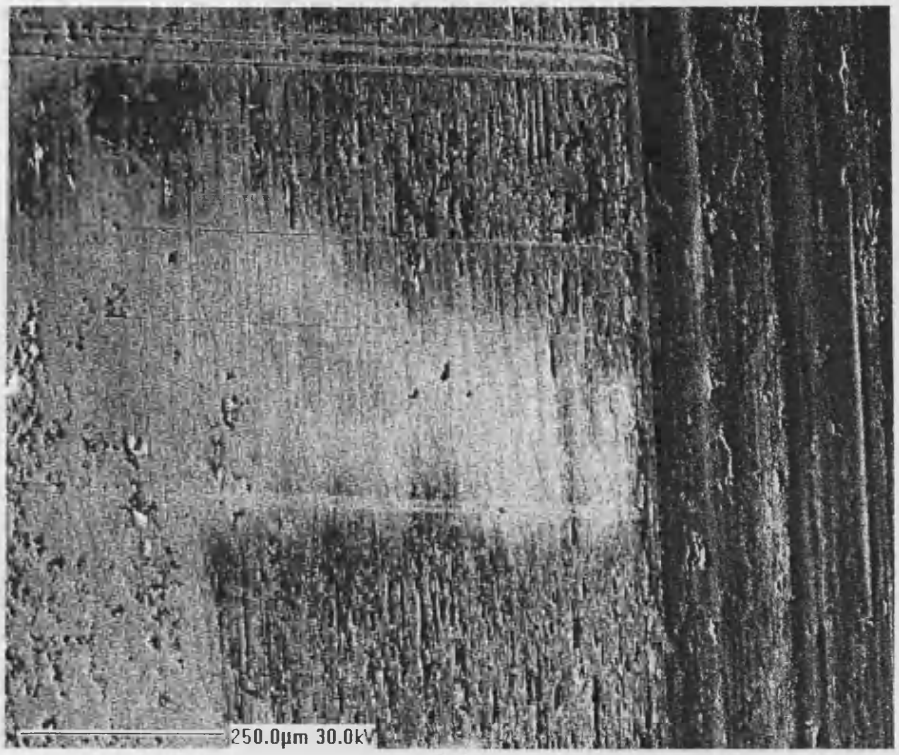

(a)

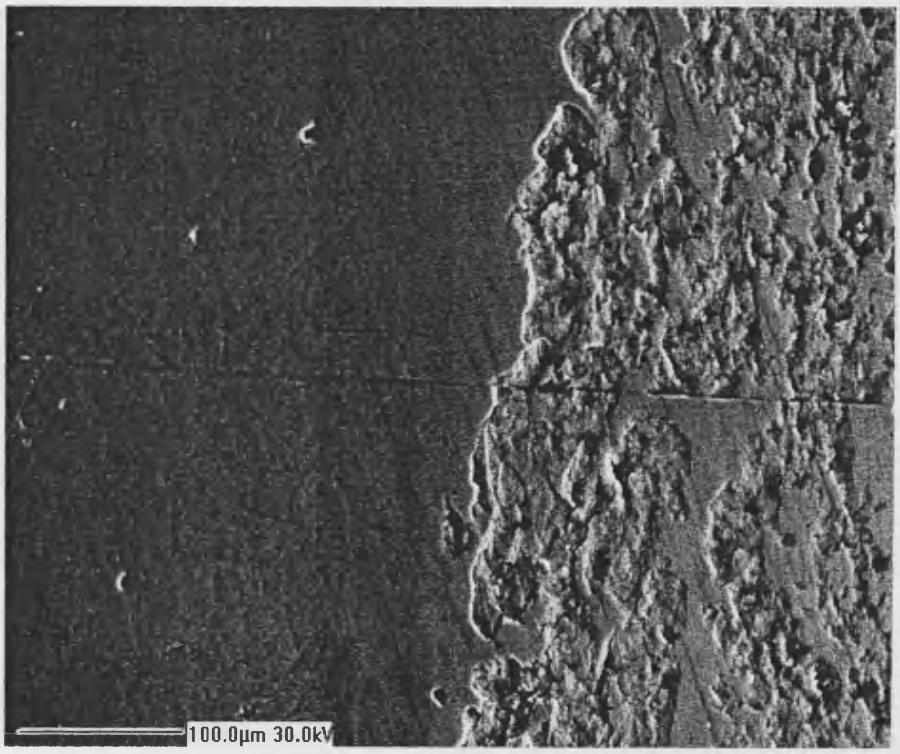

(b)

Figure 3.63. SEM images of surface of the slow disc used in test UTRC15.
(a) run in surface with the scuff track on the right
(b) run, undamaged track with scuffing mark on right

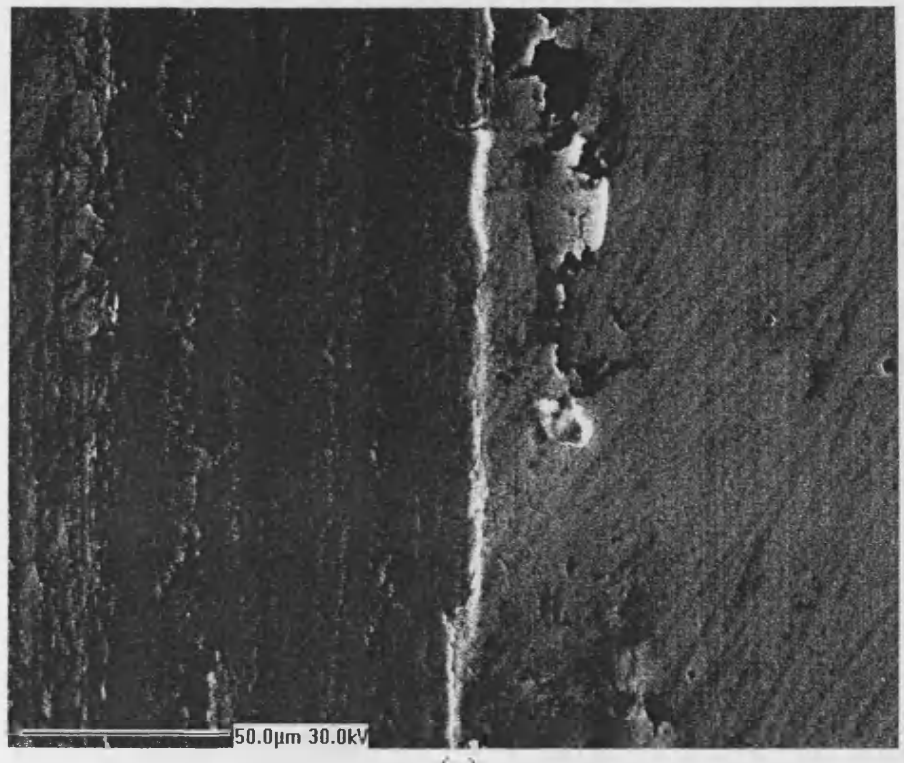

(a)

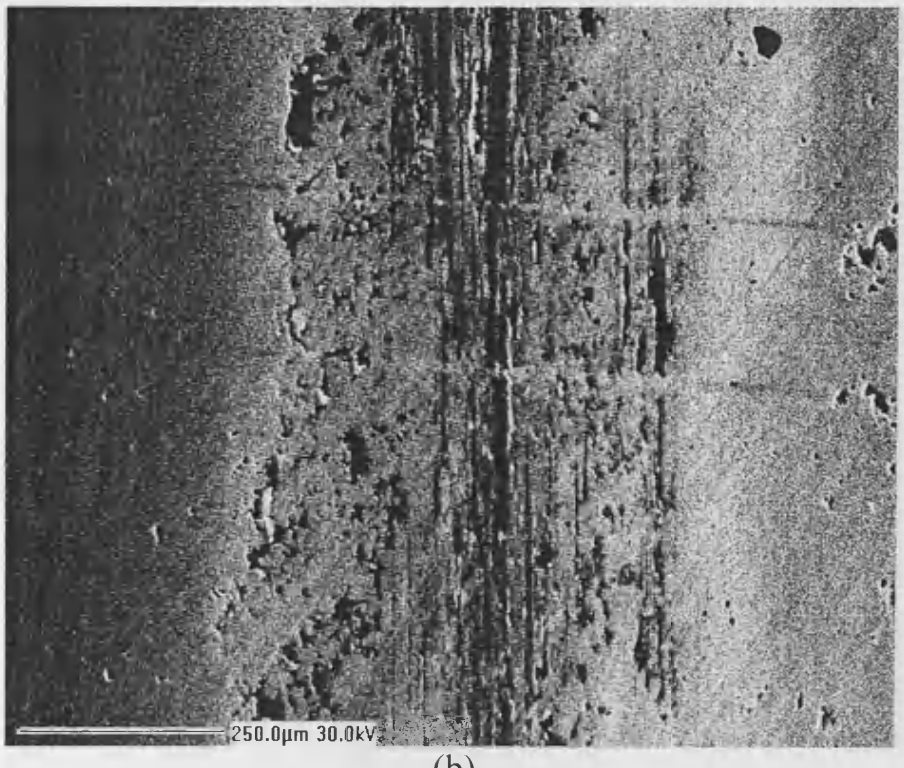

(b)

Figure 3.64. SEM images of surface of the fast disc used in test UTRC16.
(a) scuff on left with undamaged surface on right
(b) scuffing mark in the middle of the running track

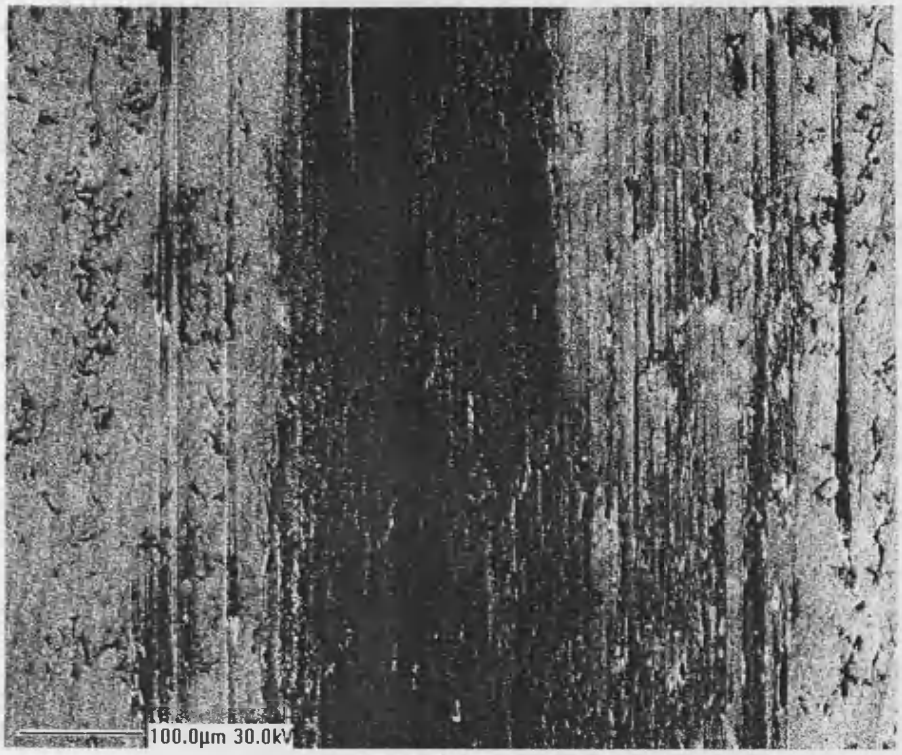

(a)

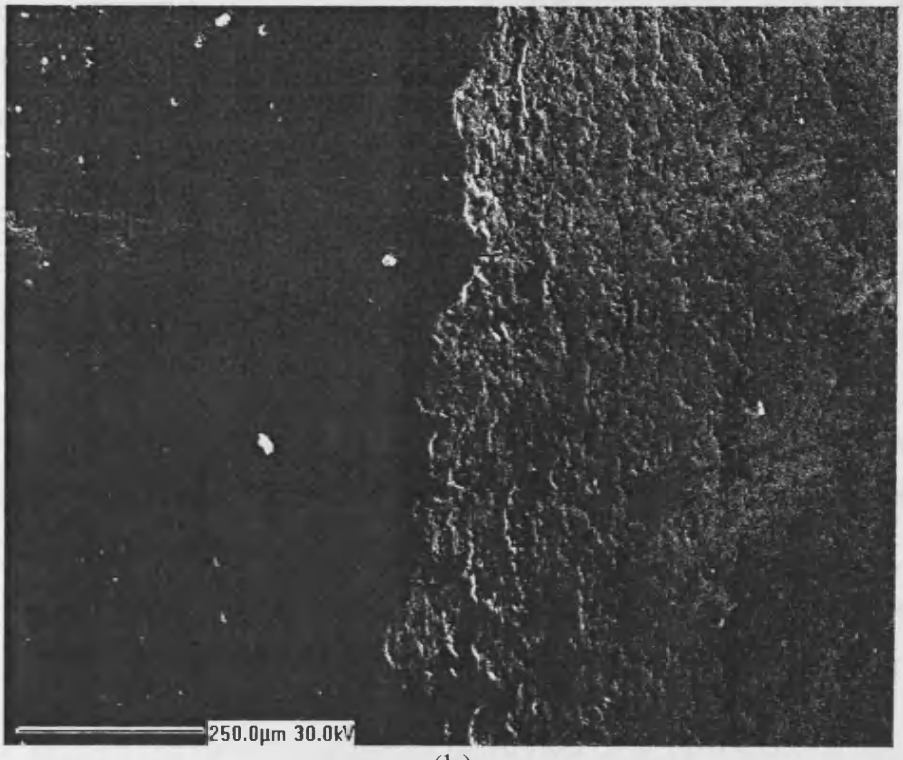

(b)

Figure 3.65. SEM images of surface of the slow disc used in test UTRC16.
(a) scuffing scar in the middle of the running track
(b) run, undamaged surface on left, scuffing scar on right

3.3.4. Ground/coated discs running against ground/un-coated discs

In this series of tests axially ground/uncoated discs of nominal surface roughness of 0.4 μm were run against discs finished in the same way, but coated (i.e. ground/coated). A total of four tests were run at a sliding speed of 16 m/s and the results obtained are summarised in Table 3.10. Records of the tests are shown in Figures 3.66 to 3.69. Tests UTRC21 and UTRC22 were carried out with ground (un-coated) disc on the fast shaft, and tests UTRC24 and UTRC26 were run with the ground/hard-coated disc on the fast shaft.

The records of these tests show some remarkable features not seen in previous work. In the case of the first two tests (i.e. ground/uncoated disc on the fast shaft) Figures 3.66 and 3.67 show that in the early stages, up to the end of stage 3, the friction force remains reasonably steady following the application of a load increment. But in the following stages there is a remarkable falling off of the friction force during a load stage. For example in Figure 3.66 the friction force falls rapidly shortly after the application of load stage 5. Indeed, the friction force at the end of this stage is almost as low as that reached at the end of the previous stage. This behaviour continues in the following stage (stage 6). At first the friction rises significantly (although not as sharply as the load, which is the usual behaviour of the friction force following a load increment) but then falls back very sharply. The application of the next load stage caused the generation of high temperatures. The temperature of the fast disc reached over 300°C. During these unexpected variations in friction the temperatures of the discs followed in the same way as expected. In this situation it was considered wise to discontinue the test (the discs were producing smoke!).

A second equally striking feature of the behaviour in these two cases is the difference in the bulk temperatures of the two discs. The temperature of the slow disc was significantly lower than that of the fast disc, when compared to the preceding test configurations. It may be noted that the behaviour seen in test UTRC21 is almost exactly repeated in test UTRC22 although the test was allowed to continue to one load stage higher (i.e. stage 8).

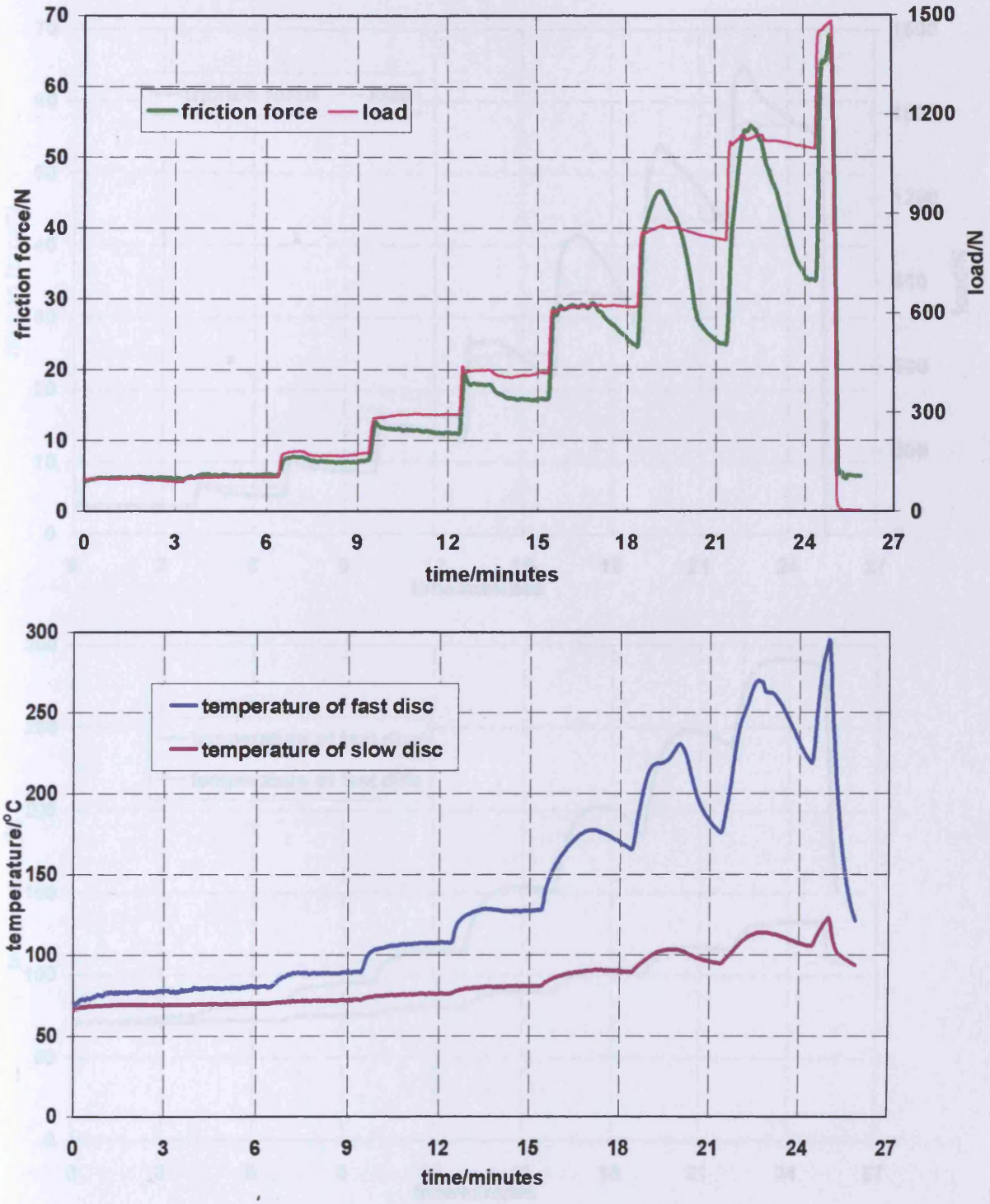

Figure 3.66. Record of test UTRC21; Upper graph shows applied load and friction force; lower graph shows bulk temperatures of the two discs

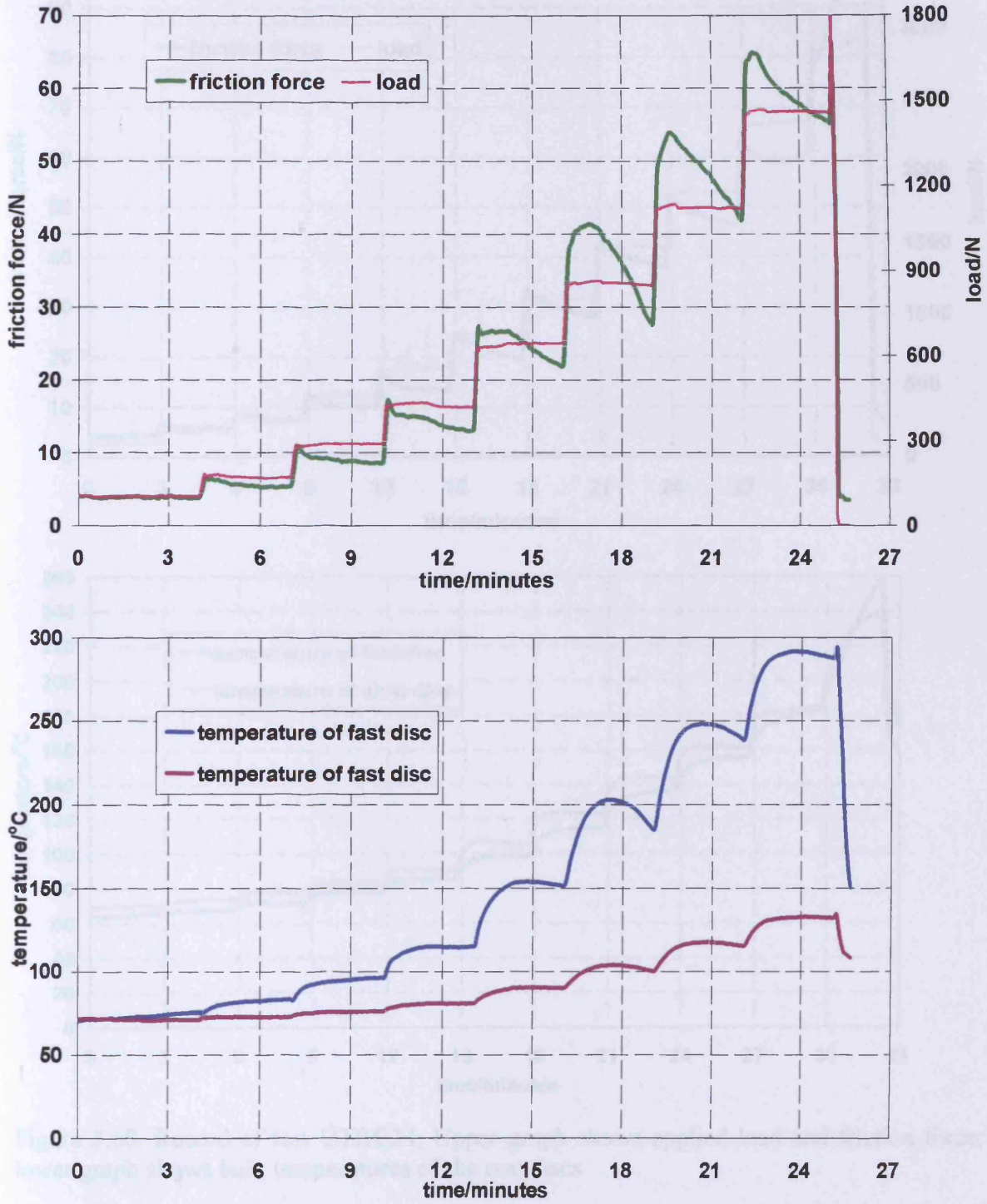

Figure 3.67. Record of test UTRC22; Upper graph shows applied load and friction force; lower graph shows bulk temperatures of the two discs

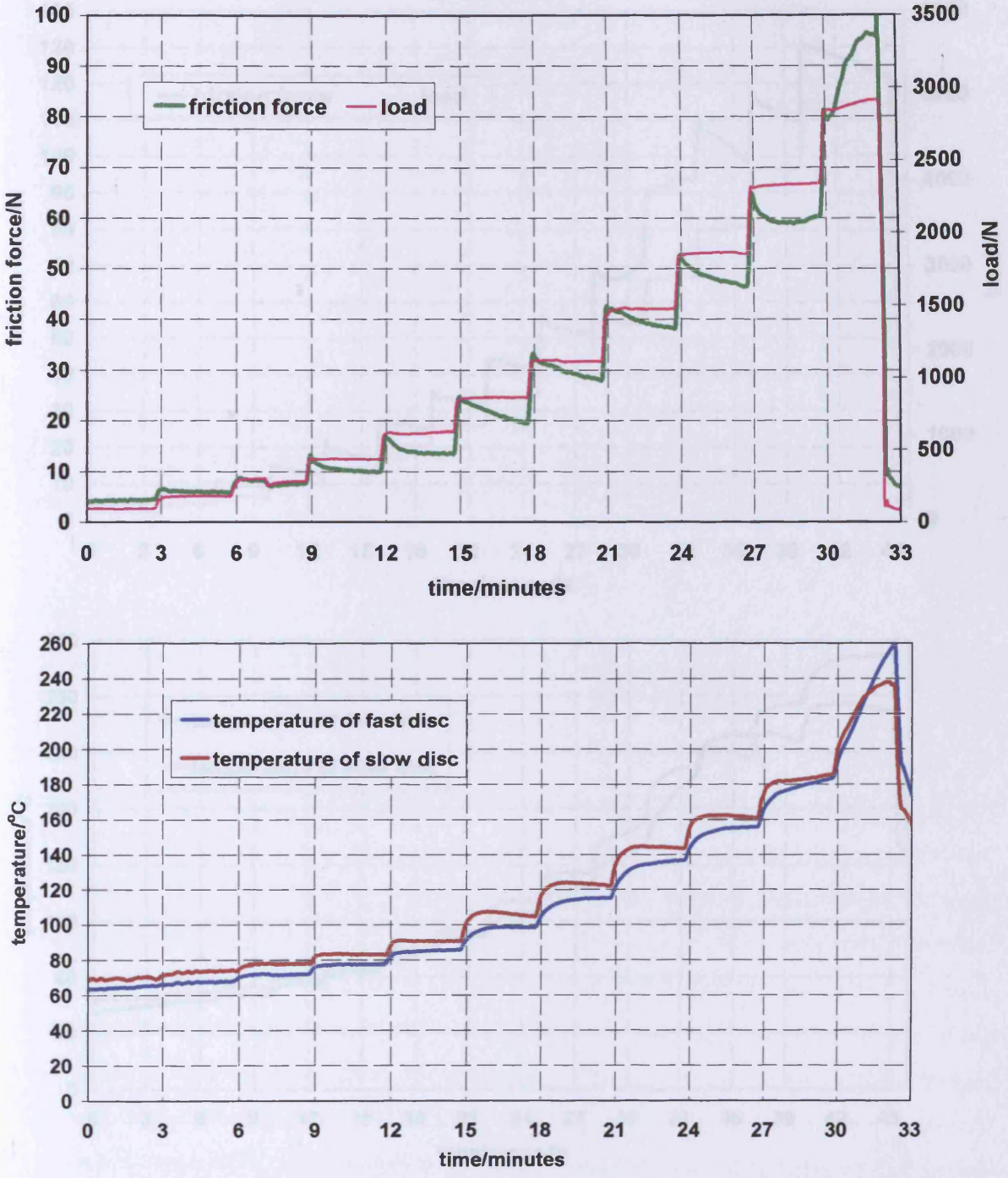

Figure 3.68. Record of test UTRC24; Upper graph shows applied load and friction force; lower graph shows bulk temperatures of the two discs

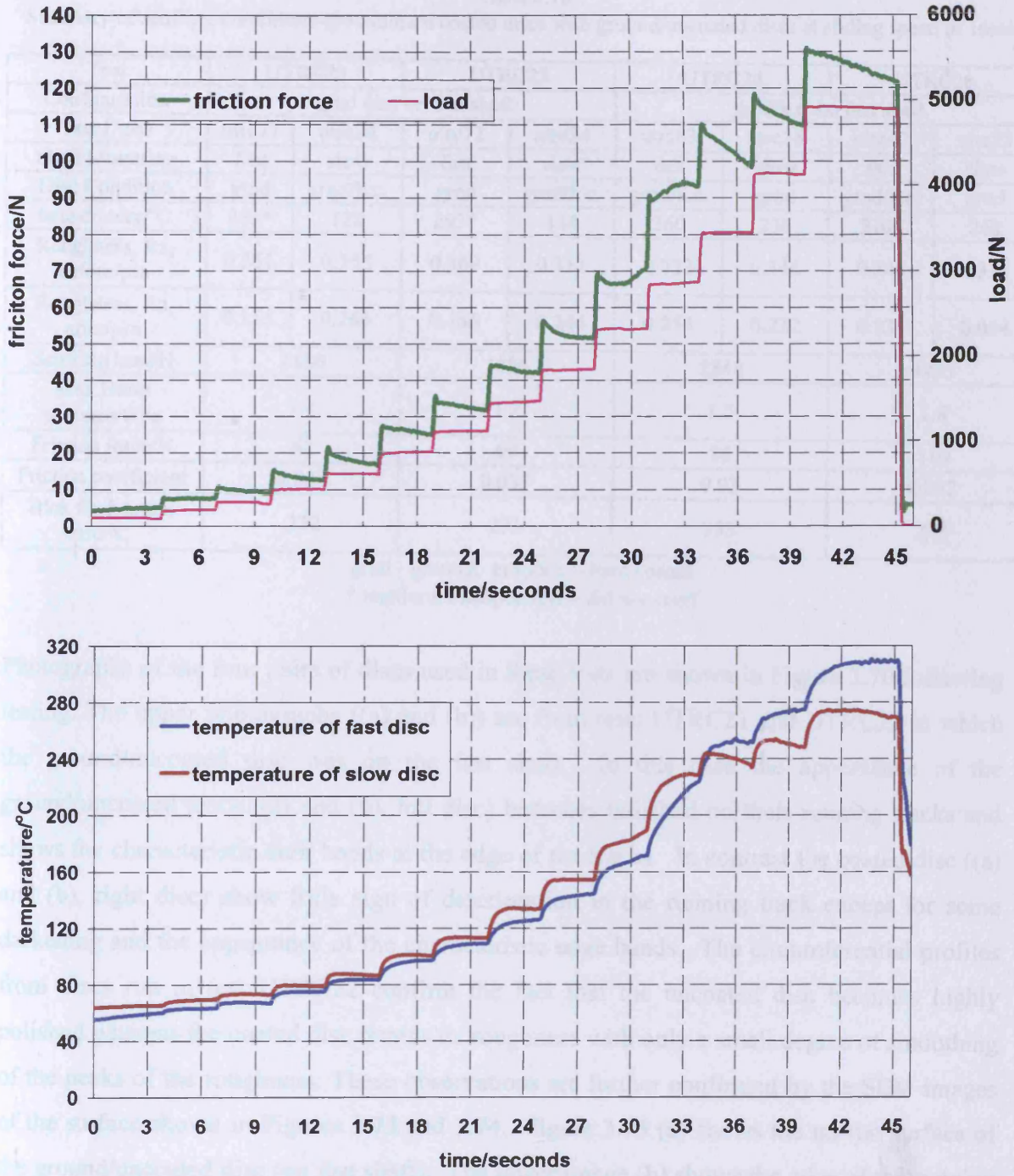

Figure 3.69. Record of test UTRC26; Upper graph shows applied load and friction force; lower graph shows bulk temperatures of the two discs

Table 3.10.
Summary of scuffing conditions-ground/hard coated discs with ground/uncoated discs at sliding speed of 16m/s

Test	UTRC21		UTRC22		UTRC24		UTRC26	
Configuration	grnd disc on fast shaft				grnd/h.c. on fast shaft			
Test Discs	utrc77	utrc34	utrc72	utrc24	utrc63	utrc36	utrc47	utrc25
Shaft Mounting	fast	slow	fast	slow	fast	slow	fast	slow
Disc Condition	grnd	grnd/h.c.	grnd	grnd/h.c.	grnd/h.c.	grnd	grnd/h.c.	grnd
temperature/°C	295*	122	293*	134	260	236	310*	268
Roughness, Ra, before/μm	0.361	0.353	0.369	0.311	0.333	0.346	0.346	0.311
Roughness, Ra, after/μm	0.155	0.266	0.156	0.244	0.254	0.222	0.134	0.034
Scuffing load/N	1480		1856		2848		4993	
Max Hertz pressure/GPa	1.2		1.3		1.5		1.8	
Friction force/N	67		69		86		110	
Friction coefficient	0.045		0.037		0.03		0.022	
Blok flash temp. rise/°C	252		231		233		225	

grnd - ground; grnd/h.c. - hard coated
* maximum temperature - did not scuff

Photographs of the four pairs of discs used in these tests are shown in Figure 3.70 following testing. The upper photographs ((a) and (b)) are from tests UTRC21 and UTRC22 in which the ground/uncoated disc was on the fast shaft. In this case the appearance of the ground/uncoated discs ((a) and (b), left disc) becomes polished on their running tracks and shows the characteristic dark bands at the edge of the tracks. In contrast the coated disc ((a) and (b), right disc) show little sign of deterioration in the running track except for some darkening and the appearance of the characteristic edge bands. The circumferential profiles from discs run in test UTRC22 confirm the fact that the uncoated disc becomes highly polished whereas the coated disc retains its roughness with only a small degree of smoothing of the peaks of the roughness. These observations are further confirmed by the SEM images of the surface shown in Figures 3.73 and 3.74. Figure 3.73 (a) shows the un-run surface of the ground/uncoated disc (on fast shaft). The lower image (b) shows the edge of the running track of the ground disc with un-run surface to the right and run in surface to the left. Even at the high magnification used in this image it can be seen that the surface appears almost perfectly smooth or polished with an absence of the damage which is characteristic of scuffing (tearing, smearing, and scoring). Figure 3.74 shows images from the coated disc (slow shaft). The upper image is taken from the un-run surface and shows the characteristic grainy appearance. The lower image is taken from the middle of the running track and

shows some brightening of the high points on the coated surface, but there is no indication of damage in the sense of scuffing or scoring.

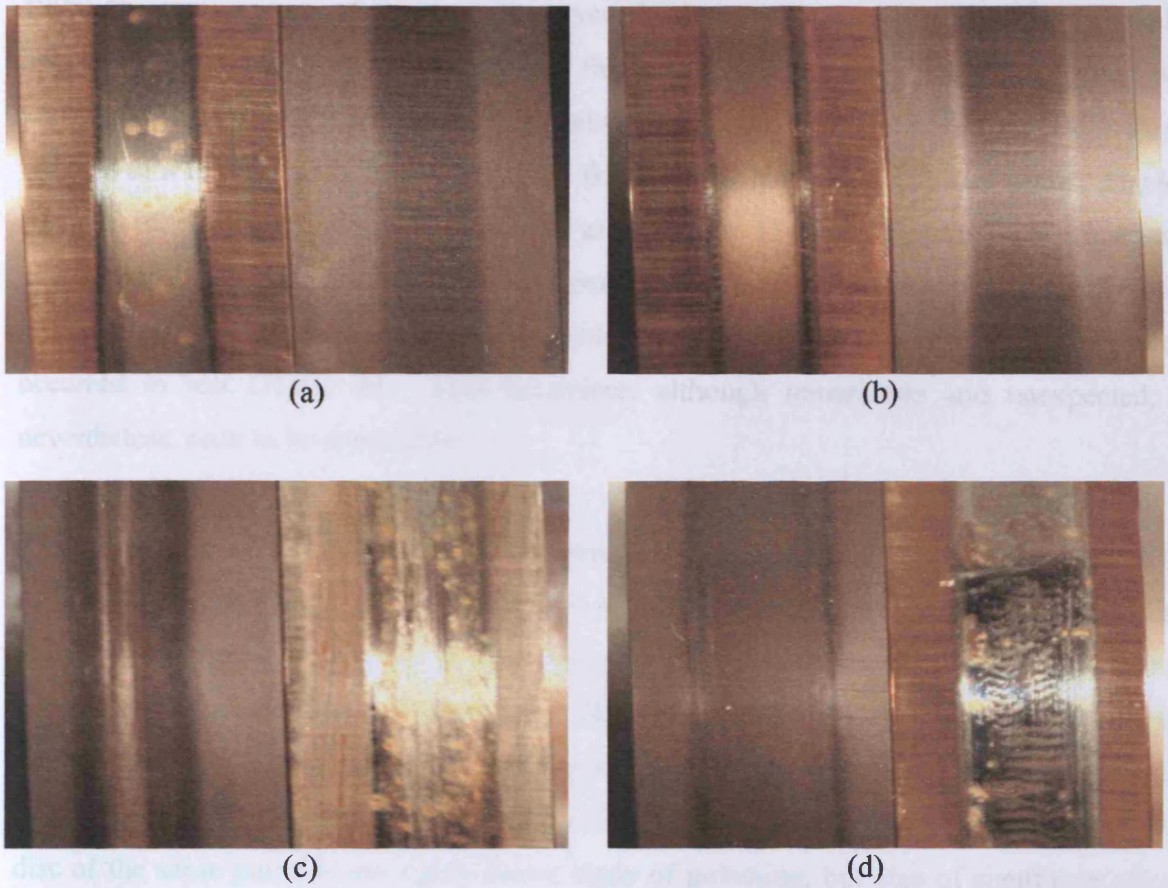

Figure 3.70. Photographs of discs following testing at a sliding speed of 16m/s
(a) UTRC21; left: ground disc on fast shaft: right: ground/hard coated disc on slow shaft
(b) UTRC22; left: ground disc on fast shaft: right: ground/hard coated disc on slow shaft
(c) UTRC24; left: ground/hard coated disc on fast shaft: right: ground disc on slow shaft
(d) UTRC26; left: ground/hard coated disc on fast shaft: right: ground disc on slow shaft

We now return to Figures 3.68 and 3.69 which show the test records of test UTRC 24 and UTRC26 in which the ground/coated discs was on the fast shaft. The behaviour in these tests is remarkably different to that seen in the preceding tests (UTRC21 and UTRC22). The behaviour of the friction force follows a more familiar pattern in that it rises sharply following an increase in the load and then falls back to some extent during the 3-minute period. In test UTRC24 scuffing, as indicated by the characteristic sharp rise in friction, occurred towards the end of load stage 10. The behaviour of the two bulk temperatures call for some comment. For most of the test the temperature of the slow (uncoated) disc was

higher than that of the fast (coated) disc. This was the case until the stage before that at which scuffing occurred. This behaviour is unique in the whole series of tests conducted so far. In all other cases of tests reported in this thesis (and in the earlier work of Patching, 1995) the temperature of the fast disc exceeds that of the slow disc. This remarkable behaviour is repeated in test UTRC26. In this case scuffing did not occur and the test was allowed to run for longer than the usual 3 minutes at load stage 13. Scuffing was anticipated because of a rather rough behaviour of the friction trace, but did not in fact occur. The test was suspended after running for 5 minutes at load stage 13 because of the high temperature developed (310°C). It is noted that the temperature of the fast disc did eventually exceed that of the slow disc during load stage 10, which is the stage at which the same behaviour occurred in test UTRC 24. This behaviour, although remarkable and unexpected, is, nevertheless, seen to be repeatable.

The appearance of the two pairs of discs used in test UTRC24 and UTRC26 is shown in the photographs presented in Figure 3.70 (c) and (d). In this pair of photographs the coated discs are shown on the left. The discs shown in (c) scuffed, as is evident from the scuffing scar on the left of the track of the coated disc. The ground/uncoated discs of this pair show a polished appearance except where scuffing occurred. The discs shown in (d) did not scuff and the coated disc (left of pair) shows no indication of distress or scoring. The uncoated disc of the same pair (d) (on right) shows signs of polishing, but also of significant plastic deformation. These observations are reinforced by the circumferential profiles shown in Figure 3.72. The upper two profiles show the coated discs before and after running and the lower pair of profiles are from the uncoated discs. These show a high degree of smoothing or polishing.

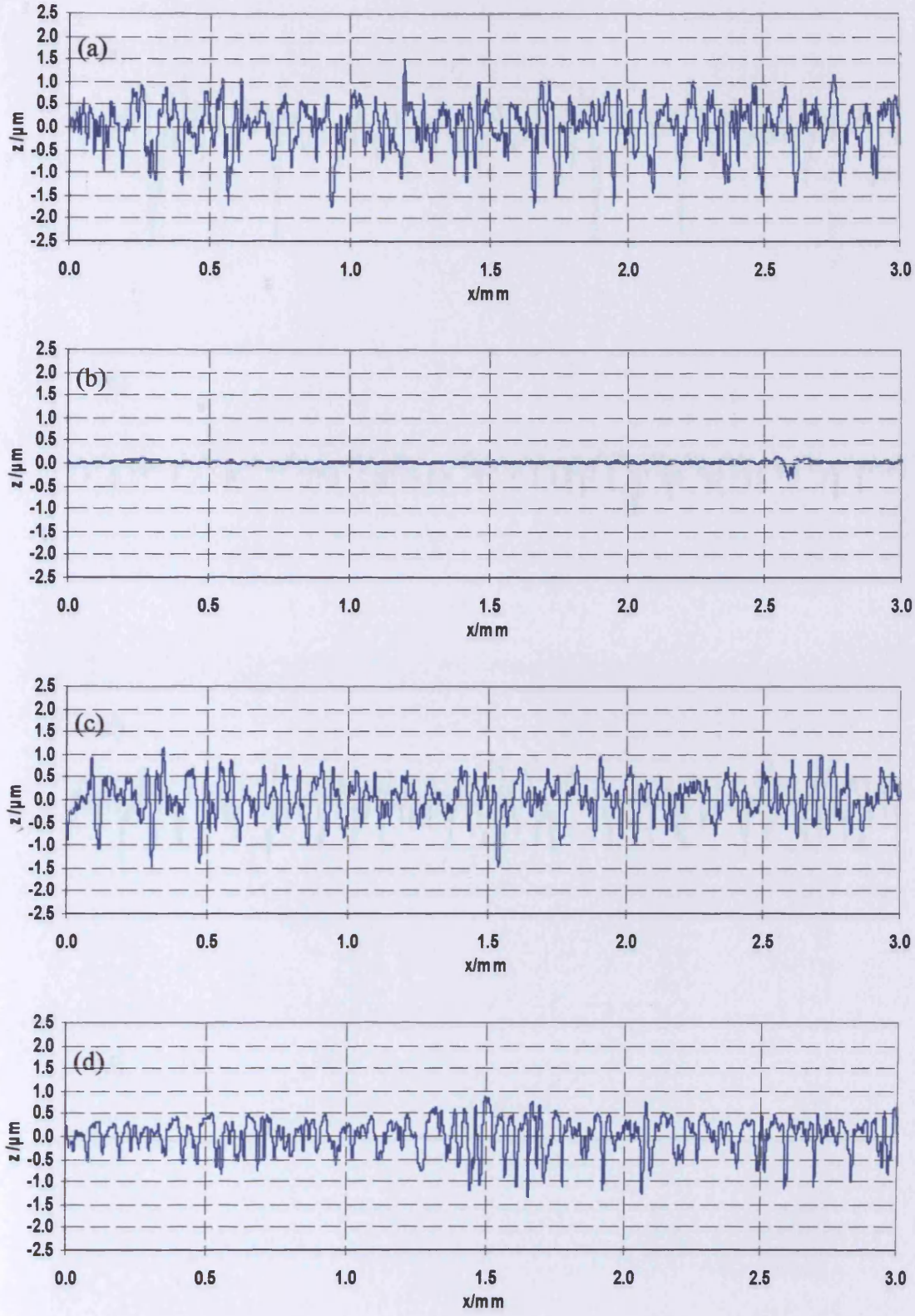

Figure 3.71. Surface profiles taken in the circumferential direction from discs used in test UTRC 22
Profiles from fast disc (a) before test; Ra =0.412µm (b) after test; Ra = 0.158µm
Profiles from slow disc (c) before test; Ra = 0.324µm (d) after test; Ra =0.240µm

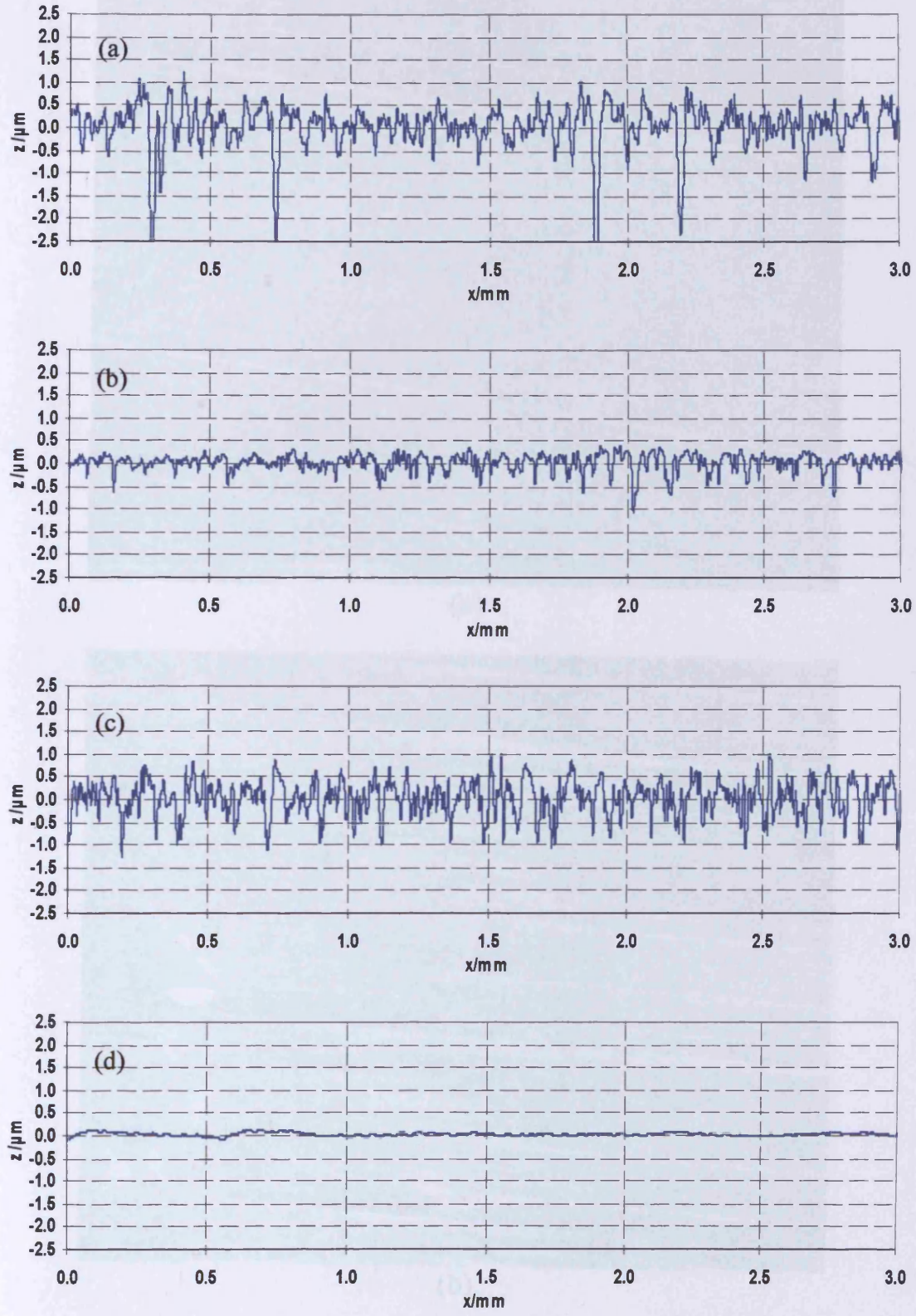

Figure 3.72. Surface profiles taken in the circumferential direction from discs used in test UTRC 26
Profiles from fast disc (a) before test; Ra = 0.362µm (b) after test; Ra = 0.144µm
Profiles from slow disc (c) before test; Ra = 0.321µm (d) after test; Ra = 0.037µm

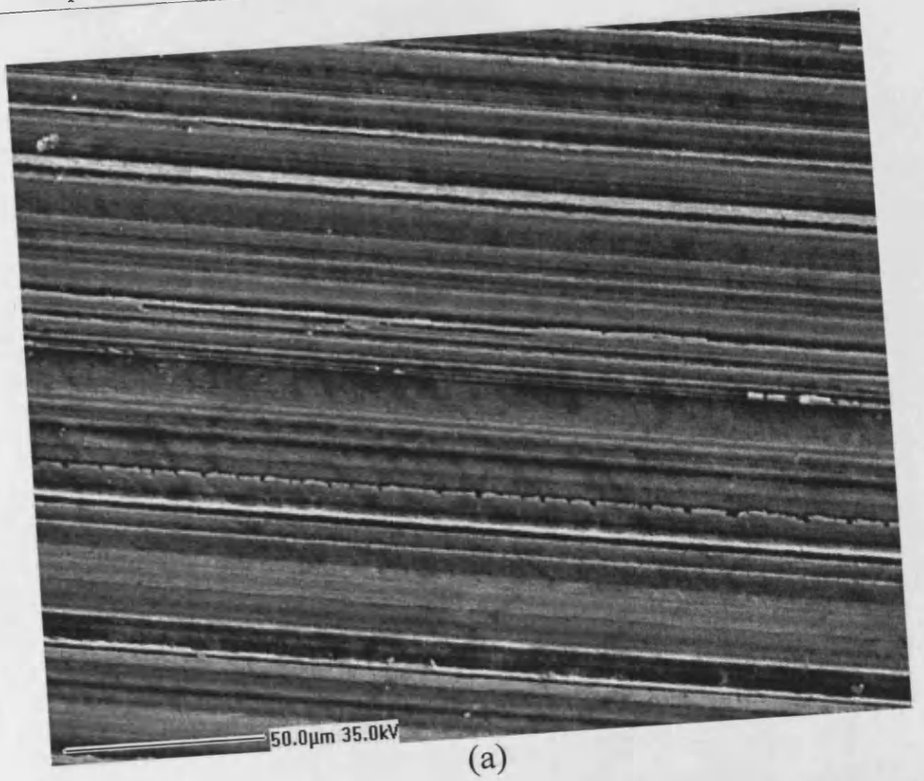

(a)

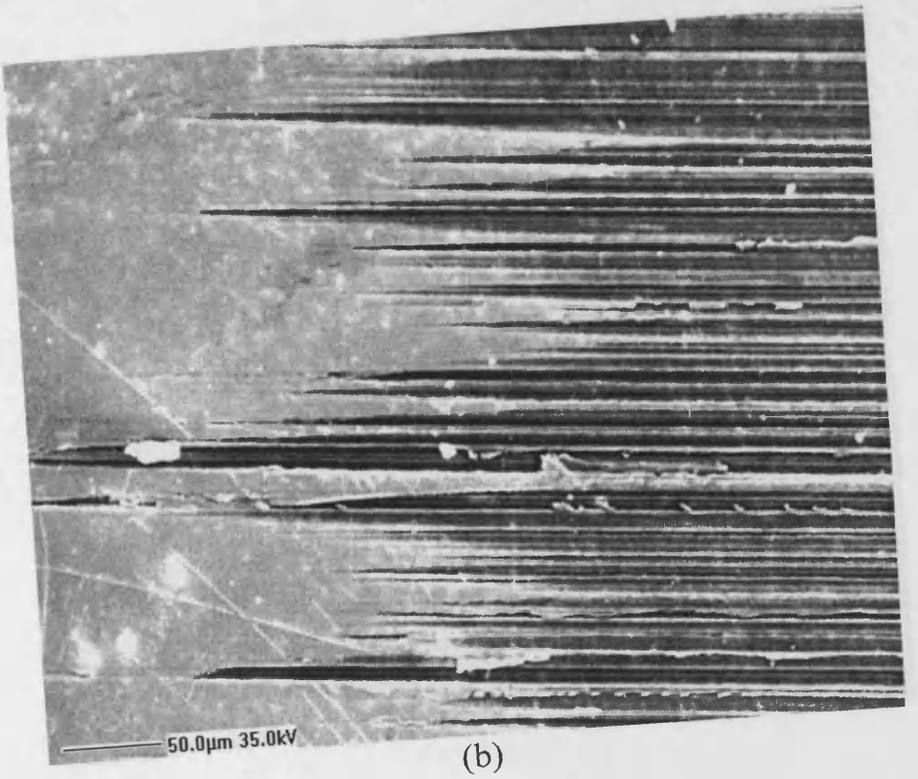

(b)

Figure 3.73. SEM images of surface of the slow disc used in test UTRC22.
(a) un-run surface
(b) polished run in surface with un run surface on the right

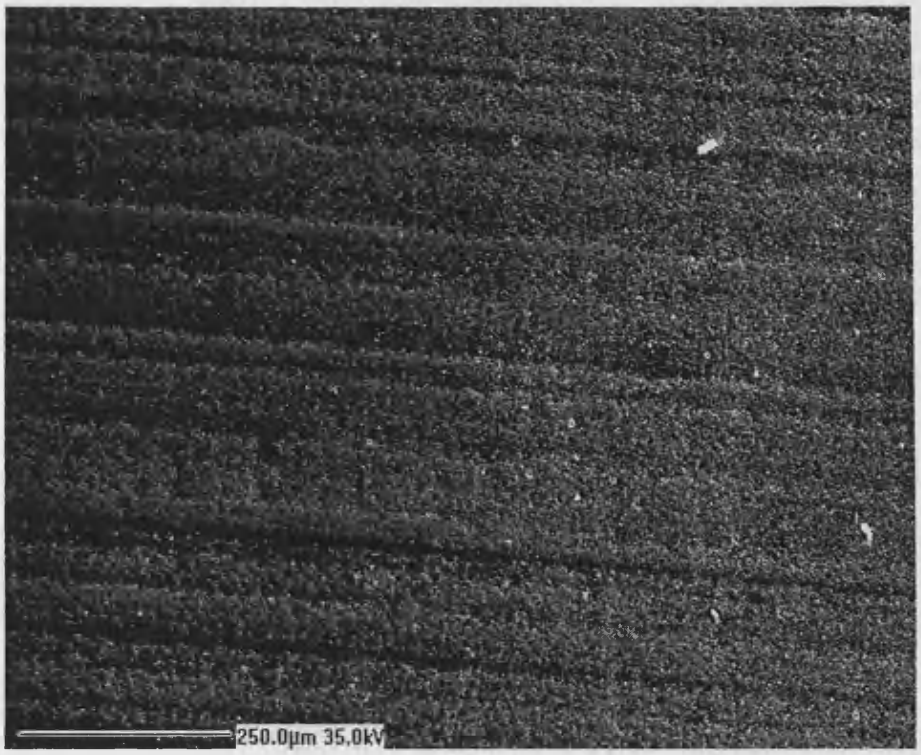

(a)

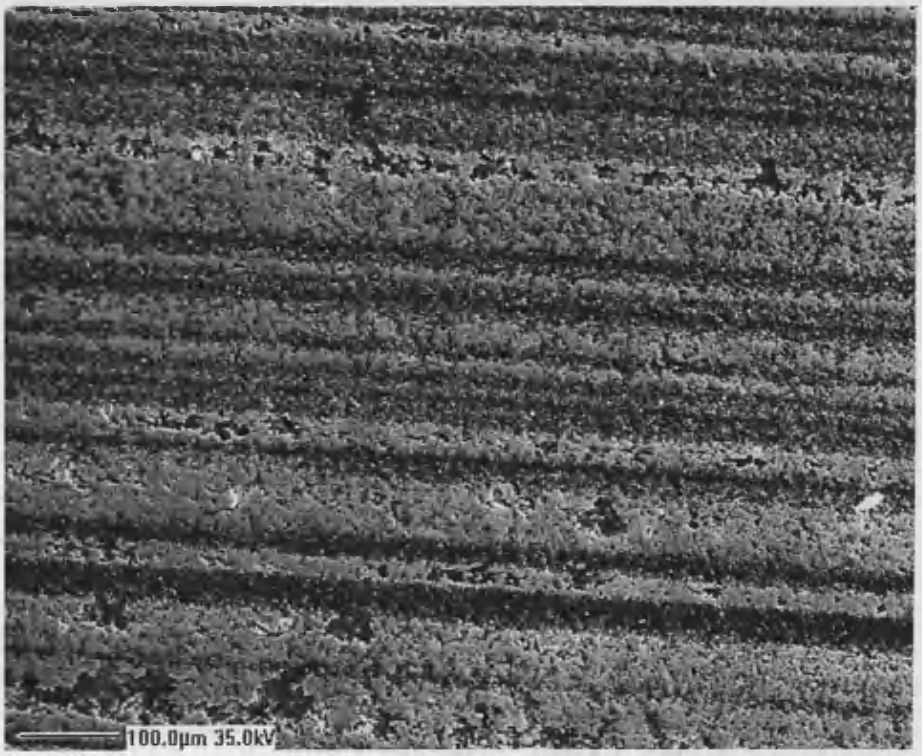

(b)

Figure 3.74. SEM images of surface of the slow disc used in test UTRC22.
(a) coated unrun part to the right and the edge of the running track to left
(b)middle of the running track with coating removed in parts

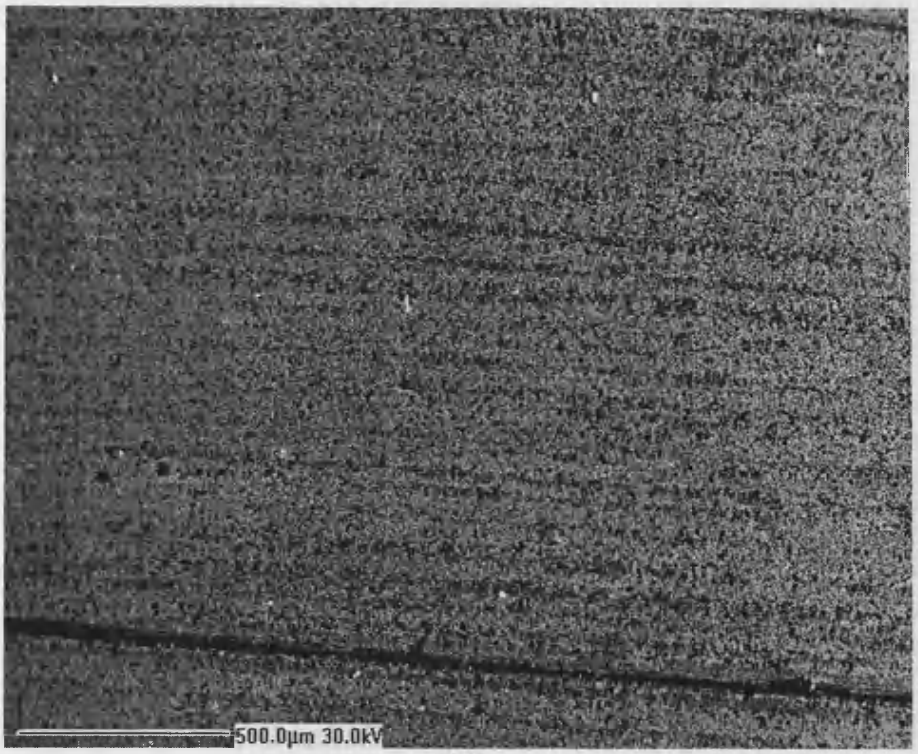

(a)

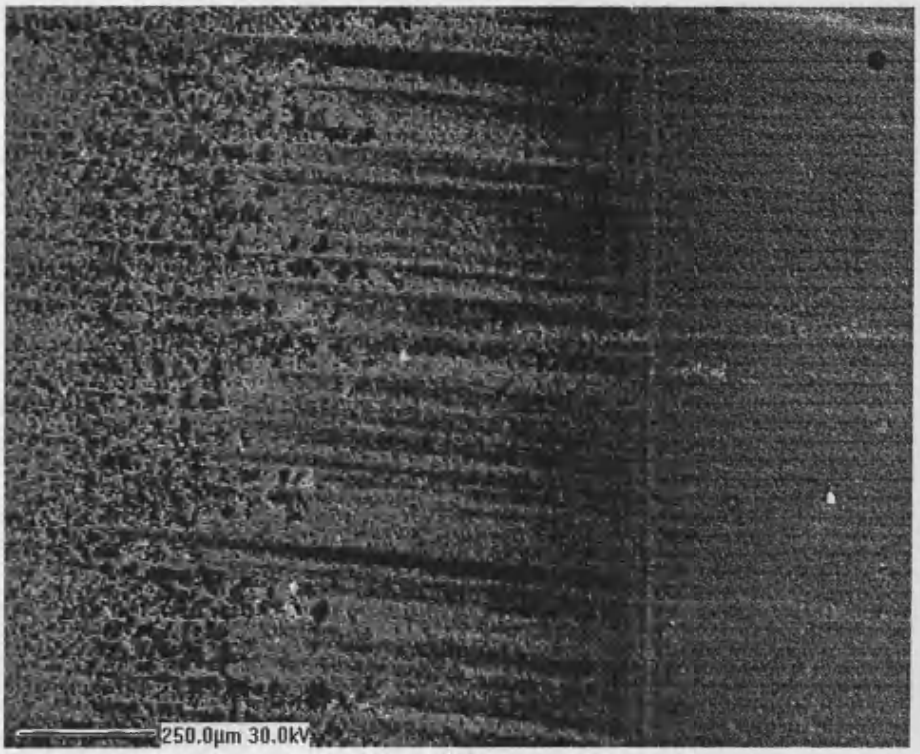

(b)

Figure 3.75. SEM images of surface of the fast disc used in test UTRC26
(a) middle of the running track
(b) edge of the running track with unrun surface on the right and run in surface to the left

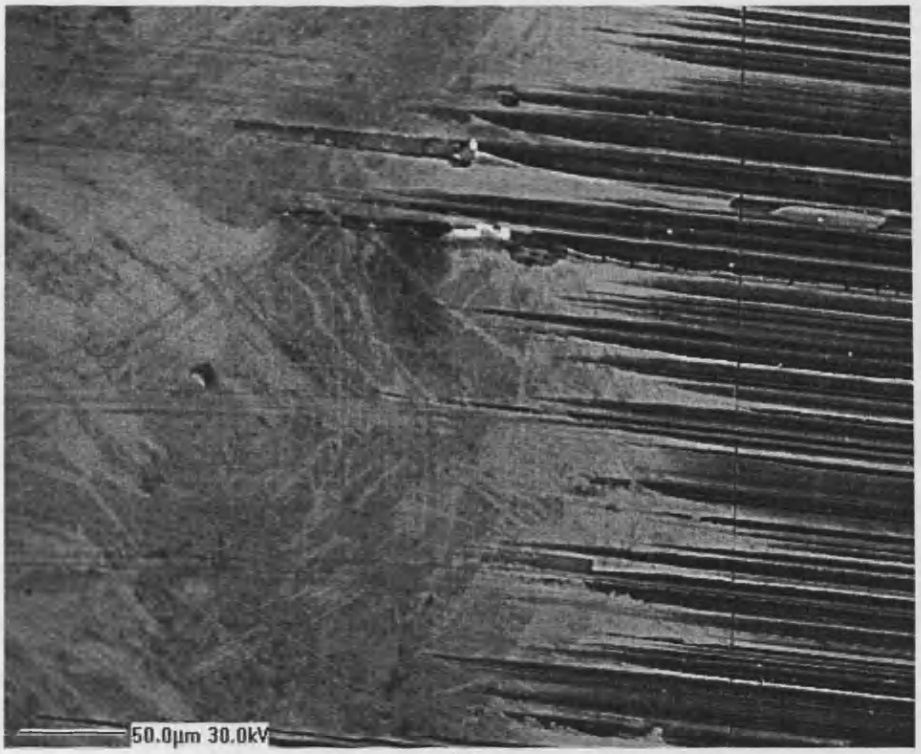

(a)

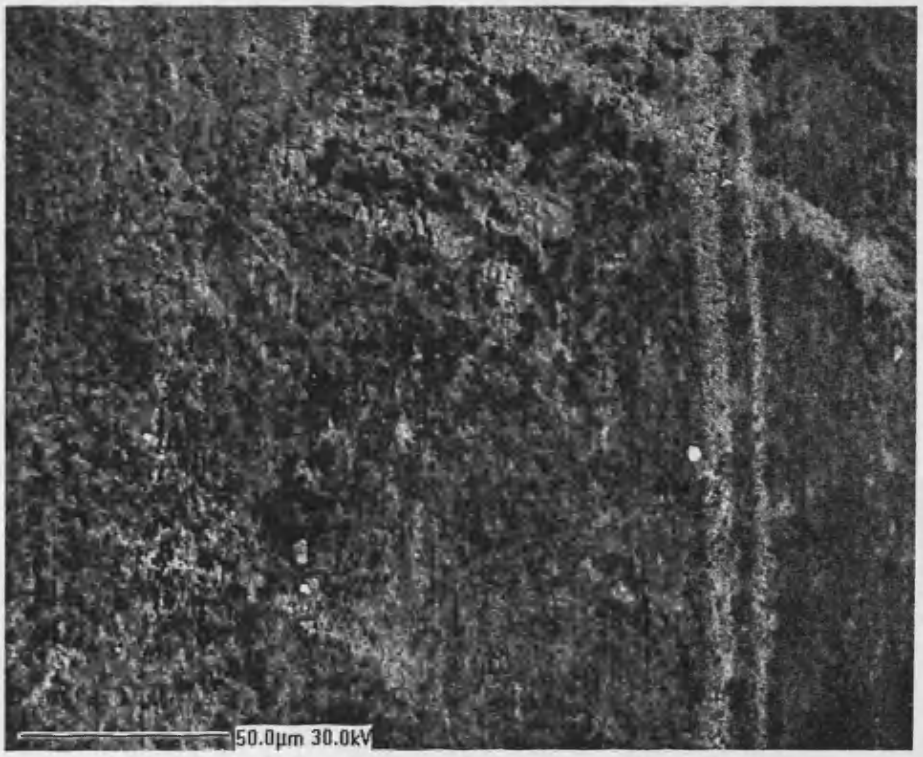

(b)

Figure 3.76. SEM images of surface of the slow disc used in test UTRC26.
(a) polished, run in surface on left with unrun surface on right
(b) deterioration of coating near the middle of the running track

SEM images from test UTRC26 are shown in Figures 3.75 and 3.76. Figure 3.75 shows images from the fast (coated) disc. The upper image is from the middle of the running track. There is no indication of distress or even slight scratching of the surface. The horizontal dark line at the lower edge of this image is a residual valley from the grinding process. The lower image is from the edge of the running track and shows un-run surface to the right and the edge of the running track to the left. The coating in this area appears to have been changed in appearance but is still intact. Figure 3.76 shows high magnification images from the ground/uncoated disc (slow shaft). The upper image shows the edge of the running track with un-run ground surface to the right and the heavily polished surface in the running track to the left. However this "polishing" has a different appearance to that found in the ground discs when this was the fastest of the pair. For example Figure 3.73 (b) shows a more smoothly uniform appearance than that of Figure 3.76(a). The surface in the latter image gives an impression of having been "pummelled".

Discussion of the results presented in this chapter will be given in Chapter 6.

Chapter 4

Experiments on scuffing with two discs having different finish; and on pre-running-in and scuffing

4.1. Introduction

In addition to the scuffing experiments designed to investigate the performance of a super-hard coating a short series of scuffing tests was also carried out using the conventional Rolls-Royce gear steel in the uncoated state. The aim of the experiments was to investigate the scuffing behaviour of a pair of surfaces, one of which was axially ground and the other was superfinished. Although the pairing of superfinished/superfinished surfaces had been studied in the work of Patching using the Rolls-Royce steel he had not considered the behaviour when the surfaces were of two significantly different roughness values. The properties of the steel in question have been given in Chapter 2. As in the series of experiments described in the previous chapter the oil used was Mobiljet 2 and the operating conditions in terms of the slide/roll ratio and loading sequence were as before. All tests in this series were carried out at a sliding speed of 12 m/s.

A second short series of tests was carried out in which a pair of ground discs was first run together under free rolling conditions at a load up the maximum load capacity of the machine. The aim in this case was to investigate the idea that by loading the surfaces together at a heavy load there would be significant smoothing of the surface profiles as a result of plastic deformation of the surface asperities, and it was of interest to discover if this had any significant subsequent effect on the scuffing performance, under sliding conditions.

4.2. Scuffing tests with two different surface finishes

Tests were conducted with two different surface finishes (described as ground and superfinished) with the discs selected from a stock of specimens that had been axially ground to a roughness of approximately 0.4μm, Ra. A batch of these discs was superfinished using the Abral polishing process as described in section 2.6 to a finish better than 0.04μm. These tests were done to confirm the scuffing behaviour of the discs with the same configuration of UTRC discs detailed in section 3.2.3. The discs used in this chapter are designated using the letters RR6010-b-*nn* where *nn* is a serial number unique to each disc. The individual tests are designated AD*mm*, where *mm* is the test serial number. The hardness of these discs (680 Vickers Hardness) is lower than that of the UTRC discs. Eight tests were conducted using this configuration, four tests with the ground disc on the fast shaft and the other four tests with the superfinished disc on the fast shaft. All the tests were conducted at the same intermediate sliding speed of 12m/s.

4.2.1. Ground on Superfinished tests with superfinished discs on the fast shaft

Four tests were conducted with the superfinished disc on the fast shaft, and a summary of the results obtained is given in Table 4.1.

Table 4.1.
Summary of scuffing conditions-grnd discs running against s.f. dics at sliding speed of 12m/s-grnd on fast shaft

Test	AD01		AD02		AD06		AD07	
Test Discs	rrc56	rrc27	rrc84	rrc18	rrc69	rrc59	rrc50	rrc15
Shaft Mounting	fast	slow	fast	slow	fast	slow	fast	slow
Disc Condition	s.f.	grnd	s.f.	grnd	s.f.	grnd	s.f.	grnd
temperature/°C	127	100	158	121	203	137	275	191
Roughness, Ra, before/μm	0.045	0.386	0.045	0.366	0.086	0.357	0.047	0.277
Roughness, Ra, after/μm	0.207	0.244	0.026	0.232	0.091	0.257	0.037	0.195
Scuffing load/N	1855		1866		2307		4927	
Max Hertz pressure/GPa	1.3		1.3		1.4		1.8	
Friction force/N	38		53		66		95	
Friction coefficient	0.021		0.028		0.028		0.023	
Blok flash temp. rise/°C	110		153		172		185	

grnd - ground; s.f. - super finished

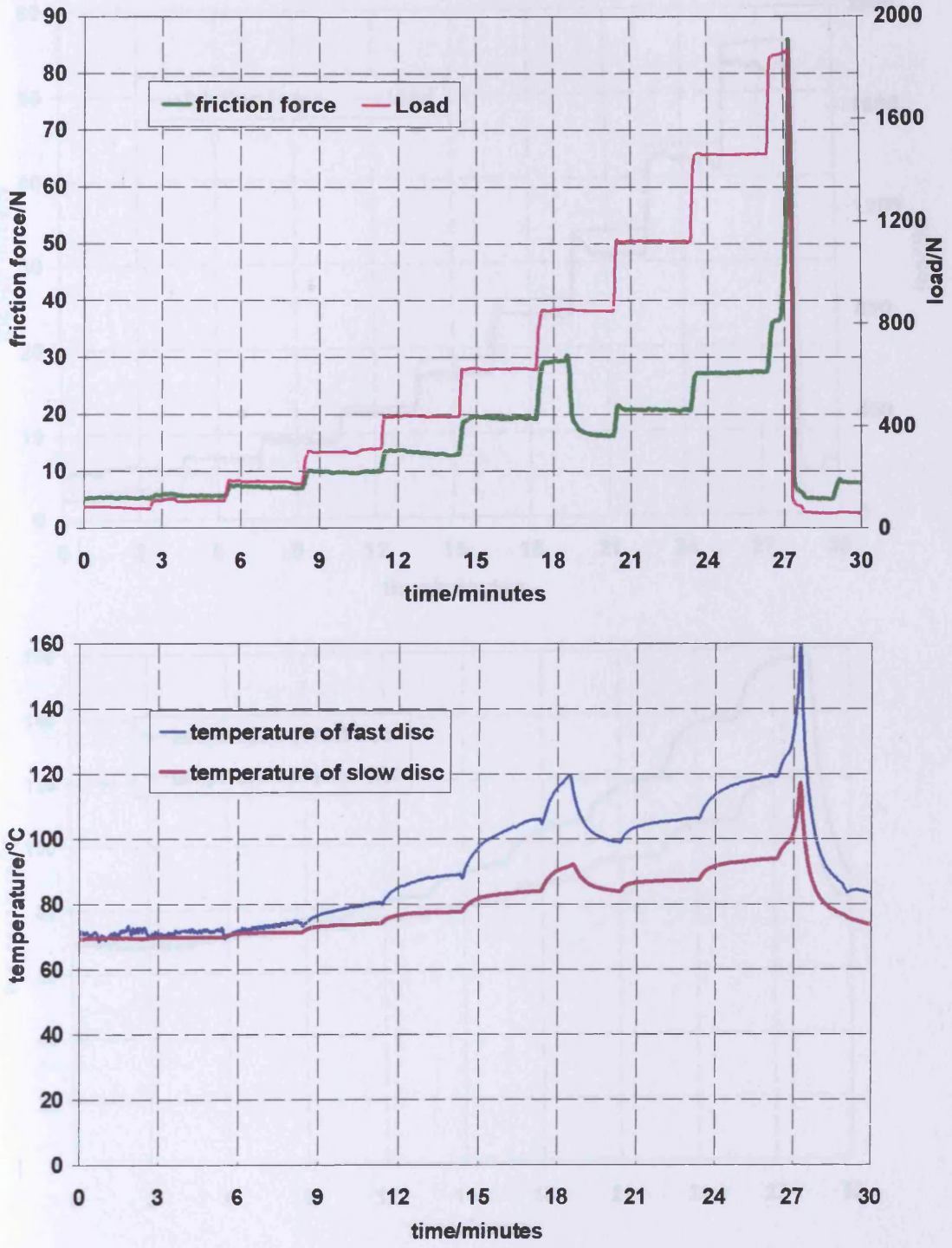

Figure 4.1. Record of test AD01; upper graph shows applied load and friction force; lower graph shows bulk temperature of the two discs.

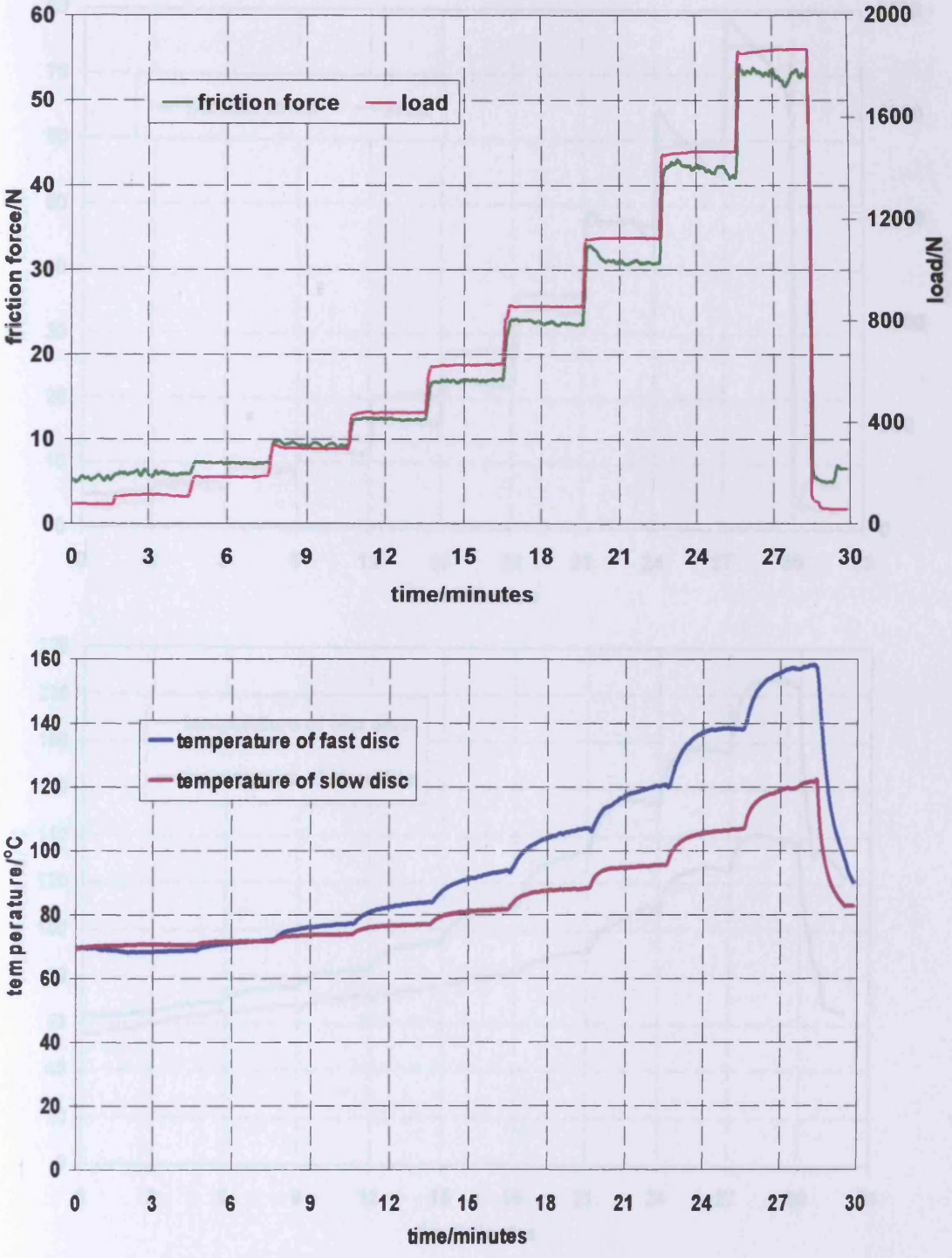

Figure 4.2. Record of scuffing test AD02, upper graph shows applied load and friction force; lower graph shows bulk temperatures of the two discs

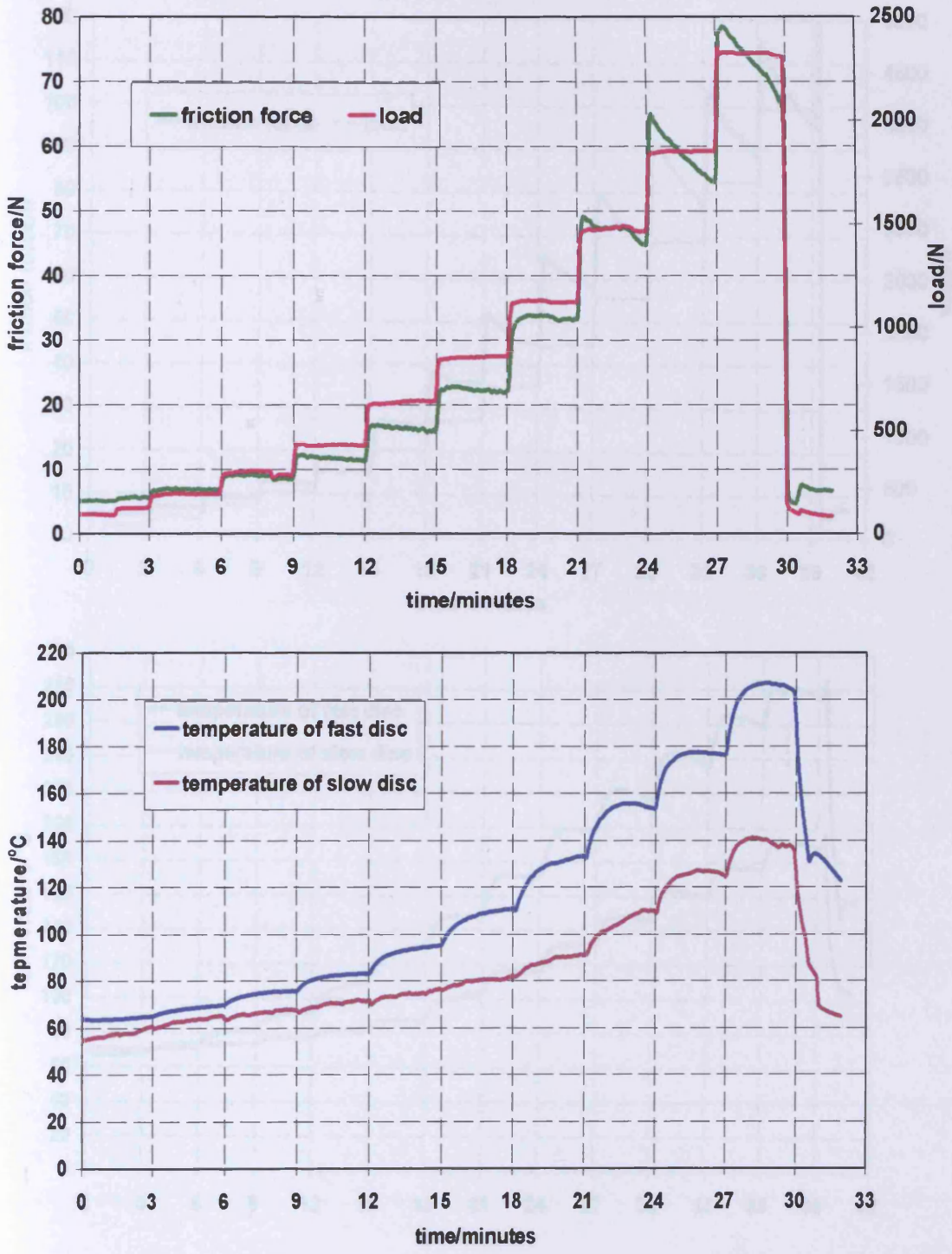

Figure 4.3. Record of scuffing test AD06, upper graph shows applied load and friction force; lower graph shows bulk temperatures of the two discs

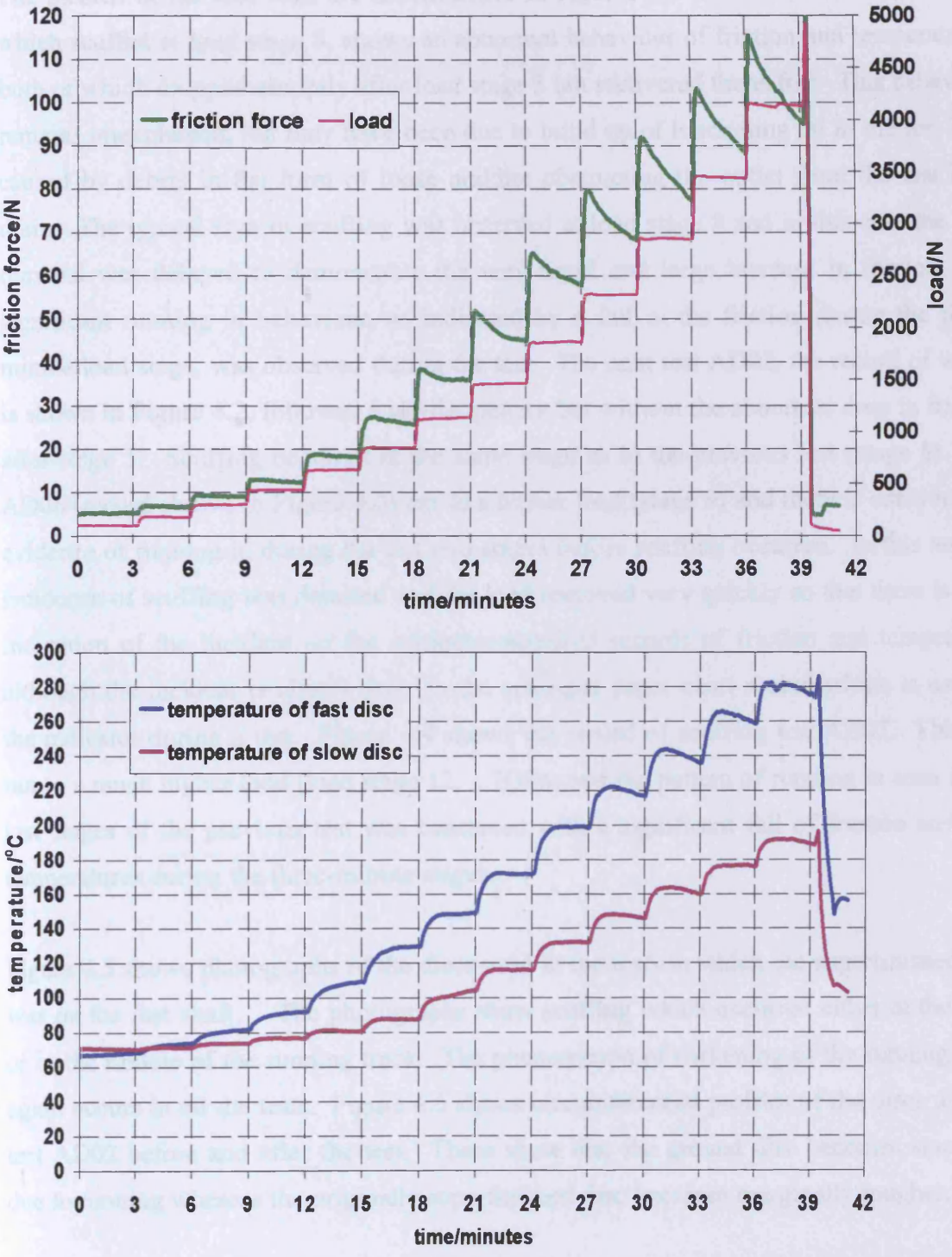

Figure 4.4. Record of scuffing test AD07, upper graph shows applied load and friction force; lower graph shows bulk temperatures of the two discs

The records of the four tests are shown above in Figures 4.1 to 4.4. The first test AD01 which scuffed at load stage 8, shows an abnormal behaviour of friction and temperatures, both of which dropped abruptly after load stage 5 but recovered thereafter. This behaviour remains unexplained, but may have been due to build up of lubricating oil in the test head caused by debris in the form of loose araldite obstructing the outlet from the test head drain. The typical sign of scuffing was observed at load stage 8 and in this case the load removal was delayed to demonstrate the very rapid and large increase in friction. No significant running in behaviour, as indicated by a fall in the friction during the three-minute load stage, was observed during the test. The next test AD02, the record of which is shown in Figure 4.2, followed a similar pattern but without the abnormal drop in friction after stage 5. Scuffing occurred at the same stage as in the previous test (stage 8). Test AD06 (record shown in Figure 4.3) ran to a higher load (stage 9) and there is considerable evidence of running in during the last two stages before scuffing occurred. In this test the incidence of scuffing was detected and the load removed very quickly so that there is little indication of the incident on the computer-acquired records of friction and temperature although the incident is clearly seen on the analogue paper chart record which is used as the indicator during a test. Figure 4.4 shows the record of scuffing test AD07. This test ran to a much higher load (load stage 12, 1.7GPa) and the pattern of running in seen in the last stages of the previous test was continued with a significant fall of friction and disc temperatures during the three-minute stages.

Figure 4.5 shows photographs of the discs used in the tests in which the superfinished disc was on the fast shaft. The photographs show scuffing which occurred either at the edge or in the middle of the running track. The phenomenon of darkening of the running track again occurs in all the tests. Figure 4.6 shows circumferential profiles of the discs used in test AD02 before and after the test. These show that the ground disc becomes smoother due to running whereas the originally superfinished disc becomes marginally rougher.

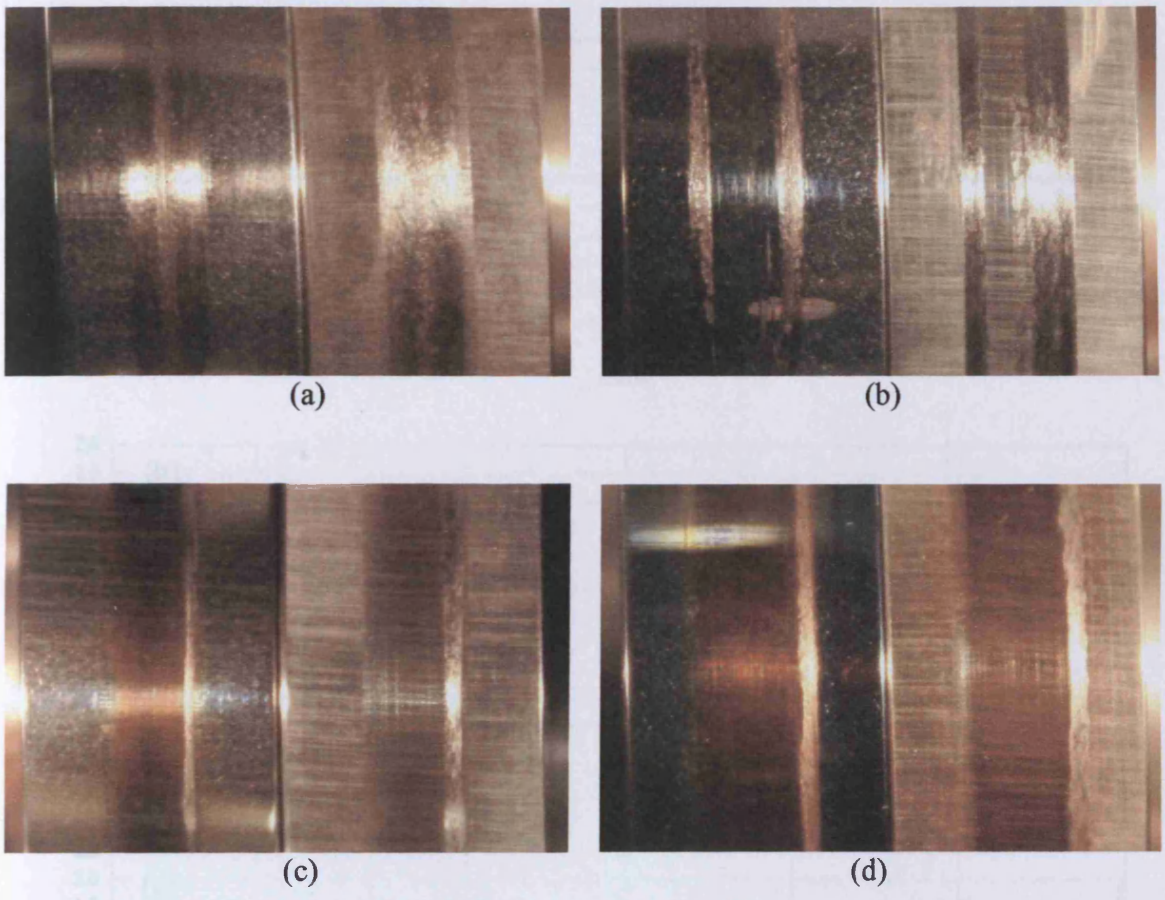

Figure 4.5. Photographs of discs following testing at 12m/s
(a) AD01; left: super finished disc on fast shaft; right: ground disc on slow shaft
(b) AD02; left: super finished disc on fast shaft; right: ground disc on slow shaft
(c) AD06; left: super finished disc on fast shaft; right: ground disc on slow shaft
(d) AD07; left: super finished disc on fast shaft; right: ground disc on slow shaft

SEM images corresponding to test AD02 are given in Figures 4.7 and 4.8. Figure 4.7 shows images from the superfinished disc used on the fast shaft. The upper image shows the edge of the scuffing region with the run part of the running track to the right. The lower image shows the other edge of the scuffing track. The upper image in Figure 4.8 shows the ground un-run surface to the right of the image and the edge of running track to the left. There is some evidence of light scoring or scratching (vertical lines) on the running track. The lower image shows the middle part of the running track with a central band of severe scuffing in the middle of the track. This image is taken from the disc shown in Figure 4.5 (b) which is an unusual case where scuffing occurred at the edges of the track and in a separate band in the middle of the track.

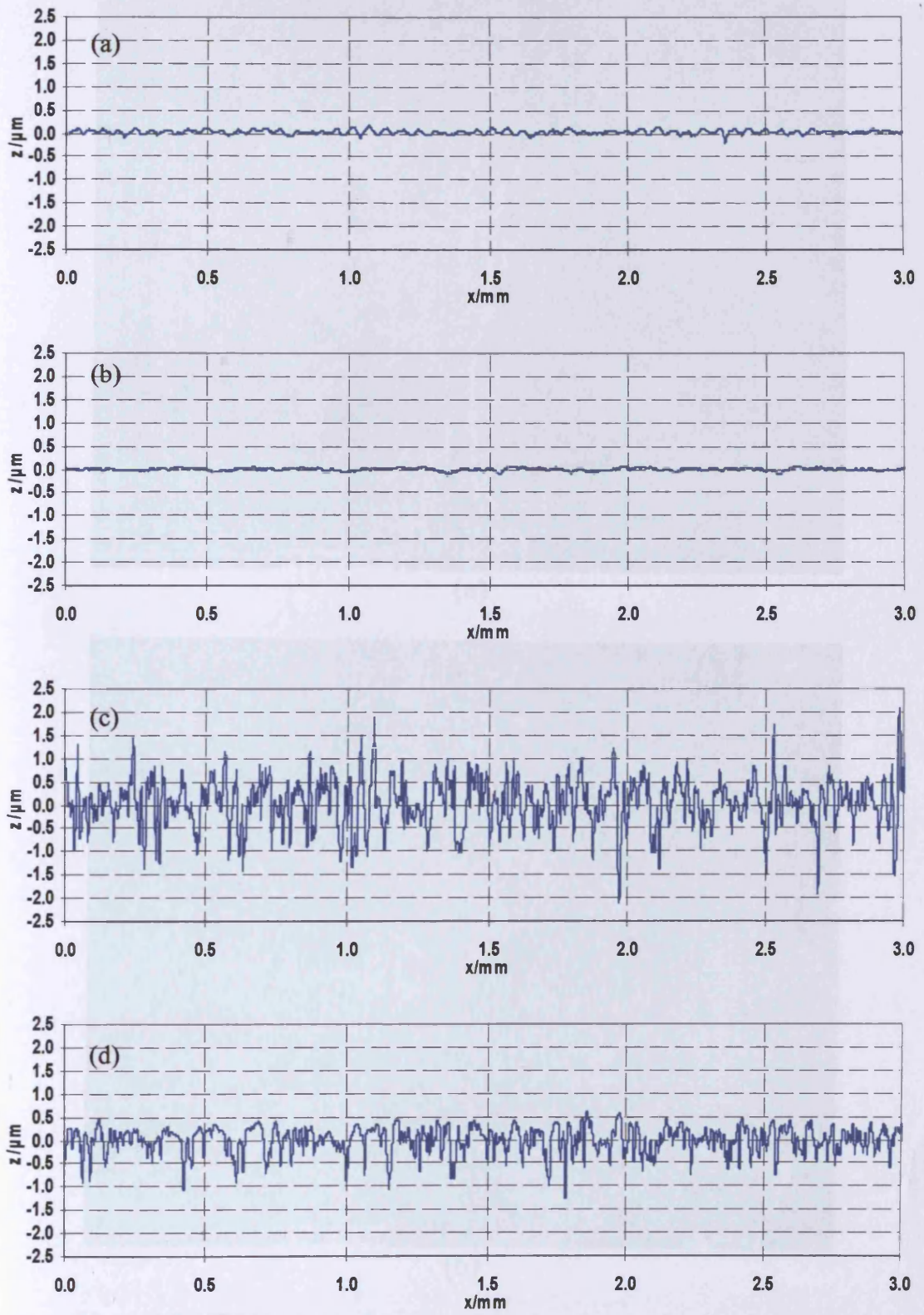

Figure 4.6. Surface profiles taken in the circumferential direction from discs used in test AD02
Profiles from fast disc (a) before test; Ra = 0.041µm (b) after test; Ra = 0.024 µm
Profiles from slow disc (c) before test; Ra = 0.379µm (d) after test; Ra = 0.222 µm

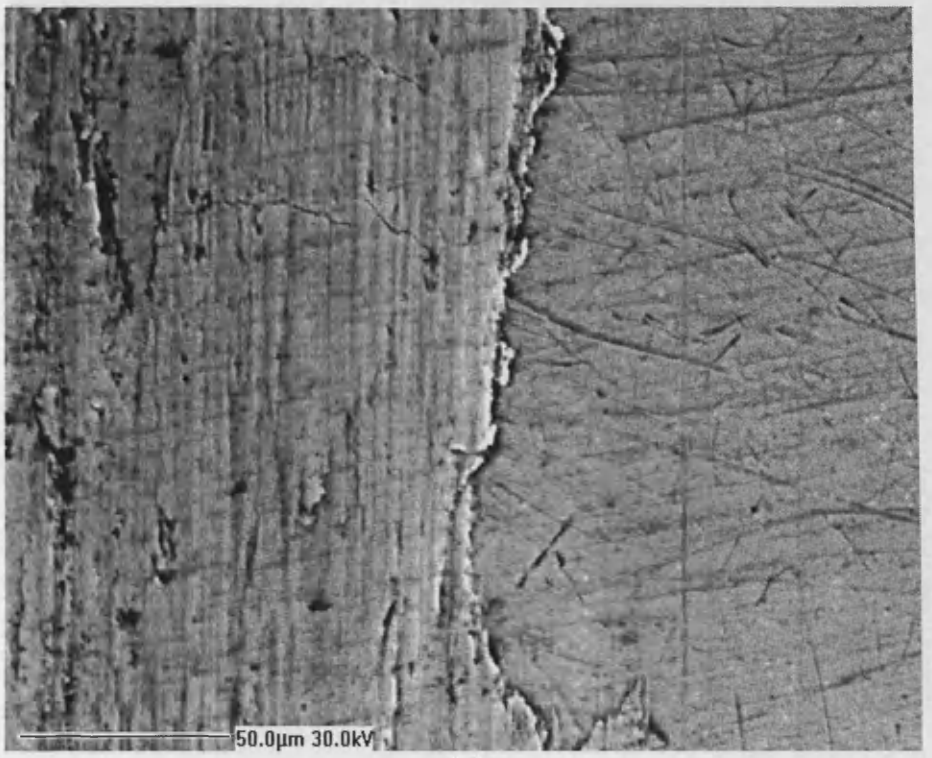

(a)

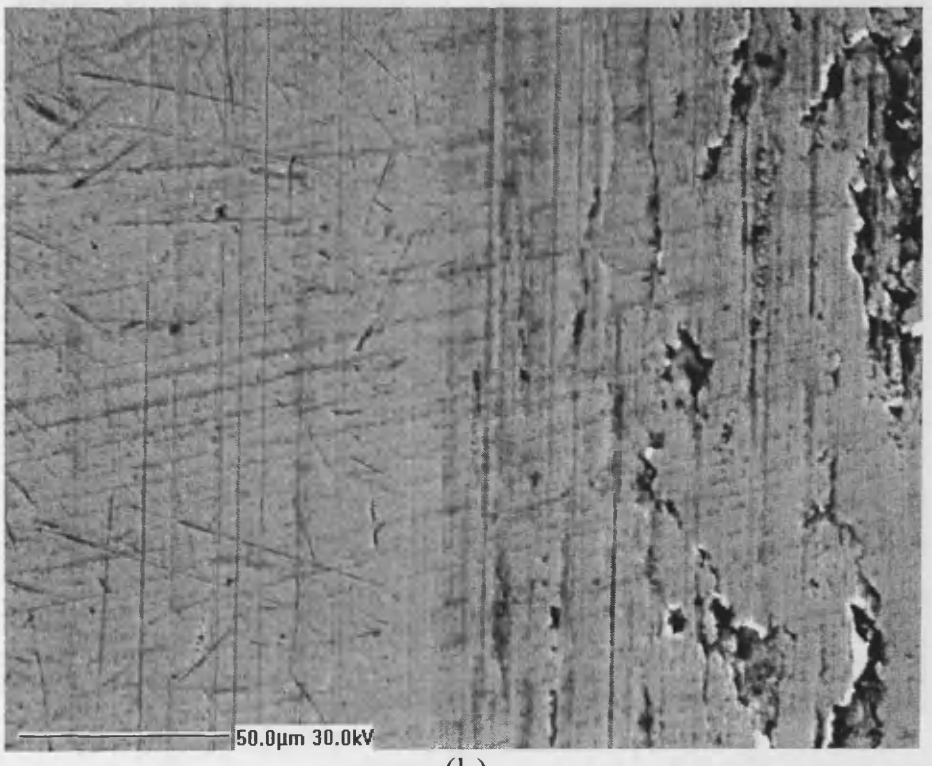

(b)

Figure 4.7. SEM images of surface of the fast disc used in test AD02.
(a) scuffed part on the left and unrun surface on the right
(b) run surface with scuffed surface to the right

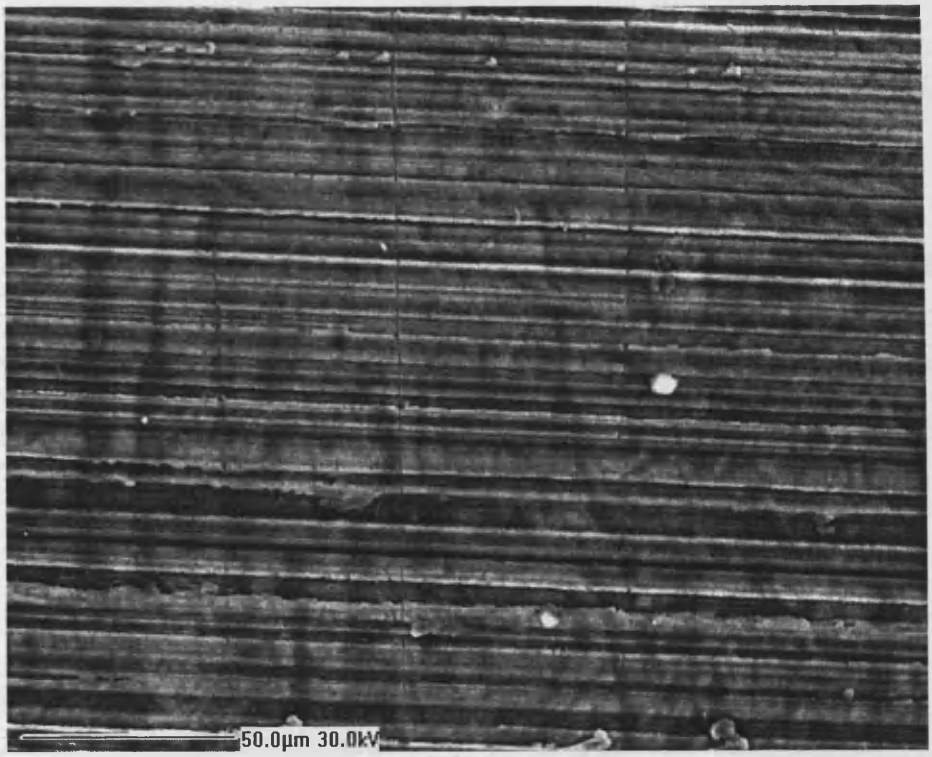

(a)

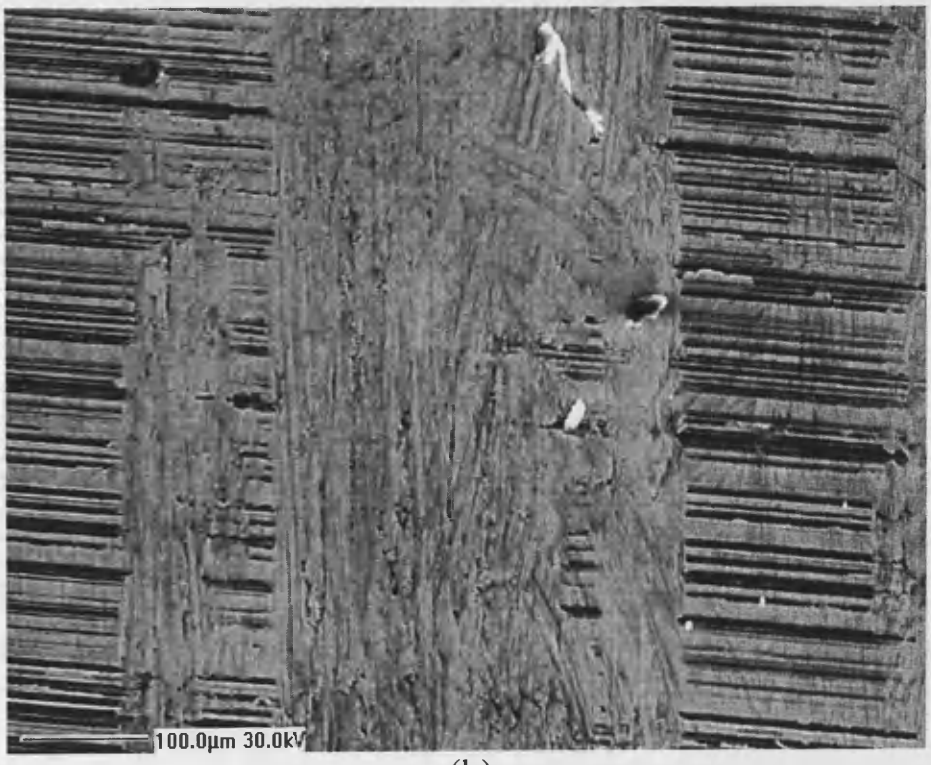

(b)

Figure 4.8. SEM images of surface of the slow disc used in test AD02.
(a) unrun condition of the disc
(b) scuffing mark in the middle with run in surface to the sides

4.2.2. Ground on superfinished tests with ground disc on the fast shaft

Four tests were conducted with this configuration at the intermediate sliding speed of 12m/s and the summary of the tests is given in Table 4.2.

Table 4.2.
Summary of scuffing conditions-grnd discs running against s.f. dics at sliding speed of 12m/s-grnd. on fast shaft

Test	AD03		AD04		AD05		AD08	
Test Discs	rrc67	rrc06	rrc24	rrc01	rrc95	rrc56	rrc81	rrc25
Shaft Mounting	fast	slow	fast	slow	fast	slow	fast	slow
Disc Condition	grnd	s.f.	grnd	s.f.	grnd	s.f.	grnd	s.f.
temperature/°C	220	162	128	101	239	178	133	102
Roughness, Ra, before/μm	0.384	0.060	0.385	0.053	0.355	0.101	0.378	0.061
Roughness, Ra, after/μm	0.266	0.062	0.217	0.054	0.192	0.069	0.164	0.061
Scuffing load/N	3450		1866		4931		1844	
Max Hertz pressure/GPa	1.6		1.3		1.8		1.3	
Friction force/N	68		39		90		28	
Friction coefficient	0.023		0.021		0.021		0.015	
Blok flash temp. rise/°C	158		113		174		82	

grnd - ground; s.f. - super finished

The records of the tests are given in Figures 4.9 to 4.12. Running in (as evidenced by a falling of friction during a load stage) was observed in all the tests but again there was an abnormal drop in friction and temperatures in two of the tests (AD04 and AD08). Figure 4.9 show the record of test AD03 which follows the expected pattern and scuffs at load stage 12. Test AD04 (record shown in Figure 4.10) exhibits the unusual behaviour of a large fall in the friction which then recovers before the scuffing stage is reached. Test AD05 (record given in Figure 4.11) shows the same behaviour as test AD03 with running in and no unusual friction and temperature drop. Figure 4.12 shows the record of test AD08 which again follows the behaviour of test AD04 with abrupt friction and temperature drops. It is of interest to point out that in spite of the unusual behaviour seen in tests AD04 and AD08 they scuffed at the same load stage.

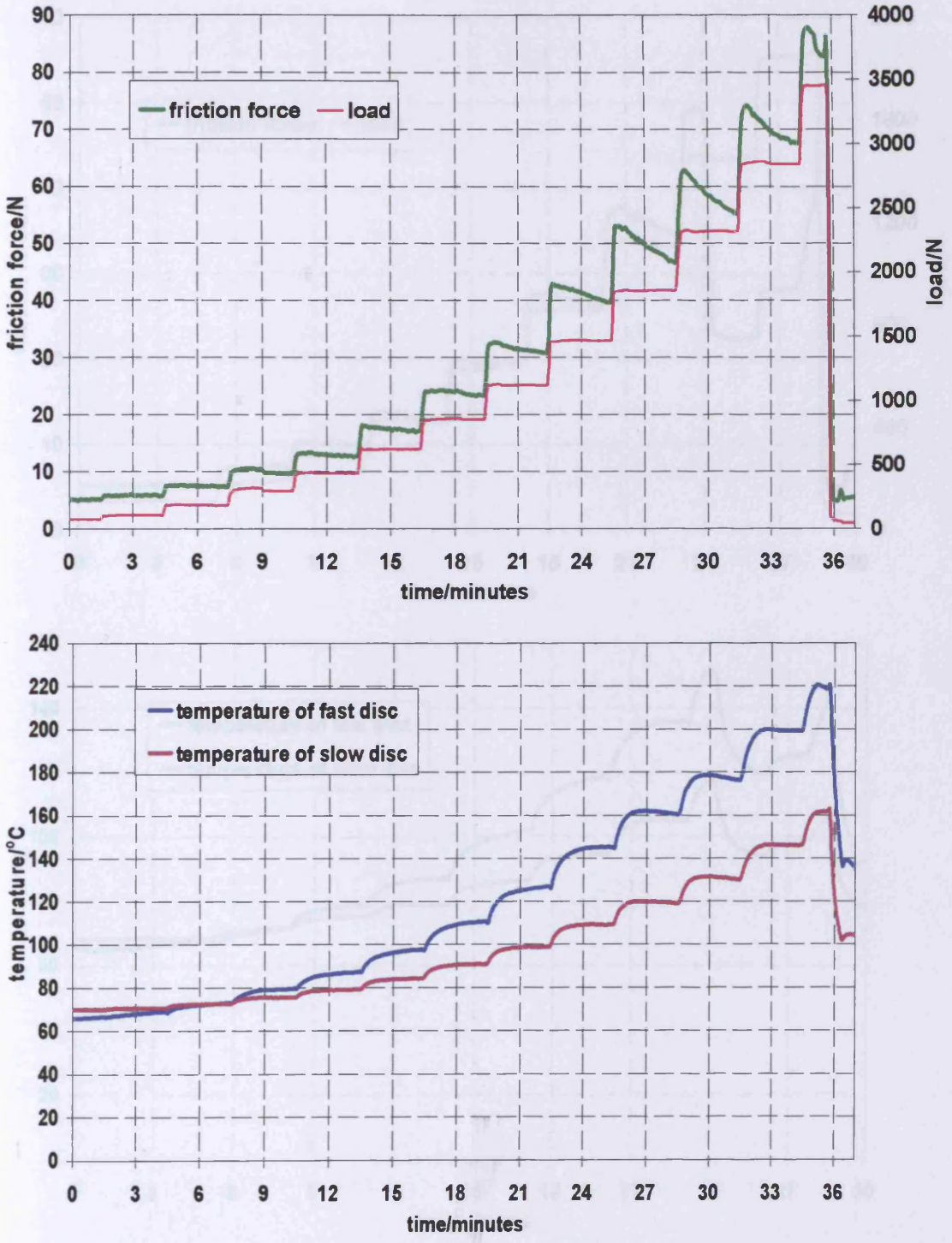

Figure 4.9. Record of scuffing test AD03, upper graph shows applied load and friction force; lower graph shows bulk temperatures of the two discs

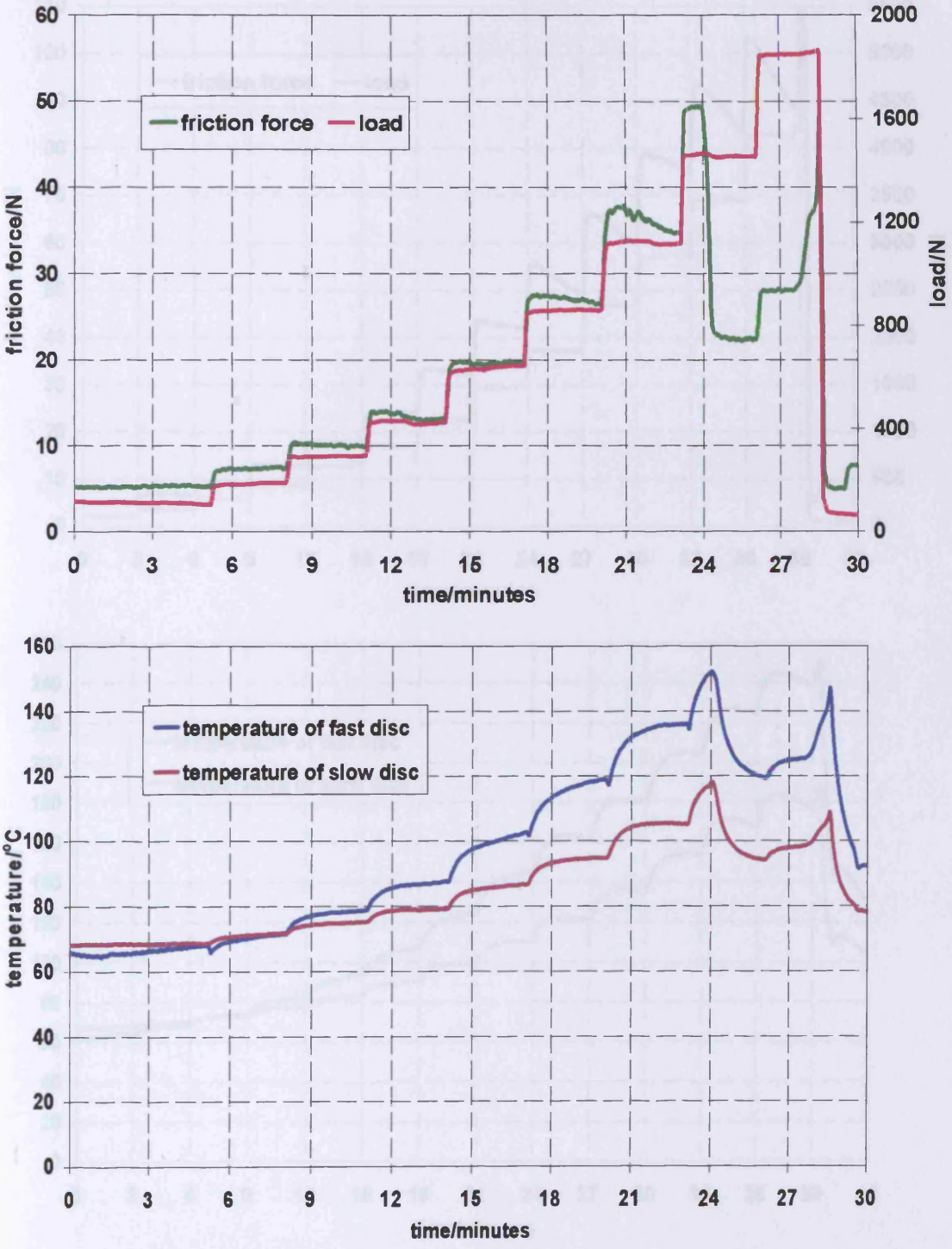

Figure 4.10. Record of scuffing test AD04, upper graph shows applied load and friction force; lower graph shows bulk temperatures of the two discs

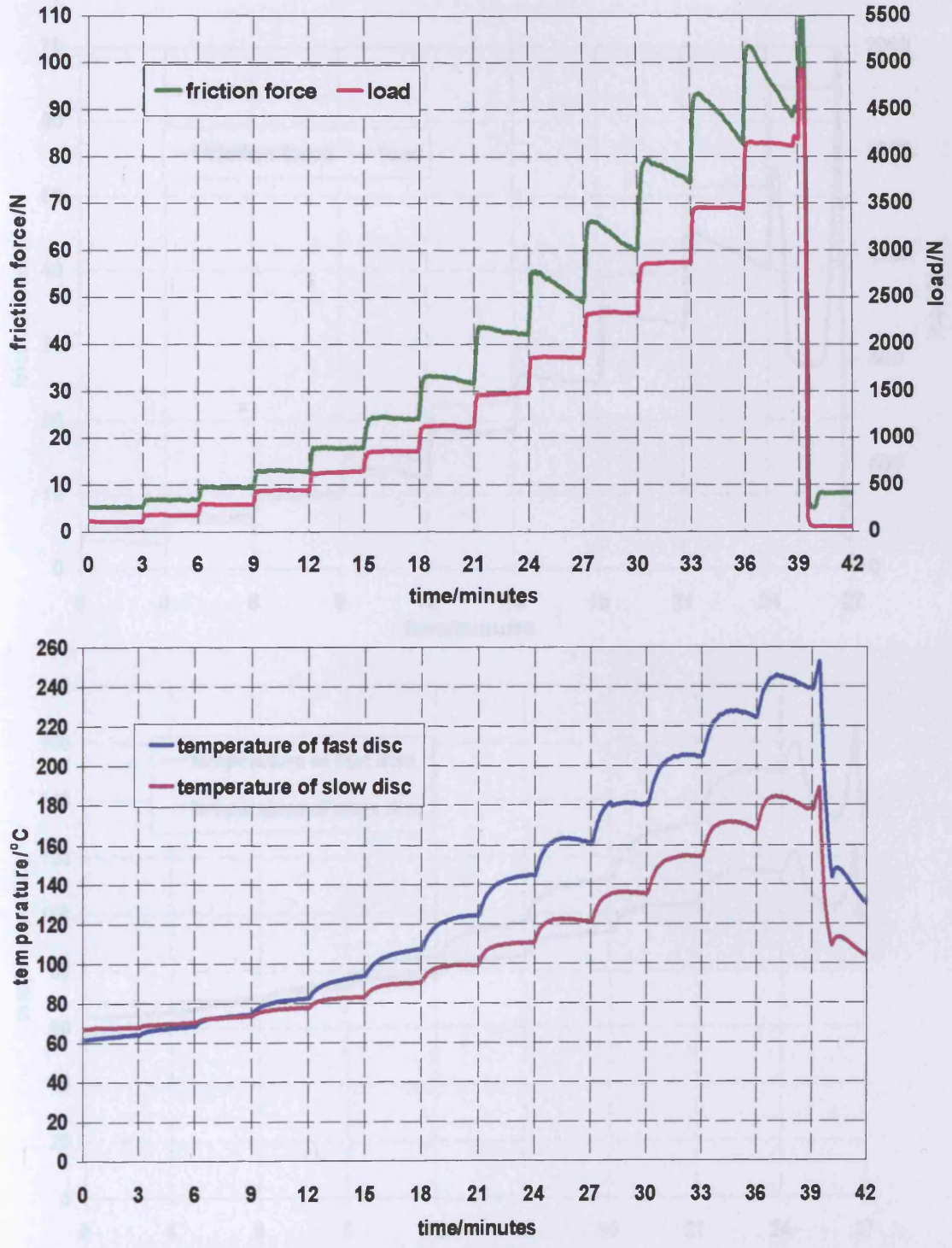

Figure 4.11. Record of scuffing test AD05, upper graph shows applied load and friction force; lower graph shows bulk temperatures of the two discs

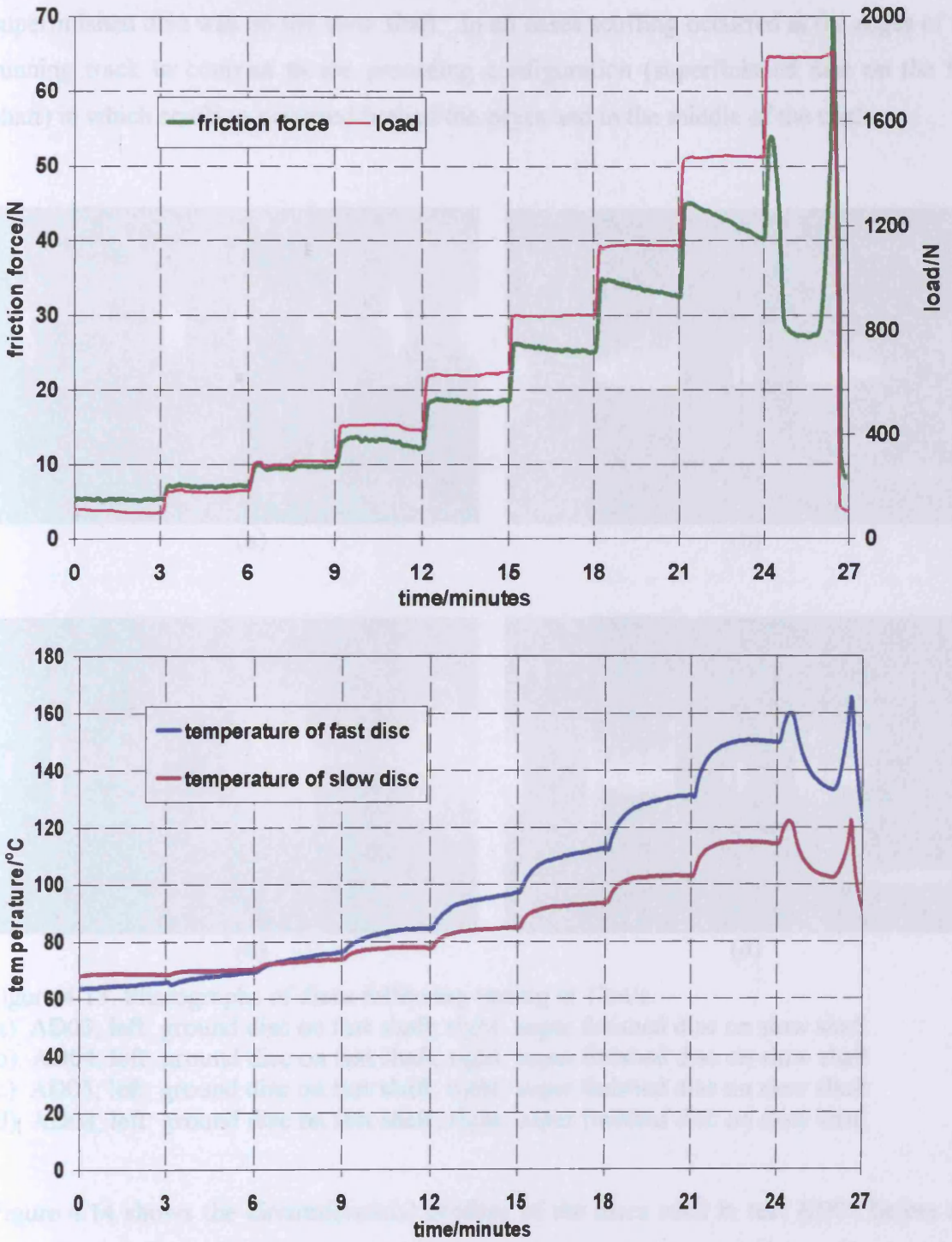

Figure 4.12. Record of scuffing test AD08, upper graph shows applied load and friction force; lower graph shows bulk temperatures of the two discs

Figure 4.13 shows photographs of the discs used in the above four tests in which the superfinished disc was on the slow shaft. In all cases scuffing occurred at the edges of the running track in contrast to the preceding configuration (superfinished disc on the fast shaft) in which scuffing occurred both at the edges and in the middle of the track.

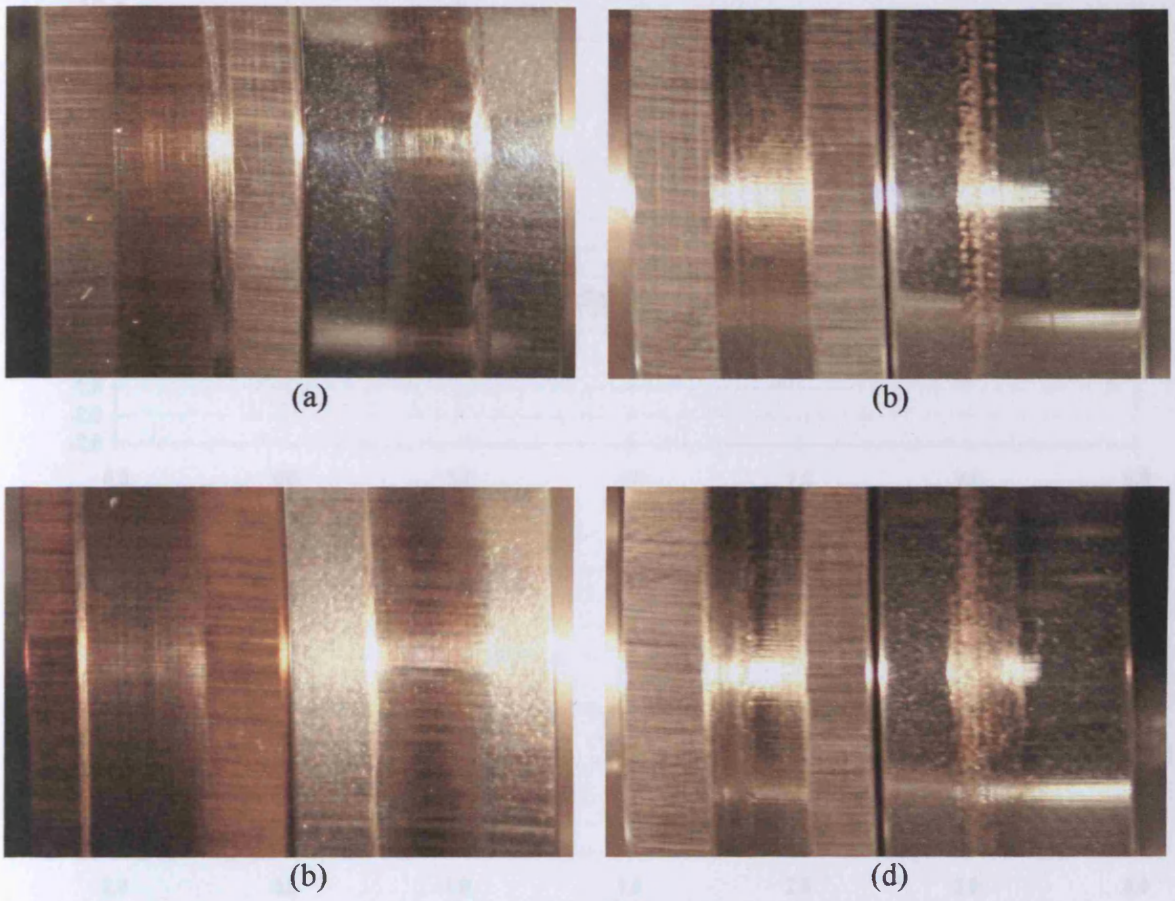

Figure 4.13. Photographs of discs following testing at 12m/s
(a) AD03; left: ground disc on fast shaft; right: super finished disc on slow shaft
(b) AD04; left: ground disc on fast shaft; right: super finished disc on slow shaft
(c) AD05; left: ground disc on fast shaft; right: super finished disc on slow shaft
(d) AD08; left: ground disc on fast shaft; right: super finished disc on slow shaft

Figure 4.14 shows the circumferential profiles of the discs used in test AD03 before and after the test. Again, the ground disc becomes slightly less rough and there is a marginal increase in the roughness of the superfinished disc.

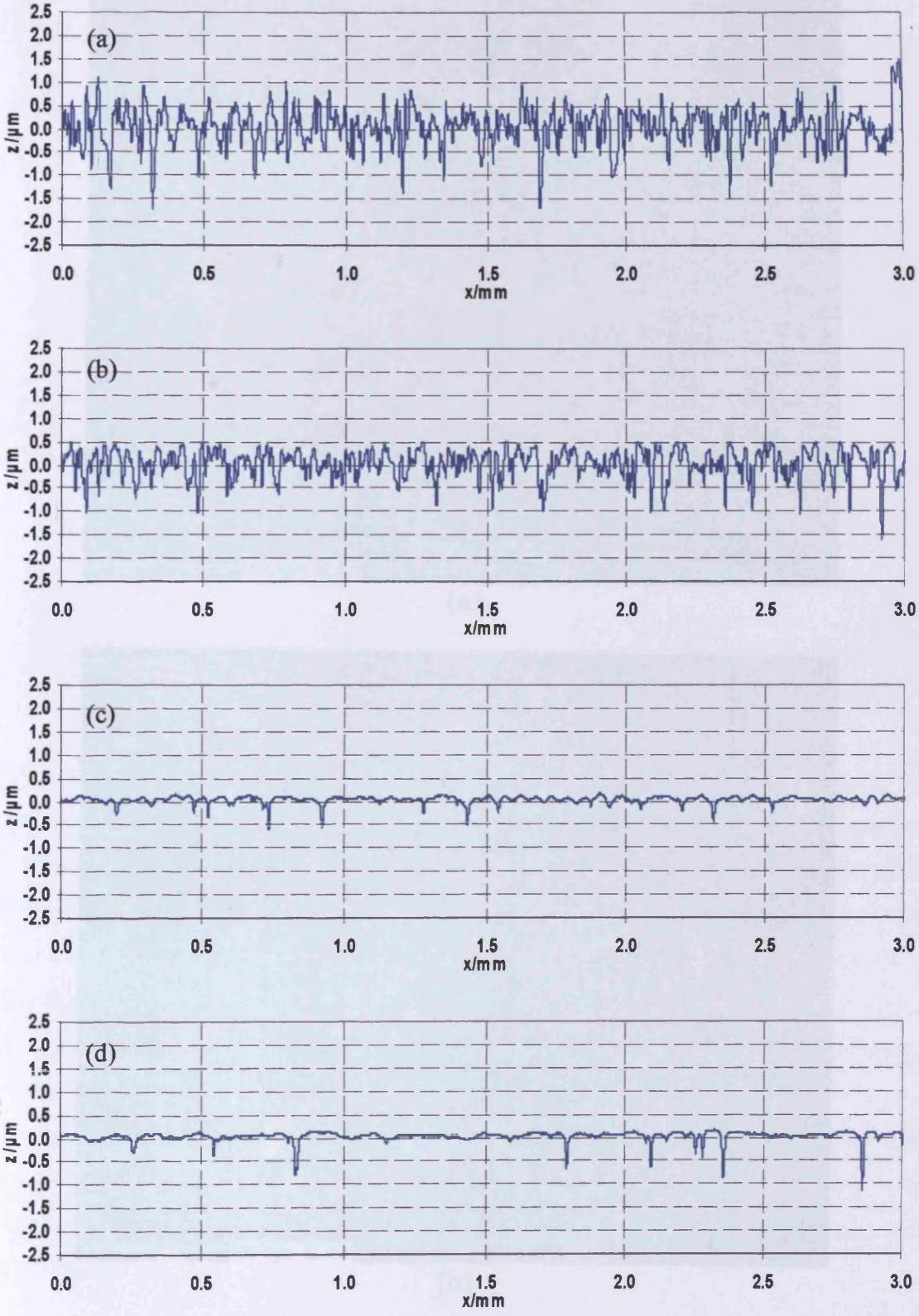

Figure 4.14. Surface profiles taken in the circumferential direction from discs used in test AD03
Profiles from fast disc (a) before test; Ra = 0.353µm (b) after test; Ra = 0.346µm
Profiles from slow disc (c) before test; Ra = 0.060µm (d) after test; Ra = 0.067µm

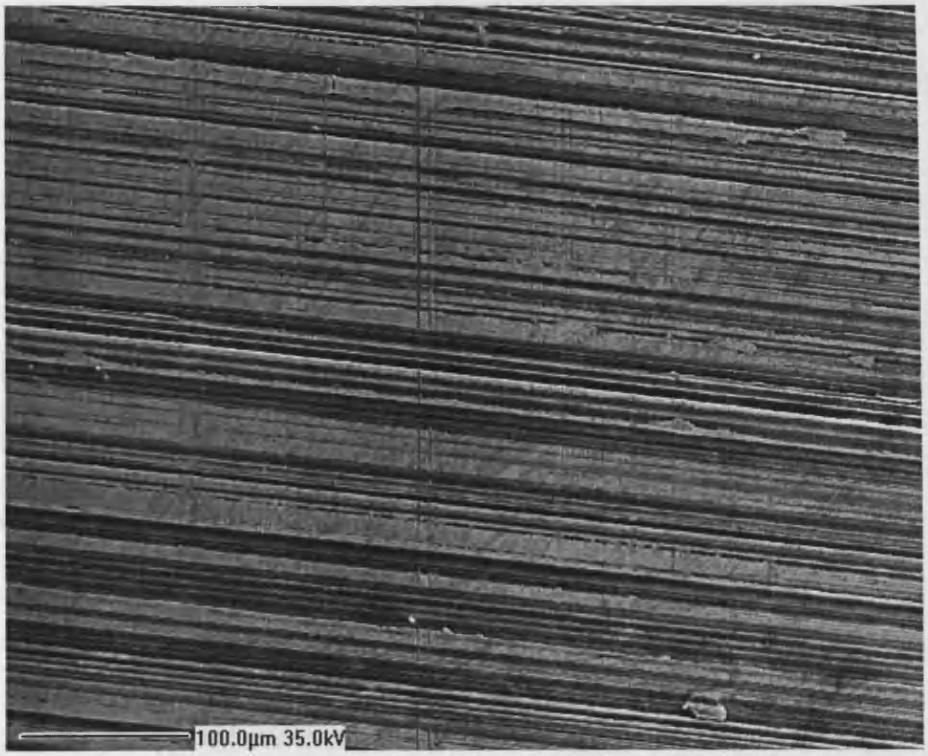

(a)

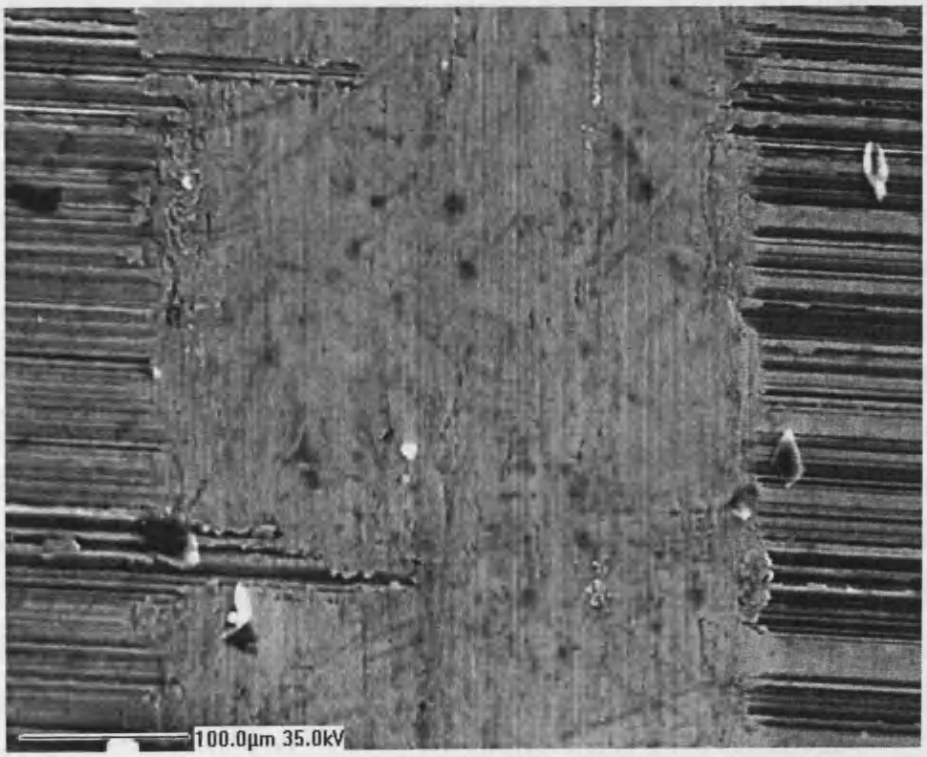

(b)

Figure 4.15. SEM images of surface of the fast disc used in test AD05.
(a) run in surface
(b) scuffing scar with run in surfaces on the sides

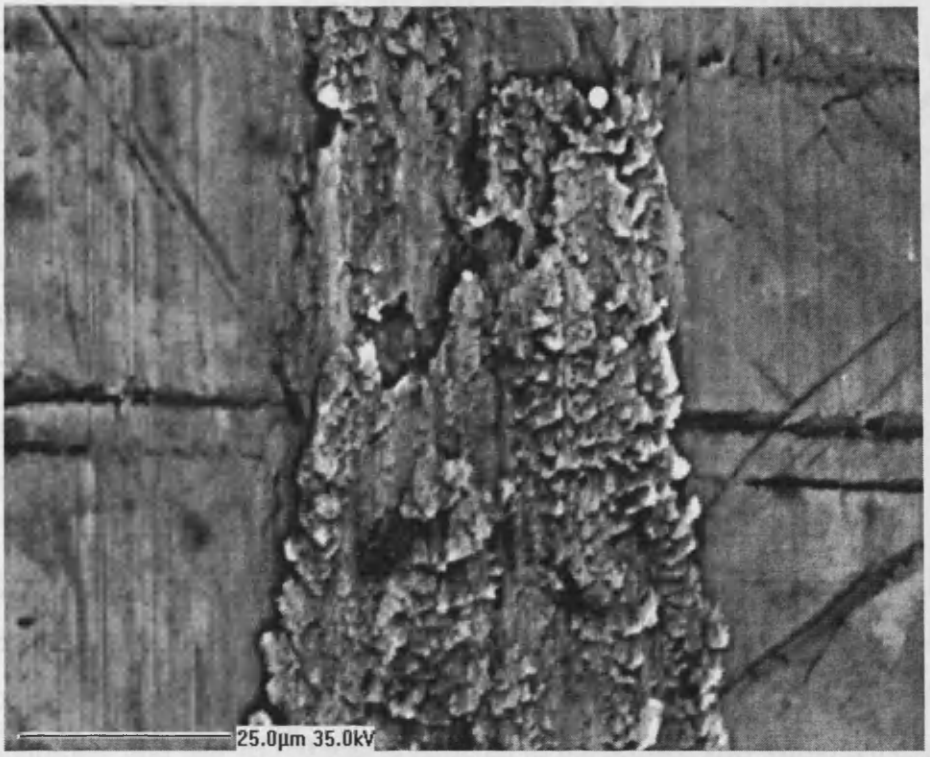

Figure 4.16. SEM image of surface of the slow disc used in test AD05.
Showing scuffing scar with run in surface at sides (note the high magnification)

SEM images of the discs used in test AD05 are given above in Figures 4.15 and 4.16. The upper image in Figure 4.15 shows the run in part of the running track on the ground disc. This shows the characteristic flattened appearance of the high points of the surface (lands). There are light scratches or scoring marks in the vertical direction. The lower image shows the scuffing track in the middle of the running track with the run in surface of the disc on both sides of the scuffing scar. Note that on the left of the scuffing scar there are regions of discontinuity (in the sliding direction) of the scuffing mark in which the undamaged ground track remains. Only one usable SEM image could be taken from the superfinished disc used in test AD05. This is shown in Figure 4.16 which shows the scuffing scar taken at a very high magnification with run in surface on both sides of the scuffing track. Note the residual deep grinding marks (dark horizontal lines) which have remained after superfinishing.

4.3. Pre-running in tests

A short series of tests was carried out with the purpose of investigating the suggestion that by running the discs at a high load under free rolling conditions (which would ensure that they did not scuff) it might be possible to increase their scuffing load in a subsequent run under sliding conditions. This suggestion is based on the idea that by running the surfaces together at a higher load than that at which they would normally have scuffed there would be a greater degree of running in or smoothing of the surfaces, and that in a subsequent scuffing test in which sliding was introduced the scuffing load would be thereby increased. Tests were carried out at two sliding speeds of 16 m/s and 12 m/s.

The results of the two tests conducted at the highest sliding speed of 16m/s are summarised in Table 4.3. The discs used in test AD09 were "pre-run" under pure rolling conditions for about 30 minutes at the maximum load capacity of the rig (6758 N) before testing under sliding conditions, and test AD10 was conducted in the normal way without a pre-run.

Table 4.3.
Summary of scuffing conditions - ground/un-coated discs at sliding speed of 16m/s

Test	AD09-prerun		AD10	
Test Discs	rrc62	rrc29	rrc80	rrc17
Shaft Mounting	fast	slow	fast	slow
Disc Condition	grnd	grnd	grnd	grnd
temperature/°C	182	132	184	137
Roughness, Ra, before/μm	0.337	0.327	0.355	0.337
Roughness, Ra, after/μm	0.247	0.257	0.275	0.227
Scuffing load/N	1465		1466	
Max Hertz pressure/GPa	1.2		1.2	
Friction force/N	44		49	
Friction coefficient	0.03		0.033	
Blok flash temp. rise/°C	166		185	

grnd - ground

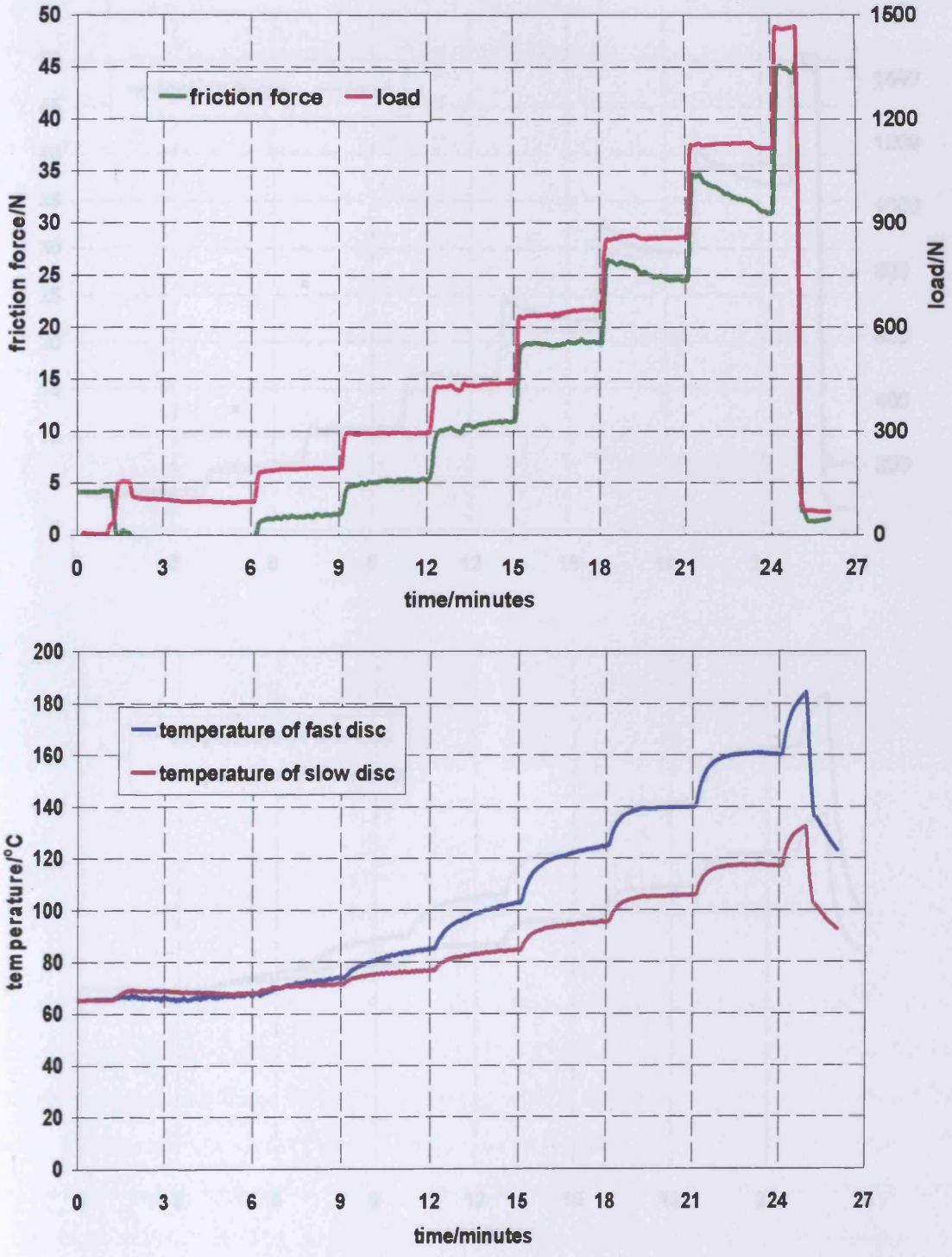

Figure 4.17. Record of scuffing test AD09(prerun), upper graph shows applied load and friction force; lower graph shows bulk temperatures of the two discs

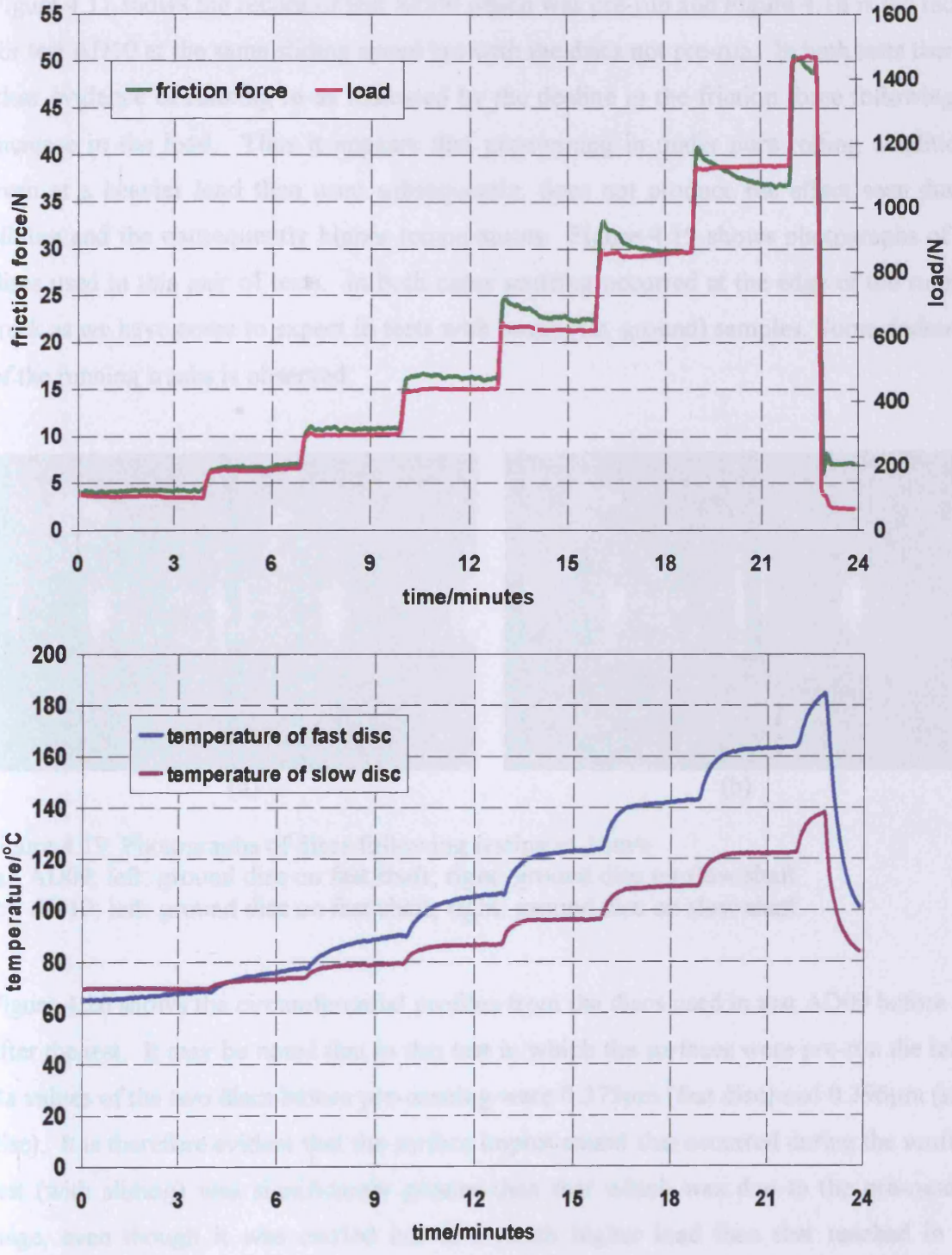

Figure 4.18. Record of scuffing test AD10, upper graph shows applied load and friction force; lower graph shows bulk temperatures of the two discs

Figure 4.17 shows the record of test AD09 which was pre-run and Figure 4.18 is the record for test AD10 at the same sliding speed but with the discs not pre-run. In both tests there is clear evidence of running in as indicated by the decline in the friction force following an increase in the load. Thus it appears that pre-running in under pure rolling conditions, even at a heavier load than used subsequently, does not produce the effect seen due to sliding and the consequently higher temperatures. Figure 4.19 shows photographs of the discs used in this pair of tests. In both cases scuffing occurred at the edge of the running track as we have come to expect in tests with rough (i.e. ground) samples. Some darkening of the running tracks is observed.

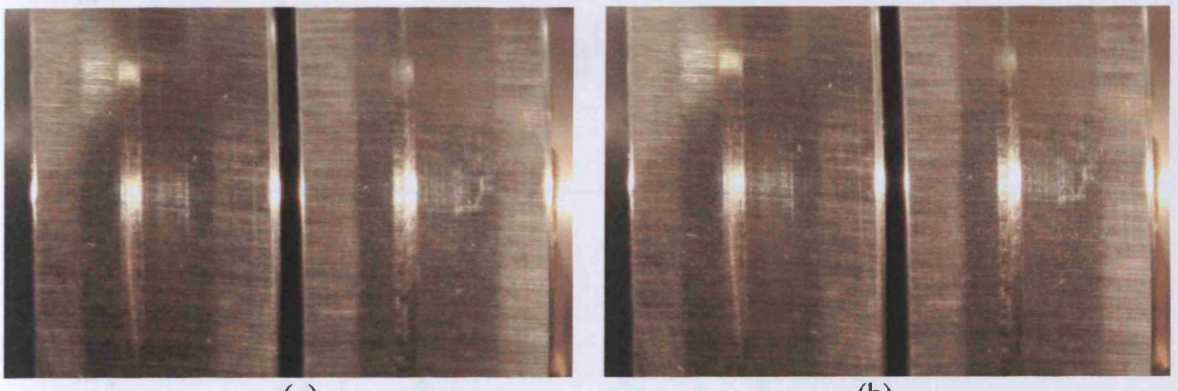

(a) (b)

Figure 4.19. Photographs of discs following testing at 16m/s
(a) AD09; left: ground disc on fast shaft; right: ground disc on slow shaft
(b) AD10; left: ground disc on fast shaft; right: ground disc on slow shaft

Figure 4.20 shows the circumferential profiles from the discs used in test AD09 before and after the test. It may be noted that in this test in which the surfaces were pre-run the initial Ra values of the two discs before pre-running were 0.375μm (fast disc) and 0.396μm (slow disc). It is therefore evident that the surface improvement that occurred during the scuffing test (with sliding) was significantly greater than that which was due to the pre-running stage, even though it was carried out at a much higher load than that reached in the scuffing test.

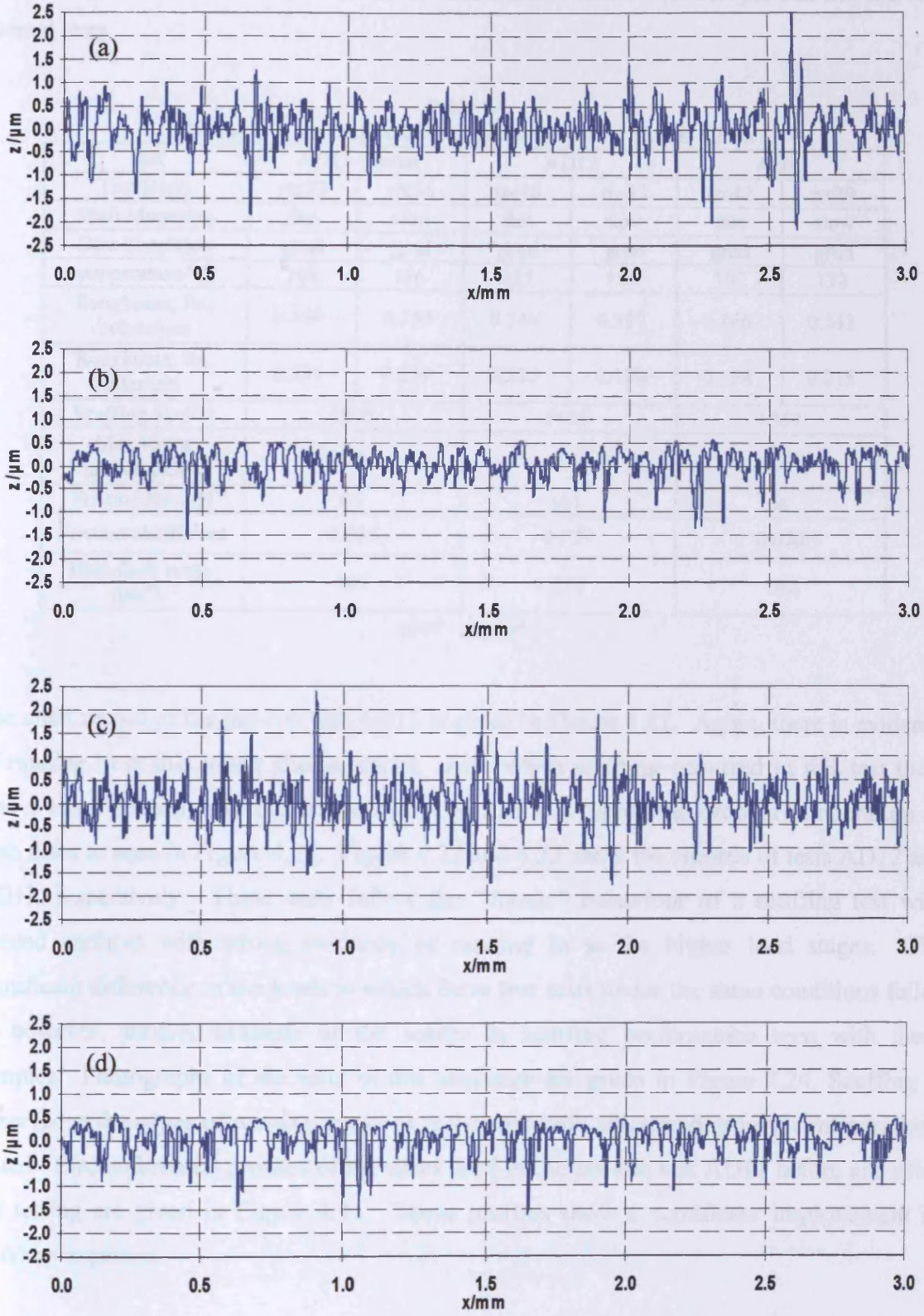

Figure 4.20. Surface profiles taken in the circumferential direction from discs used in test AD09
Profiles from fast disc (a) before test; Ra = 0.339µm (b) after test; Ra = 0.246µm
Profiles from slow disc (c) before test; Ra = 0.350µm (d) after test; Ra = 0.273µm

Table 4.4 presents a summary of the tests conducted at 12m/s with one pre-run test and two normal tests.

Table 4.4.
Summary of scuffing conditions-ground uncoated discs at 12m/s

Test	AD11-prerun		AD12		AD13	
Test Discs	rrc73	rrc35	rrc48	rrc33	rrc42	rrc39
Shaft Mounting	fast	slow	fast	slow	fast	slow
Disc Condition	grnd	grnd	grnd	grnd	grnd	grnd
temperature/°C	188	136	233	184	192	132
Roughness, Ra, before/μm	0.309	0.355	0.346	0.337	0.366	0.343
Roughness, Ra, after/μm	0.234	0.239	0.225	0.180	0.194	0.215
Scuffing load/N	1860		3461		1857	
Max Hertz pressure/GPa	1.3		1.6		1.3	
Friction force/N	66		101		66	
Friction coefficient	0.035		0.029		0.035	
Blok flash temp. rise/°C	191		215		192	

grnd - ground

The chart record of the pre-run test AD11 is given in Figure 4.21. Again, there is evidence of running in at this lower sliding speed. Just before scuffing occurred in this test there was a sharp reduction in the friction force with a corresponding drop of temperature of both discs as seen in Figure 4.21. Figure 4.22 and 4.23 show the records of tests AD12 and AD13, respectively. These tests follow the "classic" behaviour of a scuffing test with ground surfaces with strong evidence of running in at the higher load stages. The significant difference in the loads at which these two tests under the same conditions failed is, however, another example of the scatter in scuffing performance seen with these samples. Photographs of the tests in this sequence are given in Figure 4.24. Scuffing is observed at the edges of running tracks as is the case with all ground/ground configurations tested. Circumferential profiles of the discs used in the pre-run test AD11 before and after the testing are given in Figure 4.25. These profiles show a significant improvement in finish as expected.

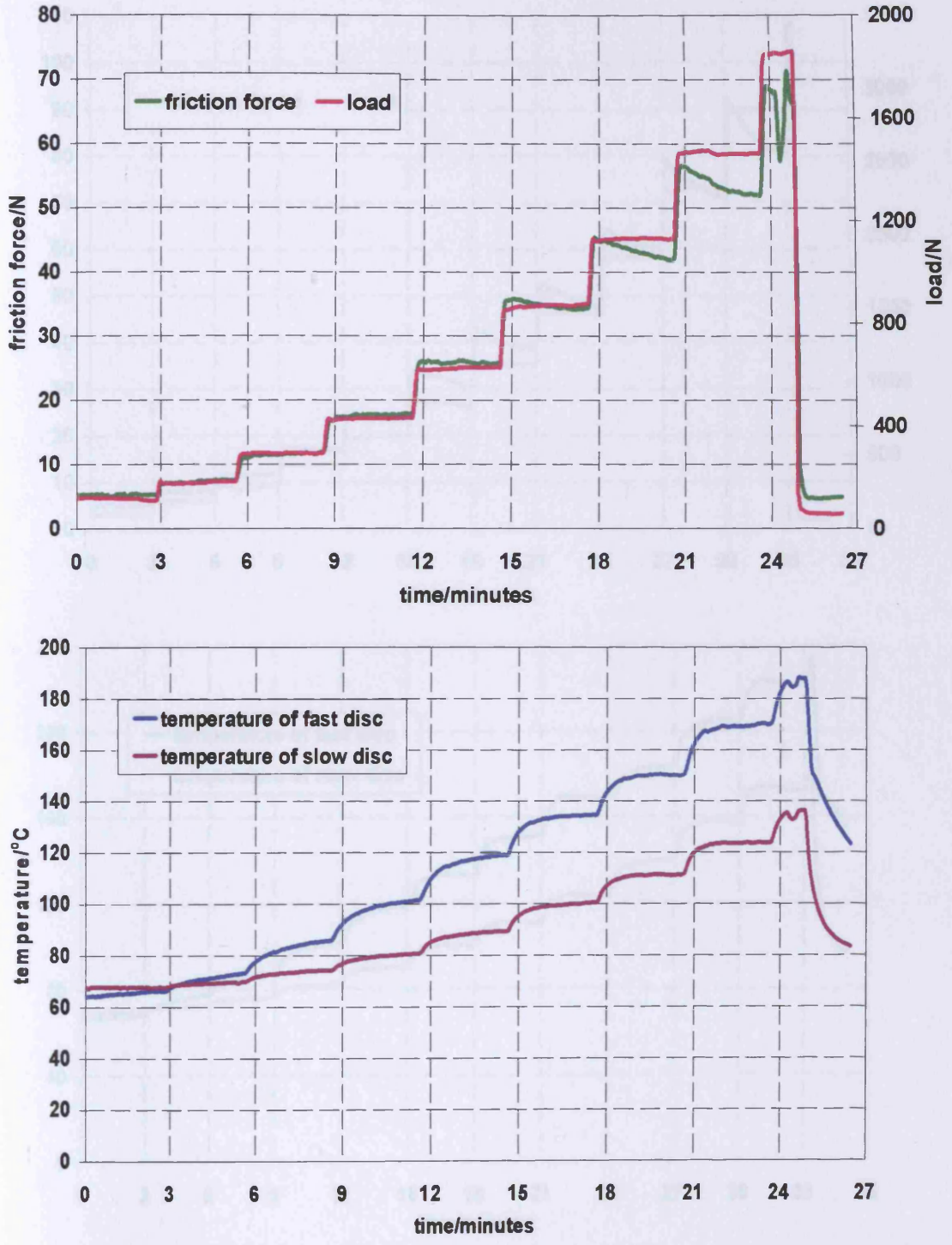

Figure 4.21. Record of scuffing test AD11, upper graph shows applied load and friction force; lower graph shows bulk temperatures of the two discs

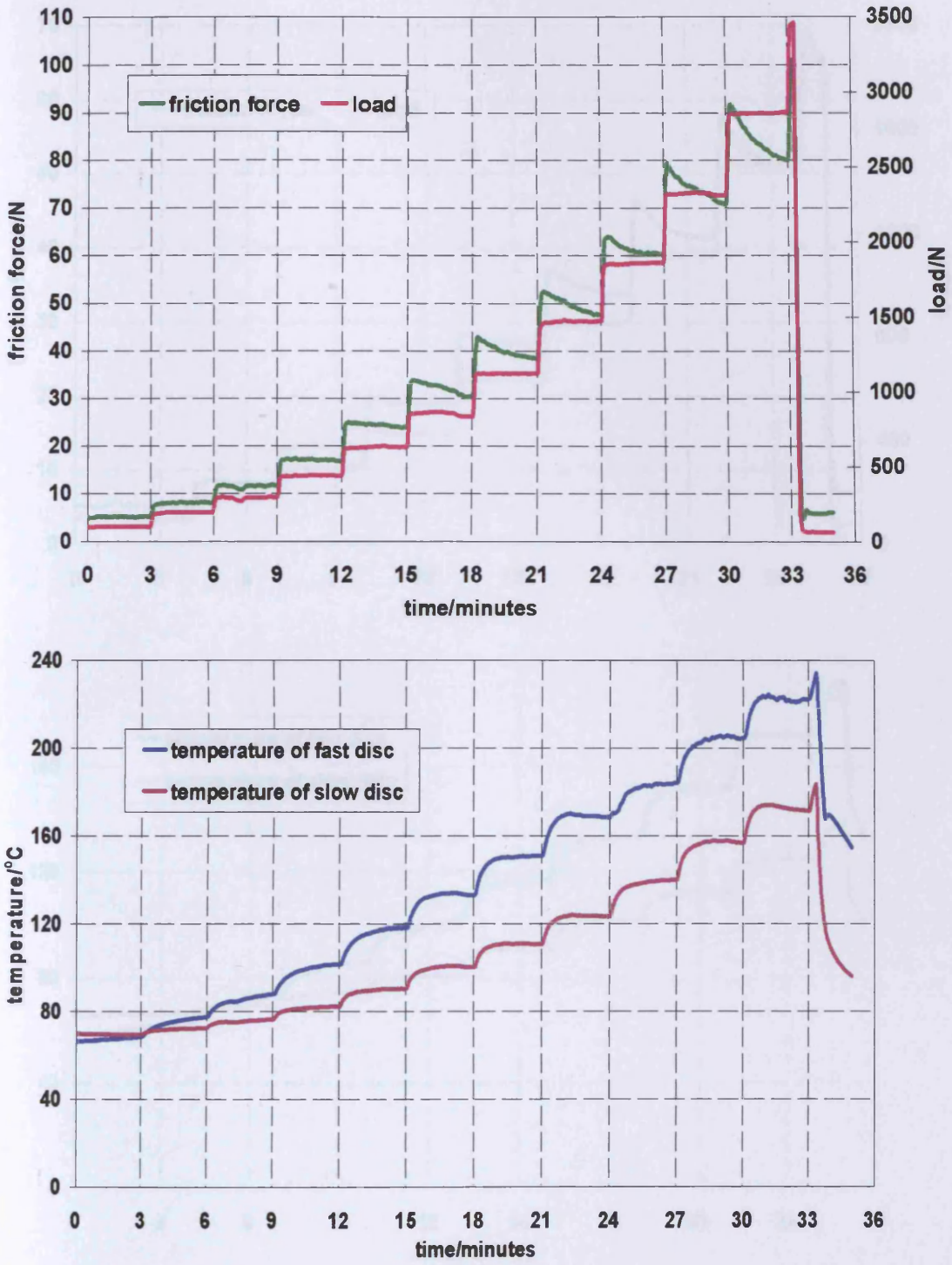

Figure 4.22. Record of scuffing test AD12, upper graph shows applied load and friction force; lower graph shows bulk temperatures of the two discs

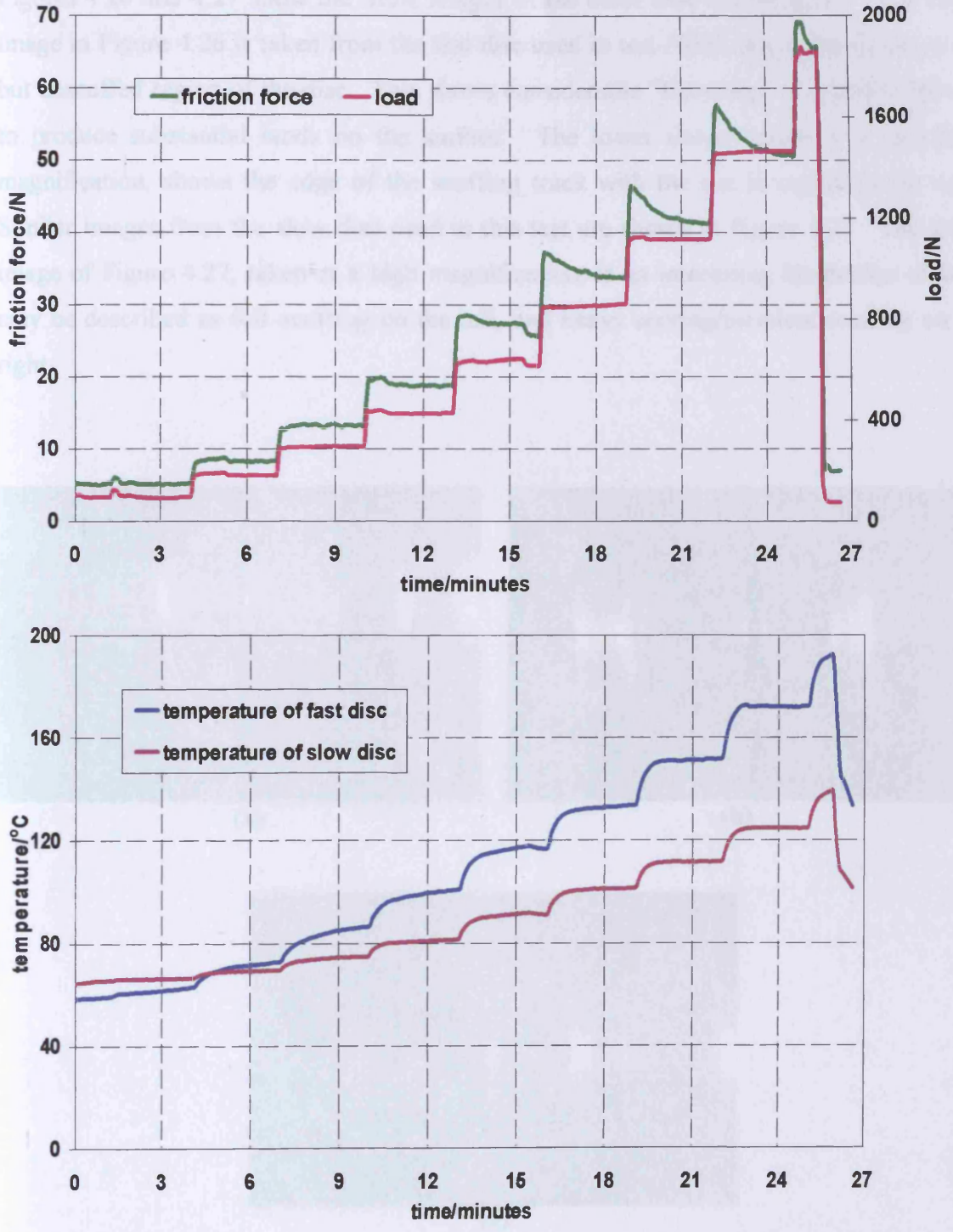

Figure 4.23. Record of scuffing test AD13, upper graph shows applied load and friction force; lower graph shows bulk temperatures of the two discs

Figures 4.26 and 4.27 show the SEM images of the discs used in test AD13. The upper image in Figure 4.26 is taken from the fast disc used in test AD13 which shows the run in but unscuffed region of the disc. This shows considerable "flattening" of asperity features to produce substantial lands on the surface. The lower image, taken at a very high magnification, shows the edge of the scuffing track with the run in region to the right. Similar images from the slow disc used in this test are shown in Figure 4.27. The lower image of Figure 4.27, taken at a high magnification, is an interesting illustration of what may be described as full scuffing on the left, and heavy scoring/incipient scuffing on the right.

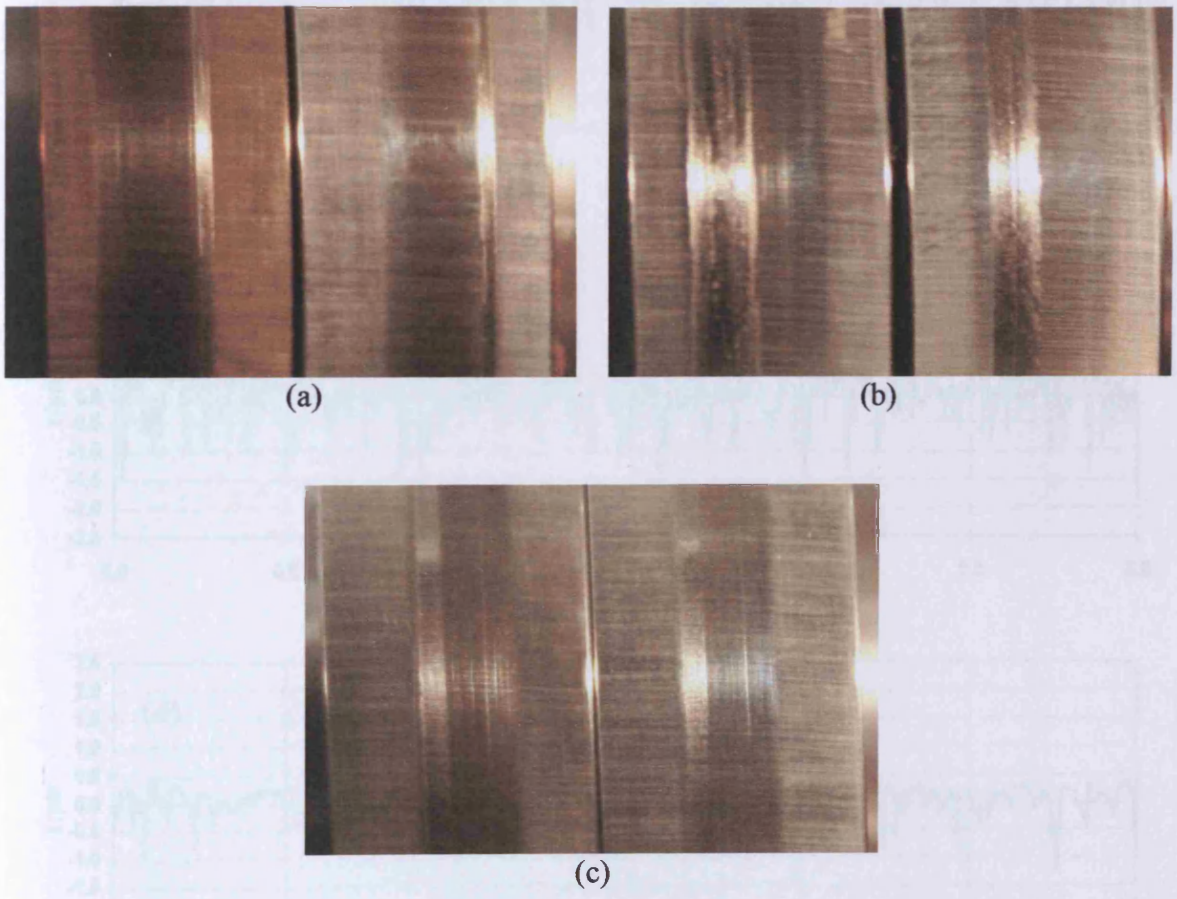

Figure 4.24. Photographs of discs following testing at 12m/s
(a) AD11; left: ground disc on fast shaft; right: ground disc on slow shaft
(b) AD12; left: ground disc on fast shaft; right: ground disc on slow shaft
(c) AD13; left: ground disc on fast shaft; right: ground disc on slow shaft

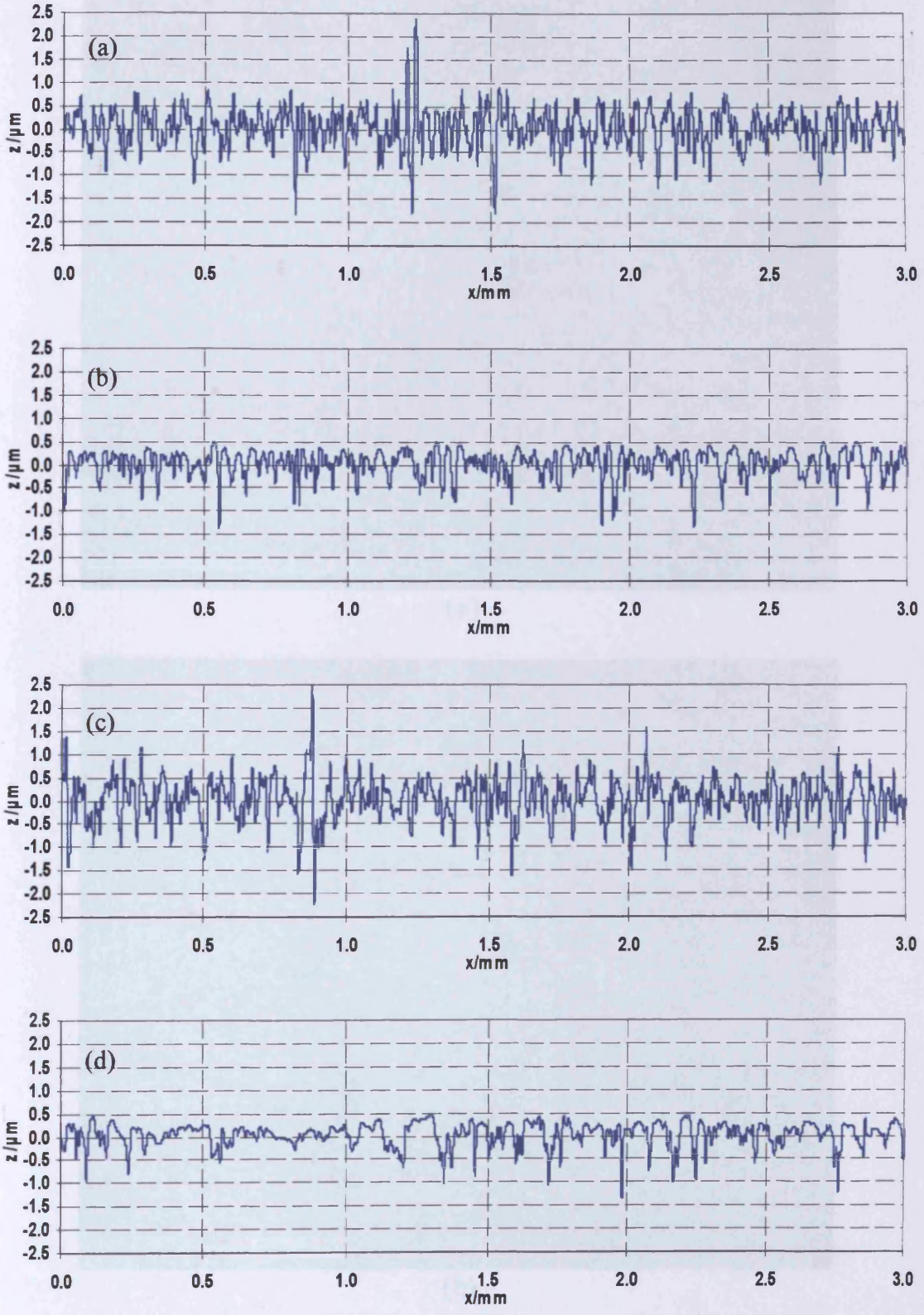

Figure 4.25. Surface profiles taken in the circumferential direction from discs used in test AD11
Profiles from fast disc (a) before test; Ra = 0.311µm (b) after test; Ra = 0.232µm
Profiles from slow disc (c) before test; Ra = 0.355µm (d) after test; Ra = 0.213µm

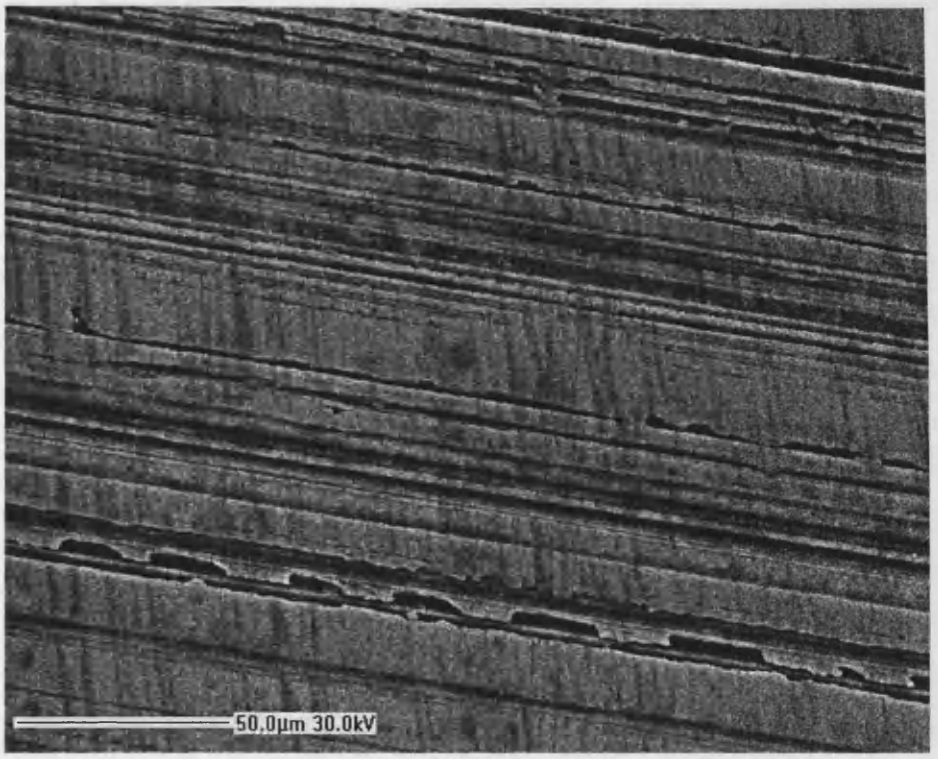

(a)

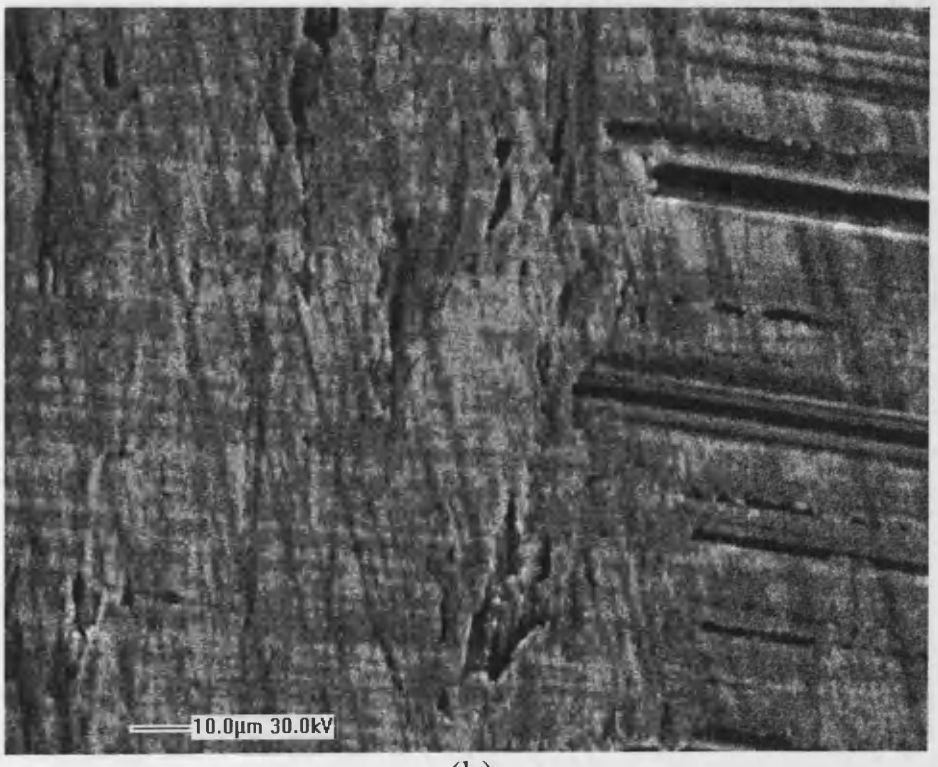

(b)

Figure 4.26. SEM images of surface of the fast disc used in test AD13.
(a) run-in surface
(b) scuffed part on the left side and run in part to the right.

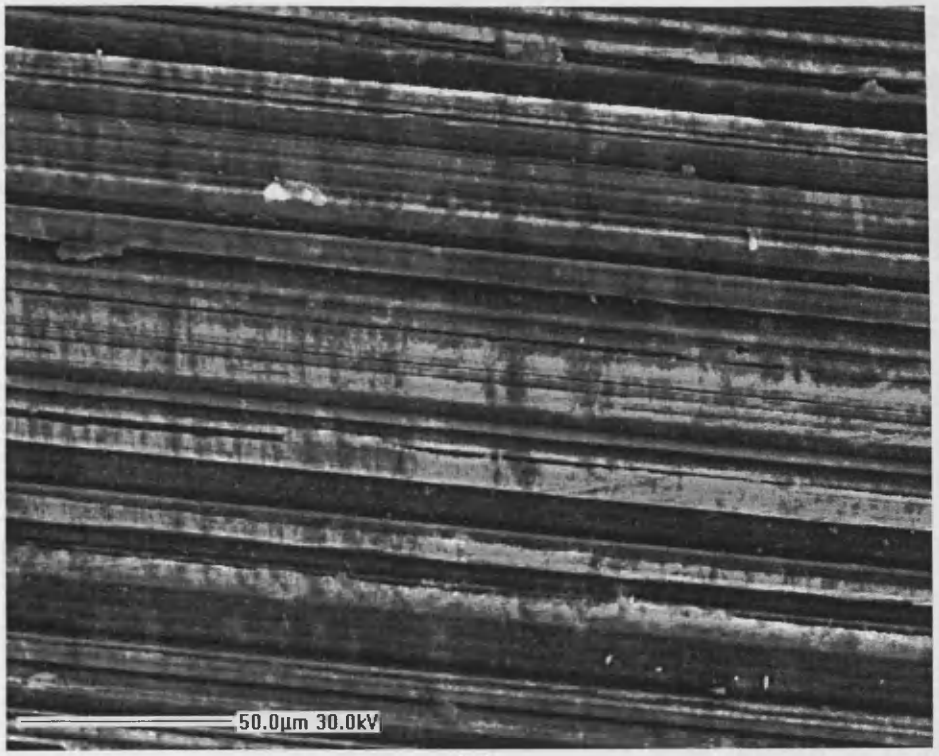

(a)

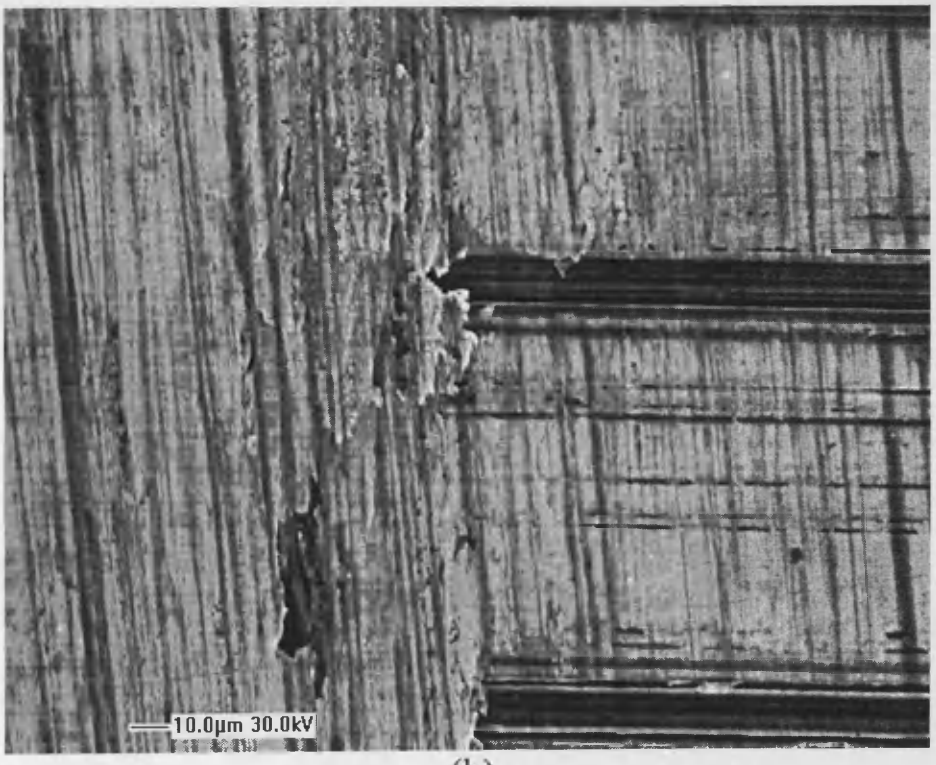

(b)

Figure 4.27. SEM images of surface of the slow disc used in test AD13.
(a) run in surface
(b) scuffing on the left and light scoring on the right.

The results of this short series on tests on pre-running in do not lend weight to the idea that pre-running at a high load under rolling conditions can improve scuffing resistance in a subsequent test under sliding conditions. In none of the tests was it possible to demonstrate an increase in the load stage at which scuffing occurred by pre-running, indeed in test AD12 in which the discs were not pre-run the scuffing load (3450 N) significantly exceeded the load at which the pre-run discs failed.

Chapter 5

Numerical EHL Simulations

5.1. Introduction

This chapter describes numerical elastohydrodynamic lubrication (EHL) simulations performed to investigate the results of three of the experimental scuffing tests carried out and described in the previous chapters. The results have been obtained using a numerical code for transient elastohydrodynamic (EHL) line contacts for rough surfaces developed at the Cardiff School of Engineering over the past ten years or so. Because the roughness moves relative to the nominal contact region it is necessary to adopt a transient (time-dependent) approach. The computer code has been applied by the present author as a "black box" in the same way that a commercial Finite Element code might be used. The author was assisted in the use of the solver by fellow researcher Giovanni Pugliese. The following section briefly outlines the formulation of the solver and its application.

5.2. Brief description of the EHL solver

Transient studies of EHL under roughness conditions (micro-EHL) have in the past been presented for sinusoidal surfaces by Chang et al (1993) and Venner et al (1994) and for individual surface defects by Chang et al (1993). Measured (i.e. "real") profiles were studied by Ai and Cheng (1994) and Elcoate et al (2000). One of the main problems encountered in these early solutions was the difficulty of dealing with conditions in which the film became very thin or even disappeared. Different approaches have been used to tackle the numerical problems involved including partitioning the contact into sub-areas where lubricant is not present, as used by Jiang et al (1999) and Zhao et al (2001), or by effectively modifying the Reynolds equation under thin film conditions in order to preserve a unified approach as proposed by Hu et al (2000). The results obtained using the latter methods have been questioned, however, by Holmes et al (2003). A truly unified approach

to thin film mixed lubrication problems involving rough surfaces has been developed at Cardiff based on the differential deflection method with full coupling of the hydrodynamic and elasticity equations in the solution phase. The basic equations to be solved in an isothermal formulation of the rough surface EHL problem are the Reynolds and elasticity equations. The active contact occurs nominally at a point, but under load this becomes an elliptical area of aspect ratio 4:1. Under these conditions it has been shown by Holmes et al (2003) that the centre line of such a contact can be modelled as a "line" contact. For the line contact situation as considered here the Reynolds equation for time-dependent conditions is

$$\frac{\partial}{\partial x}\left(\frac{\rho h^3}{12\eta} S \frac{\partial p}{\partial x}\right) - \frac{\partial(\rho \bar{u} h)}{\partial x} - \frac{\partial(\rho h)}{\partial t} = 0$$

and the elastic deflection equation in differential form is given by

$$\frac{\partial^2 h}{\partial x^2} = \frac{\partial^2 \phi}{\partial x^2} + \frac{1}{R} + \frac{2}{\pi E'} \sum_{all\ k} f_{k-i} p_k$$

The viscosity and density of the lubricant are assumed to vary with pressure as follows

$$\eta = \eta_0 \exp\left\{\ln(\eta_0 / \kappa)\left((1 + \chi p)^z - 1\right)\right\}$$

and

$$\rho = \rho_0 \frac{(1 + \gamma p)}{(1 + \lambda p)}$$

The load used in the simulation is determined by fixing the "interpenetration" of the surfaces. During the transient solution this causes the load to vary slightly about a mean value. The variation is small and has no significant effect on pressure or film thickness.

The term S in the first equation is the non-Newtonian flow factor which is obtained as a function of the local values of viscosity, shear rate and pressure gradient for a particular non-Newtonian relationship. In this work the well-known Eyring relation is assumed. The term $\phi(x,t)$ in the second equation is the composite surface roughness of the two surfaces

involved in the contact. A full description of the formulation and the fully-coupled method of solution of the above equations are given in a substantial pair of papers by Holmes et al (2003).

One of the principal advantages of the coupled formulation is that it can deal with instances of zero film thickness which occur under severe conditions of high roughness/film thickness. Such occurrences, which are transitory, are a natural consequence of the requirement to preserve continuity of flow, and are not the result of an arbitrary definition of "contact". The solver can therefore simulate, in a fully consistent way, both fully-lubricated situations in which there is complete separation of the two rough surfaces and "mixed" conditions in which some of the load is carried by "dry" contacts and the remainder by hydrodynamic pressure as discussed by Holmes (2003).

All the results presented in this thesis are limited to an isothermal analysis. Surface profiles, corresponding to tests UTRC01, UTRC07 and UTRC27, were modelled at a temperature of 100°C which corresponds to the oil supply temperature in the tests. The surface profiles used in the simulations were taken in the circumferential direction from the run but unscuffed parts of the discs following testing.

5.3. Isothermal EHL transient simulations run at temperature of 100 °C

5.3.1. Isothermal transient EHL analyses performed

All the results in this section have been obtained assuming an oil temperature of 100°C. The lubricant modelled is Mobil Jet 2 as used in the scuffing experiments. The viscosity (η_0) of this lubricant at 100 °C is 0.0048 Pas. Other lubricant properties, including non-Newtonian constants, are those at 100°C. All tests using ground discs had transverse ground finish with a nominal initial roughness (Ra) of 0.4 μm. The profiles used for the analyses were taken from the discs at the end of the tests from the run, but unscuffed, part of the running track. Following testing the surfaces became "run in" to a greater or lesser extent, and in some cases the Ra value fell to a very low value as a result of running (about 0.04 μm). Circumferential profiles were taken using a standard Talysurf profilometer and a notation was adopted in order to identify profiles from the numerous discs used in the

project. Discs and their profiles were identified using the lower-case prefix 'utrc' followed by the disc serial number. Table 5.1 gives a summary of the experimental results from the three tests presented in this section together with the Ra values of the profiles used in the theoretical simulations.

Table 5.1.
Summary of experimental conditions

Test	Disc on fast shaft	Disc on slow shaft	velocity [m/s]	Load stage reached	Maximum Hertz pressure [GPa]	Ra after running, fast disc [μm]	Ra after running, slow disc [μm]]
UTRC01	utrc 93	utrc 66	16	10	1.5	0.206	0.038
UTRC07	utrc 90	utrc 06	12	12	1.7	0.201	0.204
UTRC27	utrc 80	utrc 33	7	14	1.9	0.043	0.055

Figures 5.1 to 5.3 show sections of the profiles used in the simulations.

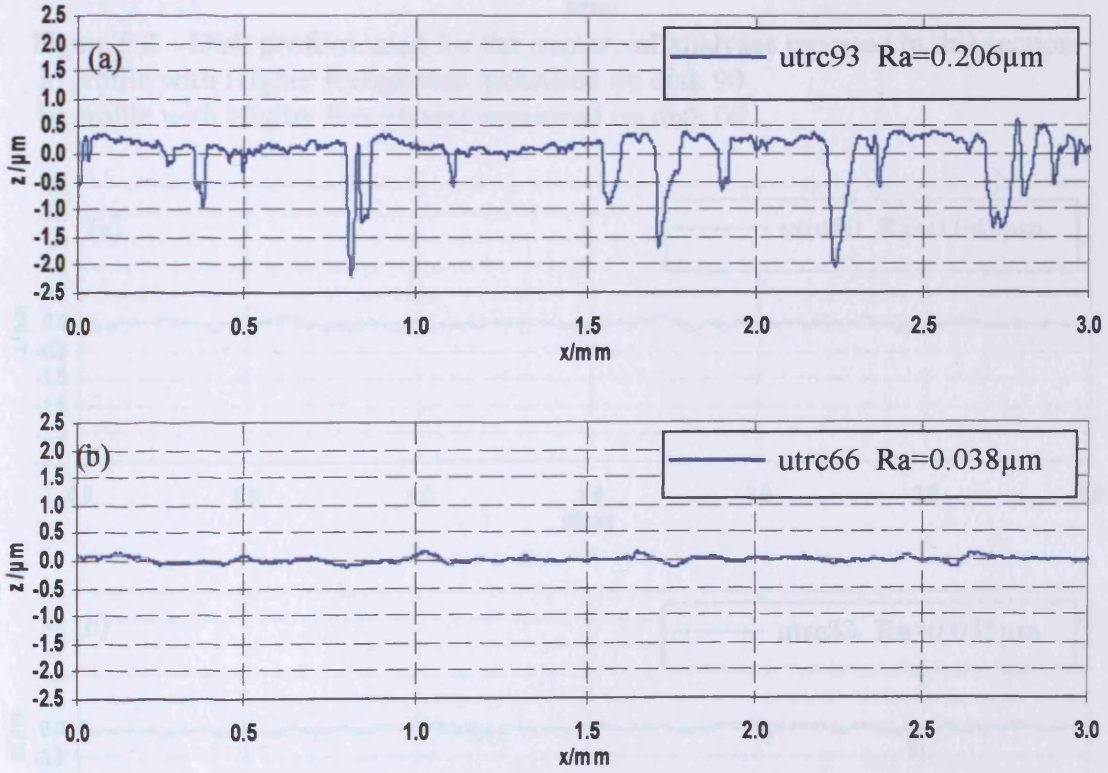

Figure 5.1. Disk profiles used for the numerical analyses reported in this section
a) profile with Higher Roughness measured on disk 93
b) profile with Lower Roughness measured on disk 66

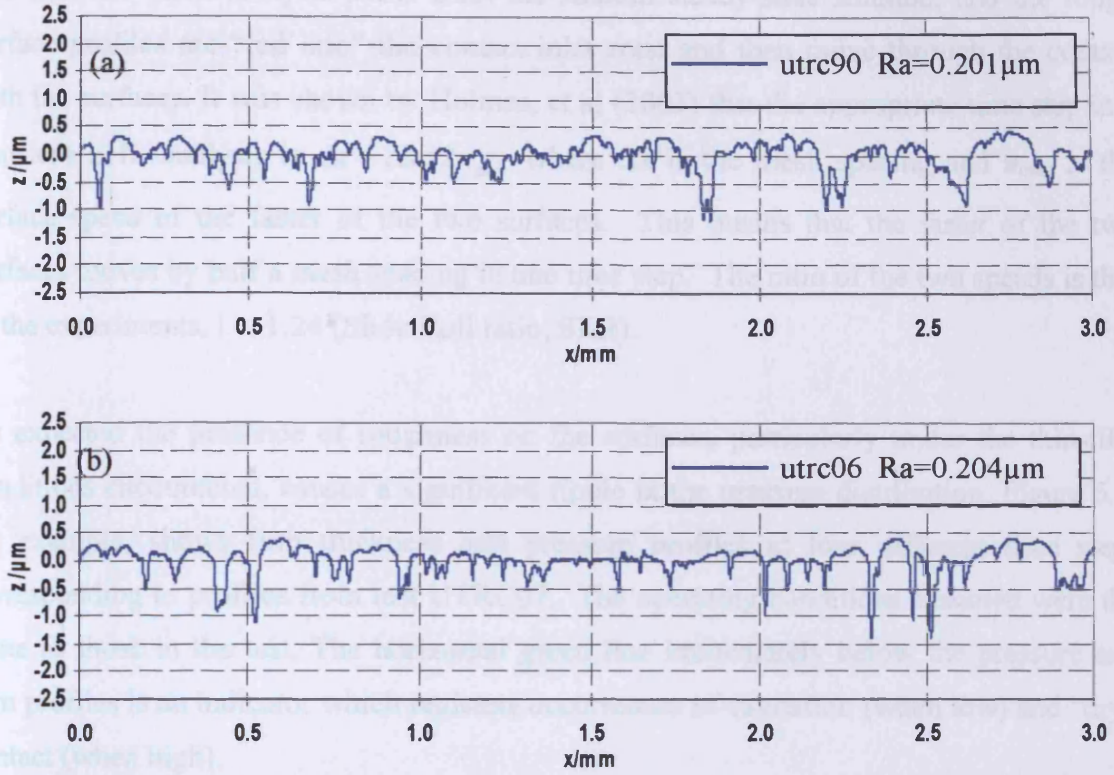

Figure 5.2. Disk profiles used for the numerical analyses reported in this section
a) profile with Higher Roughness measured on disk 90
b) profile with Higher Roughness measured on disk 06

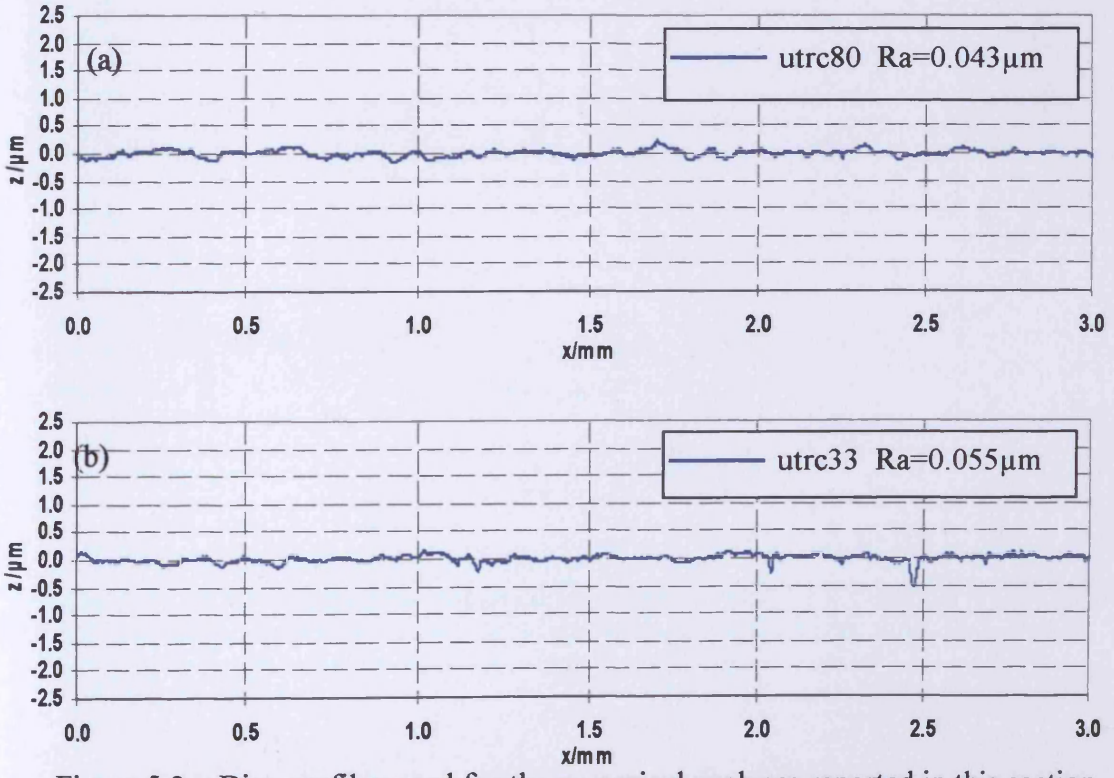

Figure 5.3. Disc profiles used for the numerical analyses reported in this section
a) profile with Lower Roughness measured on disc 80
b) profile with Lower Roughness measured on disc 33

The transient EHL analysis starts from the smooth steady-state solution, and the rough surface profiles are "fed into" the contact inlet zone and then move through the contact with the surfaces. It was shown by Holmes, et al (2003) that the appropriate time step in a transient EHL analysis is $\Delta t = \Delta x / 2u_{max}$ where Δx is the mesh spacing and u_{max} is the surface speed of the faster of the two surfaces. This means that the faster of the two surfaces moves by half a mesh spacing in one time step. The ratio of the two speeds is that of the experiments, i.e. 1.24 (Slide Roll ratio, SRR).

As expected the presence of roughness on the surfaces, particularly under the thin-film conditions encountered, causes a significant ripple in the pressure distribution. Figure 5.4, for example, shows film thickness and pressure profiles at four different time steps corresponding to profiles from test UTRC07. The operating conditions assumed were the same as those in the test. The horizontal green line immediately below the pressure and film profiles is an indicator which registers occurrences of cavitation (when low) and "dry" contact (when high).

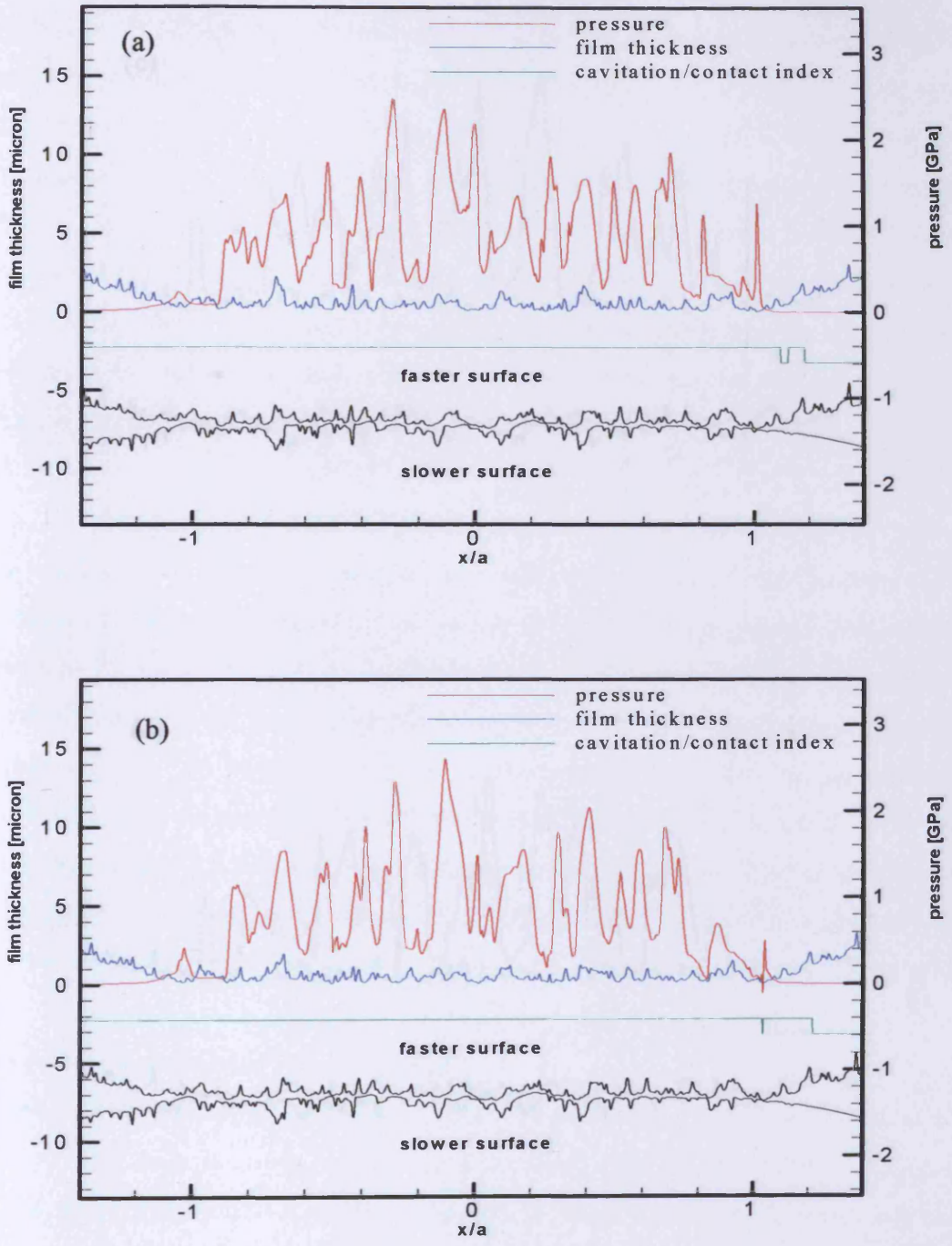

Figure 5.4. Pressure and film thickness from the analysis of contact between rough profiles from test UTRC07 at two different time steps (a) 25 time steps and (b).50 time steps. Speed = 12 m/s; load = 1.7 GPa; temperature = 100°C.

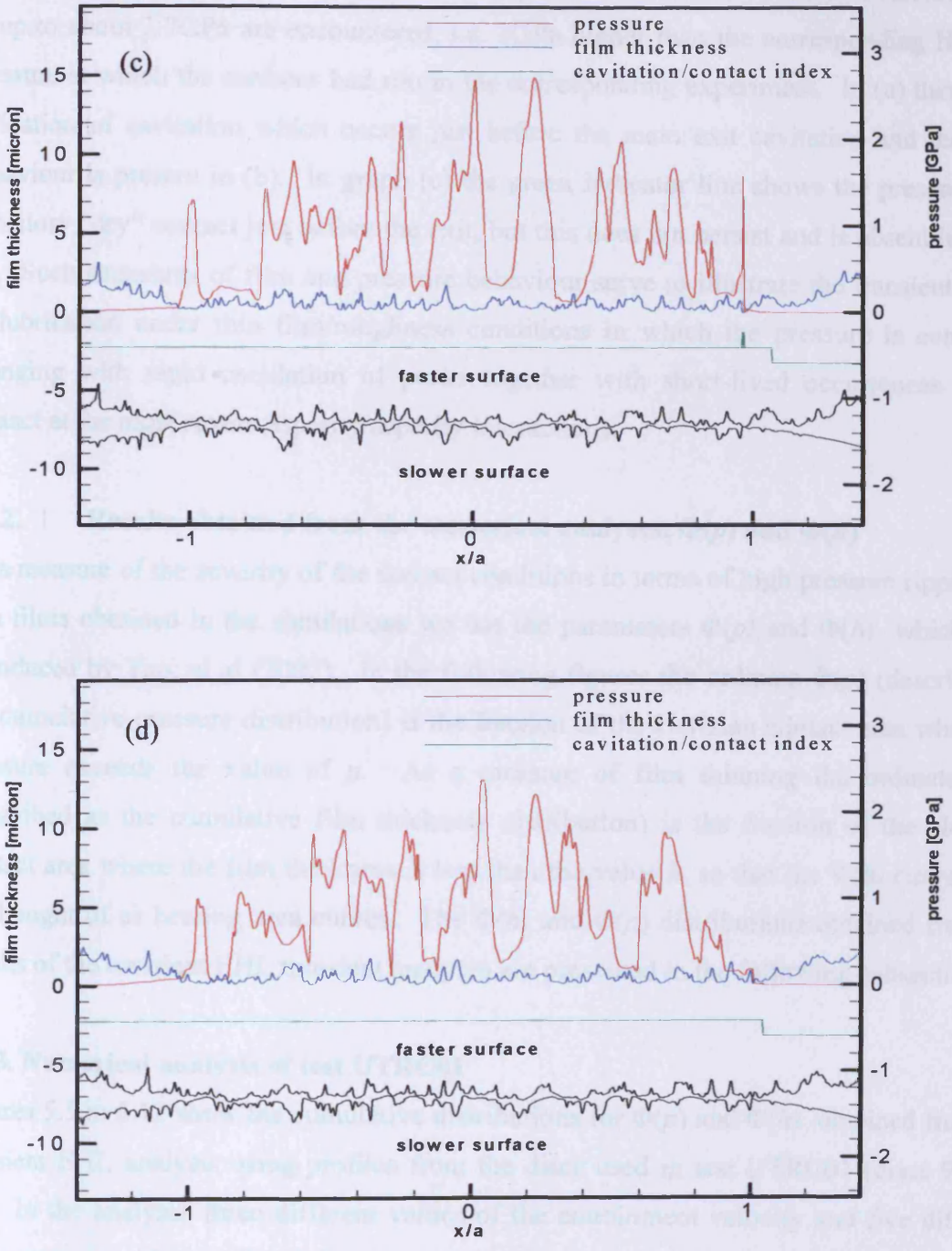

Figure 5.4. Pressure and film thickness from the analysis of contact between rough profiles from test UTRC07 at two different time steps (c) 100 time steps and (d) 200 time steps. Speed = 12 m/s; load = 1.7 GPa; temperature = 100°C.

Figures 5.4a and 5.4b show two successive positions of the roughness profiles separated by 25 time steps. There are considerable changes in the pressure and film thickness distributions. Figures 5.4c and d shows the situation after a further 100 and 200 time steps,

respectively. In all four cases the highest pressure peaks greatly exceed the corresponding maximum Hertzian pressure that would be expected for smooth surfaces. Pressure peaks of up to about 2.7GPa are encountered, i.e. 1GPa higher than the corresponding Hertzian pressure at which the surfaces had run in the corresponding experiment. In (a) there is an indication of cavitation which occurs just before the main exit cavitation and the same behaviour is present in (b). In graph (c) the green indicator line shows the presence of a transitory "dry" contact just before the exit, but this does not persist and is absent in graph (d). Such snapshots of film and pressure behaviour serve to illustrate the transient nature of lubrication under thin film/roughness conditions in which the pressure is constantly changing with rapid oscillation of peaks together with short-lived occurrences of dry contact at the most severe asperity/asperity interactions.

5.3.2. Results obtained from the numerical analyses, $\Phi(p)$ and $\Phi(h)$

As a measure of the severity of the contact conditions in terms of high pressure ripples and thin films obtained in the simulations we use the parameters $\Phi(p)$ and $\Phi(h)$ which were introduced by Tao, et al (2002). In the following figures the ordinate $\Phi(p)$ (described as the cumulative pressure distribution) is the fraction of the Hertzian contact area where the pressure exceeds the value of p. As a measure of film thinning the ordinate $\Phi(h)$ (described as the cumulative film thickness distribution) is the fraction of the Hertzian contact area where the film thickness is less than the value h, so that the $\Phi(h)$ curves may be thought of as bearing area curves. The $\Phi(h)$ and $\Phi(p)$ distributions obtained from the results of the transient EHL transient analyses are presented in the following subsections.

5.3.3. Numerical analysis of test UTRC01

Figures 5.5 to 5.12 show the cumulative distributions for $\Phi(p)$ and $\Phi(h)$ obtained from the transient EHL analysis using profiles from the discs used in test UTRC01 (discs 93 and 66). In the analyses three different values of the entrainment velocity and five different loads were considered. The following distributions therefore show the effect of load and entrainment speed on the occurrence of high pressures and the appearance of thin films.

Figure 5.5 shows results corresponding to a velocity of 7 m/s with five different loads corresponding to equivalent maximum Hertzian pressures ranging from 1.1 to 1.9GPa. These results indicate that pressure is far more sensitive to load than is the film thickness.

This is the result we would have expected on the basis of smooth surface EHL theory since in the classic film thickness formula of Dowson and Higginson (1966) the minimum film thickness is almost independent of load. It is interesting to note that the same behaviour persists under rough surface conditions.

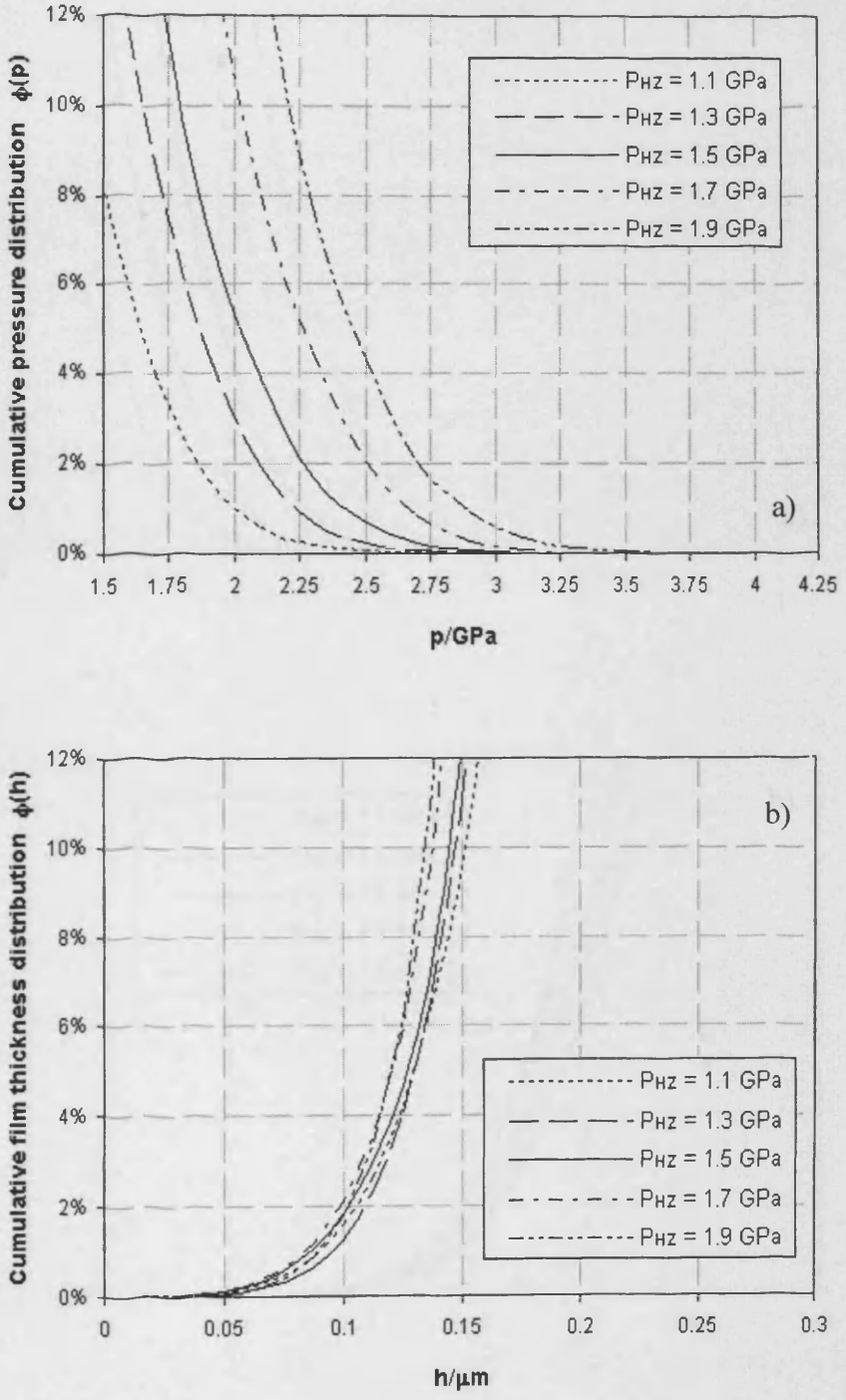

Figure 5.5. Part of cumulative pressure distribution (a) and cumulative film thickness distribution (b) over Hertzian area from EHL simulation of test UTRC01 at 7 m/s for varying loads.

The same general pattern is seen in Figures 5.6 and 5.7 which show the pressure and film distributions at the two higher speeds of 12 and 16 m/s over the same range of loads (1.1 to 1.9GPa). Again the cumulative film thickness distribution is seen to be relatively insensitive to the load at both speeds.

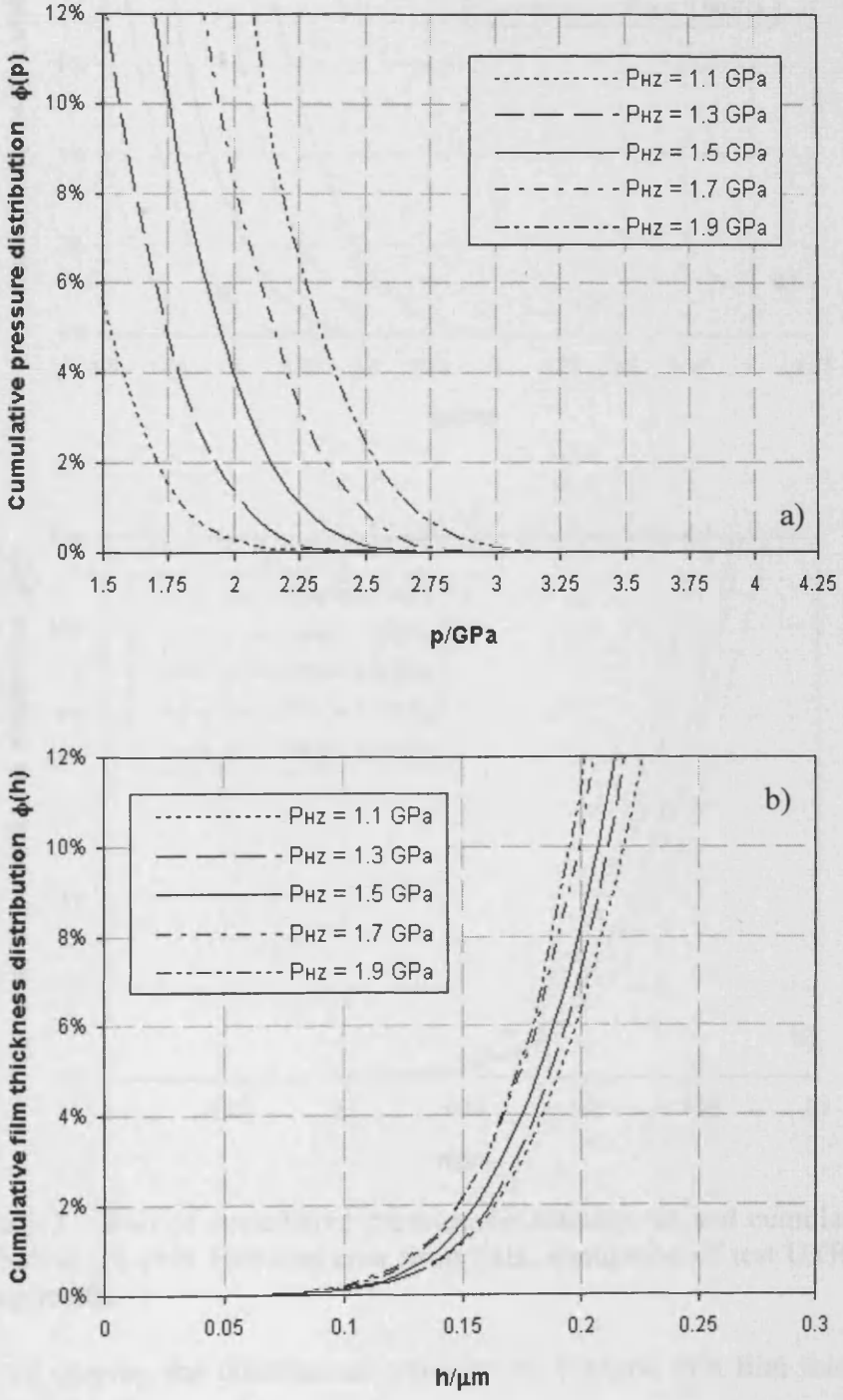

Figure 5.6. Part of cumulative pressure distribution (a) and cumulative film thickness distribution (b) over Hertzian area from EHL simulation of test UTRC01 at 12 m/s for varying loads.

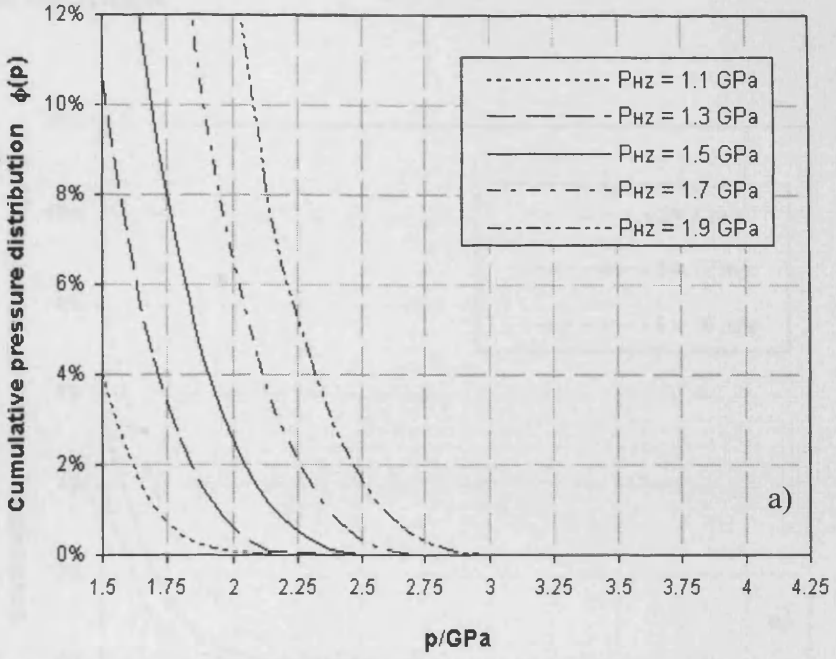

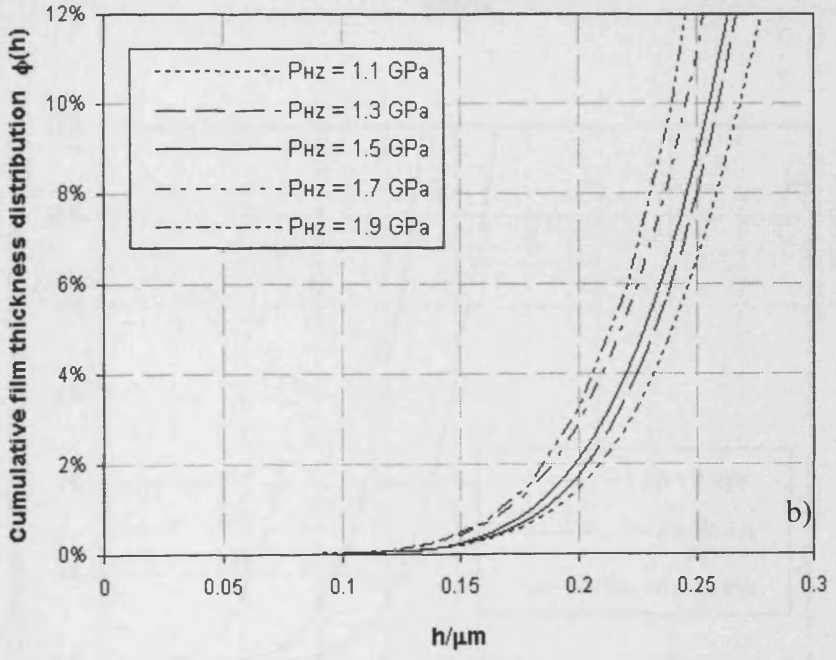

Figure 5.7. Part of cumulative pressure distribution (a) and cumulative film thickness distribution (b) over Hertzian area from EHL simulation of test UTRC01 at 16 m/s for varying loads.

The effect of varying the entrainment velocity on extreme thin film thickness and high pressure behaviour in this test, whilst keeping the load constant, is seen in Figures 5.8 to 5.12. Distributions are shown for the five load cases considered. In this case there is an

effect on both pressure and film thickness, but the influence of entrainment speed on the film is more significant.

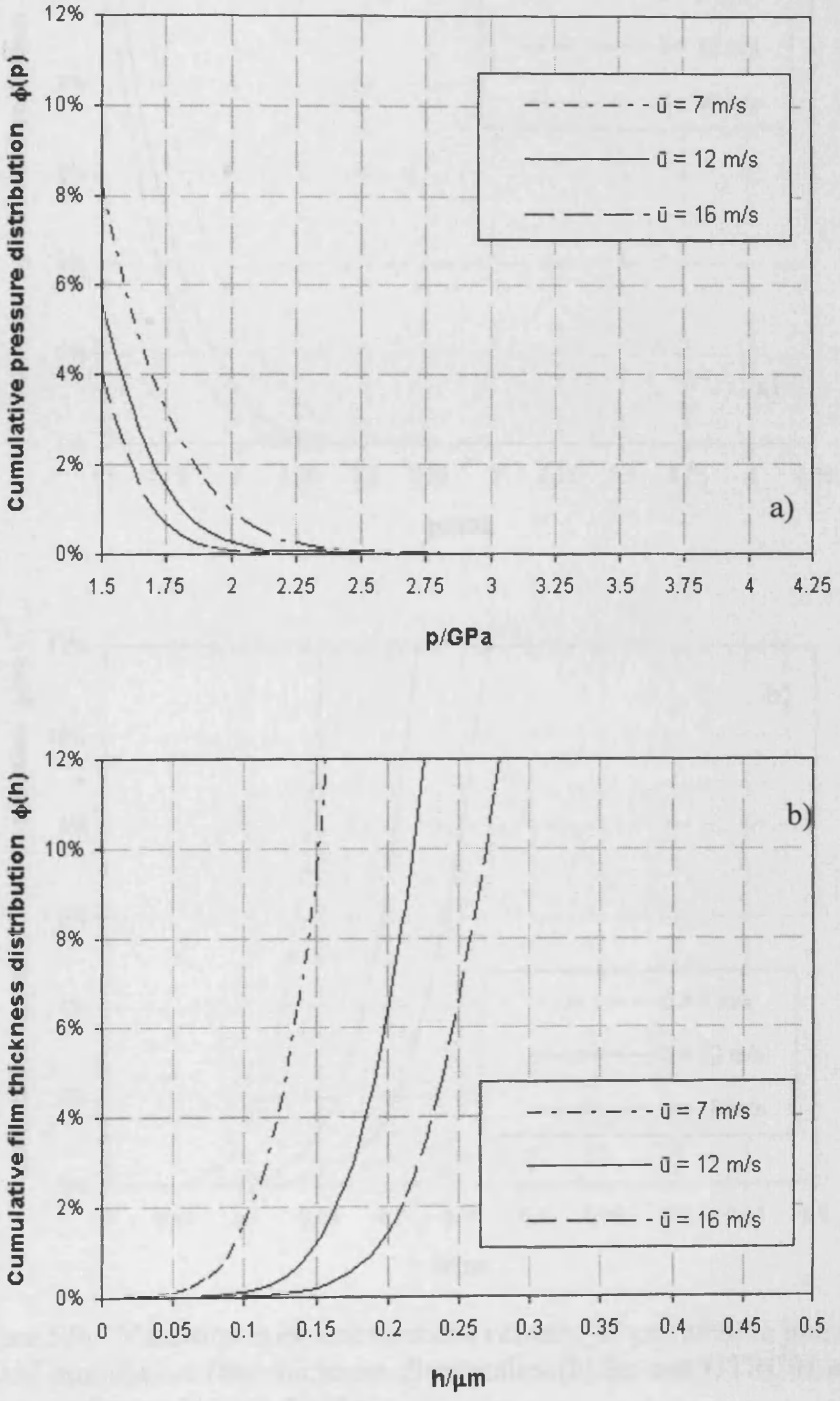

Figure 5.8. Variation with entrainment velocity of cumulative pressure distribution (a) and cumulative film thickness distribution (b) for test UTRC01 at a load corresponding to P_{Hz} = 1.1 GPa.

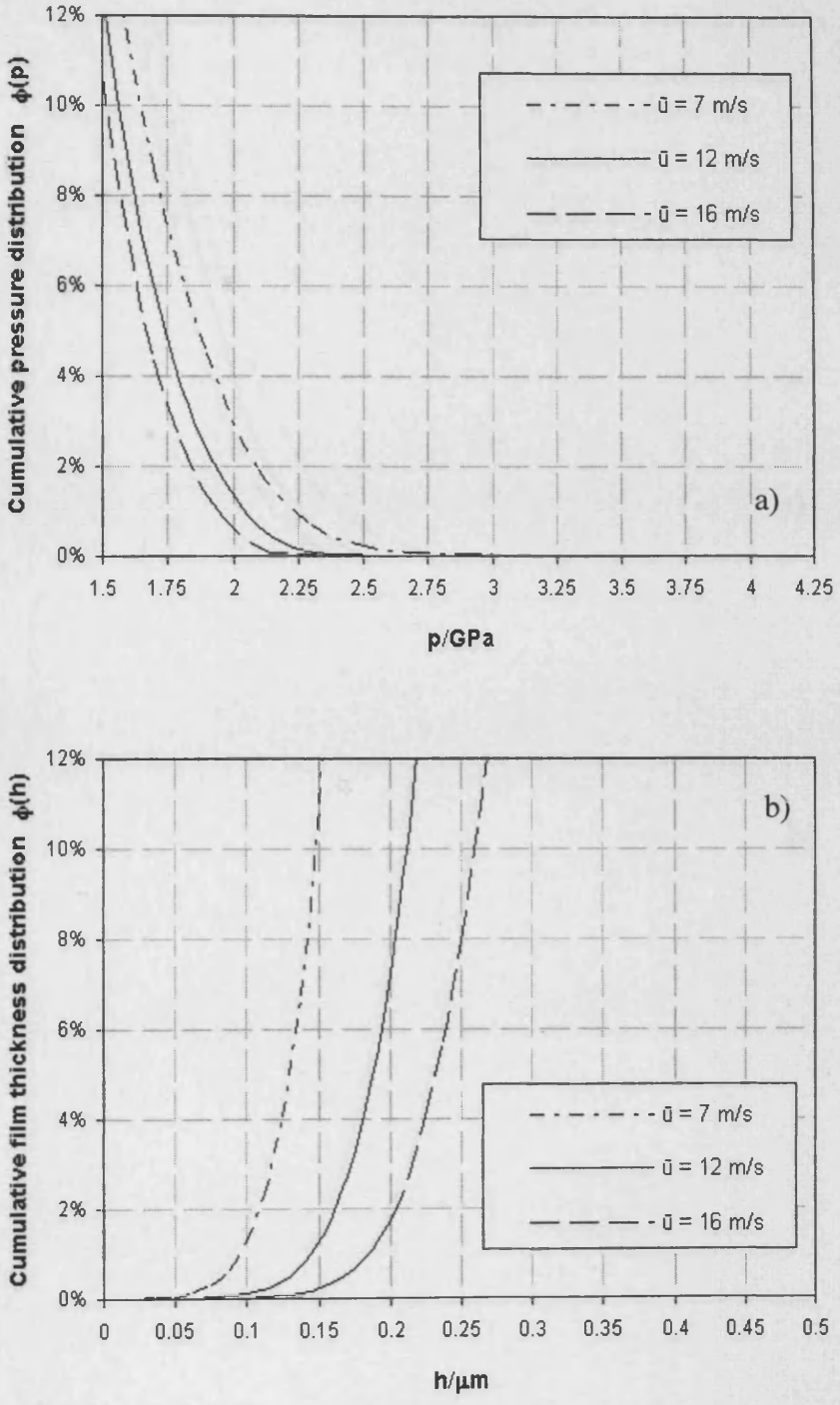

Figure 5.9. Variation with entrainment velocity of cumulative pressure distribution (a) and cumulative film thickness distribution (b) for test UTRC01 at a load corresponding to P_{Hz} = 1.3 GPa.

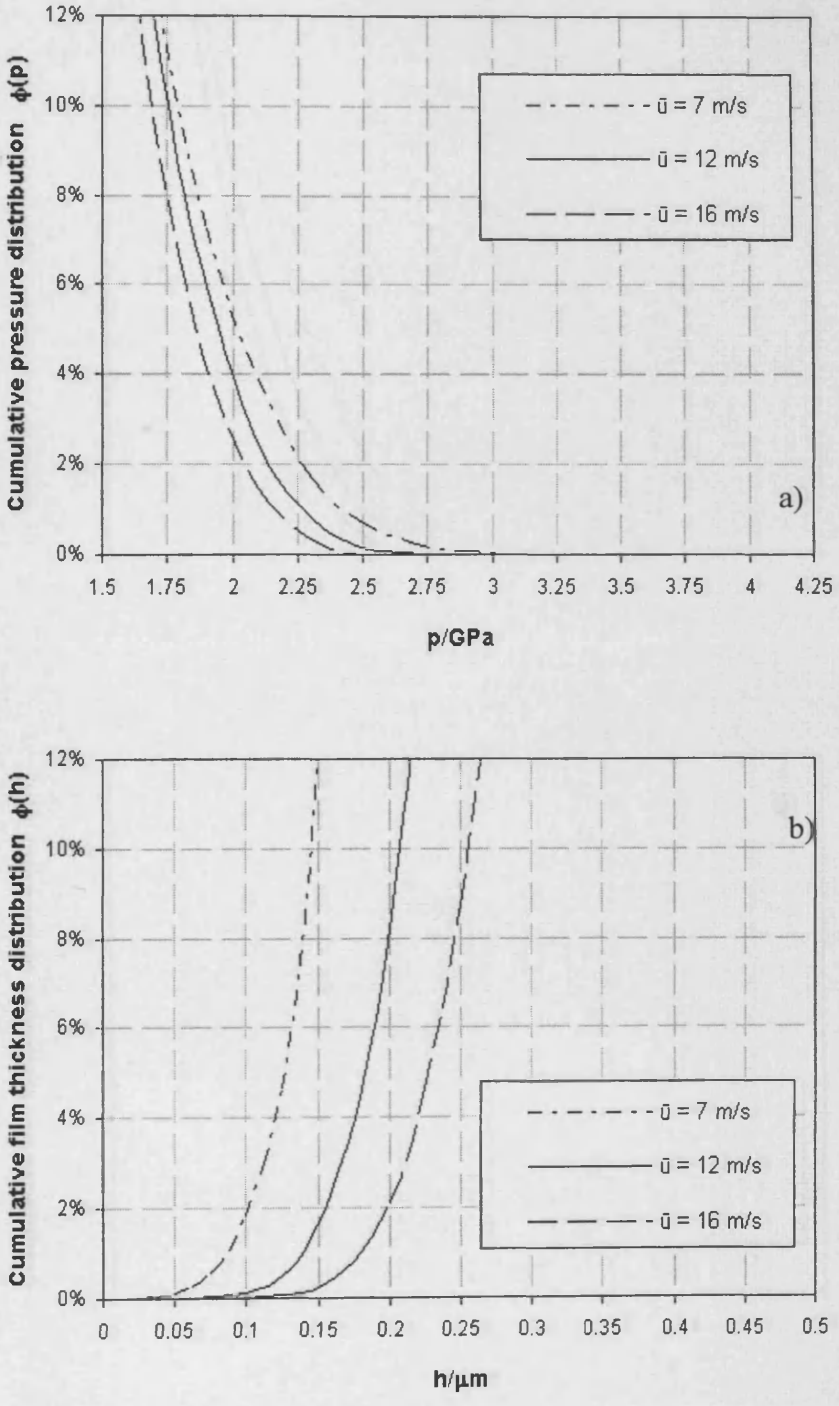

Figure 5.10.Variation with entrainment velocity of cumulative pressure distribution (a) and cumulative film thickness distribution (b) for test UTRC01 at a load corresponding to P_{Hz} = 1.5 GPa.

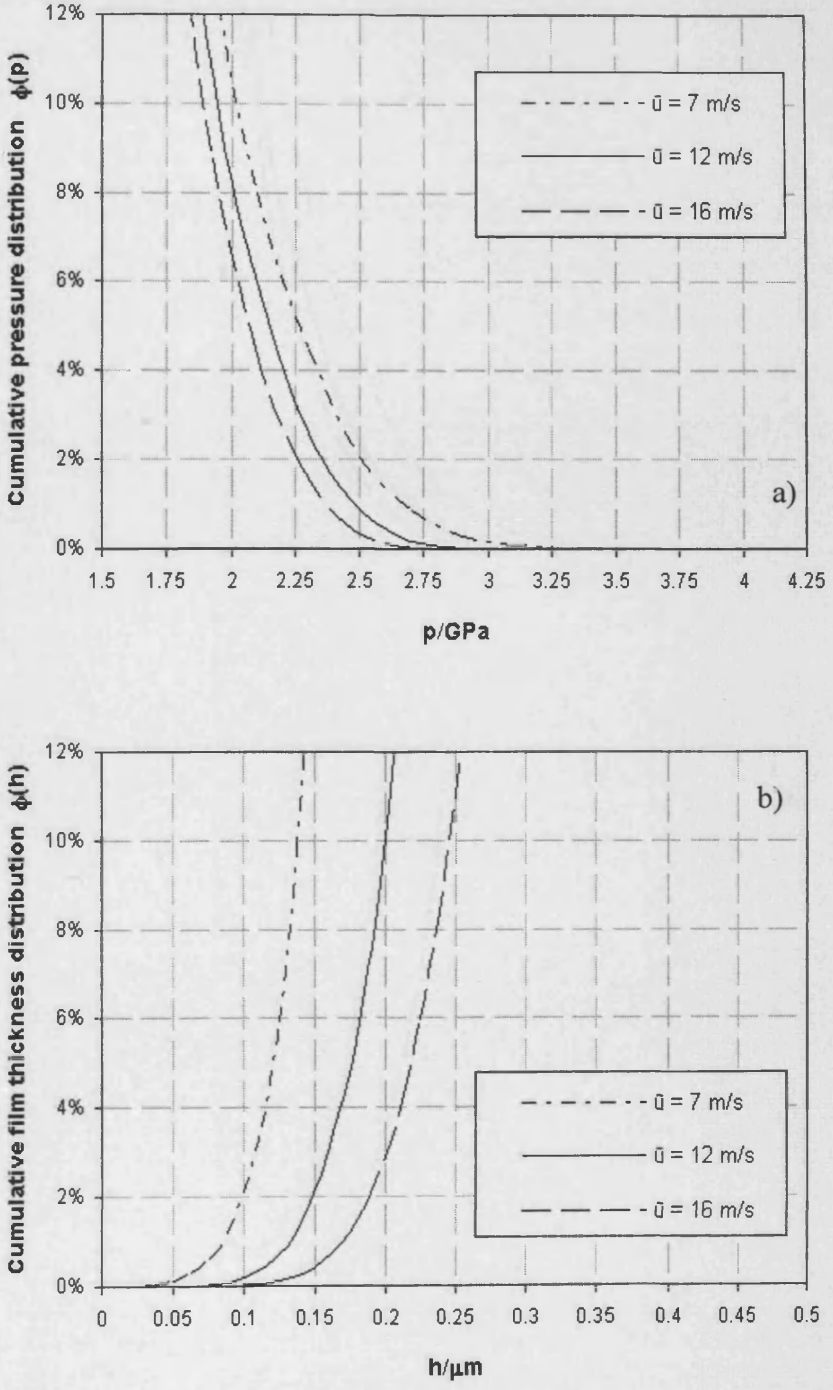

Figure 5.11. Variation with entrainment velocity of cumulative pressure distribution (a) and cumulative film thickness distribution (b) for test UTRC01 at a load corresponding to $_{PHz}$ = 1.7 GPa.

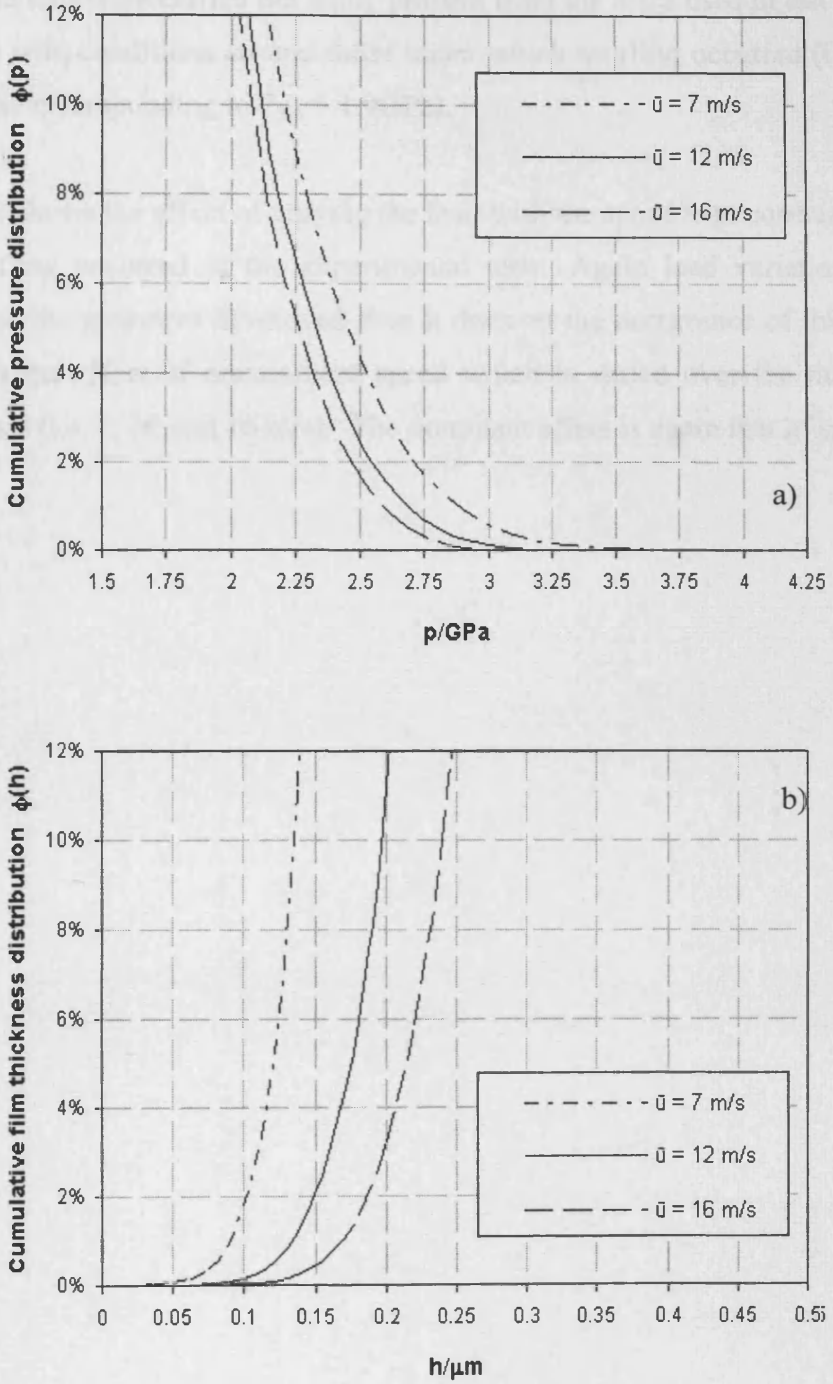

Figure 5.12. Variation with entrainment velocity of cumulative pressure distribution (a) and cumulative film thickness distribution (b) for test UTRC01 at a load corresponding to $_{PHz}$ = 1.9 GPa.

5.3.4. Numerical analysis of test UTRC27

EHL simulations were carried out using profiles from the discs used in test UTRC27 (discs 80 and 33) with conditions around those under which scuffing occurred (i.e. velocity of 7 m/s and load corresponding to P_{Hz} = 1.9GPa).

Figure 5.13 shows the effect of varying the load with the speed kept constant at the value at which scuffing occurred in the experimental test. Again load variation has a greater influence on the pressures developed than it does on the occurrence of thin films. Figure 5.14 shows the effect of entrainment speed which is varied over the range used in the scuffing tests (i.e. 7, 12 and 16 m/s). The dominant effect is again that of speed on the film thickness.

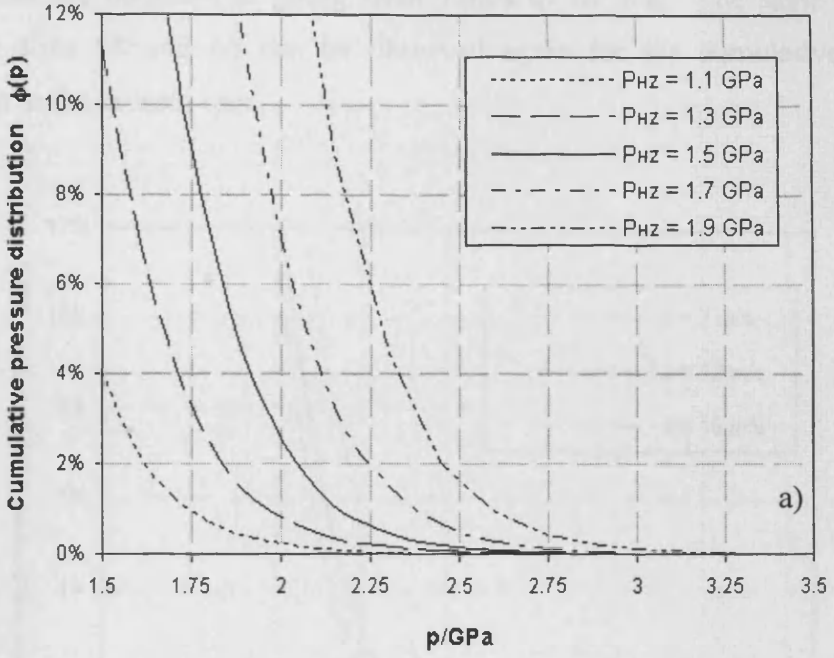

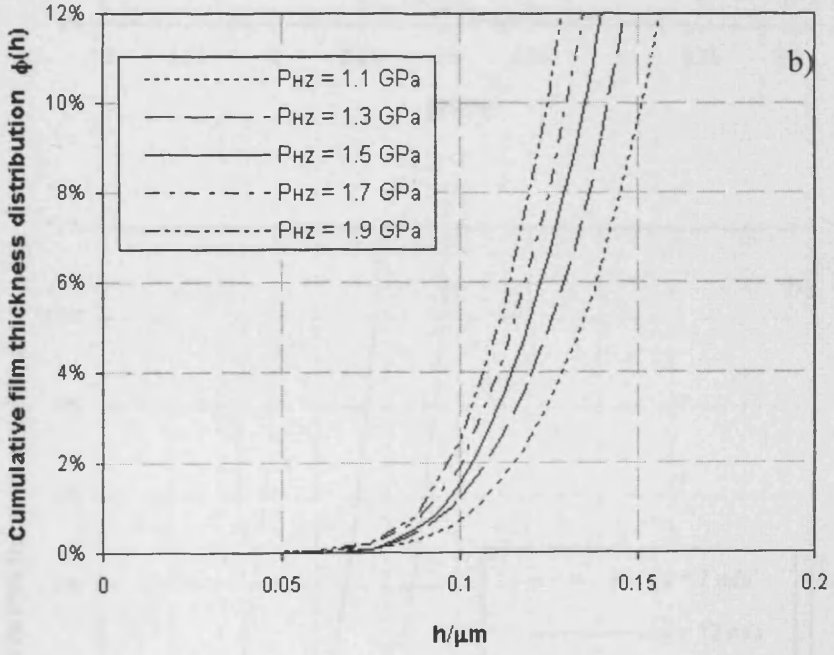

Figure 5.13. Part of cumulative pressure distribution (a) and cumulative film thickness distribution (b) over Hertzian area from EHL simulation of test UTRC27 at 7 m/s for varying loads.

The distributions obtained varying only the velocity shown in Figure 5.14 presents the same behaviour as described above for the previous case. The extreme high pressure in fact

does not show particular sensitivity to varying the velocity from 7m/s to 12m/s while higher values are obtained in going from 12m/s to 16 m/s. The same effect discussed before for discs 93 and 66 can be observed again for the cumulative film thickness distribution in the present case.

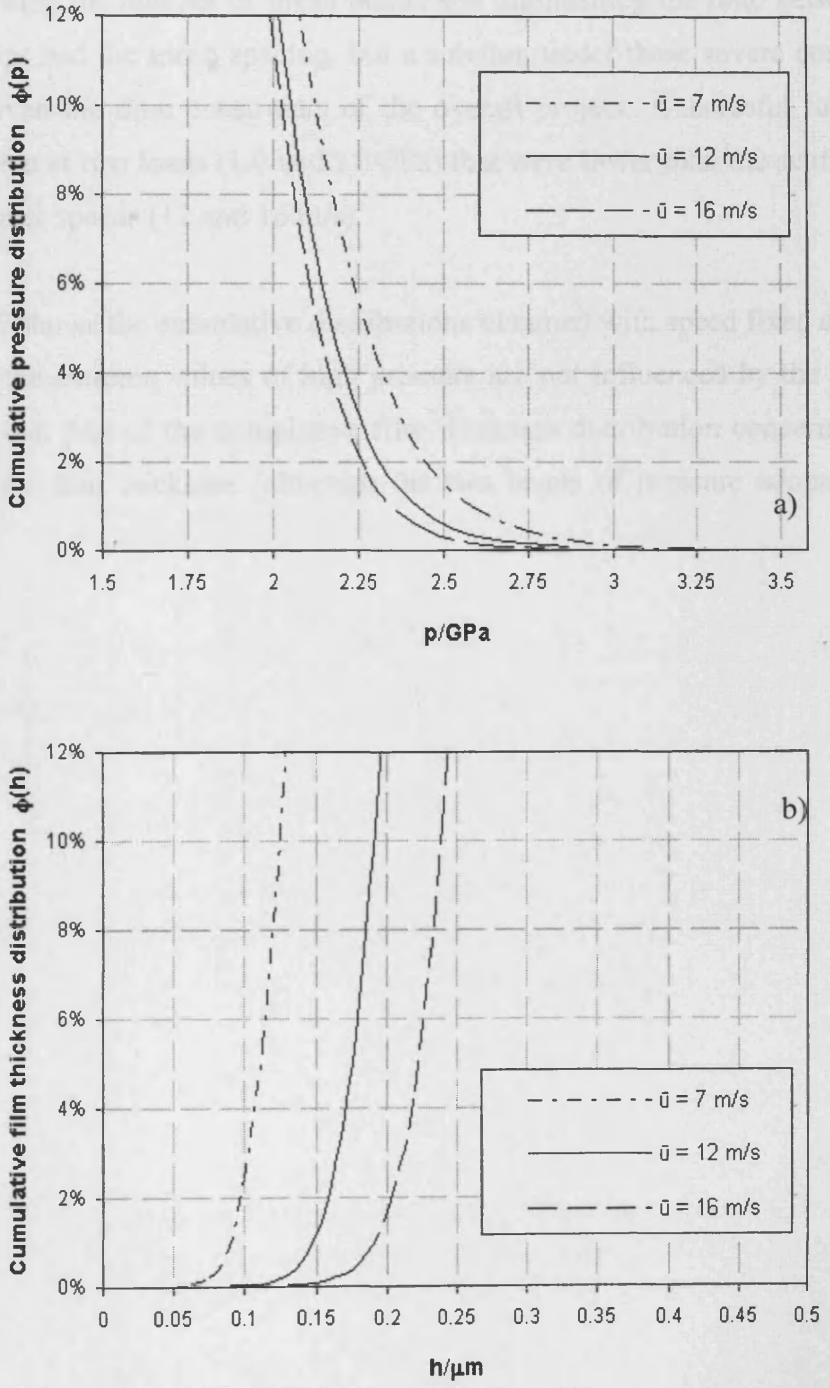

Figure 5.14. Variation with entrainment velocity of cumulative pressure distribution (a) and cumulative film thickness distribution (b) for test UTRC27 at a load corresponding to P_{Hz} = 1.9 GPa.

5.3.5. Numerical analysis of test UTRC07

Numerical analyses were carried out using profiles from the discs used in test UTRC07 (discs 90 and 06). In this case the profiles proved to be rather "aggressive" and it was not found possible to carry out simulations at the operating conditions under which scuffing occurred in the test (1.7GPa; 12 m/s). Several attempts were made to obtain a solution by both increasing the number of mesh points and diminishing the ratio between the number of time steps and the mesh spacing, but a solution under these severe conditions was not possible given the time constraints of the overall project.. Successful runs of the solver were possible at two loads (1.0 and 1.1GPa) that were lower than the scuffing load, and at the two higher speeds (12 and 16 m/s).

Figure 5.15 shows the cumulative distributions obtained with speed fixed and varying load. As shown the extreme values of high pressure are not influenced by the changes in load. Neither is that part of the cumulative film thickness distribution concerned with the thin values of the film thickness (although the two levels of pressure adopted are relatively close).

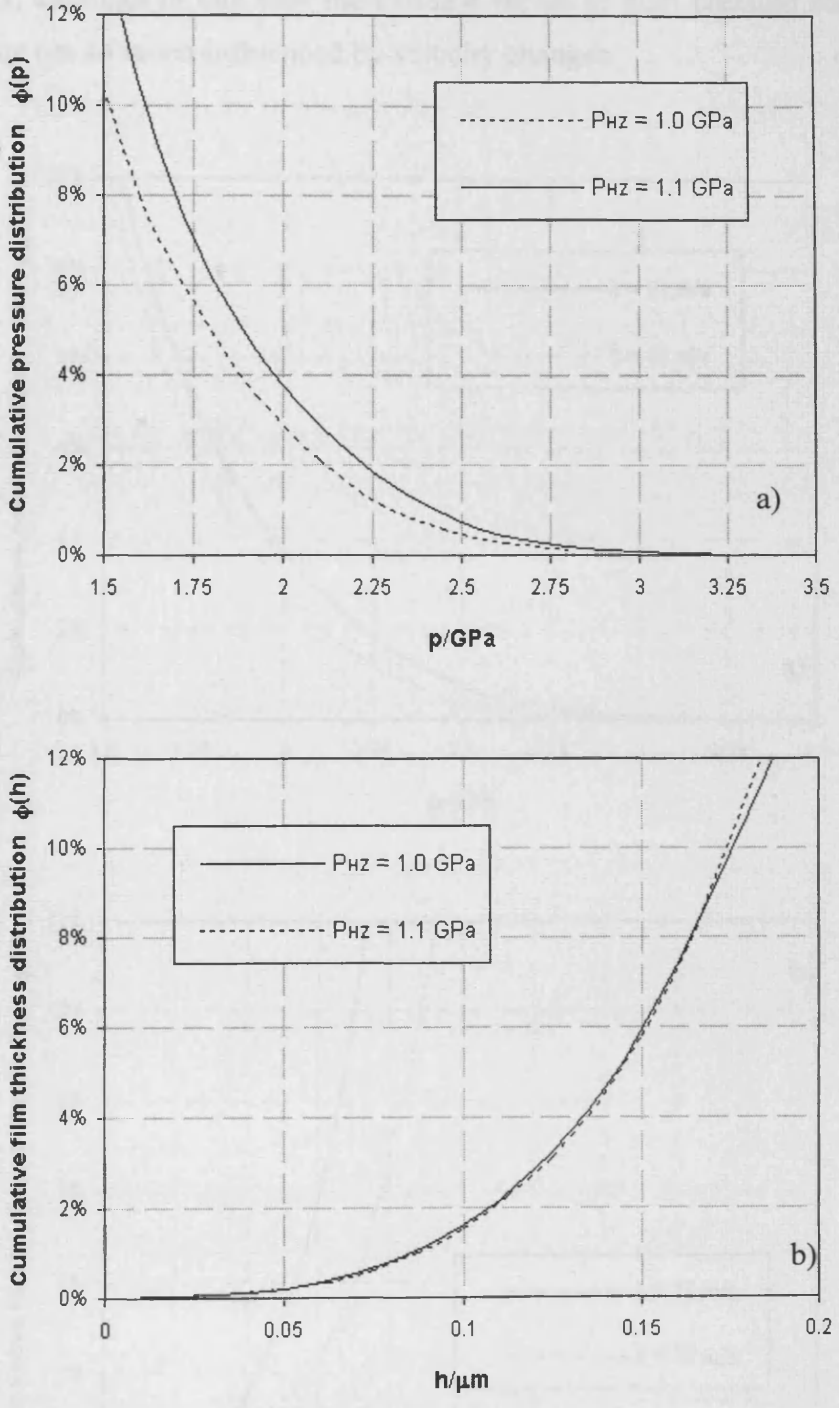

Figure 5.15. Part of cumulative pressure distribution (a) and cumulative film thickness distribution (b) for test UTRC07 at 12 m/s at two (light) loads.

Greater sensitivity is seen in Figure 5.16 which shows the distributions obtained by varying the velocity, although in this case the extreme values of high pressure and very low film thickness are not so much influenced by velocity changes.

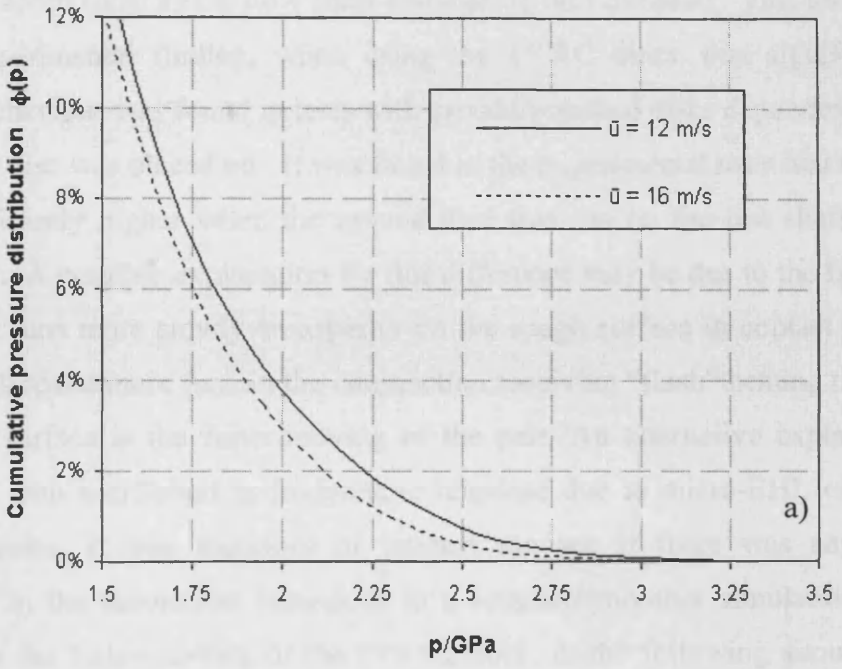

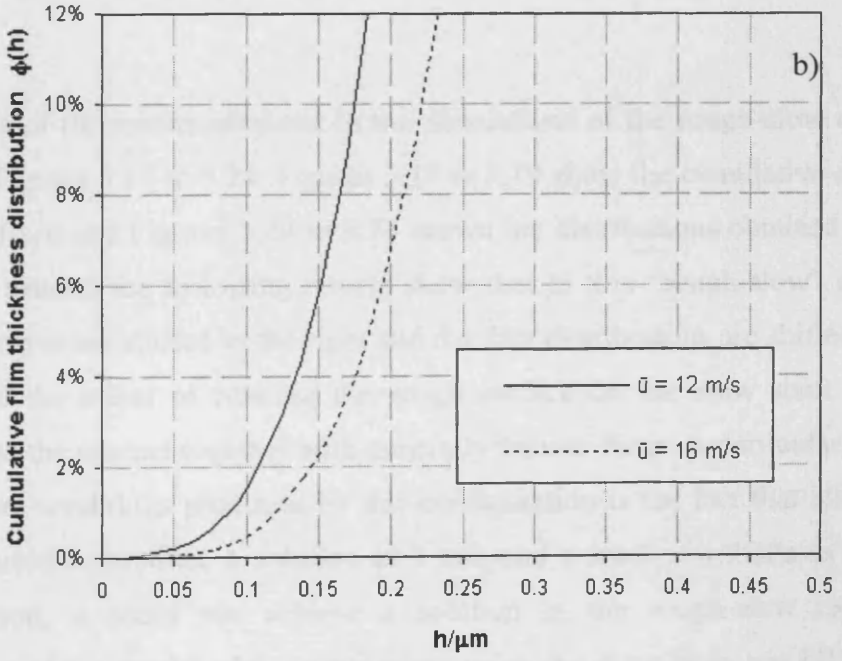

Figure 5.16. Variation with entrainment velocity of cumulative pressure distribution (a) and cumulative film thickness distribution (b) for test UTRC07 at load P_{Hz} = 1.1 GPa.

5.3.6. Numerical analysis of test UTRC01 with discs swapped

The aim in this simulation was to show the effect, if any, of swapping the profiles from the two discs, i.e. instead of the rougher of the two discs being on the fast shaft it was run at the lower speed, and the smoother disc, which was previously on the slow shaft, was run at the higher speed (disc 93 on slow shaft and disc 66 on fast shaft). This idea was suggested by the experimental finding, when using the UTRC discs, that significantly different scuffing behaviour was found in tests with ground/polished discs depending on which shaft the ground disc was placed on. It was found in the experimental tests that the scuffing load was significantly higher when the ground disc was run on the fast shaft (see Table 3.5, Chapter 3). A possible explanation for this difference may be due to the fact that when the rough disc runs more slowly an asperity on the rough surface in contact with the smooth surface will spend more time in the conjunction receiving "flash" heating than it does when the rough surface is the faster-moving of the pair. An alternative explanation might be associated with a different hydrodynamic response due to micro-EHL effects in the two different cases. It was therefore of interest too see if there was any corresponding difference in the theoretical behaviour in a rougher/smoother simulation, depending on which was the faster-moving of the two surfaces. In the following simulations the same combinations of load and velocity were used as before in the simulations using this pair of discs.

Full details of the results obtained in the simulations of the rough-slow configuration are shown in Figures 5.17 to 5.24 .Figures 5.17 to 5.19 show the cumulative distributions with the speed fixed and Figures 5.20 to 5.24 shown the distributions obtained holding the load fixed. In general the following results show that in this "rough-slow" configuration the pressure curves are shifted to the right and the film distributions are shifted to the left. This means that the effect of running the rough surface on the slow shaft produces higher pressures in the contact together with generally thinner films. A particular indication of the more severe conditions produced by this configuration is the fact that although the solver could be used to produce a solution at 7 m/s and a load of 1.9GPa in the "rough-fast" configuration, it could not achieve a solution in the rough-slow case. A detailed comparison of the results of the simulations using the discs from test UTRC01 in the two configurations is presented in the following section of this chapter.

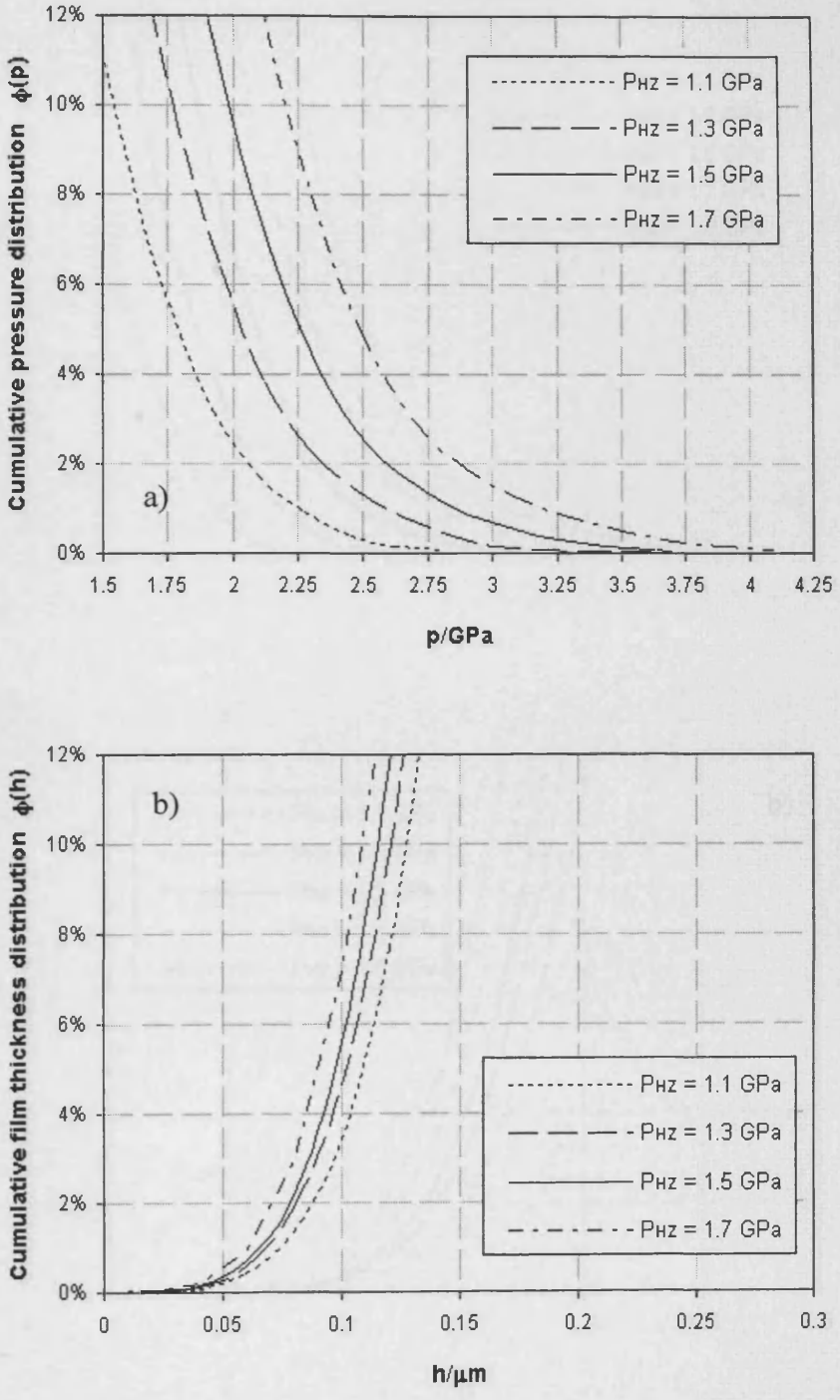

Figure 5.17. Part of cumulative pressure distribution (a) and cumulative film thickness distribution (b) from simulation of test UTRC01 with rougher profile on slower shaft at 7 m/s for varying loads.

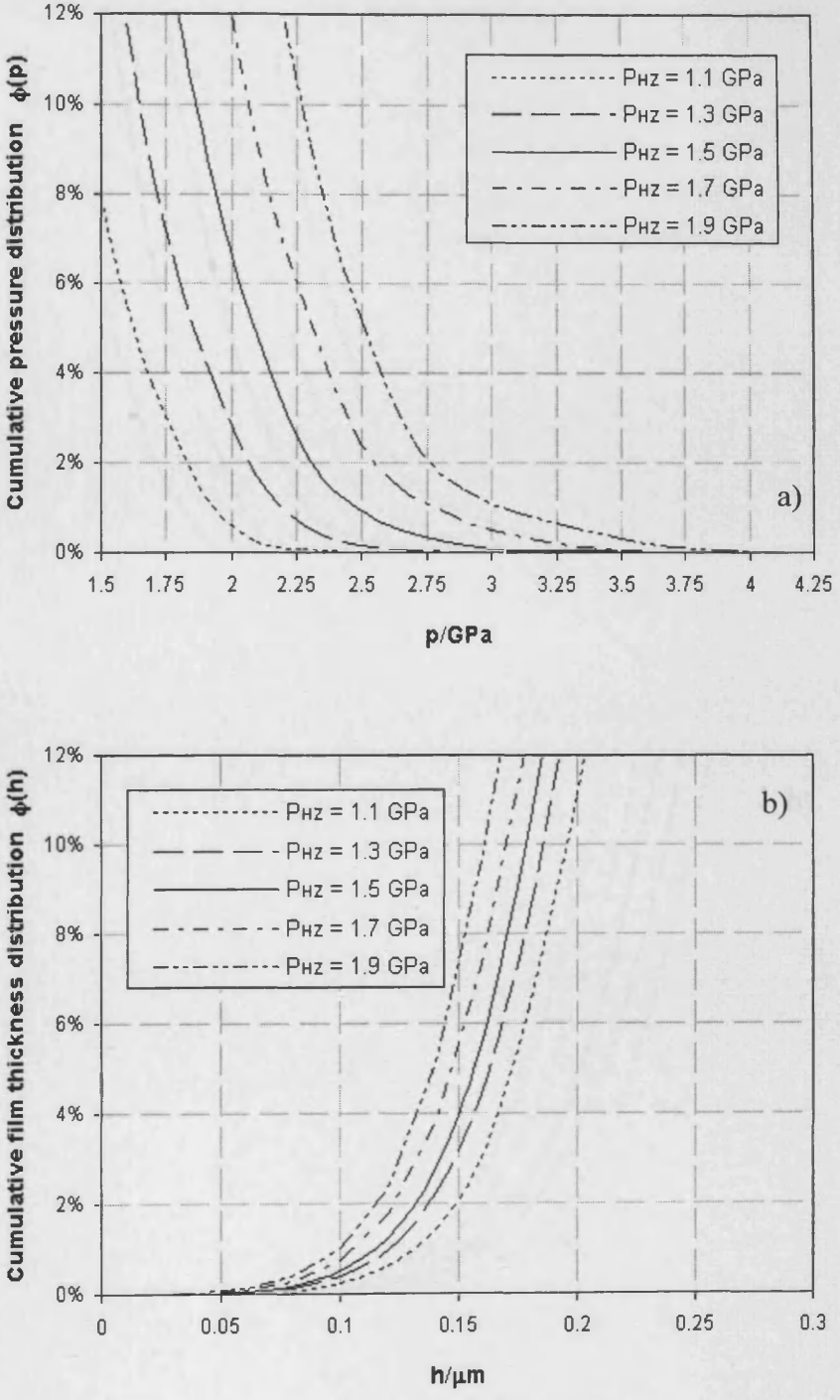

Figure 5.18. Part of cumulative pressure distribution (a) and cumulative film thickness distribution (b) from simulation of test UTRC01 with rougher profile on slower shaft at 12 m/s for varying loads.

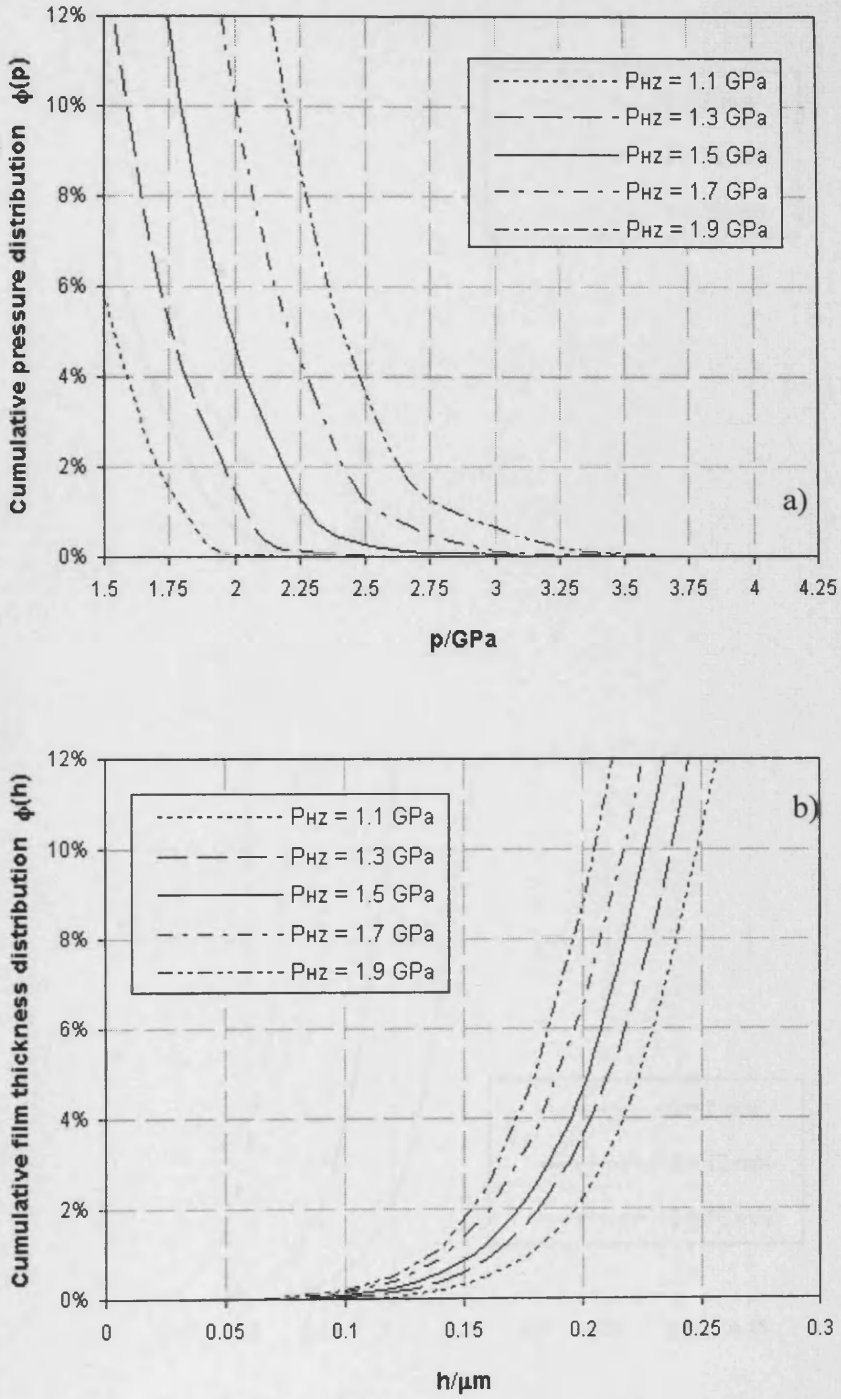

Figure 5.19. Part of cumulative pressure distribution (a) and cumulative film thickness distribution (b) from simulation of test UTRC01 with rougher profile on slower shaftat 16 m/s for varying loads.

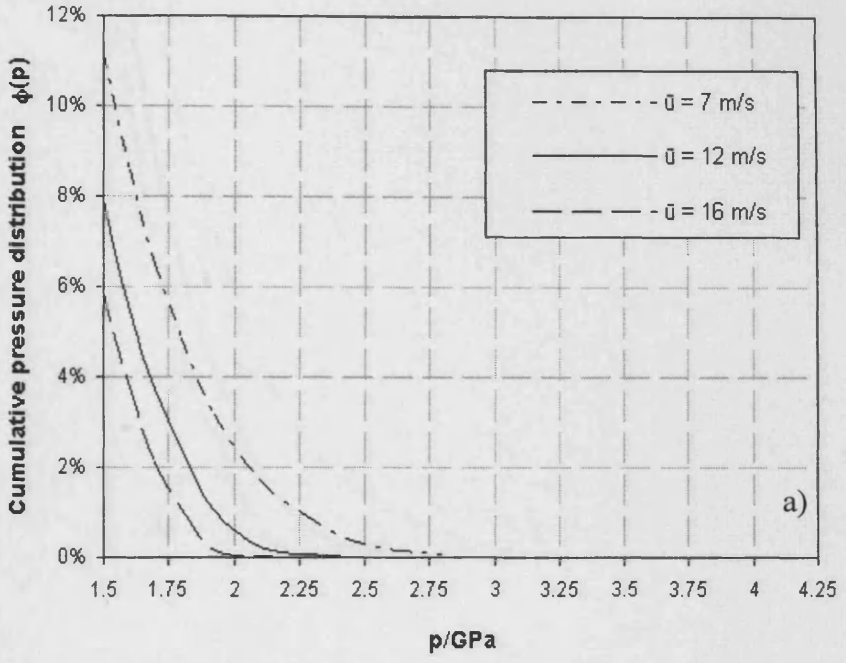

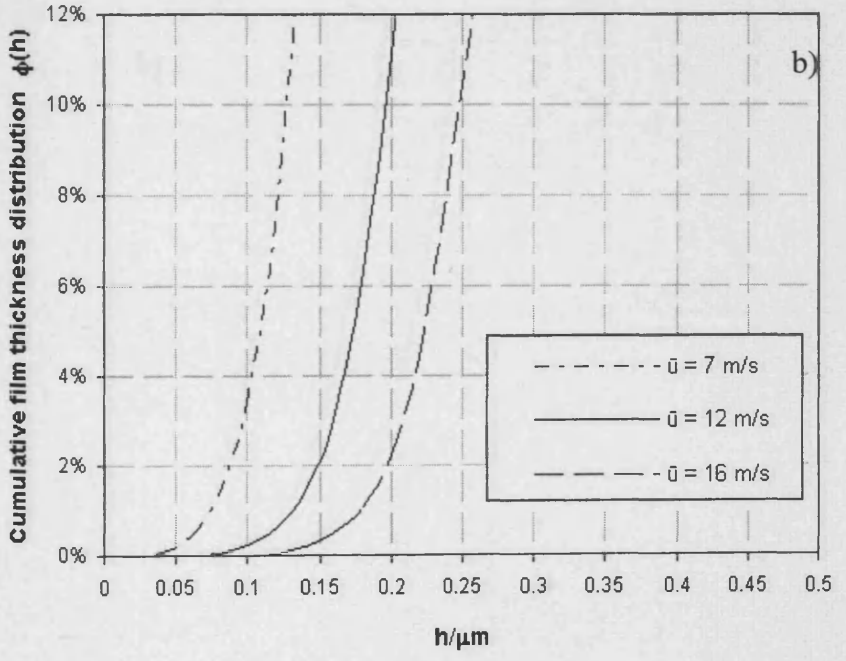

Figure 5.20. Variation with entrainment velocity of cumulative pressure distribution (a) and cumulative film thickness distribution (b) from simulation of test UTRC01 with rougher profile on slower shaft at load P_{Hz} = 1.1 GPa, for three sliding speeds.

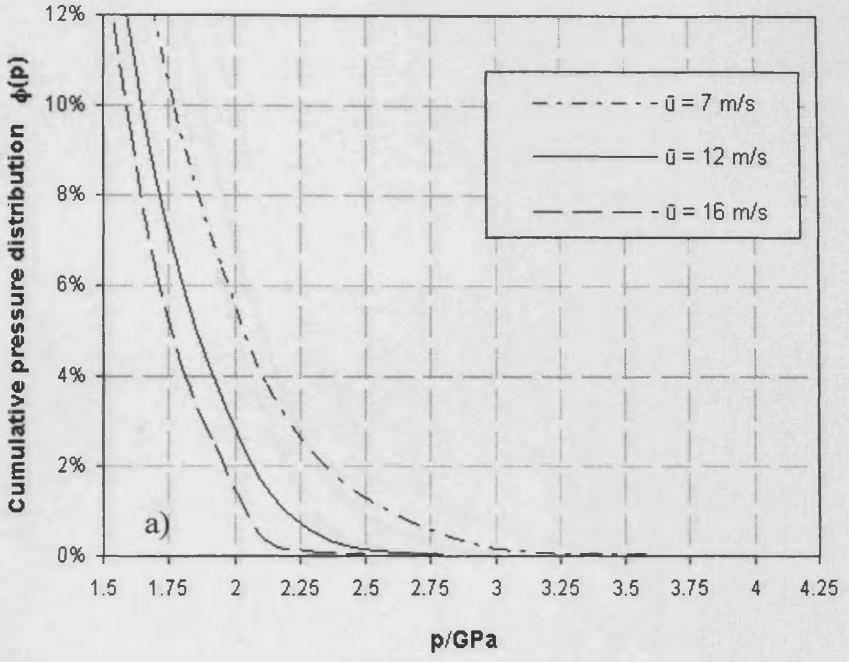

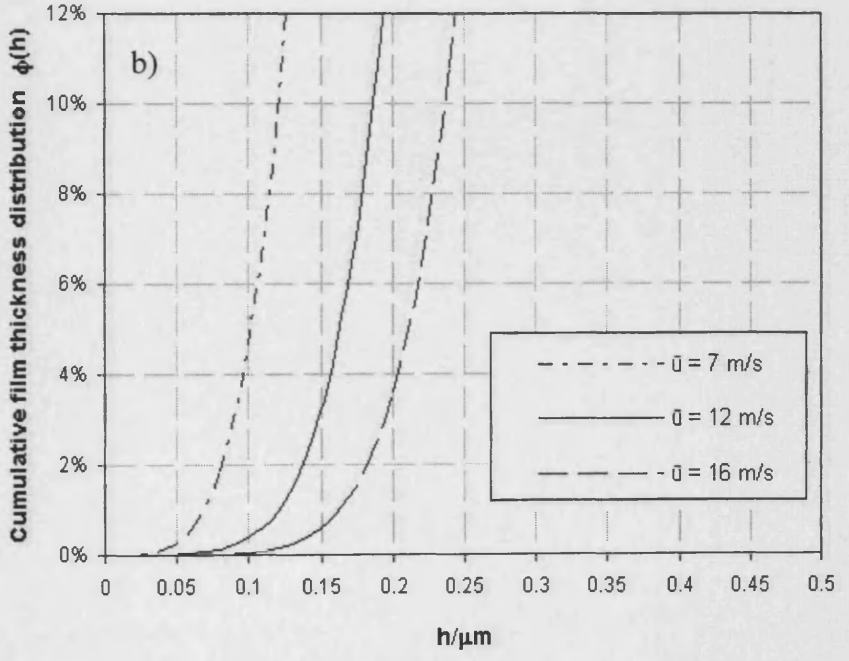

Figure 5.21. Variation with entrainment velocity of cumulative pressure distribution (a) and cumulative film thickness distribution (b) from simulation of test UTRC01 with rougher profile on slower shaft at load P_{Hz} = 1.3 GPa, for three sliding speeds.

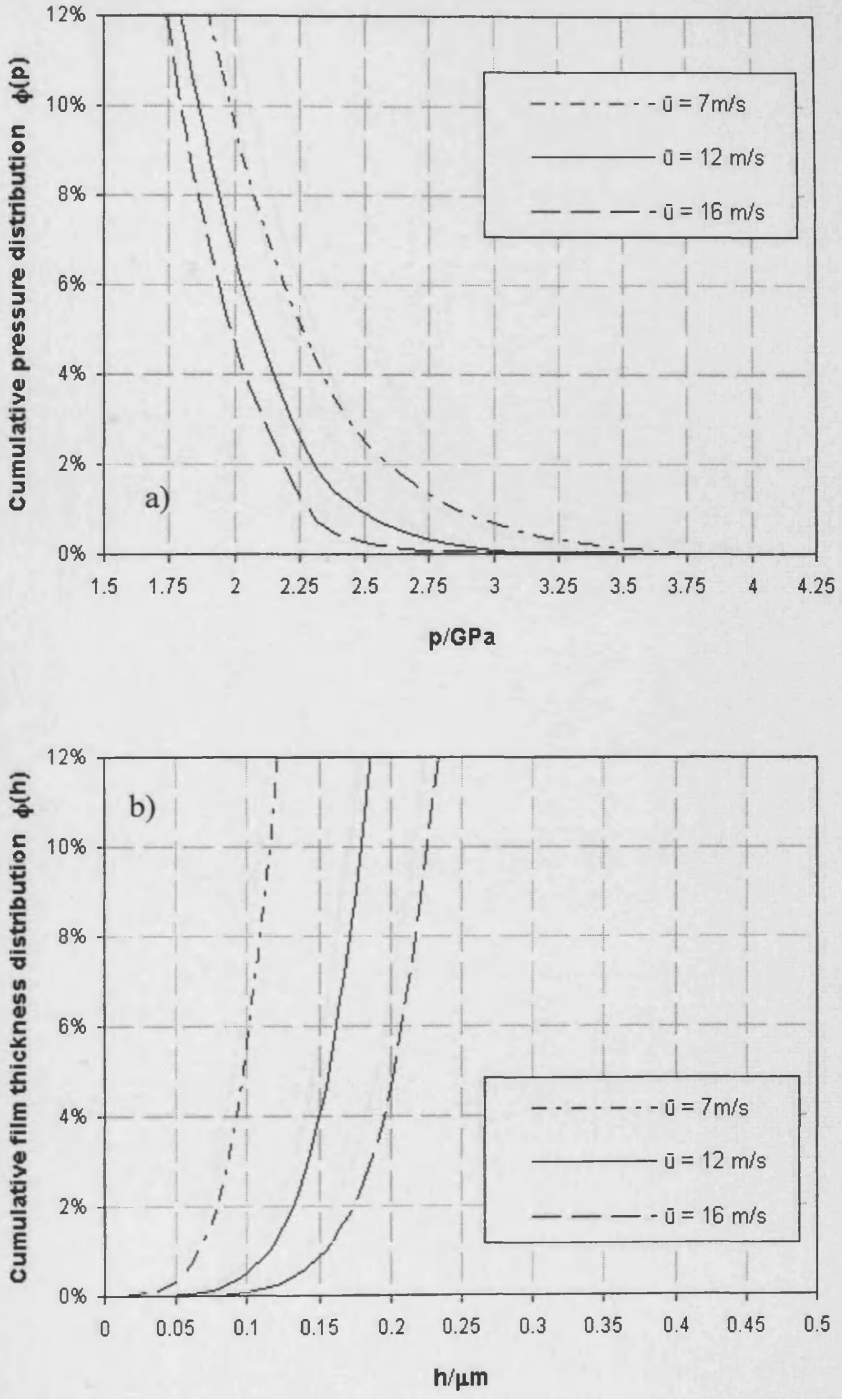

Figure 5.22. Variation with entrainment velocity of cumulative pressure distribution (a) and cumulative film thickness distribution (b) from simulation of test UTRC01 with rougher profile on slower shaft at load P_{Hz} = 1.5 GPa, for three sliding speeds.

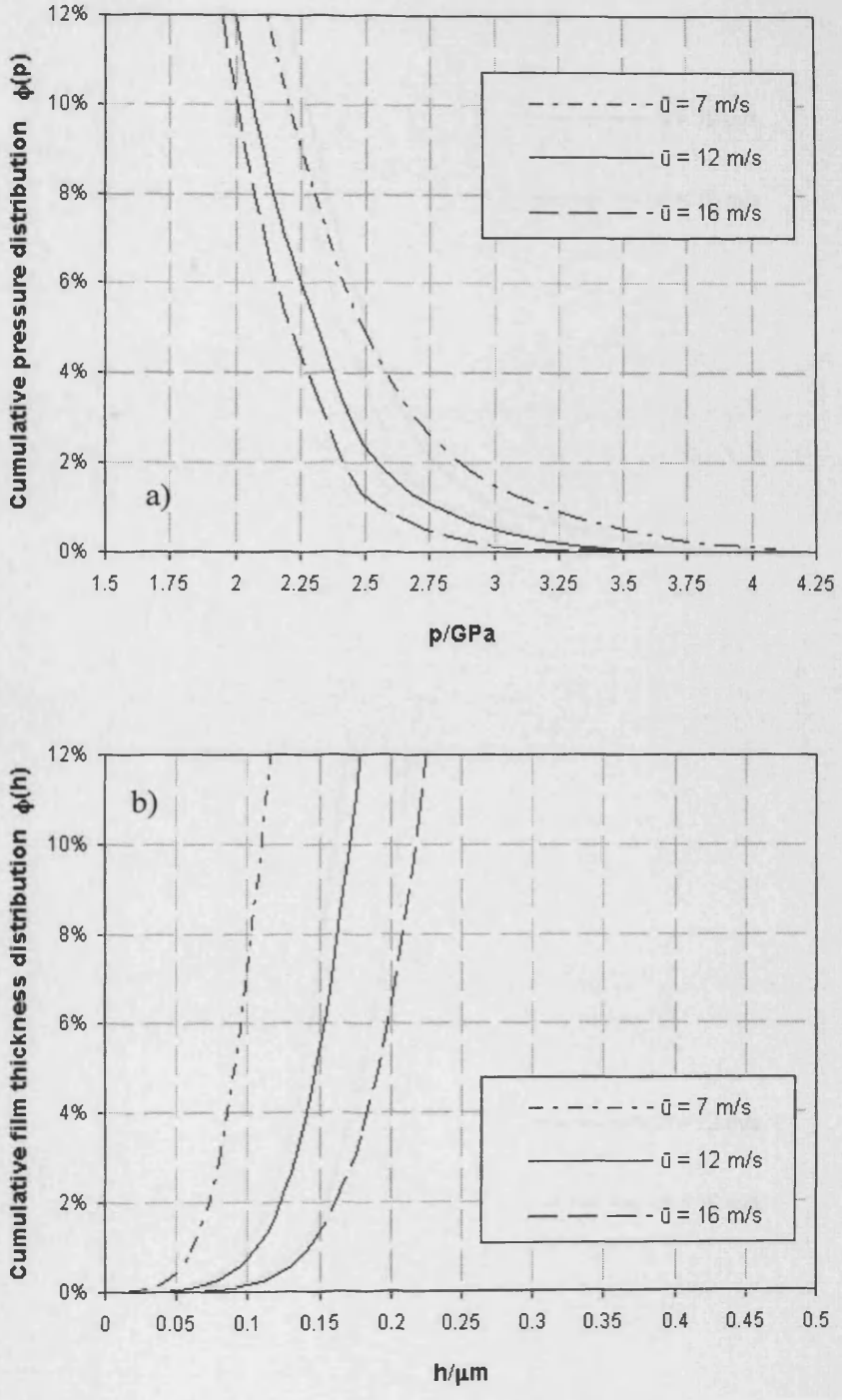

Figure 5.23. Variation with entrainment velocity of cumulative pressure distribution (a) and cumulative film thickness distribution (b) for disc 93 (fast shaft) and disc 66 (slow shaft) at load P_{Hz} = 1.7 GPa.

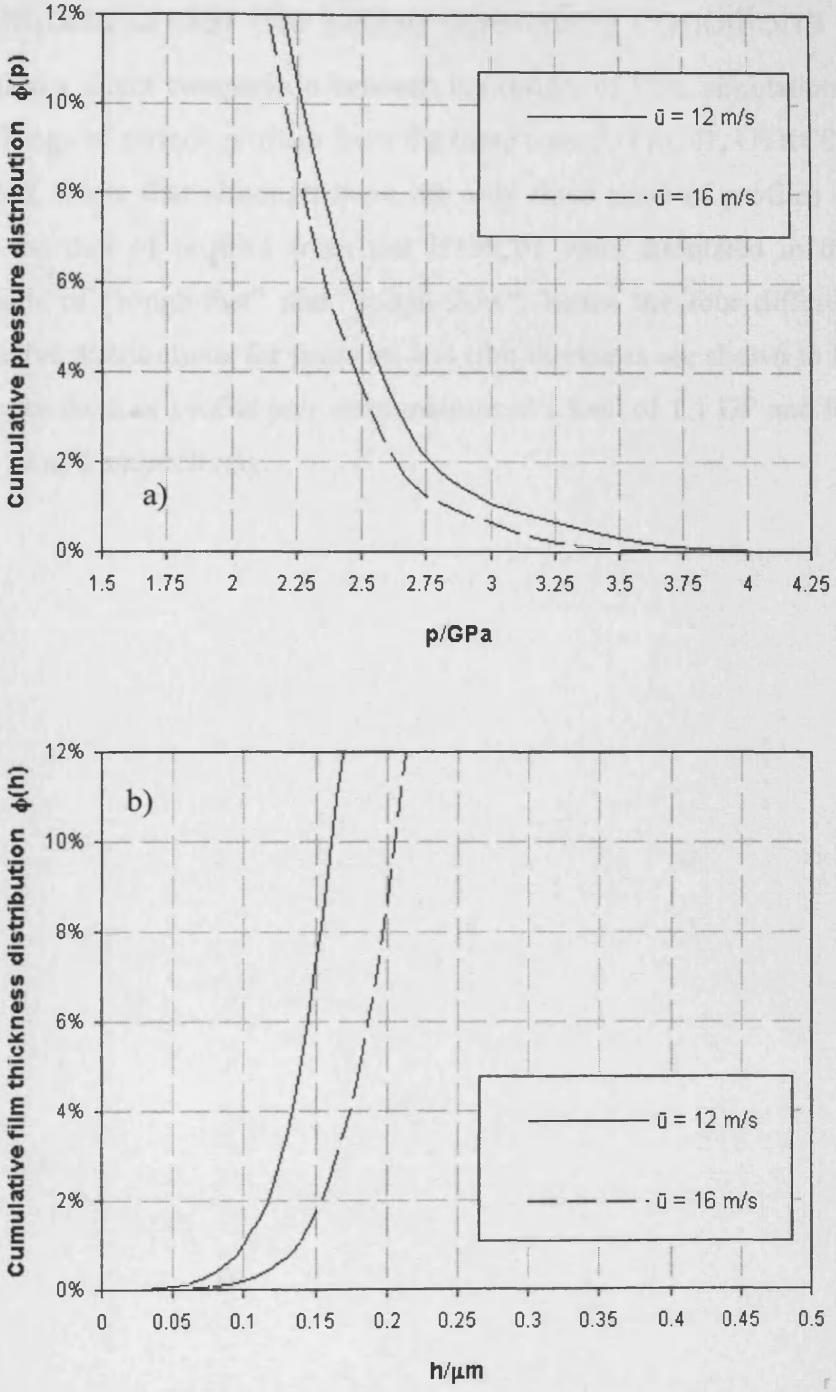

Figure 5.24. Variation with entrainment velocity of cumulative pressure distribution (a) and cumulative film thickness distribution (b) for disc 93 (fast shaft) and disc 66 (slow shaft) at load P_{Hz} = 1.9 GPa.

5.4. Comparison of simulation results of different profile combinations under the same operating conditions

In this section a direct comparison between the results of EHL simulations obtained from the four pairings of surface profiles from the three tests (UTRC01, UTRC07 and UTRC27) are described. (Note that although there are only three pairs of profiles used from these three tests the pair of profiles from test UTRC01 were simulated in the two different configurations of "rough-fast" and "rough-slow", hence the four different simulations). The cumulative distributions for pressure and film thickness are shown in Figures 5.25 and 5.26 below for the four profile pair combinations at a load of 1.1 GP and for two speeds of 12m/s and 16 m/s, respectively.

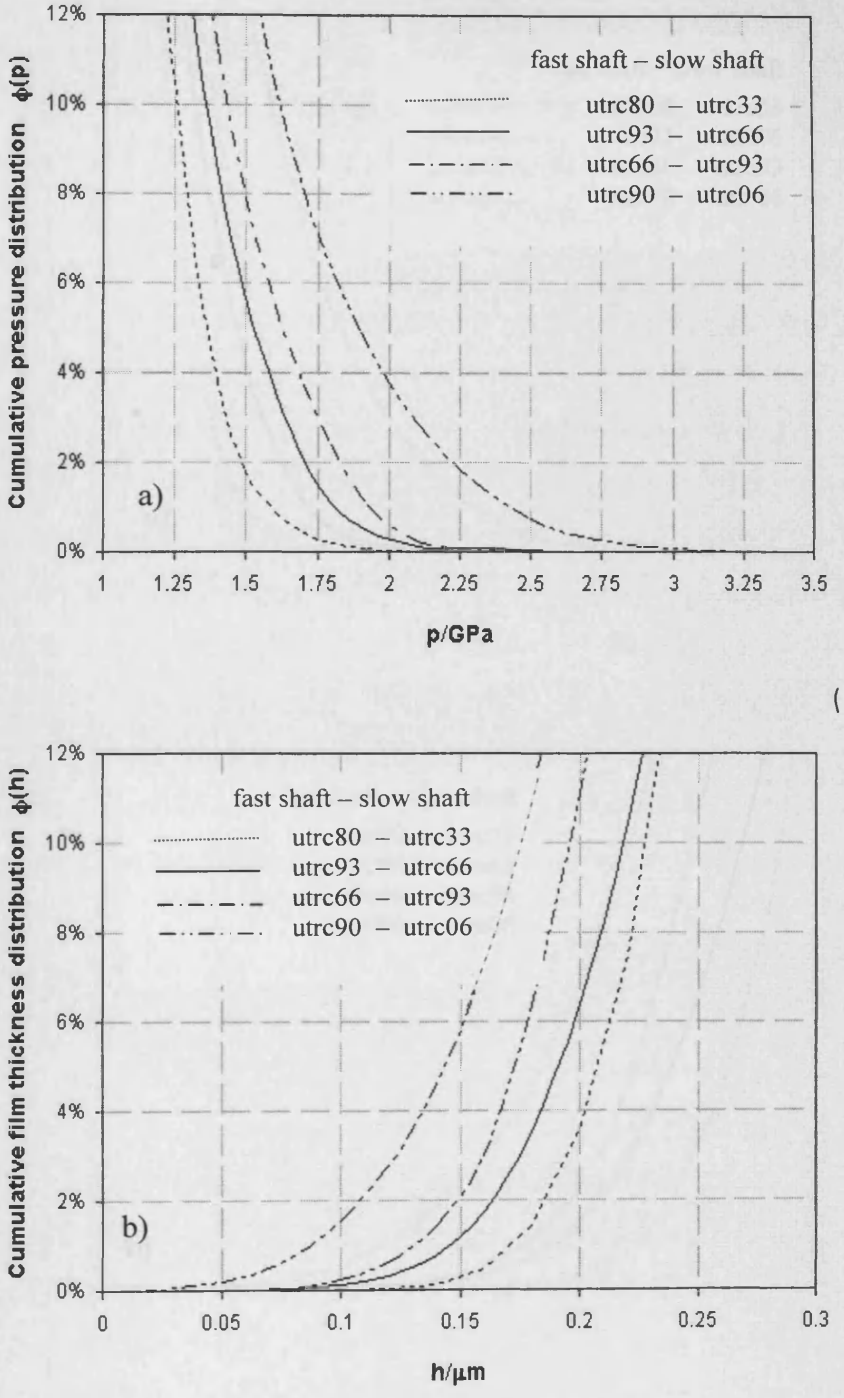

Figure 5.25. Part of cumulative pressure distribution (a) and cumulative film thickness distribution (b) for all four combinations of disc profiles at 12 m/s and P_{Hz} = 1.1 GPa.

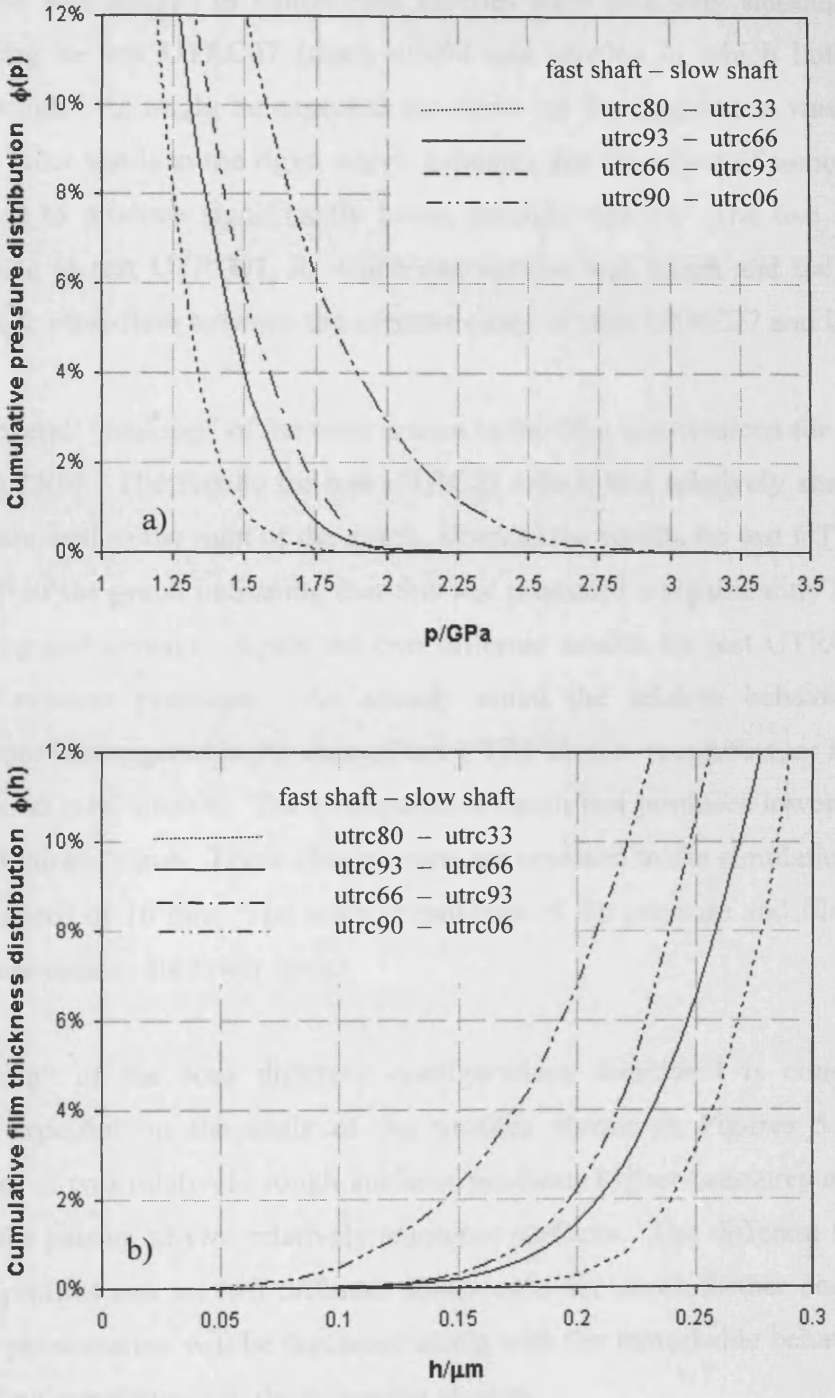

Figure 5.26. Part of cumulative pressure distribution (a) and cumulative film thickness distribution (b) for all four combinations of disc profiles at 16 m/s and P_{Hz} = 1.1 GPa.

As might be expected lower pressures are found with the profile pairs having lower roughness, and thinner films are found in the combinations of profiles with higher roughness. In Figure 5.15(a), for example, which shows the cumulative pressure

distributions at 12 m/s, there is a considerable separation of the curves for test UTRC27 (discs utrc80 and utrc33) in which both profiles were relatively smooth, and the curve corresponding to test UTRC07 (discs utrc90 and utrc06) in which both profiles were relatively rough. As might be expected the curve for the former test was to the left, and that for the latter test is to the right, which indicates that the effect of smoother surfaces on both discs is to produce significantly lower pressure ripples. The two different results corresponding to test UTRC01, in which one surface was rough and the other relatively smooth, are intermediate between the extreme cases of tests UTRC27 and UTRC07.

The same overall "ranking" of the tests is seen in the film distributions for this speed given in Figure 5.15(b). The results for test UTRC27 which had relatively smooth profiles on both discs are well to the right of the graph, whereas the results for test UTRC07 are on the extreme left of the graph indicating that this test produced a significantly higher degree of film thinning and contact. Again the two different results for test UTRC01 lie between these two extreme positions. As already noted the relative behaviour of the two configurations investigated in the case of test UTRC01 (i.e. rough/fast, as in the actual test, or rough/slow) is of interest. The configuration rough/fast produces lower pressures in the contact and thicker films. These observations are repeated in the simulations carried out at the higher speed of 16 m/s. The relative rankings of the pressure and film curves are the same as those seen at the lower speed.

The "ranking" of the four different configurations simulated is consistent with the behaviour expected on the basis of the profiles shown in Figures 5.1 to 5.3. The combination of two relatively rough surfaces produces higher pressures and thinner films than does the pairing of two relatively smoother surfaces. The different behaviour of the same two profiles run on two different shafts calls for some further comment, and this theoretical phenomenon will be discussed along with the remarkable behaviour seen in the corresponding experiments in the following chapter.

Chapter 6

Discussion, conclusions and suggestions for further work

6.1. Introduction

The work carried out during the project has been mainly concerned with experimental testing of lubricated hardened steel discs with various types of surface condition including ground, superfinished and hard-coated. The experiments were designed to investigate scuffing performance under severe conditions of load, speed and oil temperature that could be related to the extreme conditions found in aerospace transmissions such as those in a helicopter gearbox. Although plain steel surfaces have been tested in this way in the past there appears to be little in the way of testing of hard-coated surfaces under severe engineering conditions. The review carried out in Chapter 1 suggests that most of the testing that has been carried out has been done using relatively slow speed boundary-lubricated testing apparatus. It was therefore realised from the start that there was a need for the type of testing done in this project. The apparatus used in the project is described in Chapter 2. The two disc rig is capable of simulating very severe operating conditions with maximum Hertzian pressures of up to 2.0GPa, and sliding speeds at this load of the order of 20m/s. The highest sliding condition used in the study was 16m/s. The lubricant in all the tests was a typical aerospace oil, Mobiljet 2, which is a low viscosity gas turbine oil designed to lubricate the high speed rolling element bearings in an aircraft engine, but also used to lubricated and cool any gearing in the engine. Under extreme conditions the oil can operate at very high temperature and in the present study the oil was delivered to the lubricated contact between the discs at a temperature of 100°C.

In addition to the operating conditions of the rig particular attention was paid to the finish of the test discs. In most types of ground gears the teeth are finished by grinding which leaves finishing marks which are aligned in a roughly axial direction. Rolling and sliding between the teeth therefore occurs across the finish, and it was therefore considered necessary to finish the test discs in the same way by using the special finishing rig described in Chapter 2. The process also achieves a "crowned" geometry which ensures that the contact does not suffer from edge effects, which are an unpredictable feature of discs that are of a cylindrical form.

The main body of experimental work used steel discs (both hard-coated and un-coated) provided by UTRC. The results of this work are described in detail in the pages of Chapter 3, and some further discussion of the results is given in the following sections of this chapter. A short series of tests using un-coated aerospace steel supplied by Rolls-Royce was carried out and is reported in Chapter 4.

Advantage was taken of the local availability of an advanced micro-elastohydrodynamic lubrication (micro-EHL) solver to carry out simulations of the contact and lubrication of some of the steel discs used in the experimental work. This work revealed the severe nature of the lubrication regime taking place in the experiments with ground surfaces.

6.2. Discussion of the results of the disc tests

6.2.1. Ground discs on ground discs

This series of tests was carried out in order to establish a baseline against which the performance of coated and/or superfinished surfaces could be measured. The main set of eight tests was conducted using the steel samples supplied by UTRC, and a shorter group of tests was undertaken using different steel supplied by Rolls-Royce PLC. The behaviour in the tests was similar to that which had been experienced in the earlier project carried out by Patching (1995). Scuffing was experienced in all tests and the characteristic behaviour of a sudden very sharp rise in friction indicated failure of the lubrication system. In all tests there was clear evidence of "running in" as indicated by a friction reading which increased at first following an increase in the load, but then fell back to a lower level during the remaining 3 minutes in which the load remained constant. This behaviour, which was more prominent during the final stages preceding scuffing, is attributed to a

smoothing of the surfaces caused by asperity interactions. It is believed that the modification to the surface is produced as a result of plastic deformation and partial "flattening" of the high points of the finish due to the high contact pressures and frictional traction at asperity/asperity interfaces. The effects of asperity deformation in the stages before scuffing occurred are clearly evident in the SEM images such as those shown in Figures 3.8, 3.13, 3.14 in Chapter 3. The upper image of Figure 3.14, for example, shows run but unscuffed surface of the slow disc from test UTRC07 (12m/s sliding speed) to the left of the scuffing scar. It is clear that the asperity peaks have been plastically deformed to produce flat-looking "lands" and there is evidence of a "smearing" action which has displaced material over the edges of these lands in the direction of relative sliding. Deformation therefore appears to be due to a combination of normal pressure and a high effective friction coefficient. The changes that occur to the surface would appear to benefit the continuation of hydrodynamic lubrication since the measured surface roughness typically fell from about 0.4μm to less than 0.3μm prior to scuffing. The fall in friction during a load stage would also suggest improved lubrication conditions. Eventually, however, the process of surface improvement breaks down and the surfaces weld, tear and lubrication has evidently failed.

The temperatures reached in the stages preceding scuffing with the ground/uncoated samples are high. In test UTRC02 at a sliding speed of 16m/s the bulk temperature of the fast disc reached 317°C just prior to scuffing. To this bulk temperature should be added the short-lived "flash" temperature experience by the surfaces as they passed through he contact region. This temperature cannot be measured in tests with steel surfaces but can be estimated with reasonable accuracy on the basis of the measured frictional energy and the use of the Blok calculation. In the case under consideration the additional flash temperature was calculated to be 177°C giving a total maximum contact temperature of almost 500°C. A photograph of the discs after this test is shown in Figure 3.5(b) and a striking discolouration of the running parts of both discs has occurred, possibly due to oxidation of the oil film. It is perhaps surprising that hydrodynamic protection of the surfaces can persist under such extreme conditions.

Returning to the SEM image shown in Figure 3.14 we see in the lower image what may be described as an indication of the early stage of scuffing in which damage is relatively light

in extent. The smearing which is evident in a highly run in, but otherwise unscuffed, surface has in this case developed to a stage where the surfaces appear to have adhered and produced damage on the flattened "lands". A more severe displacement of material is evident and the stage has almost been reached in which displaced material is bridging the gap between one asperity and its neighbour. It is interesting to speculate that this image captures the actual moment when running in turned into scuffing.

Detailed results of the tests using ground samples are summarised as follows.

(a) 16m/s sliding speed

In the tests at the highest sliding speed of 16m/s with the UTRC discs, all four tests scuffed but the maximum Hertzian pressure at scuffing varied from 1.3GPa to 1.6GPa. Two tests were carried out with the Rolls-Royce discs at this high sliding speed. The first test was conducted with ground discs without a pre-running stage and the second pair tested after pre-running under pure rolling conditions at a heavy load of 2GPa for 30 minutes. It is perhaps surprising that the pre-running did not lead to any improvement in the scuffing load which was 1.2GPa for both tests. The generally higher loads achieved by the UTRC discs is probably due to their higher hardness which was measured using a Vickers hardness tester as 720 Vickers hardness number compared to a figure of 680 Vickers hardness number for the Rolls-Royce samples.

(b) 12m/s sliding speed

Two tests were carried out using the UTRC samples at this intermediate sliding speed. The first test scuffed at 1.7GPa and the second at 1.3GPa. Three tests at this speed were conducted using the Rolls-Royce discs. The test in which the discs were pre-run at a heavy load of 2GPa scuffed at 1.3GPa and the two tests without pre-running failed at 1.6GPa and 1.3GPa. It is clear that the suggestion that pre-running in may improve the scuffing performance has not been supported in the results obtained in this work. It is important to recall that although pre-running was carried out at a high load the temperatures attained during pre-running were low due to the lack of frictional dissipation when sliding is absent. The oil viscosity would be higher and the film thickness under these conditions would therefore be thicker and there would be less asperity contact and modification of the surfaces. This effect is borne out by the roughness figures in the pre-running tests. For example in test AD11 the initial roughness of the slow disc was 0.36μm Ra and following

pre-running it fell to 0.31μm. But the roughness of the unscuffed parts of the same discs following failure was 0.23μm. This shows that in spite of the fact that the load during the scuffing test did not reach that achieved during pre-running there was significant further smoothing because of the combination of sliding and the higher temperatures developed. This suggests that in order to achieve an improvement of finish by pre-running it may be necessary to increase the temperature by heating the samples and/or the oil, or by introducing a degree of sliding. Pre-running under the pure rolling condition does not appear to be effective.

(c) 7m/s sliding speed

Two tests were carried out using UTRC samples at the lowest sliding speed of 7m/s. The first test scuffed at 1.7GPa and the second at 1.9GPa. As expected the scuffing loads at this lowest sliding speed are generally higher than in the tests at higher speeds. No tests were carried out at this speed with the Rolls-Royce discs. In general tests carried out with ground discs on both shafts showed a higher degree of scatter, particularly at the higher speeds. Thus in the short series of tests carried out there was no significant difference in the scuffing loads achieved at 16m/s and 12m/s, although the higher sliding speeds produced significantly higher temperatures at corresponding loads

A diagrammatic comparison of the measured friction and disc bulk temperatures in tests with ground discs at three loads prior to scuffing (1.0, 1.1 and 1.2GPa), for the three sliding speeds considered is shown in Figure 6.1. This and similar bar-charts shown in this chapter show comparisons of friction and temperatures at operating conditions in load stages before scuffing occurred. It should be noted that in order to make such comparisons the highest load that can be shown in any sequence is determined by the lowest scuffing load experienced over the whole range of operating conditions which are included. In this case, therefore comparisons can only be made up to a load of 1.2GPa. This particular comparison demonstrates the result that sliding speed has only a small effect on the friction at the contact, but of course the effect of sliding speed on bulk temperature is more dramatic because the heat dissipated at the contact is proportional to the product of friction force and sliding speed.

Figure 6.1. Comparision of friction force and disc temperatures at three loads and the three sliding speeds of 16m/s, 12m/s and 7m/s for experiments with ground discs running on ground discs at conditions prior to scuffing.

6.2.2. Superfinished discs on superfinished discs

UTRC discs were used in this series of three tests in which the discs were superfinished following conventional axial grinding. Two tests were performed at a sliding speed of 16m/s which scuffed at 1.5 GPa and 1.6 GPa maximum Hertzian pressure. One test was conducted at 7m/s and this scuffed at 1.9GPa. The most striking feature of these tests is the much lower friction and bulk temperatures of the discs during corresponding load stages. For example in test UTRC02 at a sliding speed of 16m/s (ground on ground) it has already been noted that the temperature of the fast disc at the scuffing load of 1.6 GPa was 317°C, whereas the temperature of the fast disc in the corresponding test with superfinished discs (test UTRC04) was 165°C at the same load of 1.6GPa. Because of the lower friction in the test with superfinished discs the calculated flash temperature was also much lower at the same load. In the test with ground discs the flash temperature rise was calculated to be 177°C whereas in the corresponding test with superfinished discs it was 59°C. The overall effect of a lower bulk temperature and a lower flash temperature leads to a total contact temperature for the superfinished discs of 224°C (based on the bulk temperature of the fast disc) which may be compared to a total temperature of almost 500°C in the case of the ground discs at the same load. It is surprising that the two tests scuffed at the same load in spite of strikingly different temperature conditions at failure. As a side-issue this finding certainly does not add to confidence in the Blok hypothesis that the total contact temperature reaches a critical value at scuffing. The single test with superfinished discs at a sliding speed of 7m/s (UTRC06) produced a high scuffing load of 1.9GPa, but again this load was also achieved by the ground on ground discs in test UTRC27. This further emphasises the result that superfinishing has the important effect of reducing friction and temperatures, but it did not lead to any worthwhile improvement in scuffing load in these tests with the UTRC steel.

During the tests with superfinished discs on both shafts there was no indication of the running in effect that was observed in the case of the ground tests. In the record of test UTRC06, for example which ran to the high load of 1.9 GPa there was no indication of a drop in the friction force following an increase in the load. The friction force remained steady during a load stage even during the final stages before scuffing took place. The behaviour contrasts sharply with that of the ground discs in which a large fall in the friction force occurred, particularly during the last few load stages. A further way in which the

scuffing behaviour of the superfinished discs differed from that of the ground specimens was in the location of the scuffing scar. In all tests involving ground discs the scuffing scar appeared to have originated at the edge of the scuffing track, whereas with the superfinished discs the scar appeared near the middle of the track. This different behaviour suggests that in the case of the ground discs the hydrodynamic lubrication mechanism failed at the edges of the contact due to leakage of the oil in a sideways direction thus allowing the film to collapse and contact to occur. In the case of the superfinished discs a different mechanism seems to take place. The leakage of oil at the edges of the track is less easy because there are no deep valleys along which the oil can escape. But the site of failure moves to the middle of the contact where the pressures are highest. In this case it is suggested that the absence of valley features is a disadvantage because there are no longer breaks between asperity contacts which in the case of rough surfaces allows the oil to perform cooling of a transient asperity contact before its next encounter with a following asperity on the opposing surface. In contact between almost smooth surfaces such an asperity contact will tend to persist without a "cooling break" and the temperature will build up and failure will occur. Thus the importance of roughness in this case may be to provide "fire breaks".

A diagrammatic comparison of the results of the tests on superfinished discs is shown in Figure 6.2. This shows the lower friction obtained at the higher sliding speed of 16m/s which suggests a more effective hydrodynamic film due to the correspondingly higher entraining speed. There is much less of an effect of sliding on bulk temperatures because the heat dissipation at the higher sliding speed offsets the benefit of lower friction force.

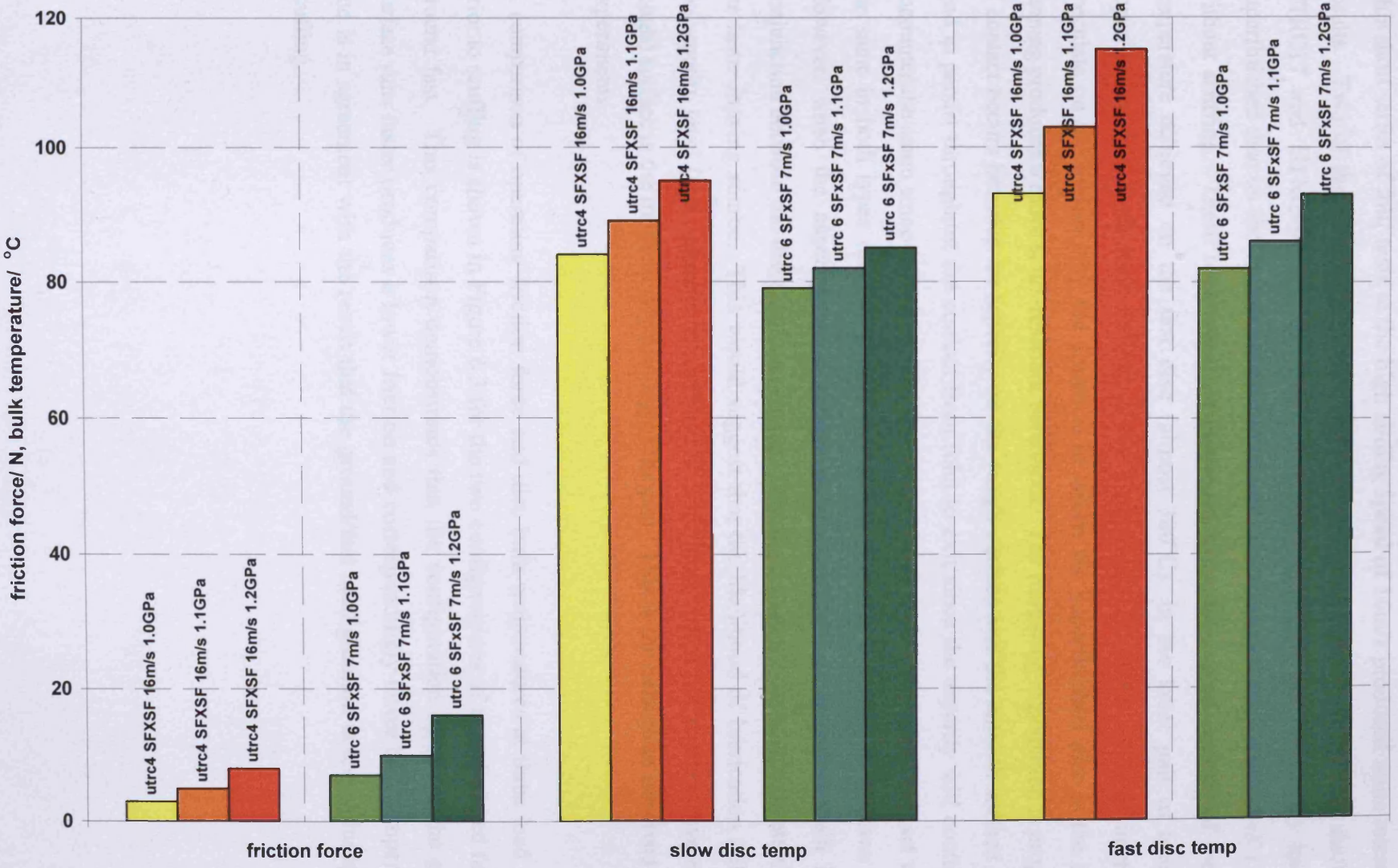

Figure 6.2. Comparison of friction force and disc temperatures at three loads and two sliding speeds of 16m/s, and 7m/s for experiments with superfinished discs running on both shafts at conditions prior to scuffing.

6.2.3. Superfinished discs on ground discs

This short series of four tests at the high sliding speed of 16m/s produced some interesting results. Two of the tests were carried out with the ground discs on the fast shaft (test UTRC17 and UTRC19) and the other two tests (UTRC18 and UTRC20) had the superfinished disc on the fast shaft. In the former case both tests ran to a load of 1.6GPa without scuffing. These tests were not continued to a higher load because of the high temperature achieved on the fast disc (almost 300°C). In the latter pair of tests (i.e. superfinished fast) both tests scuffed at the lower load of 1.3GPa. It is of interest to speculate on the reason why the situation in which the superfinished disc is the slower running produces a more scuff-resistant behaviour. The following explanation is proposed. If contact occurs between an asperity on the rough surface and the smooth surface it will tend to persist throughout the contact from inlet to exit since the asperity will continue to encounter the same smooth surface. The heat generated at such a prolonged contact will be the same in both types of test because the sliding speed is the same in the two cases. However, when the asperity is on the slower-moving surface it will remain in the conjunction between the discs and receive heat for longer than it does when it is attached to the faster moving source. This would suggest that the likelihood of lubrication failure at the asperity level (and consequent scuffing) is more likely when the asperity-covered (i.e. rough) surface is the more slowly moving of the pair. This is the behaviour observed in the experiments.

A comparison of operating friction force and disc bulk temperatures at three load stages prior to scuffing is shown in Figure 6.3 for the two configurations of superfinished fast and ground fast. This comparison demonstrates that the configuration in which the ground surface runs faster produces a lower friction and correspondingly lower bulk temperatures and is in agreement with the result that the ground/fast configuration is less vulnerable to scuffing.

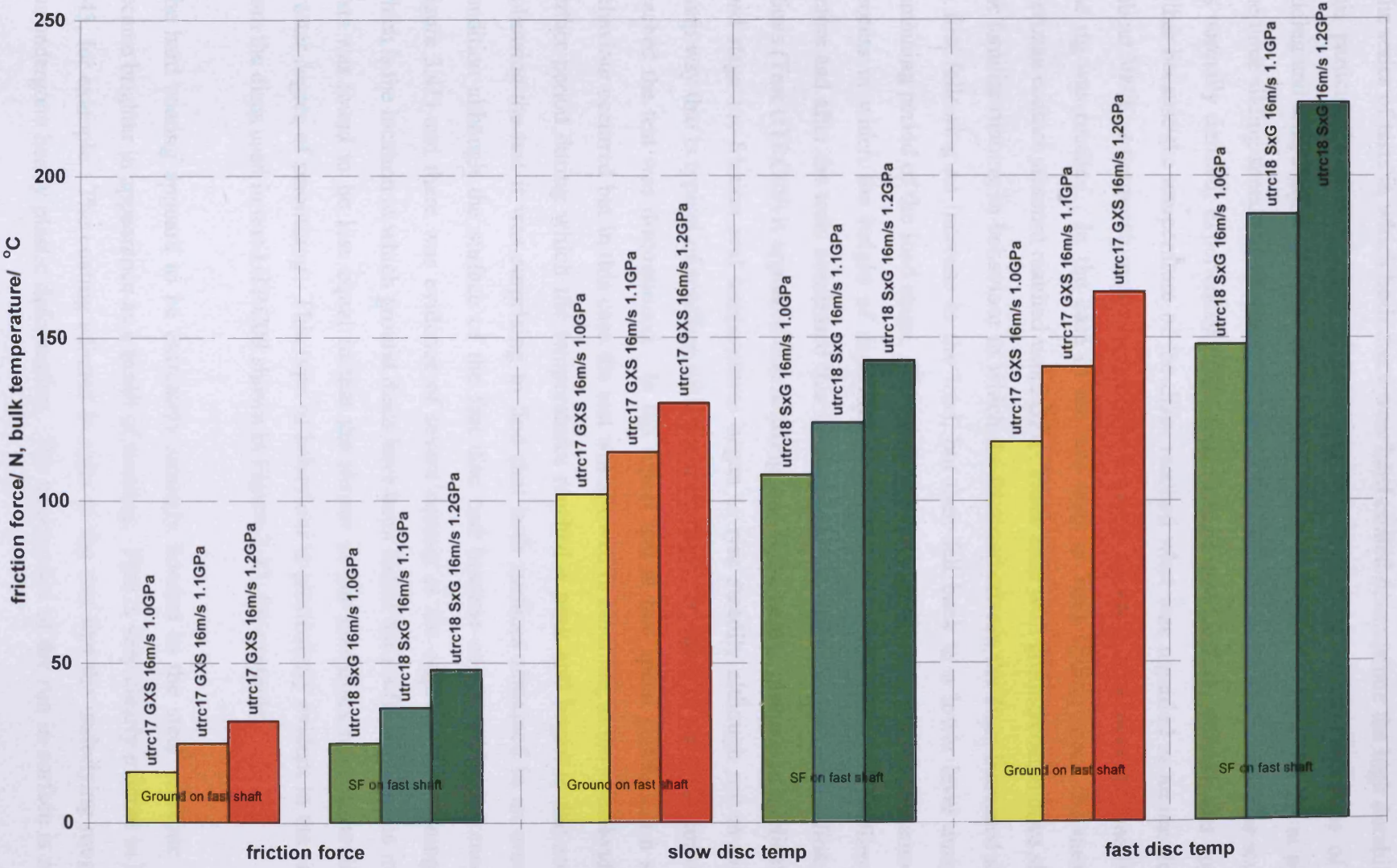

Figure 6.3. Comparison of friction force and disc temperatures at three loads and sliding speeds of 16m/s for experiments with ground discs running on superfinished discs at conditions below the scuffing load.

6.2.4. Ground coated discs on ground coated discs

The series of tests in which both discs were hard-coated demonstrate the high durability of this particular treatment when tested under very severe operating conditions of load, sliding and temperature. A total of six experiments were carried out, two tests at each of the three sliding speeds of 16m/s, 12m/s and 7m/s. In none of these six tests was scuffing, as normally defined, experienced. The tests were stopped before scuffing was apparent either because the temperature of the discs reached what was regarded as an unsafe level (about 300°C, a temperature at which smoke began to appear!) or because the load limit of the rig was reached. In the case of the two tests at 7m/s sliding speed the maximum Hertzian contact pressure reached was 2GPa. These tests with ground/coated discs showed the familiar running in behaviour in which the friction between the discs increased sharply at first following an increase in the load, but then fell back to a lower level during the remaining period of the load stage. This phenomenon was again attributed to a smoothing process in which the height of asperities was reduced. Circumferential profiles taken before and after the tests confirmed this affect as did the SEM images. In the first test at 16m/s (Test UTRC09) it appeared that scuffing was about to take place upon application of load stage 11; friction and temperatures began to rise steadily although not in the very sharp way that is typical of scuffing with uncoated discs. Because of the high temperature reached the test was discontinued. In the repeat test at this speed (UTRC12) a similar behaviour occurred but in this case the test was allowed to continue, at the same load, for a further period during which the temperatures reached a peak and began to fall steadily. Following the test it was surprising to find that both surfaces remained in an unscuffed condition although the surface of the fast disc had become considerably darkened (see Figure 3.41) and there was evidence of severe contact at the edges of the running track which is the location at which ground discs have been found the scuff. Running-in in these tests was found to be less equal in that the slower of the two discs tends to undergo a greater degree of smoothing. This type of behaviour is particularly evident in the profiles from the discs used in test UTRC09 shown in Figure 3.42, for example.

The hard coating appears to be extremely strongly bonded to the steel substrate and it became brighter in appearance as a result of running. This is very clearly evident in Figure 3.43, for example. The coating adheres in spite of the fact that the underlying roughness has undergone heavy plastic deformation. The appearance of the run in surface is similar

to that occurring in the case of ground but uncoated samples. The asperity ridges become flattened in appearance with the formation of "lands" as before. However, there is not the same smearing effect with adhesive displacement of material to form overhanging lips as is the case with the uncoated discs seen earlier. This different behaviour seems to be associated with the lower friction found with the coated samples.

The two tests carried out at the intermediate sliding speed of 12m/s behaved in a similar fashion to the tests at the higher speed. What at first appeared to be a runaway behaviour in the temperature response settled in the case of the first test (test UTRC10) and allowed a further increment of load before eventually the temperature reached an excessive level and the test was stopped. In the second test at 12m/s a similar behaviour occurred but after allowing the test to run on at constant load the temperatures began to fall and then levelled off as shown in Figure 3.46. Again there was no indication of scuffing as seen with conventional ground surfaces. The photograph of the discs used in this test shown in Figure 3.57(b) shows no indication of classical scuffing damage. Again the surface of the slower running disc becomes preferentially smoothed. The pair of tests which were run at the lowest sliding speed of 7m/s survived to the load limit of the test rig and showed considerable evidence of running in during the test as indicated by the fall-off of the friction trace following an increase in the load. The appearance of the run in surface indicated a much gentler kind of asperity deformation than was seen in the case of uncoated samples. Figure 3.56, for example, shows considerable "lands" but without the "dragged" appearance at the edges of the lands as seen in Figure 3.14, for example. This further supports the explanation that the lower friction of the coated surfaces is a significant benefit.

A bar-chart comparison of the friction and disc bulk temperatures at three loads corresponding to operating conditions below the scuffing level is shown in Figure 6.4. In this case results were obtained at all three sliding speeds of 16m/s, 12m/s and 7m/s.

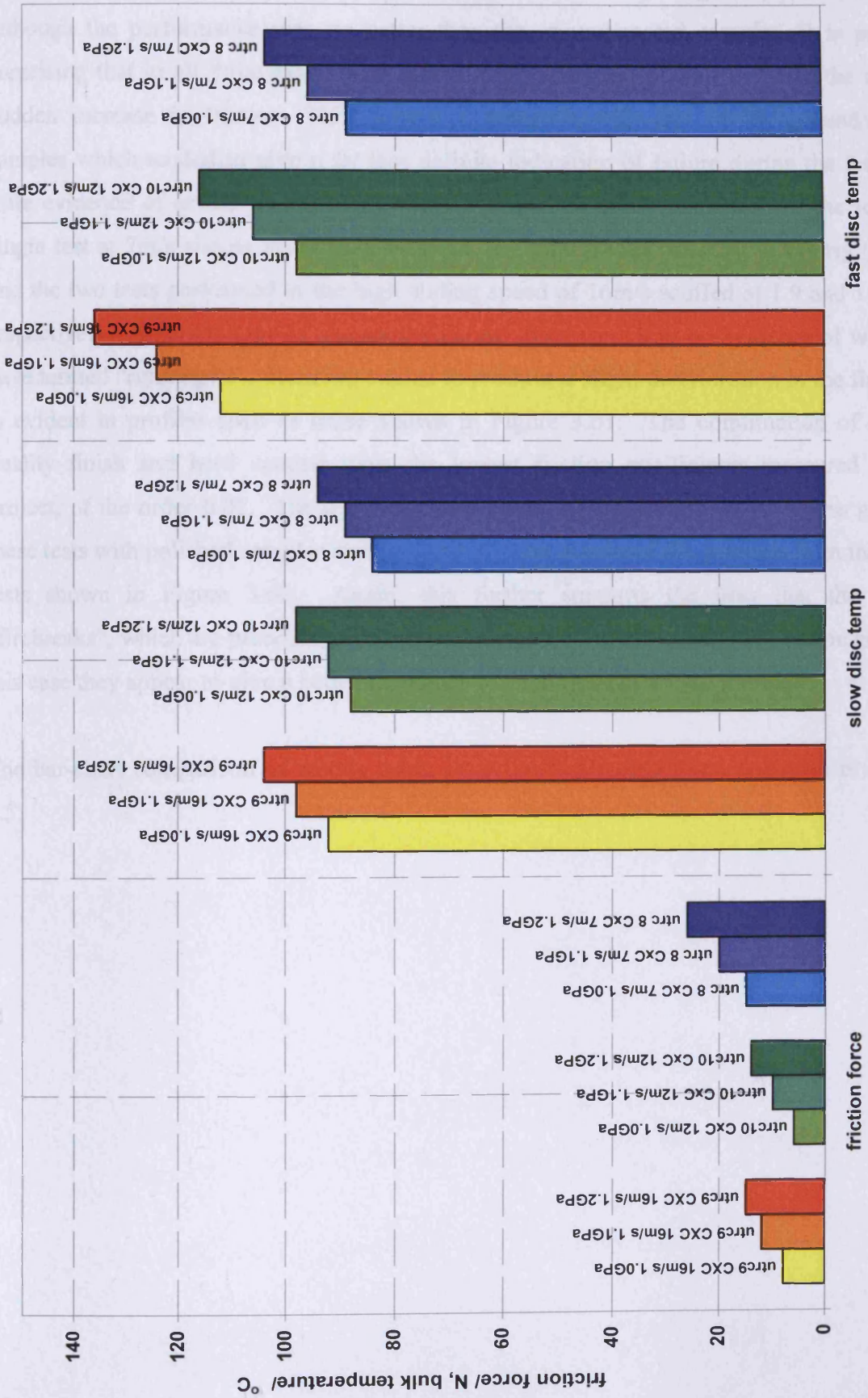

Figure 6.4. Comparision of friction force and disc temperatures at three loads and the three sliding speeds of 16m/s, 12m/s and 7m/s for experiments with ground/coated discs running on both the shafts.

6.2.5. Superfinished coated discs on superfinished coated discs

The three tests carried out with superfinished/coated samples gave excellent results although the performance was no better than the ground/coated samples. It is perhaps surprising that in all three cases there was a clear indication of scuffing with the typical sudden increase in friction. This behaviour contrasts with that of the ground/coated samples which tended to give a far less definite indication of failure during the tests and little evidence of severe damage following examination after completion of the test. A single test at 7m/s sliding speed scuffed at the maximum load capacity of the rig (2GPa) and the two tests performed at the high sliding speed of 16m/s scuffed at 1.9 and 1.8GPa, respectively. As in the case of uncoated polished discs there was no evidence of what we have termed "running in". Running tended to produce a slight deterioration in the finish as is evident in profiles such as those shown in Figure 3.61. The combination of a high quality finish and hard coating gave the lowest friction coefficients measured in the project, of the order 0.01. The durability of the coating would appear to be less good in these tests with polished samples as is evident in photographs of the samples from the three tests shown in Figure 3.60. Again, this further supports the idea that the valley "firebreaks", which are present on ground surfaces, help improve scuffing performance. In this case they appear to give a better resistance to peeling away of the coating.

The bar-chart comparison of results using superfinished/coated discs is shown in Figure 6.5.

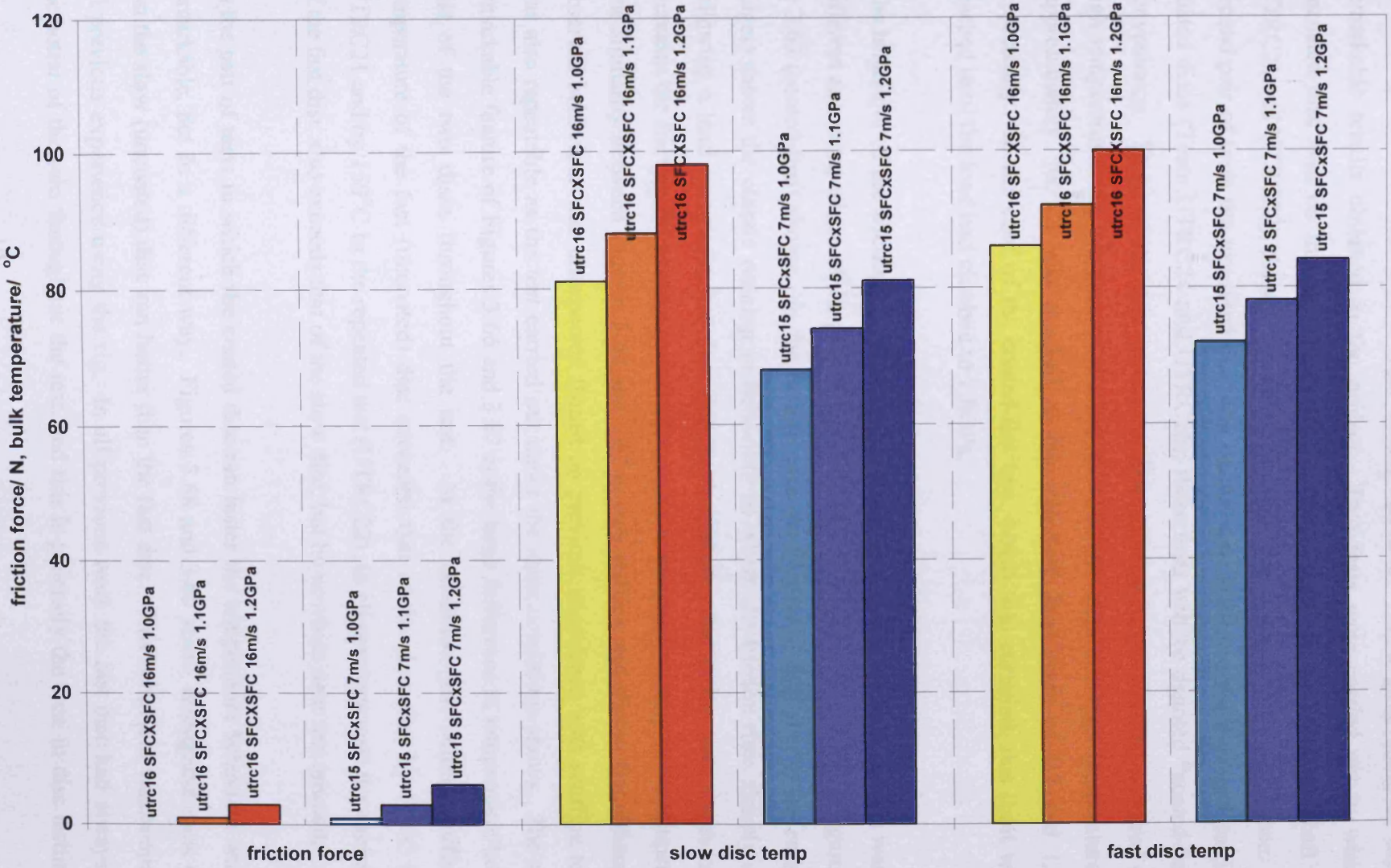

Figure 6.5. Comparison of friction force and disc temperatures at three loads and two sliding speeds of 16m/s, and 7m/s for experiments with superfinished/coated discs running on both shafts.

6.2.6. Ground coated discs on ground uncoated discs

This series of four tests at the high sliding speed of 16m/s gave some of the most remarkable results obtained in the project. Two tests were carried out in which the uncoated disc was on the fast shaft and the coated disc was on the slow shaft (Tests UTRC21 and UTRC22); these tests will be denoted "coated-slow" for convenience. In the second pair of tests the uncoated disc was on the slow shaft and the fast shaft carried the coated discs (Tests UTRC24 and UTRC26); these tests will be denoted "coated-fast" for convenience. Three of the four tests were discontinued before scuffing occurred due to high temperatures. In the case of the two coated-slow tests this high temperature limit (approximately 300°C) was reached at the relatively low loads of 1.2 and 1.3GPa, respectively. In the case of the coated-fast test, which was curtailed, this limit was not reached until the load had climbed to 1.8GPa.

The behaviour of the friction and temperature traces during the two kinds of test was quite different as a comparison of the pair of figures 3.66 & 3.67 (coated-slow) with figures 3.68 & 3.69 (coated-fast) shows. In the former case the friction at first (i.e. in the early load stages) shows the classic running in behaviour in which the friction rises sharply at first following a load increment, but then falls back slightly. But in the later stages of load increases the friction falls back considerably with a corresponding drop in the temperature. The similarity between Figures 3.66 and 3.67 is very striking and shows that although the observed behaviour was unexpected (based on previous experience with scuffing tests) it was also repeatable as the test carried out under the same conditions shows. The second remarkable feature of Figures 3.66 and 3.67 is the large difference in temperature between that of the two discs throughout the test. At the condition just before scuffing the temperature of the fast (uncoated) disc exceeded that of the slow disc by 173°C in test UTRC21 and by 159°C in the repeated test (UTRC22). In all previous tests the temperature of the fast disc also exceeds that of the slow disc, but by nowhere near this amount.

In the pair of tests in which the coated disc ran faster the temperature behaviour was also remarkable, but in a different way. Figures 3.68 and 3.69 show, throughout most of the test the slow (uncoated) disc ran hotter than the fast disc. This behaviour was contrary to all previous experience using the rig. In all previous work the fast disc had always been the hotter of the two throughout the test, and this is generally the case in disc testing. In

the final stages of tests UTRC24 and UTRC26 the usual situation (in which the fast disc was hotter) returned, but only during the final load stages. Again, this unusual behaviour was found to be repeatable as can be seen from the similarity of Figures 3.68 and 3.69. There was far less evidence of running-in in the coated-fast tests and the pattern of friction trace following an increase in the load was similar to that seen in tests with uncoated ground/uncoated discs on both shafts.

This unusual behaviour of the temperatures in both coated-fast and coated-slow tests suggests that the coating was acting as a "thermal barrier" preventing the flow of heat into the bulk of the disc. In the case of the coated-slow tests the coating on the slower-moving disc leads to it being even cooler than it would otherwise be, causing a greater difference in the temperatures of the two components; in the case of the coated-faster tests the opposite effect happens whereby the faster disc is thermally protected and is therefore cooler than it would otherwise be, and the slower disc therefore receives a greater share of the frictional heat than it did previously. The effect in the case of the coated-faster test is therefore to reduce the difference in temperature, and in fact it leads to the observed situation in which the slow disc actually becomes the hotter of the pair over most of the test. This unusual observation clearly calls for further investigation both experimentally and theoretically, but it would appear that the surface conductivity of the coated sample is significantly reduced as a result of the coating.

The running in that occurs during these tests with coated samples running against uncoated ones takes the form of polishing of the surface of the uncoated disc. This effect is dramatically illustrated in Figure 3.71, for example, which shows that the original ground surface of the uncoated disc becomes almost superfinished as a result of running. This degree of running in is not seen in any other test either with ground versus ground or with coated versus coated samples. It appears that when a coated surface runs against an uncoated surface the surface modification that takes place is no longer reliant on plastic deformation, but the process is more like abrasive polishing.

The behaviour of friction force and disc bulk temperatures under operating conditions corresponding to loads below the scuffing limit is shown in the bar-chart given in Figure 6.6. The comparison is between tests UTRC22 (ground disc fast) and UTRC26

(ground/coated disc fast). This diagrammatic comparison further reveals the strikingly different behaviour of the two configurations.

6.2.7. Comparison of performance using different surface treatments

It is of interest to compare the behaviour of all the different surface treatments (i.e. ground, superfinished, coated) under the same operating conditions prior to scuffing. All four configurations in which the two discs had the same finish and treatment were tested at the highest and lowest sliding speeds (16m/s and 7m/s). Figure 6.7 shows a comparison of the friction and disc bulk temperatures for the four configurations at 16m/s at three loads of 1.0, 1.1 and 1.2GPa which may be considered to cover the practical range of gear tooth contacts. This clearly demonstrates the benefits of hard coating in reducing friction and operating temperatures. The very low friction of superfinished/coated samples is particularly striking. A similar pattern of behaviour is seen in Figure 6.8 which shows a comparison of operating friction and temperatures at the lowest sliding speed of 7m/s. At the intermediate speed of 12m/s it is possible to show only the comparison between ground and ground/coated samples, but this does, perhaps, concentrate attention on the comparison of most practical relevance to the gearing industry. Figure 6.9 shows the comparison of friction and bulk temperatures for the sliding speed of 12m/s. The considerably lower friction of coated samples must be seen as a major advantage of the procedure, irrespective of the benefits in terms of added scuffing resistance.

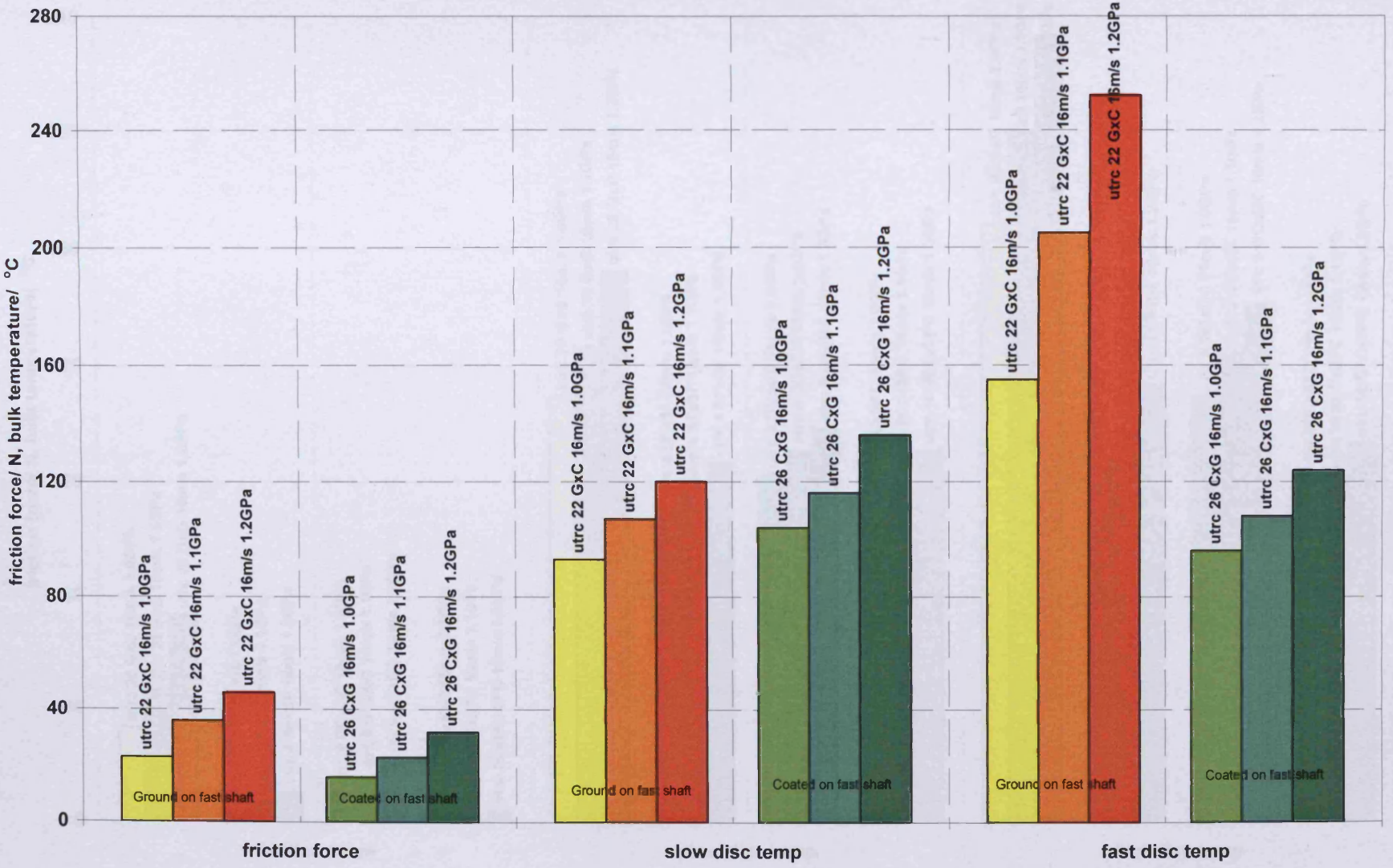

Figure 6.6. Comparison of friction force and disc temperatures at three loads and sliding speeds of 16m/s for experiments with ground/coated discs running against ground/uncoated discs in the two different configuration of coated-fast and coated-slow.

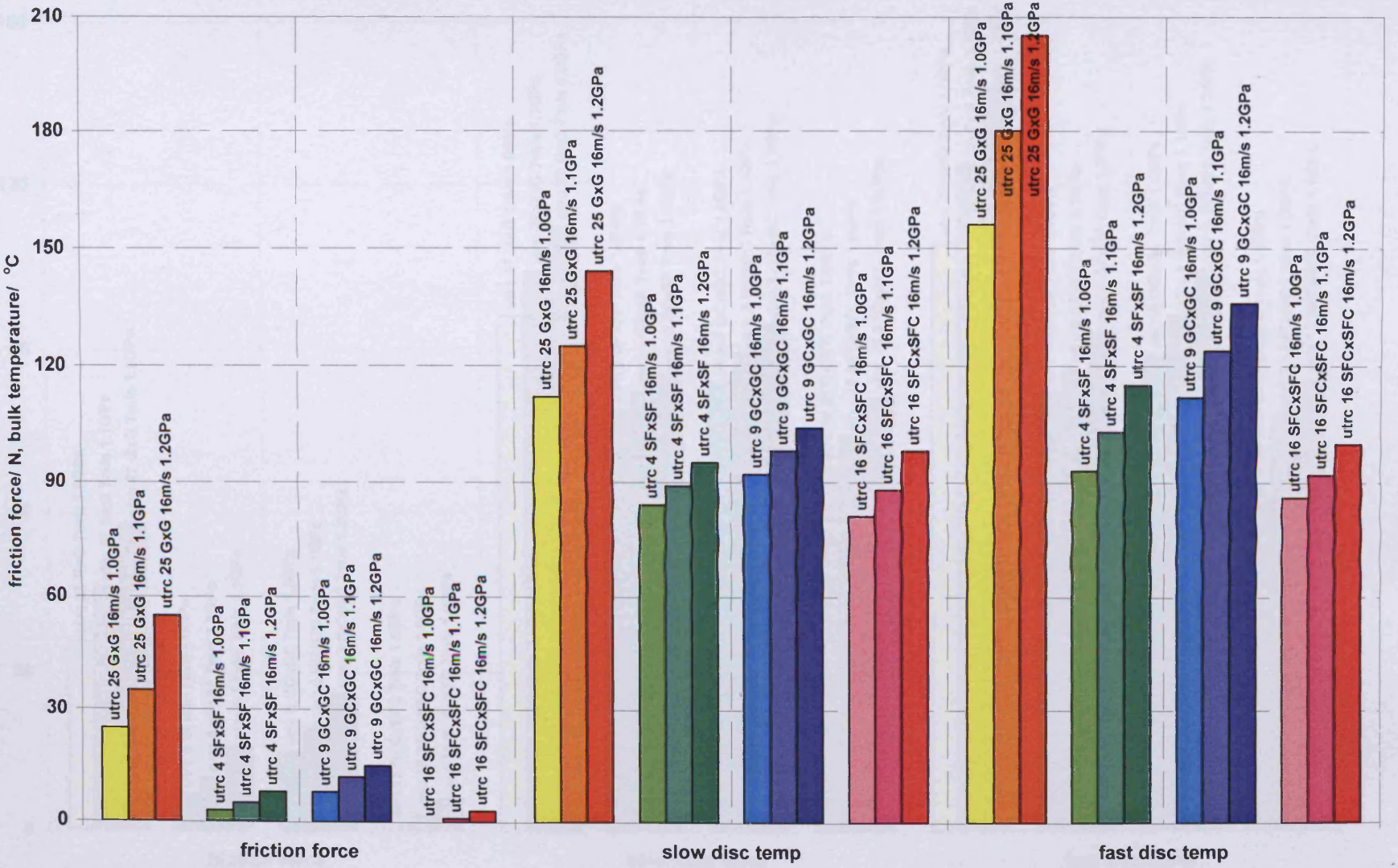

Figure 6.7. Comparision of friction force and disc temperatures at three loads and a sliding speed of 16m/s for the four different configurations in which discs of the same finish and treatment was used on both shafts

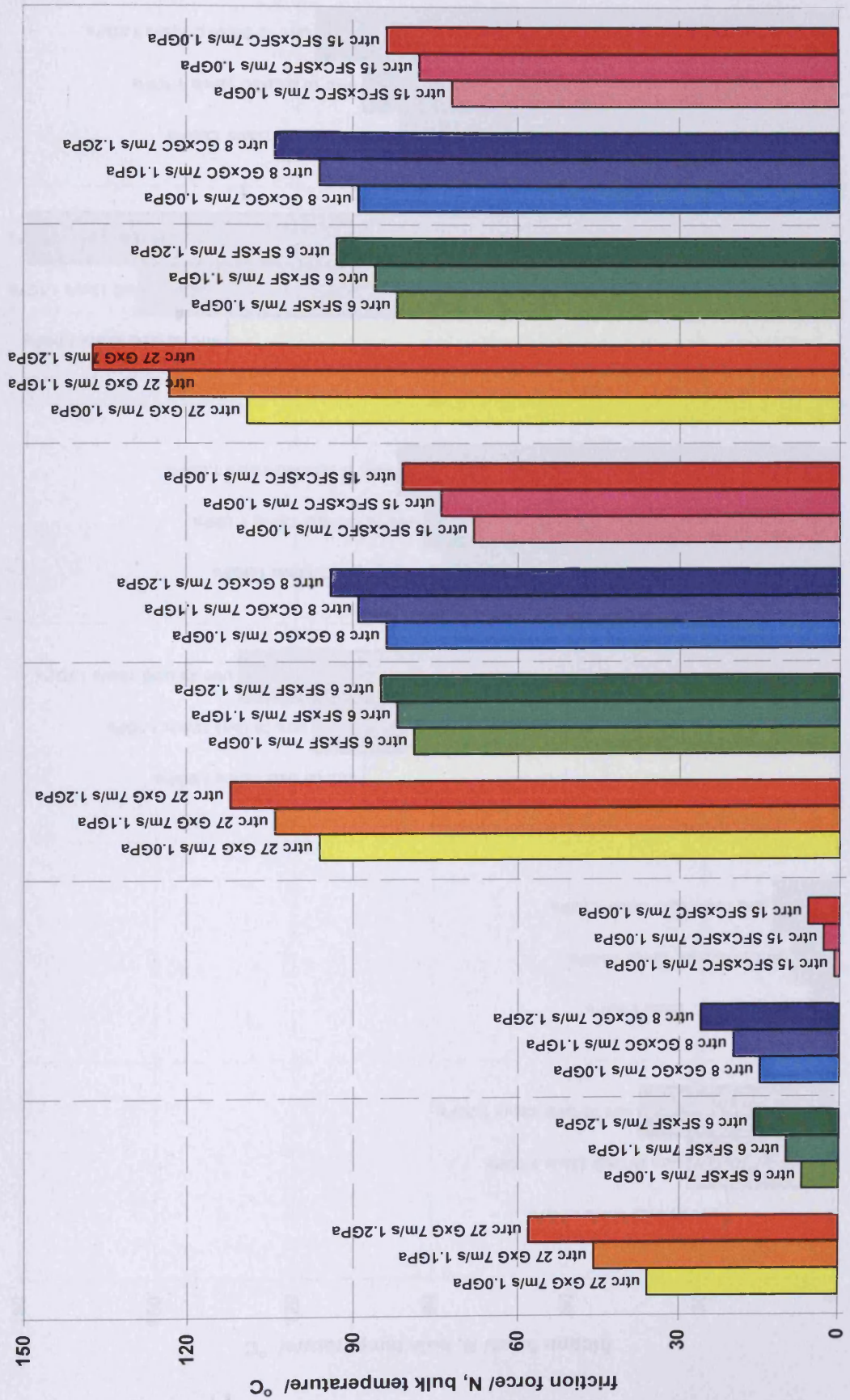

Figure 6.8. Comparision of friction force and disc temperatures at three loads and a sliding speed of 7m/s for the four different configurations in which discs of the same finish and treatment was used on both shafts

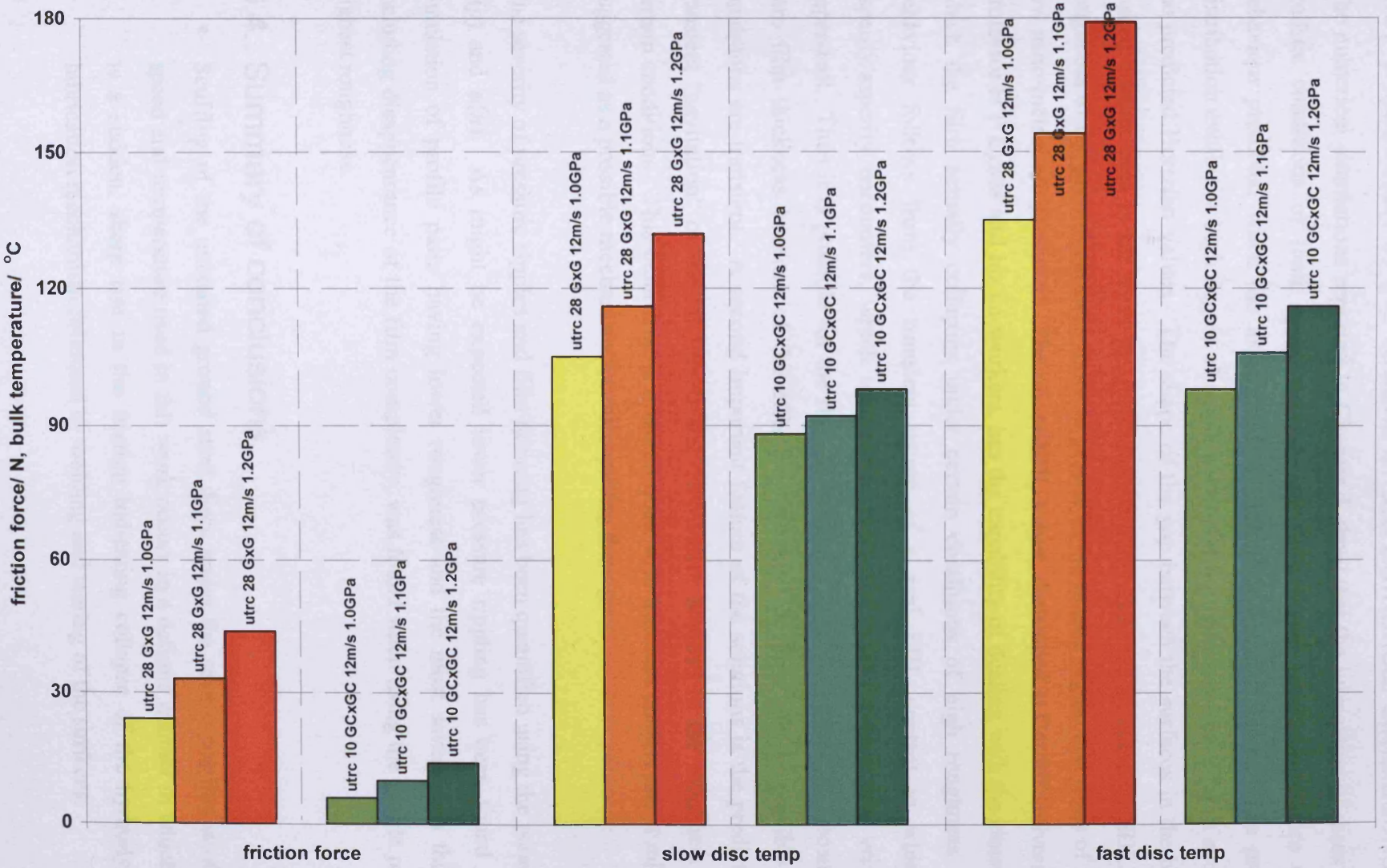

Figure 6.9. Comparison of friction force and disc temperatures at three loads and a sliding speed of 12m/s for the two configurations of ground discs on both shafts and ground/coated discs on both shafts.

6.3. Discussion of the results of the numerical simulations

The numerical simulations reported in Chapter 5 show that the lubrication of discs under realistic conditions of load, speed and surface finish bears little resemblance to the behaviour predicted when the assumption of smooth surfaces is made. The pressure distribution exhibits a high degree of ripple with maximum pressure peaks far in excess of the predicted Hertzian values. The shape of the gap between the surfaces in the heavily loaded contact area is far from the parallel separation expected in classical EHL. The roughness of the ground surfaces tends to persist in the loaded region and films of only a few nano-metres are predicted. The micro-EHL solver, developed at Cardiff University by Professor H P Evans and his co-workers, has the capability of dealing with the situation in which the film actually collapses under certain conditions of high roughness. This behaviour follows from the transient nature of a real EHL contact in which the asperity/asperity encounters, which take place within the overall conjunction, are time-dependent. Thus it is possible for the flow to be momentarily interrupted at a position of zero film thickness because of the effective "storage" of flow that is possible when conditions are transient. A second important feature of the solutions is the prediction of transient "cavitation" of the oil film in the deep valley features of the roughness under certain conditions. This behaviour is often coupled with transient contact and it might be suggested as a possible mechanism for micropitting damage.

The severity of pressure ripples and film thinning has been quantified using the parameters $\varphi(p)$ and $\varphi(h)$. As might be expected lower pressure rippling has been found in the simulation of profile pairs having lower roughness and the most severe film thinning, including disappearance of the film completely, was found when using the profile pairs of highest roughness.

6.4. Summary of conclusions

- Scuffing of the uncoated ground steel discs under the severe conditions of load, speed and temperature used in this work occurs in a definite manner in which there is a sudden, sharp rise in the friction indicating collapse of the hydrodynamic lubrication mechanism followed by welding and tearing of the surfaces.

- Prior to scuffing there is significant modification (reduction of roughness) of the surface profiles which appears to be due to plastic deformation caused by both normal and friction forces.

- The hard coating used in this work has the effect of markedly improving the scuffing resistance of the ground steel substrate. In the tests carried out scuffing did not occur and in general the limitation of loading was due to the high temperatures generated.

- In addition to improving the scuffing resistance of ground surfaces the effect of the hard coating was to reduce friction and the bulk temperatures of the samples at the same operating load.

- The use of superfinishing reduced friction and temperatures in the UTRC discs but it was not found to give any significant improvement in scuffing performance.

- Hard coated superfinished samples were not found to be superior to hard coated ground samples, although they ran at lower temperatures.

- The combination of ground/uncoated samples running against ground/coated samples produced remarkable results which strongly suggest that the hard coating acts as a thermal barrier. In the tests carried out with this configuration it was found that the usual behaviour of the temperatures of the slow and fast discs was completely altered.

- Micro-EHL analysis using profiles of discs used in the experimental work has demonstrated the very severe lubrication conditions which are present in the experiments. Pressure ripples far in excess of the calculated Hertzian pressure are predicted and the films generated by hydrodynamic action are extremely thin, and under the most severe conditions direct "dry" contact is predicted.

6.5. Suggestions for further work

This project was concerned with two steels, a single hard coating, a single oil and two surface finishes. Clearly there is a need to investigate other types of coating in the search for the optimum surface treatment. Different oils should also be investigated. The oil used in this work is a low-viscosity oil designed for use in gas turbine aero engines and may not be ideal as a gear lubricant. In any future testing of coatings for use in applications other than aerospace more appropriate oils should be used including the more common mineral oils used in industrial and automotive applications.

The unexpected behaviour of coated surfaces running against uncoated surfaces deserves further investigation, both experimentally and theoretically. It would appear that the hard coating acts as a thermal barrier which upsets the way that the frictional heat developed between the surfaces is shared between the two discs. The experiments carried out in this project were repeated to confirm the effect but further experiments under different conditions should be undertaken. Theoretical modelling of the configuration should also be carried out to quantify the changes to the division of heat necessary to explain the experimental observations. The analysis carried out by Clarke et al (2006) could be adapted for this type of investigation.

There is a need to further develop the micro-EHL analysis used in Chapter 5. The solver should be developed to include thermal effects and the effect of the hard coating both in terms of the elastic behaviour and also the thermal aspects as discussed above.

Appendix A

The Blok flash temperature equation

Notation

b	semi-dimension of line contact
k	thermal conductivity
N	$=\pi q/\rho c u$
q	heat flux density
Q	total heat flux or frictional power
t	time
u_s	sliding speed $=\lvert u_1 - u_2 \rvert$
u_1, u_2	surface speeds in x-direction relative to the contact
α	proportion of total heat conducted into body 1
θ	temperature rise
μ	coefficient of friction
ρ	mass density of solid surface
σ	thermal resistivity (=1/k)

When surfaces slide over one another frictional heat is generated and this raises the temperature of the surfaces. In concentrated (Hertzian) contacts the heating effect may be very severe because of the high pressures involved. This local rise is known as the flash temperature. The following description of the flash temperature equation attributed to Blok is given because confusion often arises in the application of the equation. Blok assumed a parabolic distribution of heat flux as shown in Figure A1 and used linear heat flow theory to find the surface temperature. Linear heat flow theory may be used to show that the temperature distribution under the heat source is given by

$$\theta(x) = (\pi k \rho c u)^{-\frac{1}{2}} \int_{x_0}^{x} q(\xi)(x-\xi)^{-\frac{1}{2}} d\xi$$

where ξ is a dummy variable for x, and x_0 is the position of the leading edge of the source. The heat source extends from $x = -b$ to $x = +b$.

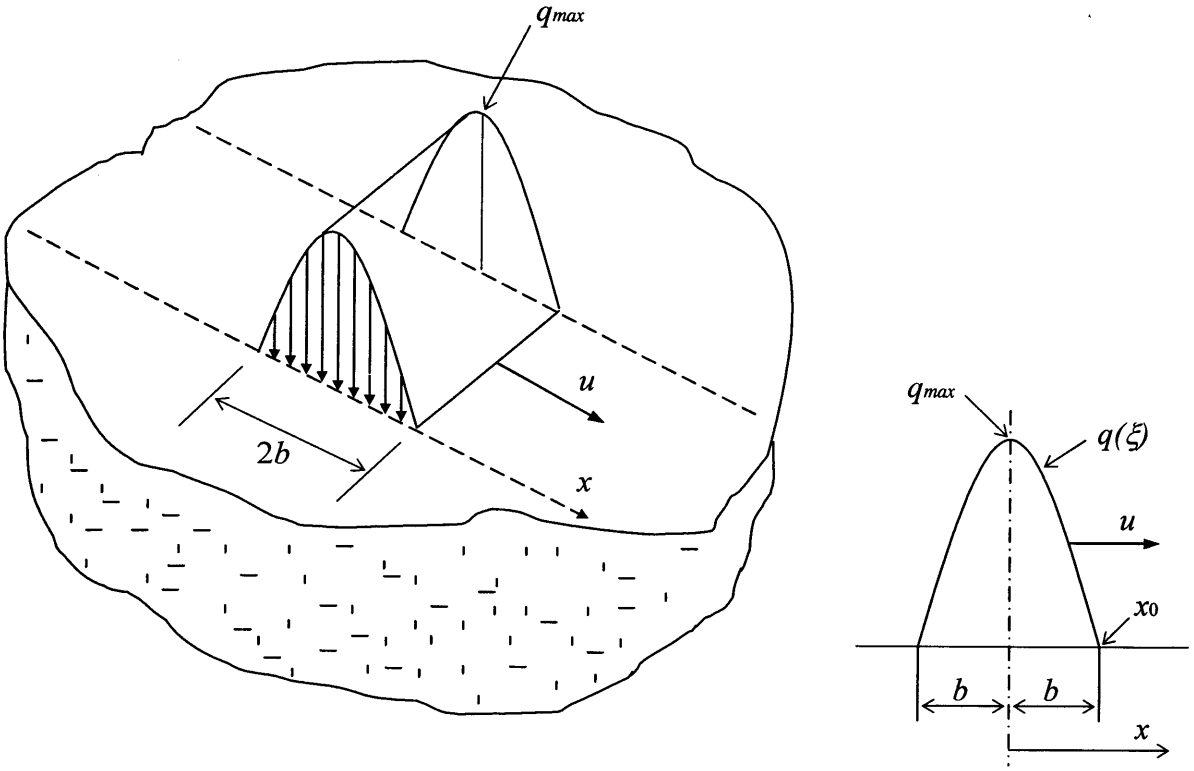

Figure A1. Parabolic distribution of heat flux assumed in Blok's flash temperature formulation

Putting $q(x) = q_{\max}\left(1 - \frac{x^2}{b^2}\right)$ and integrating gives

$$\theta_{\max} = 1.658\bar{q}\left(\frac{b}{k\rho cu}\right)^{\frac{1}{2}}$$

where $\bar{q}$ is the mean heat flux $= \frac{2}{3} q_{\max}$

If two surfaces 1 and 2 are rolling/sliding together with velocities u_1 and u_2 relative to their contact it is necessary to consider the problem of division of heat between the two surfaces. If $\bar{q}$ is the total mean heat flux generated by friction at the contact then:

body 1 receives heat $\alpha\bar{q}$ from a heat source moving at velocity u_1

body 2 receives heat $(1\text{-}\alpha)\bar{q}$ from a heat source moving at velocity u_2

If t_1 is the temperature rise of body 1 if all the heat $\bar{q}$ is conducted into body 1, and t_2 is the temperature rise of body 2 if all the heat $\bar{q}$ is conducted into body 2, then the true, common temperature rise at the contact between the bodies will be

$$\theta = \alpha t_1 = (1-\alpha)t_2$$

so $$\alpha = \frac{t_2}{t_1 + t_2} \text{ and } \frac{1}{\theta} = \frac{1}{t_1} + \frac{1}{t_2} \text{ or } \theta = \frac{t_1 t_2}{t_1 + t_2}$$

From the above $$t_1 = 1.658\bar{q}\left(\frac{b}{k_1\rho_1 c_1 u_1}\right)^{\frac{1}{2}} \quad \text{and} \quad t_2 = 1.658\bar{q}\left(\frac{b}{k_2\rho_2 c_2 u_2}\right)^{\frac{1}{2}}$$

so substituting these expressions for t_1 and t_2 into the above equation for θ gives

$$\theta_{\max} = \frac{1.658\bar{q}b^{\frac{1}{2}}}{(k_1\rho_1 c_1 u_1)^{\frac{1}{2}} + (k_2\rho_2 c_2 u_2)^{\frac{1}{2}}}$$

The mean heat flux density is given by

$$\bar{q} = \mu\bar{p}|u_1 - u_2|$$

which gives

$$\theta_{\max} = \frac{1.658\mu\bar{p}|u_1 - u_2|b^{\frac{1}{2}}}{(k_1\rho_1 c_1 u_1)^{\frac{1}{2}} + (k_2\rho_2 c_2 u_2)^{\frac{1}{2}}}$$

where $\bar{p}$ is the mean contact pressure and μ is the coefficient of friction.

If a semi-elliptic (i.e. Hertzian) distribution of q is assumed instead of a parabolic form, the numerical constant in the above becomes 1.572.

This formula is used to calculate "flash" temperatures in spur gear teeth and has been used in this thesis to estimate the additional frictionally-generated temperature of the discs. The "total contact temperature" is the sum of this flash temperature and the bulk temperature of the parts.

Note: The above Appendix is adapted from notes prepared by R W Snidle as part of his third year course on Tribology.

APPENDIX B

Setting up the Disc Machine

The following instructions are included in the thesis as a useful record of the method of dismantling and assembling the disc rig.

Machine Dismantling

Remove hood.

Remove cover (6 large bolts and 8 small ones).

Remove the oil splash cover over the two discs.

Remove the central, oil feed pipe.

Check for scuffing.

Pull off slip ring covers, undo the back plates. Note the position of the terminal spigots. Remove the short lengths of rubber retaining sheathing. The thermocouple wires are then free.

Unlock grub screws on the thermocouple drive shafts.

Lock disc shafts by inserting a rod in the holes on drive couplings and use a C spanner to undo the thermocouple drive shaft lock nut.

Remove the thermocouple drive shaft assembly.

Pull back the hydraulic ram.

Undo the slow shaft snap ring using a small screwdriver to initially prise it out of its groove.

Push back the drive coupling so that it clears the drive gear on the end of the shaft.

Rotate the restraining block and swing the slow shaft down and away from the fast shaft to give access to the bearing cap retaining capscrews.

Undo the four slow shaft bearing retaining capscrews and remove the slow shaft (note: the bearing caps are marked to be replaced in the same position).

Prise out the fast shaft snap ring and push back the drive coupling.

Undo the bearing caps and remove the fast shaft.

Replace the cover and the hood.

Dismantling of shafts

Slip off the cylindrical roller bearing outer race.

Place shaft in vice with drive gear uppermost. Use smooth vice jaws and clamp on shaft where no harm can occur.

Bend down retaining tab on tab washer securing gear.

Use castle spanner to unlock retaining nut.

Remove nut, tab washer, drive gear, thin spacer (fast shaft), thick spacer (slow shaft), retaining ring and snap ring.

Knock back tab washer on the disc-retainer nut.

Loosen and remove 40 mm disc-retaining nut using C spanner.

Remove shaft from vice.

Remove circlip from the thermocouple end of shaft.

Take to press with special tools for removing the bearings i.e. horseshoe and large tube.

Press off the double race self aligning bearing.

Press the disc from its shaft taking care not to damage it, and carefully store disc.

Disc replacement and grinding

The shaft is now ready to have a new disc fitted. Normally a spare shaft is available for building up and replacing in the machine.

Rebuild of shafts

Press on a new disc using hydraulic press, take care to align keyway and avoid damage to working surface of disc.

Using the horseshoe and the bed of the press, replace the bearings and races on the shaft.

The separate inner race of the roller bearing fits on the slip ring end which has the biggest shaft diameter.

The horseshoe must be carefully positioned both on the shaft and over the centre of the hole in the press bed to allow the shaft to be pressed through the bearing.

Care must be taken to align the bearing and the shaft initially and the press pressure released occasionally to realign them. If too much resistance is felt remove the bearing, inspect surfaces for possible damage and try again.

Replace shaft in vice as before.

Replace snap ring making sure the tang is facing the right way to allow positioning in drive collar.

Replace 40 mm tab washer and nut, spacer (thick and thin), gear, tab washer and nut, do up both nuts and bend up tabs.

Replace circlip.

Place shaft in ultrasonic cleaner for approx 15mins. Cleaning fluid is replaced every six shafts on average.

Thermocouples

Cut wire to length using old couple as guide.

Strip 5mm off one end and 10mm off the other.

Twist together the 5 mm ends, place in copper ferrule and solder up leaving a small blob of solder on the end.

When discs and shafts are clean and dry, place shaft in small alloy tube on bench with thermocouple hole facing up.

Lightly knock the soldered end of thermocouple into the 3 mm hole using the special hollow punch tool.

Glue thermocouple junction in place using araldite and leave to dry as per glue instructions.

Machine Assembly

Swing back the slow shaft yoke.

Place the fast shaft in its bearing blocks. The contact between the bearing outer race and the block should be dry i.e. free from oil.

Replace the bearing caps and capscrews but do not tighten. Check the numbers on caps and blocks.

Refit the fast shaft collar and the shaft ring in the drive coupling.

Place the slow shaft in its bearing blocks. Again keep contact dry and replace caps in right positions but do not tighten capscrews.

Align both shafts. This is important and should be done as accurately as possible. Start with the fast disc positioned so that the double roller bearing in housing 2B is aligned with the left face of the housing looking from the front of the machine. Then push the slow shaft up into position contacting the fast shaft and align the two discs as closely as possible. A small screwdriver is useful to feel for the presence of any step when run down the sides of the discs from one disc to the other.

Carefully swing back slow shaft to allow tightening of all bearing retaining capscrews.

Move slow shaft back into position and rotate the retaining block to hold it in position.

Replace the slow shaft collar and snap ring in the drive coupling. Check both couplings.

Thread the thermocouple wires through the drive shafts and through the slip rings.

Replace the drive shafts making sure all drives are engaged, tighten the locknuts and grub screws on flats.

Replace the central oil feed pipe.

Reconnect the thermocouple wires to the slip ring spigots, check output of thermocouples, and replace slip ring covers.

Replace cover and hood on machine.

APPENDIX C

Typical Test Procedure

A test starts with heating of the test oil to the desired oil feed temperature (100°C in the work reported in this thesis) and the gearbox oil to 45°C. Both test and gearbox oil circulation pumps are switched on. Allow rig to warm up for 1 hour. The thermocouple slip rings are cooled by a fan. The general test process starts with a load of 100N. The chart recorder is switched on and checked for zero readings. The chart speed is set to 10 mm/min. The main drive motor is started and set to the predetermined speed for the test. The calculated fast shaft and slow shaft speeds are given below.

Sliding speed	Fast Shaft (Rpm)	Slow Shaft (Rpm)
7m/s	2293	539
12m/s	3938	929
16m/s	5251	1238

Start the data acquisition software and take a note of the points on the chart record when the motor and the software are started and also at the end of the test. After checking the speed and oil flows the friction reading on the chart record is set to its zero position. After a few minutes of running at the light load the standard load sequence is begun with load increased every 3 minutes. During the test keep a record of the load stages and corresponding positions on the chart using the standard TEST DATA SHEET.

Scuffing is normally detected by a sudden, sharp increase in the friction and the temperatures. Scuffing can occur at any stage during the critical load. Upon detection of scuffing the load is released as quickly as possible. Allow the motor to run for a short period to provide a check on the zero-load chart and data-acquisition readings. Stop the

main drive motor and gearbox oil supply motor. Allow the rig to cool before opening the cover and removing the test shafts. Note any special features of the test on the TEST DATA SHEET.

.

Appendix D

Calibration of load and friction transducers

Calibration of load cell

The load applied between the test discs was indicated by a proprietary strain gauge load cell and electronic unit. The load cell was calibrated in situ by means of a dead-weight arrangement as shown in Figure D1. The hydraulic ram which applied the load was disconnected from the loading bell crank and the bell-crank holding the load cell was rotated though 90 degrees and locked in position with the load cell pointing vertically. A loading lever was then placed in position as shown and accurately counterbalanced. The pivot of the lever was provided with a needle-roller bearing in order to minimise friction at this point. A series of weights up to the maximum used in the project was then applied to the left end of the lever as shown in Figure D1. The digital indicator was set to correspond to the maximum load calculated from the weights applied and the lever ratio of the lever arm.

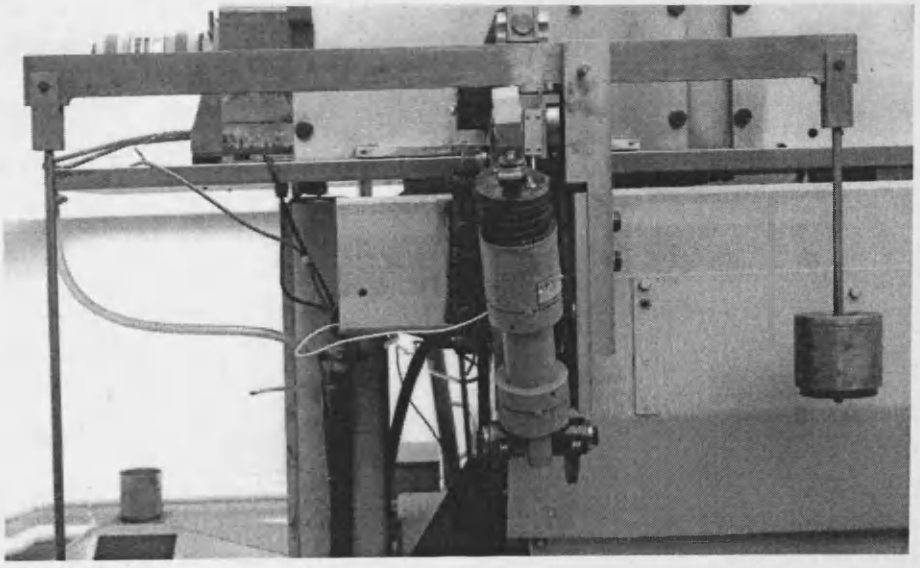

Figure D1. Arrangement for dead-weight calibration of load cell.

Calibration of friction dynamometer

The strain-gauged torque shaft in the drive to the slow speed disc was calibrated using a dead-weight loading arrangement as shown in Figure D2. The drive belt on the slow shaft pulley was disconnected and the slow disc was locked in position. The counterbalanced loading lever shown in Figure D2 was then clamped on to the slow shaft drive pulley and carefully levelled by adjusting the locked position of the slow disc. A series of weights was then added to the loading lever to calibrate the strain gauges up to a torque in excess of the highest torque used in the experiments. The gain of the chart recorder was set to give a pen displacement of 1 inch (25.4 mm) per 40 N of friction force.

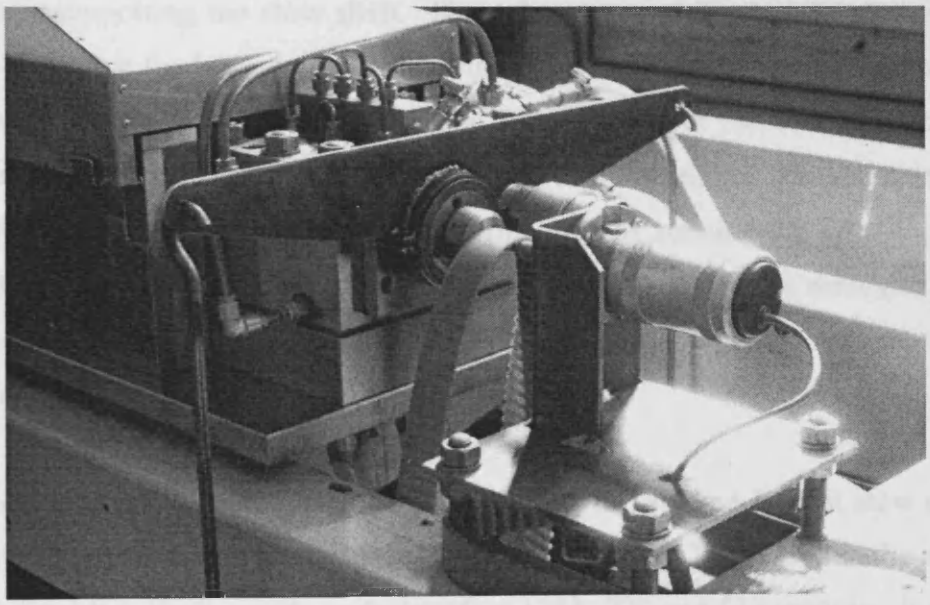

Figure D2. Arrangement for calibration of friction dynamometer

Appendix E

Calibration of load-dependent bearing friction

The friction force which is measured by the torque-shaft dynamometer includes friction in the bearings supporting the slow shaft. Since the torque applied to the slow shaft arising from the friction at the loaded contact is in the opposite direction to that due to the friction in the bearings supporting the shaft the true friction force at the contact is the measured value plus that arising from friction in the slow shaft bearings. An estimate of bearing friction was therefore required and this was obtained by running the discs together under free rolling by disconnecting the drive to the fast shaft. The friction measured in this case was then assumed to be twice that in the bearings of the slow shaft since the bearings supporting the two shafts was identical.

The bearing friction was measured as a function of the applied load at slow shaft speeds corresponding to the three sliding speeds (16m/s, 12m/s and 7m/s) used in the project. The corresponding slow shaft speeds were therefore 1238, 929 and 539 rev/min. It was decided to consider only the load-dependent bearing friction since the windage friction, which was assumed constant at constant speed, was easily offset as a constant measured value by running the rig at the operating speed and zero load. The load-dependency calibrations were run at the standard oil feed temperature of 100°C but since there was effectively zero frictional heating at the free rolling contact the temperature of the discs did not reach the temperatures experienced during a scuffing test. It was not possible to simulate high temperature conditions under free rolling conditions and hence measure the effect of temperature on bearing friction. The error involved is considered to be insignificant, however, because the measured change in effective friction force over the load range considered (0-6758 N) amounted to only about two or three Newtons which is seen to be small compared to the measured friction under conditions approaching scuffing.

The load-dependent bearing friction force obtained in this way was found to be linear as shown in Figure E1. The correction factors to take account of the load-dependent bearing friction are as follows.

$F = 2.77 \times 10^{-4} W$	at 16m/s	sliding speed
$F = 2.72 \times 10^{-4} W$	at 12m/s	sliding speed
$F = 3.69 \times 10^{-4} W$	at 7m/s	sliding speed

Where F is the friction force/N and W is the applied load/N.

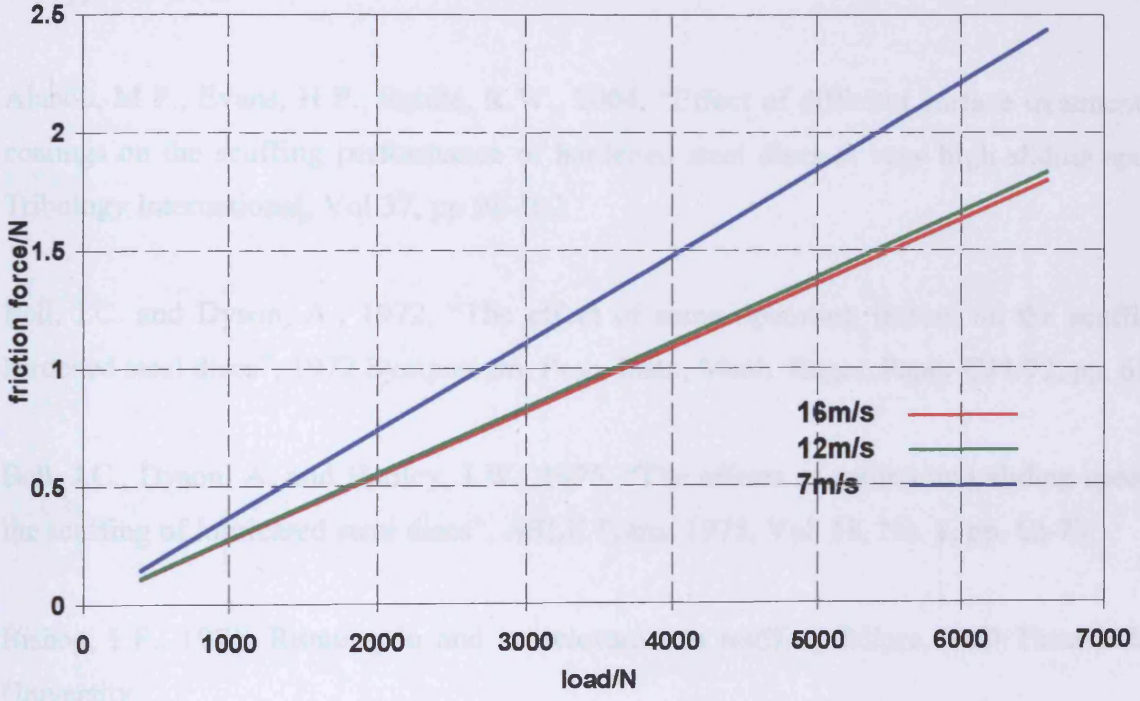

Figure E1. Determination of load-dependent bearing friction.

References

Ai, X., Cheng, H.S., 1994, "A transient EHL analysis for Line Contacts with measured surface roughness using Multi grid technique", Trans. ASME, Journal of Tribology, Vol. 116, pp. 549-556.

Alanou, M P., Evans, H P., Snidle, R W., 2004, "Effect of different surface treatments and coatings on the scuffing performance of hardened steel discs at very high sliding speeds", Tribology International, Vol 37, pp 93-102.

Bell, J.C. and Dyson, A., 1972, "The effect of some operating factors on the scuffing of hardened steel discs", 1972 Symposium, Proc, Instn, Mech. Engrs. Paper C11/72, pp. 61-67.

Bell, J.C., Dyson, A. and Hadley, J.W., 1975, "The effects of rolling and sliding speeds on the scuffing of lubricated steel discs", ASLE Trans. 1975, Vol. 18, No. 1, pp. 62-73.

Bishop, I F., 1981, Running in and its relevance to scuffing failure, PhD Thesis, Cardiff University.

Bjerk, R O., 1973, "Oxygen-An "Extreme-Pressure agent"", ASME Transactions, Vol 16, pp 97-106.

Blok, H., 1937, "Theoretical study of temperature rise at surfaces of actual contact under oiliness lubricating conditions", Instn. Mech. Engrs., Proceedings of the General Discussion on Lubrication and Lubricants, 2, pp 222-235.

Blok, H., 1939, "Seizure delay method for determining the protection against scuffing afforded by extreme pressure lubricants", J. Society of Auto Engrs., Vol 44, No 5, pp 193-210.

Borodich, F M., Keer, L M., Harris, S J., 2003, "Self-Similarity in abrasiveness of hard carbon-containing coatings", ASME Journal of Tribology, Vol 125, pp 1-7.

Britton, R.D., Elcoate, C.D., Alanou, M.P., Evans, H.P., Snidle, R.W., 2000, "Effect of surface finish on gear tooth friction", Trans. ASME, Journal of Tribology, Vol. 122, pp. 354-360.

Chang, Y Y., Wang, D Y., Chang, C H., Wu, W., 2004, "Tribological analysis of nano-composite diamond-like carbon films deposited by unbalanced magnetron sputtering", Surface & Coatings Technology, Vol 184, pp 349-355.

Chang, L., Webster, M.N., Jackson, A., 1993, "On the pressure rippling and roughness deformation in Elastohydrodynamic Lubrication of rough surfaces", Trans. ASME, Journal of Tribology, Vol. 115, pp. 439-444.

Cheng, H S., 1983, "Micro-Elastohydrodynamic Lubrication", NASA International Conference, Trib. II, pp 615-629.

Clarke, A., Sharif, K.J., Evans, H.P. and Snidle, R.W., 2006. "Heat partition in rolling/sliding elastohydrodynamic contacts", Trans ASME, Journal of Tribology, Vol. 128, pp. 67-78.

Dearnaley, G., Arps, J H., 2005, "Biomedical applications of diamond-like carbon (DLC) coatings: A review", Surface & Coatings Technology, Vol 200, pp 2518-2524.

Donnet, C., 1998, "Recent progress on the Tribology of doped diamond-like and carbon alloy coatings: a review", Surface and Coatings Technology, Vol. 100-101, pp. 180-186.

Donnet, C., Grill, A., 1997, "Friction control of diamond-like carbon coatings", Surface and Coatings Technology, Vol. 94-95, pp. 456-462.

Dowson, D., Higginson, G R., 1966, "Elastohydrodynamic Lubrication", Wear, Vol. 10, Issue 3, pp. 246-261.

Dyson, A., 1975, "Scuffing – a review", Tribology International, Vol 8, Pt 1, pp 77-87, Pt 2, pp 117-122.

Dyson, A., 1976, "The failure of elastohydrodynamic lubrication of circumferentially ground discs", Proc. Inst. Mech. Engrs, Vol 190, No 52, pp 699-711.

Dyson, A., Evans, H P., Karami, G., Paliwal, M C., Snidle, R W., 1990, "Scuffing failure of steel discs: conditions for failure of elastohydrodynamic lubrication", Proc Instn Mech Engrs., Vol 204, pp 91-97.

Elcoate, C.D., Evans, H.P., Hughes, T.G., Snidle, R.W., 1999, "Thin film, time dependent, micro-EHL solutions with real surface roughness", Proc. 25th Leeds-Lyon Symposium on Tribology, Elsevier, Amsterdam, pp. 163-174.

Field, S K., Jarratt, M., Teer, D G., 2004, "Tribological properties of graphite like and diamond like carbon coatings", Tribology International, Vol 37, pp 949-956.

Grill, A., 1997, "Tribology of diamond like carbon and related materials: an updated review", Surface & Coatings Technology, Vol 94-95, pp 507-513.

Harris, S.J., Weiner, A.M., Meng, W, 1997, "Tribology of metal containing diamond like carbon coatings", Wear, Vol. 211, pp. 208-211.

Harris, S J., Weiner, A M., Grischke, M., 1999, "Effects of load on the abrasion of steel by metal-containing diamond-like carbon", Surface & Coatings Technology, Vol 120-121, pp 561-564.

Hershberger, J., Ajayi, O O., Zhang, J., Yoon, H., Fenske., 2005, "Evidence of scuffing initiation by adiabatic shear instability", Wear, Vol 258, pp 1471-1478.

Hirst, W., Hollander, A E., 1974, Surface Finish and damage in Sliding, Proc. R. Soc. A337, pp 379-394.

Hogmark, S., Jacobson, S., Larsson, M., 2000, "Design and evaluation of tribological coatings", Wear, Vol 246, pp 20-33.

Holmberg, K., Matthews, A., Ronkainen, H., 1998, "Coatings Tribology – contact mechanisms and surface design", Tribology International, Vol 31, No 1-3, pp 107-120.

Holmes, M.J.A., Evans, H.P., Snidle, R.W., 2003, "Transient elastohydrodynamic point contact analysis using a new coupled differential deflection method Part 1: theory and validation" & "Transient elastohydrodynamic point contact analysis using a new coupled differential deflection method Part 2: results", Proc. Inst. Mech. Engrs. Part J: Journal of Engineering Tribology, Vol. 217, pp. 289-304 & 305-322.

Hu, Y., Zhu, D., "A full numerical solution to the mixed lubrication in point contacts", 2000, Trans. ASME, Journal of Tribology, Vol. 122, pp. 1-9.

Institution of Mechanical Engineers, 1957
Conference on Lubrication and Wear, London, England, Proceedings, p 4

Jiang, X., Hua, D.Y., Cheng, H.S., Ai, X., Lee, S.C., 1999, "A mixed elastohydrodynamic lubrication model with asperity contact", Trans. ASME, Journal of Tribology, Vol. 121, pp. 481-491.

Kalin, M., Vizintin, J., 2005 (a), "The tribological performance of DLC-coated gears lubricated with biodegradable oil in various pinion/gear material combinations", Wear, Vol 259, pp 1270-1280.

Kalin, M., Vizintin, J., 2005 (b), "A comparison of the tribological behaviour of steel/steel, steel/DLC and DLC/DLC contacts when lubricated with mineral and biodegradable oils", Wear, Article in Press.

Kim, J W., Lee, Y Z., 2001, "The residual stresses on lubricated sliding surfaces during break-in and up to scuffing", Wear, Vol 251, pp 985-989.

Kodali, P., Walter, K C., Nastasi, M., 1997, "Investigation of mechanical and tribological properties of amorphous diamond-like carbon coatings", Tribology International, Vol 30, No 8, pp 591-598.

Krantz, T.L., Alanou, M.P., Evans, H.P., Snidle, R.W., 2001, "Surface fatigue lives of Case-Carburized gears with an improved surface finish", Trans. ASME, Journal of Tribology, Vol. 123, pp. 709-716.

Krantz, T., Cooper, C., Townsend, D., Hansen, B., 2004, "Increased surface fatigue lives of spur gears by application of a coatings", Journal of Mechanical Design, Vol 126, pp 1047-1054.

Ludema, K C., 1984, "A review of scuffing and running-in of lubricated surfaces, with asperities and oxides in perspective", Wear, Vol 100, Issue 1-3, pp 315-331.

Lee, S C., Cheng, H S., 1991, "Scuffing Theory Modelling and Experimental Correlations", Journal of Tribology, Vol 113, pp 237-334.

Leach, E F., Kelley, B W., 1965, "Temperature, the key to lubricant capacity", Trans. ASLE, Vol 8, No 3, pp 271-285.

Martin, M J.,Alanou, M P., Evans, H P., Kawamura, H., Dodd, A., 2001, "Scuffing performance of M50 bearing steel lubricated with a gas turbine engine oil at high sliding speeds", Tribology Transactions, Vol 44, pp 465-471.

Matveevsky, R M., 1965, "The Critical Temperature of Oil with Point and Line Contact Machines", Trans. ASME Jn. Basic Engineering., 89, pp 754-760.

Neimann, G., Lechner, G , 1967, "Scuffing load of steel gears", Erdoel & Kohle, Erdgas, Petrochemie, Vol 20(2), pp 96-106.

O. E. C. D, 1969, Glossary of terms and definitions in the field of friction, wear and lubrication. Wear and Lubrication, pp 52-53.
Niemann & Lechner (1967)

Padmore, E I., and Rushton, S G., 1964, "Effects of loading procedure on surface failure in spur gears", Proc. Inst. Mech. Engrs, Vol 179, Part 3J 12, pp 78-97.

Paliwal, M C., 1987, Running In and scuffing failure of marine gears, PhD thesis, Cardiff University.

Patching, M.J., 1994, The effects of Surface Roguhenss on the Mirco-Elastohydrodynamic Lubrication and Scuffing performance of Aerospace Gear Tooth Contacts, PhD Thesis, University of Wales, Cardiff

Patching, M.J., Kweh, C.C., Evans, H.P., Snidle, R.W., 1995, "Condtitions for scuffing failure of ground and super finished steel discs at high sliding speeds using a gas turbine engine oil", Trans. ASME, Journal of Tribology, Vol 117, pp. 482-489.

Persson, K., Gahlin, R., 2003, "Tribological performance of a DLC coating in combination with water based lubricants", Tribology International, Vol 36, pp 851-855.

Podgornik, B., Jacobson, S., Hogmark, S., 2005, "Influence of EP additive concentration on the tribological behaviour of DLC-coated steel surfaces", Surface & Coatings Technology, Vol 191, pp 357-366.

Polonsky, I A., Chang, T P., Keer, L M., Sproul, 1997, "An analysis of the effect of hard coatings on near-surface rolling contact fatigue initiation induced by surface roughness", Wear, Vol 208, pp 204-219.

Qu, J., Truhan, J J., Blaue, P J., 2005, "Investigation of the scuffing characteristics of candidate materials for heavy duty diesel fuel injectors", Tribology International, Vol 38, pp 381-390.

Sheeja, D., Tay, B K., Krishnan, S M., Nung, L N., 2003, "Tribological characterization of diamond-like carbon (DLC) coatings sliding against DLC coatings", Diamond and related materials, Vol 12, pp 1389-1395.

Snidle, R W., Rossides, S D., Dyson, A., 1984"The failure of elastohydrodynamic lubrication", Proc R Soc London, Ser. A, 395, 291-311.

Staph, H E., Ku, P M., and Carper, H J., 1973, "Effective of Surface Roughness and Texture on Scuffing", ASME-AGMA-IFTMM Symposium, San Francisco, Oct 1972.

Story, D L., Archard, J F., and Baglin, K P., 1980, "A Reassessment of the Scuffing Failure Data of Discs", Proc. Int. Symposium on Performance and Testing of Gear Oils and Transmission Fluids, Inst Petrol., 177-192

Suh, A Y., Polucarpou, A A., Conry, T F., 2003, "Detailed surface roughness characterization of engineering surfaces undergoing tribological testing leading to scuffing", Wear, Vol 255, pp 556-568.

Tallian, T E., 1972, "The theory of partial elastohydrodynamic contacts", Wear, Vol 21, pp 49-101.

Tao, J., Hughes, T G., Evans, H P., Snidle, R W., 2002, "Elstohydrodynamic response of transverse ground gear teeth", Proc. 28th Leeds-Lyon Symposium on Tribology, Elsevier, Amsterdam, pp 447-458.

Venner, C.H., Lubrecht, A.A., 1994, "Transient analysis of surface features in an EHL line contact in the case of sliding", Trans. ASME, Journal of Tribology, Vol. 116, pp. 186-193.

Wanstrand, O., Larsson, M., Hedenqvist, P., 1999, "Mechanical and tribological evaluation of PVD WC/C coatings", Surface and Coatings Technology, Vol. 111, pp. 247-254.

Wong, S K., Kapoor, A., 1996, "Effect of hard and stiff overlay coatings on the strength of surfaces in repeated sliding", Tribology International, Vol 29, No 8, pp 695-702.

Yokoyama, J., Ishikawa and Hayashi, K., 1972, "Effect of tooth profile modification on the scoring resistance of heavy duty spur gears", Wear, Vol 19, Issue 2, pp 131-141.

Zaidi, H., Frene, F., Senouci, A., Schmitt, M., Paulmier, D., 2000, "Carbon surface modifications during sliding test and friction behaviour of carbon thin films against XC steel", Surface and Coatings Technology, Vol. 123, pp. 185-191.

Zhao, J., Sadeghi, F., Hoeprich, M.H., 2001, "Analysis of EHL Circular contact start up. Part I-Mixed contact model with pressure and film thickness results", Trans. ASME, Journal of Tribology, Vol. 123, pp. 67-74.

Zhang, C., Cheng, H S., Wang, Q J., 2004, "Scuffing behaviour of piston-pin/bore bearing in mixed lubrication-part II: Scuffing mechanism and failure criterion", Tribology Transactions, Vol 47, pp 1-8.